The Trident of Climate Change Impacts on Marine Ecosystems: Warming, Acidification and Deoxygenation – Insights from Mediterranean sedimentary records

Sven Pallacks

Universitat Autònoma de Barcelona

ICTA Institute of Environmental Science and Technology - UAB

Doctoral thesis

Ph.D. in Environmental Science and Technology

June 2023

The Trident of Climate Change Impacts on Marine Ecosystems: Warming, Acidification and Deoxygenation – Insights from Mediterranean sedimentary records

Sven Pallacks

Tutor and thesis director:

Dr. Patrizia Ziveri

Co-director:

Dr. Eric Galbraith

This PhD thesis was funded by the fellowship from the Ministry of Economy and Competitiveness (FPI/BES-2017-080730) granted in August 2018 to December 2022). Funding was also provided by the consolidate research group MERS - Marine and Environmental Biogeosciences Research Group (SGR 2017 – 1588). This PhD thesis contributes to the ICTA-UAB "Unit of Excellence" (FPI/MDM-2015-0552-16-2; CEX2019-000940-M).

“You thought I should find nothing but ooze”

H. G. Wells, Into the Abyss (1897)

To my family

Content

Acknowledgements

It will be difficult to acknowledge and thank everybody who has helped me with this thesis over almost the past five years. However, I will give it a try!

Firstly, I want to thank both of my supportive supervisors Patrizia Ziveri and Eric Galbraith. Patrizia, I know you now since almost a decade, from when I first stumbled into your office in 2016 as a student to ask for an opportunity to do a master thesis with you. A master thesis became a PhD, through which you guided me with a lot of patience. Many thanks for your faith and trust in me, and that you gave me the opportunity to find my path in academic research. Thank you, Eric, for your constructive comments and suggestions at the right time. Your ideas lead me into directions I have not thought about before. I hope that our paths will cross many times more in the future.

I also want to send a special thank to Richard Norris, who was like a third supervisor for the last part of my thesis. He allowed me to do my research stay abroad at the marvelous Scripps Institution of Oceanography. I really hope we will have some common topics in the future to work on together, and who knows, maybe it will be the fantastic record in the Bay of Navarino.

A big thank is send to my research group, as you made me feel always welcome during my entire PhD. Thanks to my former/actual PhD student colleagues Roberta, Laura, Miki, Griselda, Stephanie, Arturo, Mouna, Eloise, Shania, Henrique to sustain the young spirit in science. Thanks to the research colleagues Michael Grelaud, Gerald Langer, Graham Mortyn and the people from Physics department. Every morning I walked with a good feeling through the main entrance of ICTA, which is mainly your merit, as all of you created a very friendly working atmosphere. Also big thanks to all of my co-authors and your endurance to comment on my never-ending drafts. Thanks to the ICTA administration, who was always very helpful and supportive.

Endless thanks to my family, without you I would not be where I am. Only with your emotional, intellectual, and financial support I was able to go down this road. Thanks, Muddern, for your infinite patience and not giving up practicing German spelling with

me in fifth grade, even if it seemed hopeless. Thanks, Vaddern, for all the detailed explanations on how the human organism works, I am certain it helped me a lot in the understanding of my research. Thanks for waken and keeping my enthusiasm for sports during my youth, as a lot of skills learned there were quite useful during my PhD. I cannot thank you both enough for your faith in me, I appreciate your trust very much and all the freedom you allowed me. Big gratitude to my two sisters, Wiebke and Frauke, I am pretty sure you made me a better person and prevented me from being an idiot sometimes. Thanks to all my four grandparents, as they are responsible for the education of my parents, and so set the foundation for mine. Thanks to my grandmother Renate and the interest you show for the research I am doing. I am always astonished by your never-ending curiosity and powers of comprehension. Thank you, Lukas, for a long-term friendship since kindergarten, I have always looked up to you. Thanks Oriol, it was a pleasure to share more than 3 PhD years with you in Communidadje. Your stoicism inspired me. Good luck with your PhD! Many many thanks to all my friends in Germany and Barcelona and wherever. You have all contributed a huge part to this!

Abstract

Humankind's great hunger for cheap, instant fossil energy has led to exponential carbon dioxide (CO_2) accumulation in the atmosphere since the onset of the Industrial Revolution. The accumulation of atmospheric CO_2 not only heats our planet but has adverse knock-on effects for our ocean and its ecosystem functioning. Owing to its large specific heat capacity and volume, the global ocean accounts for about 95% of Earth System warming. Accelerated ocean warming decreases the mixing in the upper 2000m of the water column and impacts the nutrient budget in surface waters, which further influences marine primary production. Around 25% to 30% of the accumulated atmospheric CO_2 is absorbed by the ocean every year, altering the carbonate chemistry of seawater. Calcifying marine organisms are particularly affected by declining surface water pH and carbonate ion concentrations [CO_3^{2-}], in a phenomenon known as ocean acidification. Closely linked to ocean warming, ocean deoxygenation, specifically at mesopelagic depths, also threatens great parts of the marine ecosystem. Therefore, the synergistic effects of ocean warming, acidification and deoxygenation will have unpredictable consequences for global marine ecosystem services like climate regulation, biodiversity and food security. However, the lack of oceanographic long-term records relating to biological and physicochemical parameters prevents a comprehensive assessment of how those climate change drivers affect marine ecosystems. The main objective of this thesis is to contribute to the understanding of the ocean in high CO_2 conditions by reconstructing marine ecosystem dynamics beyond the temporal scale of instrumental records. This will place recent observations into the context of past climate change when human influence was minor or even absent. Additionally, field observations allow us to capture the complex natural environment of the Mediterranean Sea, a region highly sensitive to anthropogenic and natural climate change, through which the synergistic effects of changing physical and chemical conditions on key marine organisms can be directly assessed.

To investigate marine environmental changes as a response to human induced ocean warming and acidification, we reconstruct fossil planktic foraminiferal changes over

the last 2000 years in the western Mediterranean Sea. Planktic foraminifera are globally distributed, calcifying marine zooplankton, and valuable recorders of physicochemical and biological changes at the sea surface. How sensitive those key organisms are to the combined effects of climate change drivers on timescales beyond observational records is still unknown. Chapter 2 and 3 of the thesis are dedicated to analyzing changes of planktic foraminifera composition, abundance, and test calcification along with multi-proxy data from three high resolution multicores, collected in the Alboran Sea, Balearic Sea and the Strait of Sicily. Our findings suggest that in the pre-industrial era, changes in planktic foraminiferal productivity and species composition can be explained primarily through natural climate variability. Starting from about 1800 CE, foraminiferal dynamics are linked to accelerated sea surface temperature warming, indicating decreased marine productivity due to thermally induced water column stratification. Reduced test weights imply that anthropogenic CO_2 has already affected planktic foraminiferal calcification during the 20th century, corroborated by carbon and boron isotope data indicating enhanced anthropogenic CO_2 uptake and decreasing pH at our study sites. Our studies detect a basin-wide imprint of anthropogenic CO_2 induced changes in western Mediterranean sediment records.

Moreover, the thesis provides a glimpse on how ocean deoxygenation may impact oceanic fish ecology. Open ocean deoxygenation is hypothesized to pose severe threats, specifically to the mesopelagic fish community, by enhancing physical stress, shifting their habitat into the photic zone, and so changing prey-predator relationships, with negative effects for their abundance and composition. Mesopelagic fish are key players in ocean food webs, an abundant nutritional resource for aquaculture and nutraceutical markets and of highest importance for climate change mitigation as they transport carbon from the surface to the deep sea. In chapter 4, we investigate the impacts of ocean deoxygenation on the midwater fish community by using Holocene otoliths from an Eastern Mediterranean sediment core. Extremely low overall abundances of otoliths are detected between 7 and 11 kyr ago, when bottom to mid-waters were highly anoxic, and surface waters were remarkably productive. During that time the otolith composition is dominated by fish adapted to the epipelagic zone,

while mesopelagic species are nearly absent. After re-oxygenation at about 6 kyr ago, mesopelagic fish species dominate the otolith record to the present day. Our results suggest a likely negative response of midwater fish to ongoing intensification and expansion of Oxygen Minimum Zones over coming centuries, which would have major impacts on marine fisheries, marine conservation, ocean food web structure and carbon storage capacity.

These long-term records capture the complex natural environment throughout periods of intense human and naturally induced climate pressure. Together, they allow us to assess the impact of ocean warming, acidification and deoxygenation on the ecology and calcification of planktic foraminifera, and on midwater fish dynamics, both key groups of organisms that are highly important for the structure and functioning of global marine ecosystem services and food webs. Our findings may help to better project future ocean food web dynamics and will serve to facilitate marine policy decision making.

CHAPTER 1

1 Introduction

1.1 Anthropogenic CO_2 increase and impacts on marine ecosystems

Humankind has developed a great hunger for fossil fuels during the last centuries. Particularly, since the onset of the Industrial Revolution, our novel demand for energy needs to be satisfied by the combustion of coal, oil and natural gas, leading to an exponential increase of human-induced carbon dioxide (CO_2) in Earth's atmosphere (Crutzen, 2002; Waters et al., 2016). The global atmospheric CO_2 concentrations rose from 280 ppm during pre-industrial times to about 421 ppm in May 2022, an increase of more than 50% (Lan et al., 2023), and a level that probably has not been reached for the last 3 million years (Guillermic et al., 2022; Pagani et al., 2010). The recent anthropogenic CO_2 pollution, which is in humanity's past unprecedented in rate and amplitude, leads to ocean warming, ocean acidification, and ocean deoxygenation. The combination of those CO_2 induced climate change stressors, referred to as the "deadly trio" (Bijma et al., 2013), is assumed to have severe consequences for marine ecosystem functioning, with adverse knock on effects for marine fishery, conservation and climate regulation.

1.1.1 Ocean warming and productivity changes

Enhanced anthropogenic CO_2 emissions are responsible for shifting the energy balance of Earth's climate system and so heating up our planet (Rhein et al., 2013). Owing to its large specific heat capacity and volume, the lion's share of energy imbalance is taken up by the ocean accounting for approximately 93% of Earth system warming that has occurred since the mid-20th century (Cheng et al., 2019; Levitus et al., 2012). Observational records covering the last decades, show accelerated warming of the sea surface compared to the ocean interior, with global sea surface temperatures (SSTs) increasing at a rate of 0.13 °C per decade during the last 100 years (Levitus et al., 2000; Reid & Hill, 2016). This is corroborated by several proxy records describing unprecedented SST increase with the onset of the Industrial Era (IE) (Abram et al., 2016) and models projecting surface waters to warm faster than deeper ocean regions (Bopp et al., 2013; Cheng et al., 2019), with an estimated mean global ocean temperature rise between 1 to 4 °C by the end of the 21st century (Reid & Hill, 2016).

Accelerated warming of the upper ocean enhances the vertical temperature gradient which implicates stronger water column stratification (Hoegh-Guldberg et al., 2014). Human-induced warming during the last decades has significantly contributed to global upper-ocean stratification (Cheng et al., 2023; Li et al., 2020), impacting marine life. Stronger vertical gradients prevent nutrient enriched deep-water from being mixed into nutrient depleted surface waters, and therefore deepening the nutricline, with negative consequences for primary producers (Chavez et al., 2011; Longhurst, 1995). Although the relationship between global surface ocean primary productivity and warming seems to be complicated (Dunstan et al., 2018), there is a growing body of evidence that thermally induced stratification leads to a decline in biological marine surface productivity. Satellite images reveal that expansion of low surface chlorophyll areas and low phytoplankton productivity is closely coupled to ocean warming and stratification strength (Behrenfeld et al., 2006; Martinez et al., 2009; Polovina et al., 2008), further corroborated by model projections, estimating a reduction of 2-16% in global net primary production (NPP) and 7-18% in global export production (EP) throughout the 21st century, induced by more stratified ocean (Fu et al., 2016). Accordingly, ocean warming impacts the entire marine ecosystem, as it cuts of nutrient supply at the sea surface, negatively impacting primary productivity, and so limiting food supply for upper trophic levels in the ocean.

1.1.2 Ocean acidification and calcification loss

Every year, about 25-30% of anthropogenic CO_2 accumulating in the atmosphere is absorbed by the global ocean (Friedlingstein et al., 2022; Gruber et al., 2023; Gruber et al., 2019). The dissolved CO_2 reacts with sea water and forms carbonic acid (H_2CO_3), followed by an instant release of hydrogen ions (H^+) and bicarbonate ions (HCO_3^{1-}), which increases sea water acidity. The chemical reaction decreases pH and the availability of CO_3^{2-} in sea water, a phenomenon referred to as ocean acidification (Caldeira & Wickett, 2003; Zeebe, 2012). While global mean ocean pH has decreased by 0.1 units compared to pre-industrial levels, it may drop below 7.8 by the end of 2100 Common Era (CE) (IPCC, 2019; Jacobson, 2005), also lowering carbonate ion concentrations in the global ocean significantly, which is expected to have detrimental

implications for abundance and shell structure of marine calcifying organisms (Kroeker et al., 2010).

Planktic foraminifera and coccolithophores are two of many calcifying organisms which form their shells and outer skeletal structures using calcium carbonate ($CaCO_3$) through a process known as biogenic calcification. As the build-up of their calcite structures is dependent on pH and carbonate ion concentration, those taxa are particularly prone to seawater chemistry changes, facing severe consequences with ongoing ocean acidification (Fabry et al., 2008; Kroeker et al., 2010; Leung et al., 2022; McNeil & Matear, 2008; Orr et al., 2005). This is supported by a comprehensive amount of laboratory experiments investigating the responses of coccolithophores (Meyer & Riebesell, 2015) and planktic foraminifera (Bijma et al., 1999; Lombard et al., 2010; Russell et al., 2004) to CO_2 induced changes in seawater chemistry.

Further insights on how marine calcifying organisms respond to ocean acidification events is given through the fossil record. The Paleocene-Eocene Thermal Maximum (PETM) was an episode of large geologic carbon release into the ocean atmosphere system that occurred 55.9 to 55.7 Ma ago, decreasing global sea surface pH by about 0.30 units (Penman et al., 2014), concomitant with an extinction of marine calcifying organisms (Zachos et al., 2005). The amplitude of pH decline was similar compared to the projected 21st century pH decrease of 0.33 units (Bopp et al., 2013; Gattuso et al., 2015), however, the rate of change was one order of magnitude slower, making today's ocean acidification rate unprecedented during the last 66 Ma (Zeebe et al., 2016), and will likely result in widespread future extinctions of marine calcifying organisms that will significantly exceed those at the PETM (Zeebe & Zachos, 2013). Another past analogue for CO_2 changes comparable to the IE provides the Last Deglacial Transition (LDT) between 18-11 kyr BP, when atmospheric CO_2 levels rose by around 80 ppm (Marcott et al., 2014), causing a sea surface pH drop between 0.15-0.05 units (Henehan et al., 2013; Hönisch & Hemming, 2005). Even though CO_2 related changes during the LDT are slightly below current rates and amplitudes (Bopp et al., 2013; Gattuso et al., 2015), substantial calcification loss has been reported across the last glacial-interglacial transition for planktic foraminifera (Barker &

Elderfield, 2002; Moy et al., 2009) and coccolithophores (L. Beaufort et al., 2011). Both geological periods can be used as natural experiments, testing the response of marine calcifying plankton to anthropogenic ocean acidification.

1.1.3 Ocean deoxygenation and midwater fish decline

Open ocean deoxygenation occurs over the entire upper global ocean but is particularly severe in Oxygen minimum Zones (OMZs), which are mainly located in eastern boundary upwelling systems of the Atlantic and Pacific Ocean and the Arabian Sea (Bindoff et al., 2019; Gilly et al., 2013; Helm et al., 2011; Ito et al., 2017; Schmidtko et al., 2017). Since the mid-20th century global ocean oxygen content has decreased between 0.5-3.3% in the upper 1000m, while OMZs expanded in volume, surface area, and shifted their hypoxic boundary layer (HPL) further upwards to the sea surface. Open ocean deoxygenation is strongly coupled to CO_2 induced climate warming, as it is mainly driven through changes in solubility effects, ocean ventilation and marine oxygen respiration (Bindoff et al., 2019; Brewer & Peltzer, 2017; Helm et al., 2011; Oschlies et al., 2018). Further evidence for the strong link between ocean warming and deoxygenation derives from geological records (A. J. Dickson et al., 2012; Praetorius et al., 2015), suggesting that throughout Earth's history, OMZs tend to be stronger, shallower and bigger during warmer periods with impacts on ancient marine ecosystems (Jenkyns, 2010; Yasuhara et al., 2019). Therefore, it is assumed that anthropogenic warming in combination with positive biogeochemical feedbacks might tip our ocean into larger scale anoxia (Watson, 2016), which is in agreement with model projections, showing unambiguous decline of ocean oxygen levels for the coming century (Bindoff et al., 2019; Bopp et al., 2013; Keeling et al., 2010; Shaffer et al., 2009), with adverse knock-on implications for marine life.

Intensification and shoaling of OMZs in the future are expected to alter marine pelagic ecosystems. In general, lower oxygen levels have negative impacts for fairly most marine organisms (Claireaux & Chabot, 2019), with fish being one of the most sensitive groups to hypoxia (Vaquer-Sunyer & Duarte, 2008). Reduced midwater oxygen levels affect mesopelagic organisms directly by decreasing oxygen supply at their tissue level, thus enhancing physiological stress (Seibel & Wishner, 2019;

Wishner et al., 2013). As the vertical habitat depth range of many mesopelagic taxa is strongly controlled by oxygen levels (D. Bianchi et al., 2013; Klevjer et al., 2016; Maas et al., 2014; Netburn & Koslow, 2015), shoaling of OMZs would compress their vertical habitat range and push those species into better illuminated regions at the sea surface, enhancing their visibility to predators with negative consequences for their survival (Gilly et al., 2013; Seibel & Wishner, 2019). Whether epipelagic species benefit from enhanced prey availability or deprive from reduced vertical habitat range through OMZ shoaling is less well understood yet (Prince & Goodyear, 2006; Prince et al., 2010; Stramma et al., 2012; Stramma et al., 2010). In any case, oxygen deoxygenation in future warming oceans is expected to alter both epipelagic and mesopelagic ecosystems.

1.2 The lack of long-term time series and their relevance to study ecosystem change

Availability of marine environmental data based on monitoring programs and instrumental measurements is too limited in time and space to comprehensively assess the effects of natural versus anthropogenic climate change on marine ecosystems. First in situ measurements have been performed from ships or at coastal sites since the early 19th century (Kent et al., 2017). However, fine temporal and spatial coverage of SST and marine biological productivity are just accessible since the start of satellite remote sensing programs in the late 20th century (Madrid, 1978; Merchant et al., 2019), and instrumental measurements of seawater carbonate chemistry and oxygen content at certain locations in the global ocean are at best a couple of decades long (Bates et al., 2014; Yasuhara et al., 2019). Past changes in marine food web dynamics and fish stock changes remain largely undocumented as time-series of modern scientific surveys like the Continuous Plankton Recorder (CPR) (Richardson et al., 2006) or the California Cooperative Fisheries Investigations Program (CalCOFI) (Ohman & Venrick, 2003) have just started in the early 20th century, while historical data is often fragmentary in time and space, making it difficult to study long term plankton and fish population dynamics.

The concern of human impacts on marine ecosystems is continuously growing, but the spatial and temporal limitation of oceanographic observational data hinders us to separate anthropogenic from natural climate change. Through paleorecords we can reconstruct environmental changes and ecosystem dynamics covering times scales further beyond the temporal coverage of instrumental and monitoring data, allowing for the development of adequate baselines to test human impact on marine life. Paleorecords can provide preconditions for conducting geohistorical natural experiments, capturing the complex interplay of many environmental parameters to test the combined effects of global climate change stressors on marine ecosystems. Therefore, paleorecords are crucial to better understand the synergistic impacts of anthropogenic and natural climate change stressors on key marine organisms over different (decadal to millennial) timescales.

1.3 Paleoenvironmental tools to extend instrumental time series

One of the most common tools used in paleo studies are proxy data derived from environmental archives. These proxy data are measurable descriptors in terms of physical characteristics of the environment, which stand in for desired, direct measurements like temperature, productivity or pH (Wefer et al., 1999). Proxy data is derived from environmental archives like ocean sediments or microfossils, which record the natural variability of ecosystems. This approach has the potential to reconstruct diverse aspects of the system, from the physical and chemical state of the water column to ecosystem productivity and structure. Below, selected types of proxy data and environmental archives used for this work are listed and briefly described.

1.3.1 Marine sediment cores – Travelling back in time

As historians use written chronicles to conceive human history, paleoceanographers read environmental archives to get a better understanding of past climate changes. As 6 to 11 billion metric tons of sediment accumulating every year on the seabed, ocean sediments are an important environmental archive, containing information about past changes in the ocean and the adjacent land masses, in form of biogenic (Fig. 1.1) and terrigenous material (Bradley, 2015b). Under ideal circumstances, layer after layer of

sediment is laid down at the seabed in undisturbed succession, forming continuous sequences of uninterrupted deposits. Those deposits can persist more than tens of millions of years at the seabed before tectonic processes might destroy them (Ruddiman, 2008). Ocean corer systems like Multi Cores and Kasten Cores (appendix in Gersonde, 2012) are typical devices to sample marine sediments (Fig. 1.2).

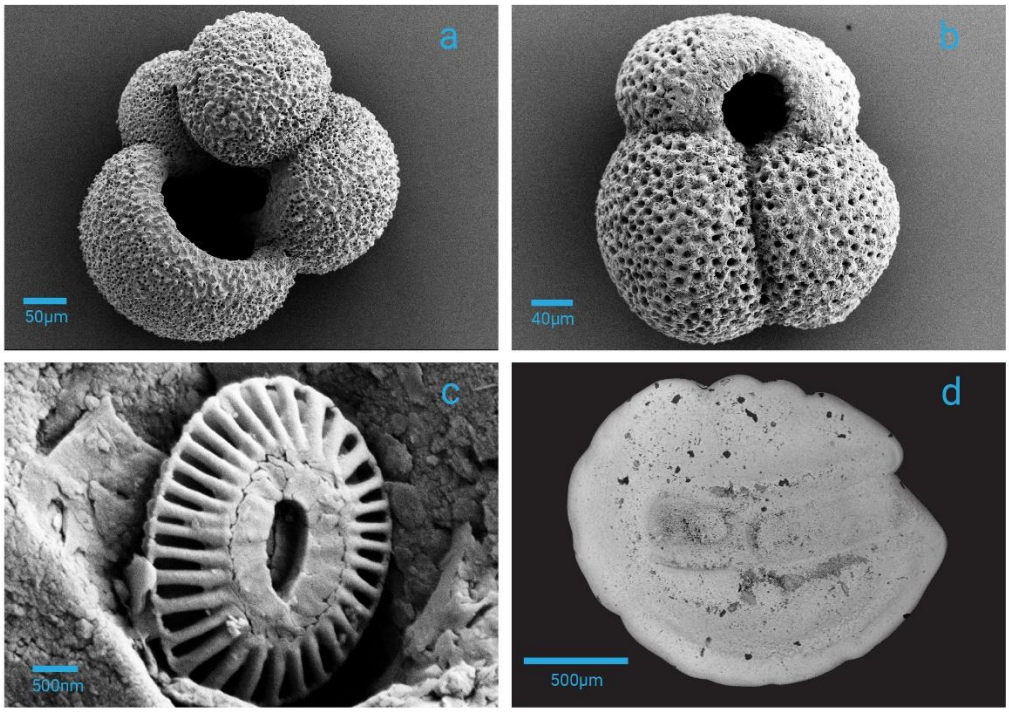

Figure 1.1: *Biogenic material in form of calcareous microfossils deposited in Mediterranean marine sediments. (a-b) Planktic foraminiferal shells of the two species Globigerina bulloides (a) and Globigerinoides ruber (b). (c) Coccolith of Emiliania huxleyi. (d) Fossil otolith of a spotted lanternfish (Myctophum punctatum).*

Accurate dating is crucial to palaeoceanographic studies to test synchronism between certain events in the past and to accurately define the rate of environmental change. Through measuring the decay of radioactive isotopes in the sediment, absolute ages can be assigned to certain depths in the record, allowing for precise dating throughout the ocean record (Bradley, 2015a). Through carbon exchange, all living organisms incorporate the radioactive isotope ^{14}C. After their death, radiocarbon decays within a half-life of 5780 years, making radiocarbon an ideal tool to date Holocene and Late Pleistocene carbon bearing sediments (Libby et al., 1949). As part of the radioactive

decay chain of ^{238}U, the natural radionuclide ^{210}Pb is produced constantly in the atmosphere through a series of short-lived daughter isotopes, before ending up in ocean sediments (Appleby & Oldfield, 1992). Owing to its shorter half-life of 22.3 years, ^{210}Pb chronologies cover the last 100 to 150 years, making it an ideal dating method for studying oceanographic changes during the IE, when human impact was most significant (Nriagu, 1990, 1996). Additionally, artificial radionuclides like ^{137}Cs tracking nuclear weapon testing and the Chernobyl accident, hence can serve as time markers in marine sediments (Garcia-Orellana et al., 2009).

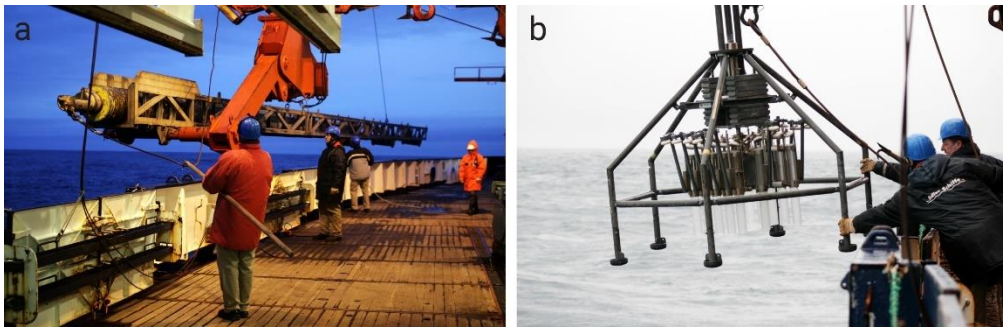

Figure 1.2: *Ocean sediment coring devices. (a) Kasten core system. (b) Multi core system (Images: Young Nam Kim/AWI).*

1.3.2 Calcifying plankton assemblages – Recorders of past environmental conditions

Planktic foraminifera and coccolithophores are within the most productive calcifying plankton on Earth, generating constant calcium carbonate rain from sea surface down to the seabed, being responsible that almost half of the modern ocean's seabed is covered by calcareous ooze (Rothwell, 2004). Planktic foraminifera / coccolithophores are single-celled zooplankton / phytoplankton, both building skeletal calcite structures, forming an excellent marine sedimentary record. Their good preservation in sediments and the species-specific morphology of their shells allows to reconstruct their population dynamics which is closely linked with environmental conditions in the past. Planktic foraminiferal changes are controlled by several surface water properties (Bé, 1977; Bé & Tolderlund, 1971; Schiebel & Hemleben, 2017), making their shell accumulation rates and species composition changes in marine sediments a good recorder for past variabilities in SST (A.

Incarbona et al., 2019; Jentzen et al., 2018; Morey et al., 2005; Rutherford et al., 1999), primary productivity (Hemleben et al., 1989; Herguera & Berger, 1991; Imbrie & Kipp, 1971; Schiebel & Hemleben, 2005) or hydrography (Lirer et al., 2014; Margaritelli et al., 2018; Vallefuoco et al., 2012). Similarly, coccolithophores are sensitive tracers of past and ongoing changes in the marine environment (Baumann et al., 2005; Baumann et al., 1999). Accordingly, both planktic foraminiferal and coccolithophore dynamics can be used as tracers for recent human-induced climate change (Beaugrand et al., 2013; Field et al., 2006; Jonkers et al., 2019).

1.3.3 Calcifying plankton shells – Tracing oceans chemistry

Morphometry and chemical composition of marine plankton carbonate shells contain important information about the oceanographic conditions which prevailed during their biogenic calcification, and provides an archive of past biological, environmental, and human-induced changes. Shell mass is associated with planktic foraminiferal calcification, thus it can be used as a tracer for changes in ocean surface chemistry, temperature and productivity (Weinkauf et al., 2016). However, alterations in sea water pH and [CO_3^{2-}] seem to be the dominant driver for biological precipitation of the calcite test, and therefore shell weight (A. N. Davis et al., 2019; Marshall et al., 2013; Osborne et al., 2016), making shell mass of fossil planktic foraminifera an ideal indicator for industrial CO_2 induced changes in the past ocean (Béjard et al., 2023; Moel et al., 2009; Moy et al., 2009; Osborne et al., 2020).

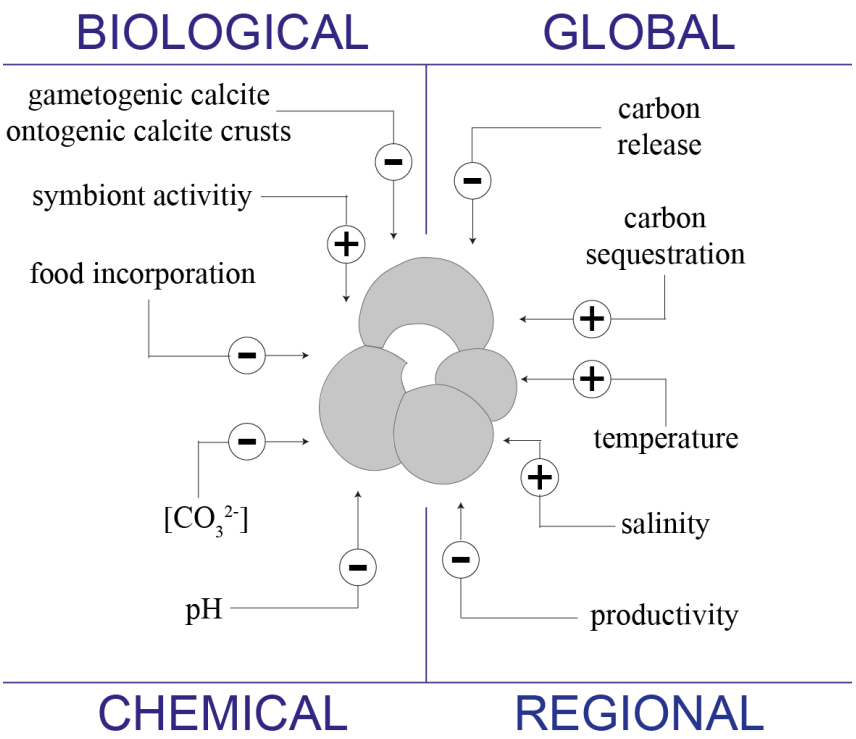

Figure 1.3: *Effects on the stable carbon isotope incorporation of planktic foraminiferal tests produced in the average surface pelagic ocean, modified after (Schiebel & Hemleben, 2017). Positive and negative coupling marked by (+) and (-).*

Stable isotopes are one of the most powerful tools in paleoceanography. Carbon isotopes recorded within the calcareous shell of planktic foraminifera are directly related to the carbon isotope signature of seawater, while their composition can be affected by a variety of biological, chemical, global and regional effects (Fig. 1.3). Variations in the ratio of light (^{12}C) vs. heavy (^{13}C) isotopes can serve as indirect measurements of past environmental changes (Schiebel & Hemleben, 2017). Particularly, the signal of enhanced uptake of isotopically light $^{12}CO_2$ by the ocean (Friedlingstein et al., 2022; Gruber et al., 2023; Gruber et al., 2019) due to anthropogenic carbon emissions since the onset of Industrial Revolution is carried in the $\delta^{13}C$ signal of planktic foraminiferal shells, referred to as the Suess effect (Eide et al., 2017; Mellon et al., 2019; Quay et al., 1992). Boron isotopes ($\delta^{11}B$) consist of the two naturally occurring stable isotopes ^{10}B and ^{11}B. Unlike $\delta^{13}C$, their composition in planktic foraminiferal calcite is compromised via vital effects, changing the pH of the shell microenvironment (Glas et al., 2012; Toyofuku et al., 2017). However, a robust

correlation between $\delta^{11}B$ calcite and ocean pH has been reported (Foster & Rae, 2016; James W. B. Rae, 2018), why stable boron isotopes in planktic foraminiferal shells have been used to detect and asses the amplitude of ocean acidification events in the geological past (Azharuddin et al., 2022; Harper et al., 2020).

Alkenones are organic compounds, comprising a suite of long-chain unsaturated ethyl and methyl ketones, detected in the ubiquitous coccolithophore *Emiliania huxleyi* and *Gephyrocapsa oceanica* (Eglinton et al., 2001; Volkman et al., 1995; Volkman et al., 1980). As the relative proportions of di- ($C_{37:2}$) and tri- ($C_{37:2}$) unsaturated methyl ketones are closely related to the growth temperatures of coccolithophores (Marlowe et al., 1984), the sedimentary unsaturation index ($U^{k'}_{37}$) can be applied as a paleothermometer (Brassell et al., 1986). Additionally, C_{37} alkenone cannot only serve as a proxy for primary production but also total phytoplankton biomass (Raja & Rosell-Melé, 2021).

1.3.4 Fossil fish ear bones (otoliths) – Reconstructing fish population dynamics

The application of fossil fish otoliths in paleoecology began more than 100 years ago (Koken, 1884), however, to this point their use as a proxy to reconstruct fish population dynamics is rather young (Elder et al., 1996). Each fish possesses three pairs of otoliths made of $CaCO_3$, serving as the hard structures for the gravity and auditory receptors. Due to its morphological variability and size, the largest of the three otolith pairs, the *saggitae*, provides the most valuable information for community reconstruction (Tuset et al., 2008). Morphometric analysis of the *saggitae* is used for taxonomic fish identification (Lombarte et al., 2006; Parisi-Baradad et al., 2010), and can be applied to reconstruct past fish assemblages from fossil otoliths (Cartes et al., 2017; W. A. Jones & Checkley, 2019; Lin et al., 2018; Lin et al., 2016; Lin et al., 2017). Their ubiquitous distribution in ocean sediments, makes fossil otoliths a promising new proxy to enhance our understanding of fish population dynamics in the past, which is insufficiently understood yet.

1.4 Natural experiments in the Mediterranean Sea

The semi-enclosed Mediterranean Sea is characterized by two large deep sub-basins (Eastern and Western Mediterranean Sea) connected through the shallow Strait of Sicily channel (Fig. 1.4). The modern arid climate and net buoyancy loss from west to east results in an anti-estuarine thermohaline circulation and a pronounced longitudinal surface gradient in physical and chemical characteristics in the Mediterranean Sea (Rohling et al., 2009; Schroeder et al., 2012). It's geographical location between two climate regimes, the subtropical high and the westerly wind zone, makes it highly sensitive to changes in atmospheric forcing and anthropogenic impacts. Several large rivers discharge their high sediments loads into the Mediterranean causing enhanced sedimentation rates in the basin, which provides a temporally highly resolved sediment archive for those changes. Owing to the small volume and the limited communication to the open ocean, those environmental signals are recorded instantaneously and in an amplified fashion (Rohling et al., 2009). Accordingly, Mediterranean ocean sediments provide excellent preconditions to test the response of a highly sensitive ecosystem to natural versus anthropogenic climate change stressors over long time scales.

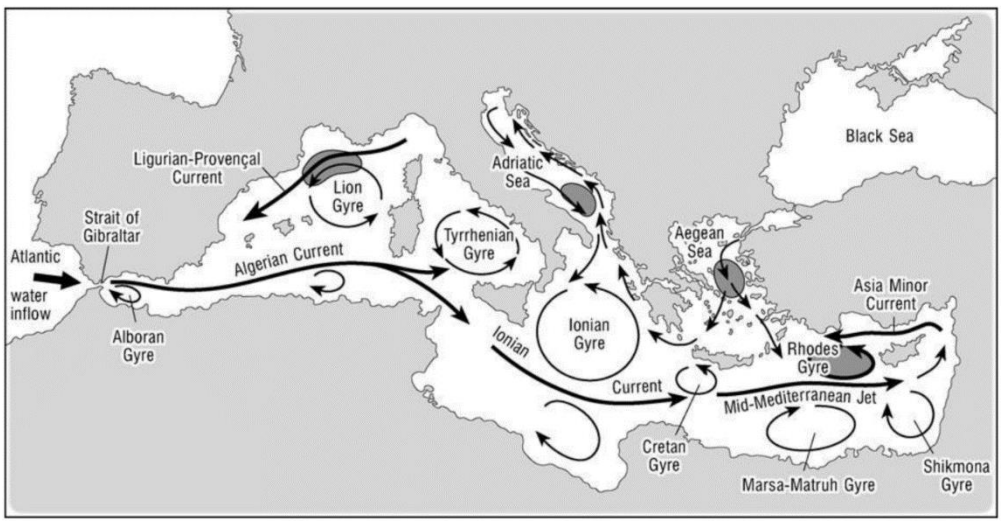

Figure 1.4: *Surface water circulation and intermediate and deep water formation in the Mediterranean Sea (Rohling et al., 2009).*

1.4.1 Natural experiment 1: The Mediterranean Anthropocene

Owing to its climatic conditions and hydrodynamic features, the Mediterranean Sea shows amplified and very rapid response to climate change, hence can be acknowledged as a climate change hot spot (Cramer et al., 2018; Giorgi, 2006). Accelerated recent warming of the Mediterranean region with a rate above global average (Lionello & Scarascia, 2018; MedECC, 2020), is also reflected in increasing Mediterranean SSTs trends with a rate around 0.4 °C per decade (Macías et al., 2013; Pisano et al., 2020; Shaltout & Omstedt, 2014). High alkalinity and low residence times of water masses with fast turnover rates (60 to 220 years) makes the Mediterranean Sea susceptible to the uptake of anthropogenic carbon (Hassoun et al., 2022; A. Schneider et al., 2010; A. Schneider et al., 2007; Touratier & Goyet, 2009), however, surface pH decreased by -0.08 units during the IE (MedECC, 2020), which is in agreement with global trends (Gattuso et al., 2015). Those anthropogenic changes are also captured in Mediterranean paleorecords like the unprecedented increase of SST (Marriner et al., 2022) or the enhanced accumulation of heavy ^{13}C isotopes in carbonate deposits (Amitai et al., 2020). We can make use of the Mediterranean Sea as a geohistorical natural laboratory, by comparing anthropogenic environmental changes with plankton dynamics, both recorded in the sediment record of the last centuries, to assess the impacts of ocean warming and ocean acidification on the marine ecosystem.

1.4.2 Natural experiment 2: The Eastern Mediterranean Sapropels

Strong oceanographic contrasts occur during the Eastern Mediterranean Holocene (Fig. 1.5), which help to investigate the response of marine pelagic ecosystems to intensification and shoaling of OMZs. During the Early Holocene, between approximately 10 to 6 kyr BP, changing orbital configurations lead to a shift of evaporation and precipitation patterns over eastern Mediterranean surface waters (Rohling, 1994), enhancing rainfall and river runoff, and so the freshwater and nutrient input into the eastern Mediterranean Sea (Kallel et al., 1997; Rohling & Hilgen, 1991). Consequently, Eastern Mediterranean surface waters became highly productive, whereas mid- to bottom waters suffered from hypoxia, due to a freshwater lid at the sea surface, impeding oxygen rich waters from being mixed into deeper

regions (Stratford et al., 2000). This period is reflected in the formation of sapropel S1 deposits, characterized by dark, organic rich sediment layers, resulting from enhanced export production and bottom water anoxia (Rohling et al., 2015; Schmiedl et al., 2010). Sapropel formation ended with a shift in precipitation patterns and the re-establishment of well oxygenated, ultraoligotrophic conditions, comparable to those of the modern Eastern Mediterranean Sea (Kontakiotis, 2016; Zielhofer et al., 2017). By comparing reconstructed fish dynamics with changing geohistorical oxygen levels, the hypoxic Eastern Mediterranean during S1 formation can serve as an extreme natural experiment, to study the response of pelagic ecosystems to future ocean deoxygenation.

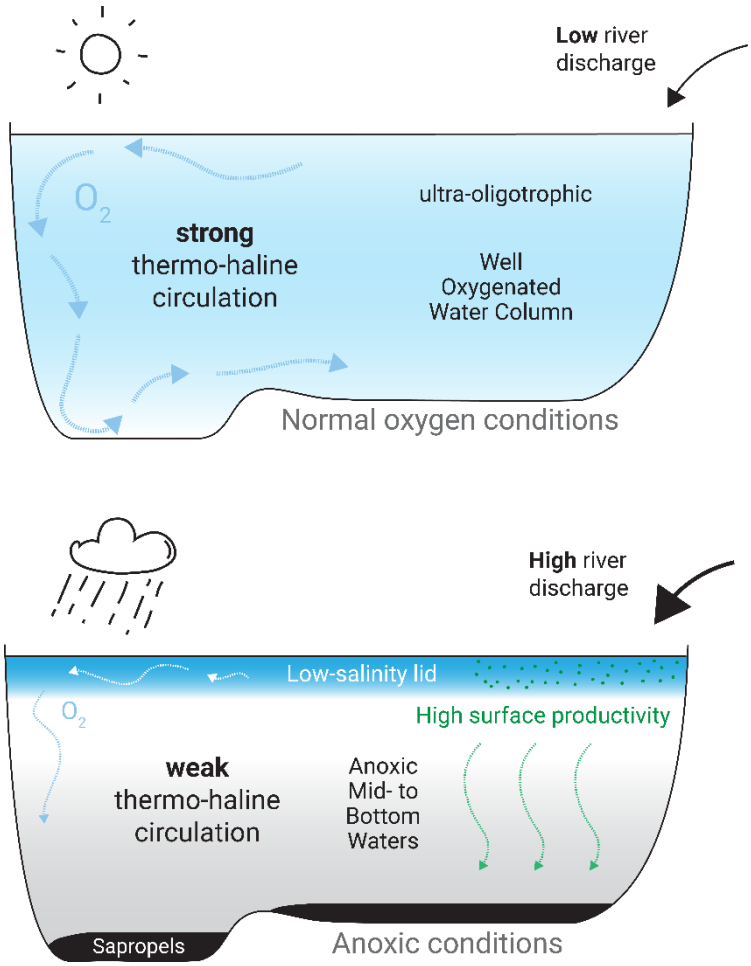

Figure 1.5: *Climatic and oceanographic conditions in the Eastern Mediterranean during (top) normal oxic and (bottom) anoxic conditions, modified after (Rohling et al., 2015; Ruddiman, 2008).*

CHAPTER 2

2 Planktic foraminiferal changes in the western Mediterranean Anthropocene

Abstract

The increase in anthropogenic induced warming over the last two centuries is impacting marine environment. Planktic foraminifera are a globally distributed calcifying marine zooplankton responding sensitively to changes in sea surface temperatures and interacting with the food web structure. Here, we study two high resolution multicore records from two western Mediterranean Sea regions (Alboran and Balearic basins), areas highly affected by both natural climate change and anthropogenic warming. Cores cover the time interval from the Medieval Climate Anomaly to present. Reconstructed sea surface temperatures are in good agreement with other results, tracing temperature changes through the Common Era (CE) and show a clear warming emergence at about 1850 CE. Both cores show opposite abundance fluctuations of planktic foraminiferal species (*Globigerina bulloides, Globorotalia inflata* and *Globorotalia truncatulinoides*), a common group of marine calcifying zooplankton. The relative abundance changes of *Globorotalia truncatulinoides* plus *Globorotalia inflata* describe the intensity of deep winter mixing in the Balearic basin. In the Alboran Sea, *Globigerina bulloides* and *Globorotalia inflata* instead respond to local upwelling dynamics. In the pre-industrial era, changes in planktic foraminiferal productivity and species composition can be explained mainly by the natural variability of the North Atlantic Oscillation, and, to a lesser extent, by the Atlantic Multidecadal Oscillation. In the industrial era, starting from about 1800 CE, this variability is affected by anthropogenic surface warming, leading to enhanced vertical stratification of the upper water column, and resulting in a decrease of surface productivity at both sites. We found that natural planktic foraminiferal population dynamics in the western Mediterranean is already altered by enhanced anthropogenic impact in the industrial era, suggesting that in this region natural cycles are being overprinted by human influences.

Chapter based on: Pallacks, S., Ziveri, P., Martrat, B., Mortyn, P. G., Grelaud, M., Schiebel, R., . . . Anglada-Ortiz, G. (2021). Planktic foraminiferal changes in the western Mediterranean Anthropocene. Global and Planetary Change, 204, 103549. doi.org/10.1016/j.gloplacha.2021.103549

2.1 Introduction

Mankind's influence on the climate has grown over the last two centuries, with exponential enrichment of greenhouse gases in the atmosphere (Abram et al., 2016; Crutzen, 2002). As observed by comparing data retrieved from instrumental measurements and ice core records (Bauska et al., 2015; Friedli et al., 1986; Tans & Keeling, 2020), the unprecedented increase of atmospheric CO_2 accelerated during the 20th century, warming surface oceans (Gleckler et al., 2012) and depleting marine surface production through enhanced vertical stratification (Behrenfeld et al., 2006; Li et al., 2020). In a world subjected to high anthropogenic pressure and affected by a continuous increase in atmospheric CO_2 since the Industrial Revolution, knowledge about the impacts of rising SST on changes in marine productivity plays an important role in understanding biological and environmental changes in the ocean.

The Mediterranean Basin, as a climate change hotspot (Giorgi, 2006), is particularly affected by environmental changes. The western Mediterranean is under the influence of large scale atmospheric patterns like the North Atlantic Oscillation (NAO), since fluctuations of the atmospheric pressure gradient between the Icelandic Low and the Azores High are associated with changes in climatic and oceanographic conditions (Hurrell, 1995; Tsimplis et al., 2013; Ulbrich et al., 2012), altering marine ecosystems (Drinkwater et al., 2003). The Atlantic Multidecadal Oscillation (AMO) is closely linked to SST variations in the western Mediterranean Sea (Marullo et al., 2011). NAO and AMO varies on multidecadal to centennial time scales (Mann et al., 2009; Olsen et al., 2012; Trouet et al., 2009) with positive phases prevailing during the Medieval Climate Anomaly (MCA), a warm period which begins in the western Mediterranean at roughly 800 CE. With the onset of the Little Ice Age (LIA), a subsequent, cold period lasting from around 1300 CE to 1800 CE, negative NAO phases became predominant (S. T. Gray et al., 2004; Lüning et al., 2019; Moreno et al., 2012; J. Wang et al., 2017). The first part of the 20th century was characterized by low pressure gradients, whereas from the 1970s on, positive NAO phases were stronger and occurred more frequently (Hurrell, 2020). The high NAO index by the end of the 20th century appears unprecedented during the last 130 years (Osborn, 2004), but is not unusual in the context of the past centuries (Hernández et al., 2020).

The close relation between NAO, AMO, and SST in the pre-industrial Mediterranean (Lüning et al., 2019) was superimposed by anthropogenic induced warming during the second half of the 20th century (Macías et al., 2013). Since 1880 CE, the annual mean air temperature has warmed more abruptly in the Mediterranean region compared to the global average (Cramer et al., 2018), accelerating the increase of SSTs in the Mediterranean at a rate of 0.35 °C per decade (Shaltout & Omstedt, 2014). Direct (changes in reproducibility, behavior, fitness and survival of marine organisms) and indirect (changes in biotic interactions or hydrography, e.g. displacement and intensity of marine currents, sea surface stratification) effects of ocean warming resulting in biogeographical shifts of species, mainly towards the northwest, causing a tropicalization and homogenization of the Mediterranean biota, and altering biodiversity and ecosystem functioning (C. N. Bianchi, 2007; Lejeusne et al., 2010; Philippart et al., 2011). Enhanced stratification as a consequence of sea surface warming is predicted to lower the primary production rate in the western basin, causing biomass loss in the entire Mediterranean Sea (Coma et al., 2009; Macías et al., 2015). Particularly calcifying organisms seem to be affected by climate-induced warming (Beaugrand et al., 2013).

The northwestern and southwestern Mediterranean regions are ideal locations to study impacts of natural versus anthropogenic climate change on surface ocean properties, since deep water formation in the Gulf of Lion is strongly connected to NAO variability (Josey et al., 2011; Vignudelli et al., 1999), driving surface productivity in the Alboran Sea (Macías et al., 2008; Macías et al., 2016; Macías et al., 2007). The see-saw pattern between high productive phases linked to strong deep water formation and vice versa is described in several Holocene marine sediment records (Ausín et al., 2015; Bazzicalupo et al., 2020; Cacho et al., 2000; Cisneros et al., 2019; Nieto-Moreno et al., 2015; Schirrmacher et al., 2019), while anthropogenic warming has affected both study regions, as reported through instrumental data and paleoenvironmental archives (Nieto-Moreno et al., 2013; Sicre et al., 2016).

Planktic foraminifera are single-celled marine eukaryotes producing calcite and yield an excellent marine sedimentary record. The sensitivity of planktic foraminifera to

changing physical and chemical conditions and their good preservation in marine sediments makes them good tracers of changing environmental conditions, regardless of whether alterations are caused by natural or anthropogenic drivers. Planktic foraminifera are under the influence of several surface seawater properties (Bé, 1977; Bé & Tolderlund, 1971; Schiebel & Hemleben, 2017), although the most important factor controlling assemblage composition and diversity is SST (Jentzen et al., 2018; Morey et al., 2005; Rutherford et al., 1999). On a regional and seasonal scale, quality of food plays a crucial role for the distribution of surface to subsurface dwelling species (Schiebel et al., 2001), indicated by the close relation between marine primary production and flux rates of planktic foraminiferal tests (Kucera, 2007). Water column configuration and food availability are supposed to be the main factors controlling foraminiferal distribution, abundance and diversity in the Mediterranean Sea (Bárcena et al., 2004; Giamali et al., 2020; Pujol & Grazzini, 1995; Rigual-Hernández et al., 2012; Zarkogiannis et al., 2020), whereas differences in the seawater carbonate chemistry between the eastern and western basin play a minor role (Mallo et al., 2017). Post-industrial age changes in planktic foraminiferal assemblages in oceans are subtle, limited to ~ 600 km latitudinal shift compared to pre-industrial communities (Field et al., 2006; Jonkers et al., 2019; Schiebel et al., 2018). In the Mediterranean Sea, no evidence of anthropogenic influence on planktic foraminiferal assemblages has been documented. Even over the latest climate anomalies (e.g. MCA, LIA), the planktic foraminiferal response appears weak, with small percentage changes in selected species and/or in the ratio between taxa that indicate different local hydrographic conditions (A. Incarbona et al., 2019; Lirer et al., 2014; Margaritelli et al., 2018; Vallefuoco et al., 2012).

The main objectives of this study are to determine how natural climate change, in particular large scale atmospheric oscillations like the NAO and AMO, have driven planktic foraminiferal assemblage dynamics during the Common Era at two strategically ideal locations in the western Mediterranean to study high-frequency changes in water mass dynamics and marine surface productivity, and to assess if the signal of natural variability in planktic foraminiferal composition is superimposed by accelerated anthropogenic SST warming, starting with the onset of the Industrial

Revolution. For this reason, we investigate the planktic foraminiferal accumulation rate records in two high resolution multicores collected in the Alboran Sea and the Balearic Sea spanning approximately the last 1.2 and 1.7 ky. We also report abundances of selected taxa in the > 150 μm fraction, to test the impact of large-scale atmospheric oscillations like the NAO and AMO during the Common Era. The planktic foraminiferal palaeoecological reconstruction is carried out along with data on alkenone-derived SST, organic biomarkers, and coccolithophore (calcifying phytoplankton) assemblage that provide evidence of a simultaneous modification in water column dynamics and in the planktic ecosystem network. Especially significant are $U^{k'}_{37}$ estimates that capture a pronounced post-industrial SST rise in both the Balearic and the Alboran seas, which is in line with instrumental measurements.

2.2 Study area

2.2.1 Oceanographic settings

The semi-enclosed Mediterranean Sea is separated by the Sicily Strait sill into the western and eastern Mediterranean basins. It is characterized by an anti-estuarine thermohaline circulation with eastward surface and westward subsurface flow, due to net buoyancy loss from west to east as a consequence of changes in evaporation, precipitation and runoff (Millot, 1999; Rohling et al., 2009; Schroeder et al., 2012; Schroeder et al., 2008). The Mediterranean Sea features large eastward surface gradients in physical and chemical characteristics with increasing salinity, SST, and alkalinity, and decreasing surface nutrient concentrations and dissolved inorganic carbon (A. Schneider et al., 2007; Shaltout & Omstedt, 2014; Stambler, 2014; Tanhua et al., 2013).

The two study sites, as shown in Figure 2.1, are under the influence of large-scale atmospheric phenomena. The differences of atmospheric sea level pressure between the Icelandic Low and the Azores High, known as the NAO, is influencing the climate and oceanographic conditions of the western Mediterranean (Hurrell, 1995). Positive NAO phases characterized by a strong subtropical high-pressure cell and a deeper Icelandic Low generate strong westerly winds, crossing the Atlantic on a more northerly track and result in warm and dry conditions over the Mediterranean Sea with

reduced storm activity and below average precipitation rates. A weak pressure gradient between the Azores High and the Icelandic Low (negative NAO phase) causes a more southeasterly pathway and enhanced storminess in southern Europe, which brings more moisture to the Mediterranean region (Ulbrich et al., 2012). NAO phases vary on annual to multicentennial time scales and are recorded in environmental archives like lake sediments, tree rings and speleothems, thus allowing for reconstructing high resolution records dating back several thousand years (Faust et al., 2016; Olsen et al., 2012; A. C. Smith et al., 2016; Trouet et al., 2009).

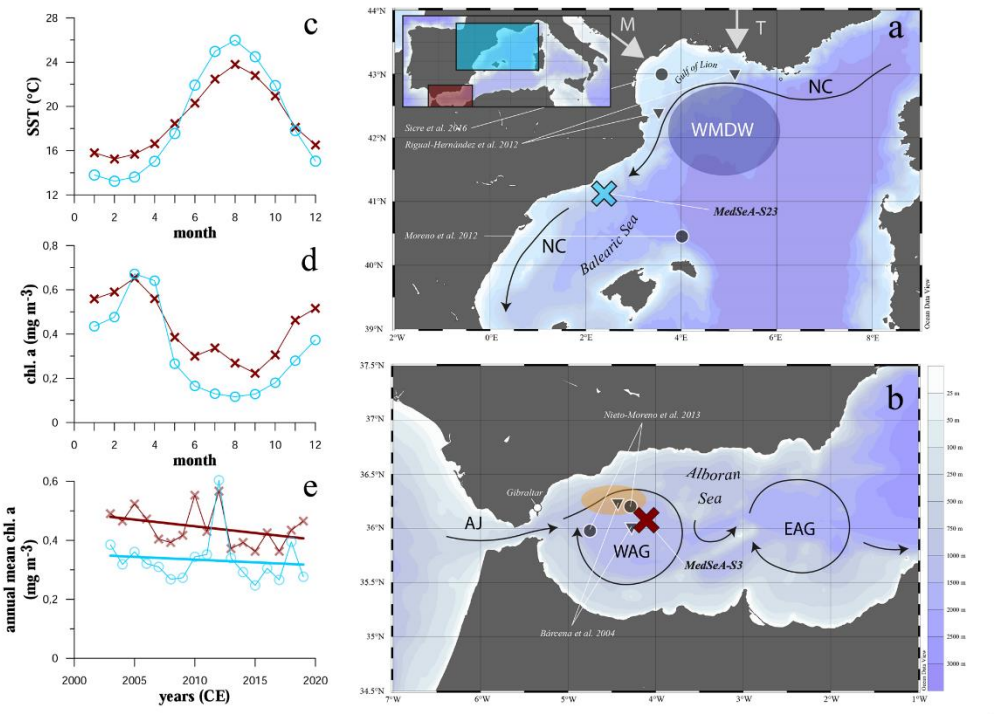

Figure 2.1: *Locations of the study areas in the western Mediterranean Sea, bathymetry, hydrography, SST, and chlorophyll-a data. (a-b) Ocean Data View (ODV) bathymetric maps (Schlitzer, 2019). Dark arrows represent surface currents and gyres. (a) Station MedSeA-S23 in the Balearic Sea. Core location indicated by a blue cross. NC: Northern Current (surface). WMDW: Western Mediterranean Deep Water formation. M: Mistral. T: Tramontana. (b) Station MedSeA-S3 in the Alboran Sea. Core location indicated by a red cross. AJ: Atlantic Jet (surface). WAG: Western Alboran Gyre. EAG: Eastern Alboran Gyre. Upwelling area (orange). References of studies close to core location cited in text. (c) Monthly sea surface temperature (SST), (d) Monthly surface chlorophyll-a concentration (e) annual mean chlorophyll-a concentration from 2003 to 2019 CE at the Balearic (blue open circles) and Alboran Sea (red crosses) core site. Linear fit for both time series indicated by blue (Balearic Sea) and red (Alboran Sea) line. Data is retrieved from AQUA-Modis, Level 3 sensor, covers the period from July 2002 to February 2020, and is centered at the exact core location, covering 16 km^2.*

The AMO is a climate cycle varying on multidecadal to -centennial timescales, which affects SST of the North Atlantic Ocean. SST changes vary with an amplitude of 0.4 °C at their extremes on a 65-80 year cycle (Enfield et al., 2001; Schlesinger & Ramankutty, 1994). The AMO has a strong connection to SST changes in the western Mediterranean Sea. SSTs in the Mediterranean region exhibit a 70 year cyclicity, which is similar to the AMO variability, when looking at instrumental data (Marullo et al., 2011).

Each study site shows a characteristic hydrography, influenced by the previously described large-scale atmospheric patterns. As an end-member of the Mediterranean Atlantic Water (MAW) flowing through the Tyrrhenian Sea, the Northern Current (NC) connects the Gulf of Lion with the study area in the Balearic Sea (Millot, 1999). Primarily in the Gulf of Lion, Western Mediterranean Deep Water (WMDW) is formed through two oceanographic processes described as dense shelf water cascading and open-sea deep convection mainly in January to February due to cold air masses (Canals et al., 2006; Rohling et al., 2009). Cold, orographically channeled air from the northern European continent is causing strong evaporation and surface water cooling and results in buoyancy loss in the Gulf of Lion, thus affecting deep water formation (Medoc, 1970; Mertens & Schott, 1998; R. O. Smith et al., 2008). Interannual variabilities between cold and dry or warm and wet air masses have been detected and linked to the winter state of the NAO (Ausín et al., 2015; Cisneros et al., 2019; Josey et al., 2011; Vignudelli et al., 1999).

The hydrography of the Alboran Sea is mainly characterized by two anticyclonic, quasi-permanent gyres, the Western Alboran Gyre (WAG) and the Eastern Alboran Gyre (EAG) both spanning around 100 km in diameter (Gascard & Richez, 1985; Heburn & La Violette, 1990). Driven by the strength of the Atlantic Jet (AJ) (Bormans & Garrett, 1989; Flexas et al., 2006), the Alboran gyre system is characterized by a complex mesoscale variability and can vary between a one gyre (1G), two gyre (2G) or three gyre (3G) system (Peliz et al., 2013; Renault et al., 2012; Vargas-Yáñez et al., 2002). Variations in the Mediterranean Thermohaline Circulation (MTHC) during winter months force surface net water flux into the Mediterranean Sea through the

Strait of Gibraltar (SoG), to compensate for water masses transported to the interior during deep water formation. The MTHC is the main mechanism controlling velocity and direction of the AJ, whereas local wind forcing and sea level pressure are playing a minor role (Macías et al., 2016). Upwelling in the region is controlled by winds and direction and velocity of the AJ (Macías et al., 2008; Macías et al., 2007; Sarhan et al., 2000). A strong AJ located northwards along the Spanish coast and prevailing westerlies cause coastal upwelling and result in highly fertile, nutrient rich surface water. Weak Atlantic water inflow and presence of easterlies induces a southward shift of the AJ, moving the upwelling area further offshore and generating less fertile surface water conditions in the northwestern Alboran region (Fig. 2.1b).

2.2.2 SST and surface productivity at the two study sites

Satellite-derived data from 2003 to 2019 (AQUA-Modis, Level 3) shows with 18.8 °C (Balearic Sea) and 18.9 °C (Alboran Sea) an almost equal mean annual SST at both study sites, whereas higher mean annual chlorophyll-a concentrations of 0.44 mg m^{-3} at the Alboran core station, compared to 0.33 mg m^{-3} in the Balearic Sea site, confirm the Alboran Sea to be a high productivity area (NASA Goddard Space Flight Center, 2020). The Balearic Sea is characterized by lower productivity levels compared to the Alboran Sea, but is still one of the high productivity regions in the Mediterranean Sea (Colella et al., 2003; Stambler, 2014). As shown in Figure 2.1c, seasonal SST variations in the Balearic Sea (August: 26.0 °C; February: 13.2 °C) have a higher amplitude compared to the Alboran Sea (August: 23.7 °C; February: 15.2 °C). In the Balearic Sea, SSTs are mainly controlled by warm summer and cold winter airflow, coming from the European continent, whereas cold Atlantic water inflow influences SST at the Alboran study site.

With highest productivity in March (0.64 mg m^{-3}) and lowest values in August (0.12 mg m^{-3}), primary production is driven by the annual cycle of the thermal structure of the water column in the northwestern Mediterranean. High summer SSTs cause a strong stratification of the water column, impeding vertical advection of nutrients to the surface causing oligotrophic conditions. Cold katabatic winds during winter enhance deep mixing and surface nutrient supply, which leads to high primary

production by late winter to early spring, amplified by higher solar radiation. Interannual variabilities between cold and dry or warm and wet air masses influencing the deep water formation in the Gulf of Lion through buoyancy loss, have been detected and linked to the winter state of the NAO (Cisneros et al., 2019; Josey et al., 2011; Vignudelli et al., 1999). At the Alboran core station, highest chlorophyll-a concentrations occur in March (0.66 mg m^{-3}) and lowest ones in August (0.22 mg m^{-3}). High primary productivity levels are the consequence of fresh nutrient rich upwelled water at the northern Alboran Sea (Bárcena & Abrantes, 1998; Bárcena et al., 2004; Garcia-Gorriz & Carr, 2001), the local occurrence of which is highly dependent on the hydrography of the WAG system.

2.3 Material and Methods

2.3.1 Material

The study is based on high resolution multicore records (MedSeA-S3-c1; MedSeA-S23-c1; MedSeA-S23-c3), collected at two sites of the western Mediterranean Sea with a MC400-Multicorer system during the MedSeA cruise (Mediterranean Sea Acidification in a changing climate) on 2 May to 2 June 2013 onboard the R/V Àngeles Alvariño. Core MedSeA-S3-c1 was retrieved in the Alboran basin (Lat. 36.0746° N, Long. 04.11040° W) at a water depth of 1137 m, with a core length of 33 cm. Cores MedSeA-S23-c1 and MedSeA-S23-c3 were recovered at a water depth of 1156 m in the Balearic basin offshore Barcelona (Lat. 41.1121° N, Long. 2.38200° E) with core lengths of 43 cm. MedSeA-S23-c3 was sliced onboard every cm, whereas MedSeA-S23-c1 was processed after the cruise and sliced every 0.5 cm.

2.3.2 Radiocarbon and radionuclides analysis

Determination of total ^{210}Pb activities was accomplished through the measurement of its alpha-emitter daughter nuclide ^{210}Po, following the methodology described in Sánchez-Cabeza et al. (1998) at the Autonomous University of Barcelona. After addition of ^{209}Po as an internal tracer, sample aliquots of 200–300 mg were totally digested in acid media by using an analytical microwave oven and Po isotopes plated on silver discs in HCl 1N at 70 °C while stirring for 8 h. Po emissions were subsequently counted using α-spectrometers equipped with low-background silicon

surface barrier (SSB) detectors (EG&G Ortec) for $4x10^5$ seconds. The concentrations of excess ^{210}Pb used to obtain the age models were determined as the difference between total ^{210}Pb and the uniform ^{210}Pb at depth. Maximum mean sediment accumulation rates and therefore the age-depth model over the last decades / century was estimated using the Constant Flux : Constant Sedimentation (CF:CS) model (Krishnaswamy et al., 1971; Robbins, 1978).

Radiocarbon dating (^{14}C) was performed on the lower part of cores MedSeA-S3-c1 and MedSeA-S23-c1. Planktic foraminifera (*Globorotalia inflata*) isolated from the 250 – 315 µm fraction from two different depths (MedSeA-S3-c1: 15-16 cm, 30-31 cm and MedSeA-S23-c1: 19.0-19.5cm, 39.0-39.5 cm) were used for radiocarbon dating. Analysis was performed by using accelerator mass spectrometry (AMS) at the NOSAMS facility at Woods Hole Oceanographic Institution (Volkman et al., 1995). Taking the marine radiocarbon reservoir effect into account, with an offset of 400 years (Siani et al., 2000), radiocarbon ages were calibrated to calendar ages by using Marine13 calibration curve (Reimer et al., 2013) where ages were reported with a 2σ uncertainty. The age-depth models of the sediment records were obtained by combining the surficial age models obtained from the ^{210}Pb activity-depth profiles with the ages obtained using the ^{14}C technique from planktic foraminifera from sections 15.5 cm to 30.5 cm (MedSeA-S3-c1) and 19.25 cm to 39.25 cm (MedSeA-S23-c1) (Appleby & Oldfield, 1992; Bradley, 2015a).

The age-depth models for the entire sediment cores in the Alboran and the Balearic Seas were calculated considering both ^{14}C dates and the ages from the 20th century reported by the ^{210}Pb age model (up to 5.5 cm core depth of MedSeA-S3-c1, up to 11.5 cm core depth of MedSeA-S23-c1 and MedSeA-S23-c3) and using Bayesian statistics applied by the R-code package “rbacon” (Blaauw & Christen, 2011) shown in Figures S2.1, S2.3 and S2.4.

2.3.3 Biomarkers

Alkenones (heptatriaconta-8E,15E,22E-trie2-one and heptatriaconta-15E,22E-die2-one) of core MedSeA-S3-c1 and MedSeA-S23-c3 were extracted from sediments, purified using organic solvents and quantified with a Varian gas chromatograph

Model 450 equipped with a septum programmable injector, flame ionization detector and a CPSIL-5 CB column (coated with 100% dimethyl siloxane; film thickness of 0.12 µm; L(m) * ID(mm) * OD(mm): 50 * 0.32 * 0.45). Hydrogen was the carrier gas (2.5 mL min^{-1}). Concentrations were determined using n-hexatriacontane ($CH_3(CH_2)_{34}CH_3$) as an internal standard. Absolute concentration errors were below 10% (resolution between the alkenones from 1.5 to 1.7). Reproducibility tests showed that uncertainty in the $U^{k'}_{37}$ determinations was lower than 0.015 (ca. 0.5 ºC) (Cacho et al., 1999; Martrat et al., 2004; Martrat et al., 2014; this study), confirming the precision of this paleothermometry tool (Eglinton et al., 2001). SST reconstructions are based on the global calibration of Conte et al. (2006), estimating the standard error on surface sediments at 1.1 °C.

2.3.4 Planktic foraminifera

2.3.4.1 Taxonomic concept

Analysis of planktic foraminiferal tests was performed on cores MedSeA-S3-c1 and MedSeA-S23-c1. The five morphospecies *Globigerinoides ruber* (d'Orbigny 1839), *Globigerina bulloides* (d'Orbigny 1826), *Globorotalia inflata* (d'Orbigny 1839), *Globorotalia truncatulinoides* (d'Orbigny 1839), and *Orbulina universa* (d'Orbigny 1839) were isolated. Classification of the different foraminiferal species was carried out by visual identification using a binocular stereo microscope (magnification 10× - 20×) and a bifurcated illuminator. Taxonomic identification of the target species was based on Schiebel and Hemleben (2017). The white (*G. ruber*$_{WHITE}$) and pink (*G. ruber*$_{PINK}$) varieties were collected separately. A distinction between the two morphotypes of *G. ruber*$_{WHITE}$, *G. ruber* sensu lato (*G. ruber*$_{SL}$) and *G. ruber* sensu stricto (*G. ruber*$_{SS}$) was made, based on differences in test morphology (Kontakiotis et al., 2017; Numberger et al., 2009; L. Wang, 2000).

2.3.4.2 Analyzed size fraction

Bulk sediment mass was obtained after drying samples at 60 °C for approximately 24 hours. Samples were washed over a 63 µm screen using distilled Elix water. The size fraction larger than 63 µm was oven dried at 60 °C for 1 - 2 hours. Samples were dry sieved and divided by a Riffle Splitter at the chosen size fractions, 150-250, 250-315

and > 315 µm. Results are presented and discussed for > 150 µm size fraction. More than 300 specimens were identified in the > 150 µm size fraction in all samples.

The standard > 150 µm analysis for planktic foraminifera analysis in the oceans is a legacy of the CLIMAP project (CLIMAP Project Members et al., 1984), mainly aimed at reconstructing SST variations in the oceans over glacial-interglacial cycles and benefits from a huge modern reference database (Schmidt et al., 2004). This fraction is commonly used by Mediterranean specialists even if some species would be underrepresented, among others *Turborotalita quinqueloba*, an important proxy for surface productivity during glacials (Capotondi et al., 2004; Di Donato et al., 2015; Sprovieri et al., 2003). The number of total planktic foraminiferal shells and their total accumulation rate was evaluated on the > 150 µm size fraction.

2.3.5 Coccolithophore sedimentary record

Analysis of relative abundance of calcareous nannoplankton assemblages (coccolithophores) was done on core MedSeA-S3-c1. Following standard procedures in Bown and Young (1998) smear slides of each sample (<63 µm) were prepared and analyzed by a polarized microscope (x 1000 magnification). Considering around 20 taxonomic units, at least 500 specimens were counted and identified by taxonomic concepts of extant coccolithophores (Young et al., 2003).

2.4 Results

2.4.1 Age Model

Concentrations of $^{210}Pb_{tot}$ and $^{210}Pb_{xs}$ with depth in the sediment records are shown in Figures S2.1, S2.3 and S2.4. $^{210}Pb_{tot}$ activity of the 3 analyzed cores is decreasing from the surface, reaching a constant average value ($^{210}Pb_{sup}$) of ~31 ± 2 Bq kg^{-1} at ~12.5 cm depth (MedSeA-S3-c1), ~35 ± 3 Bq kg^{-1} at ~20.5 cm depth (MedSeA-S23-c1) and ~33 ± 2 Bq kg^{-1} at ~18.5cm depth (MedSeA-S23-c3). Applying the CF:CS model the maximum mean mass accumulation rate (MAR) is 0.047 ± 0.002 g cm^{-2} yr^{-1} (MedSeA-S3-c1), 0.105 ± 0.008 g cm^{-2} yr^{-1} (MedSeA-S23-c1), and 0.110 ± 0.004 g cm^{-2} yr^{-1} (MedSeA-S23-c3). Combining the calculated ^{210}Pb ages for the upper core parts (first 5.5 cm and 11.5 cm for cores MedSeA-S3-c1 and MedSeA-S23-c1,

respectively) with calibrated ^{14}C ages at depth 15.5 cm (1297 yr CE, 2σ cal 1257 – 1337 yr CE) and 30.5 cm (433 yr CE, 2σ cal 358 – 534 yr CE) of core MedSeA-S3-c1, and at depth 19.25 cm (1481 yr CE, 2σ cal 1442 – 1529 yr CE) and 39.25 cm (1050 yr CE, 2σ cal 992 – 1140 yr CE) of core MedSeA-S23-c1, through Bayesian modelling approach, an age depth model was calculated. The mean sedimentation rate (SR) is 33.45 cm kyr^{-1} (MedSeA-S3-c1), 50.60 cm kyr^{-1} (MedSeA-S23-c1), and 53.79 cm kyr^{-1} (MedSeA-S23-c3) (Table S2.1).

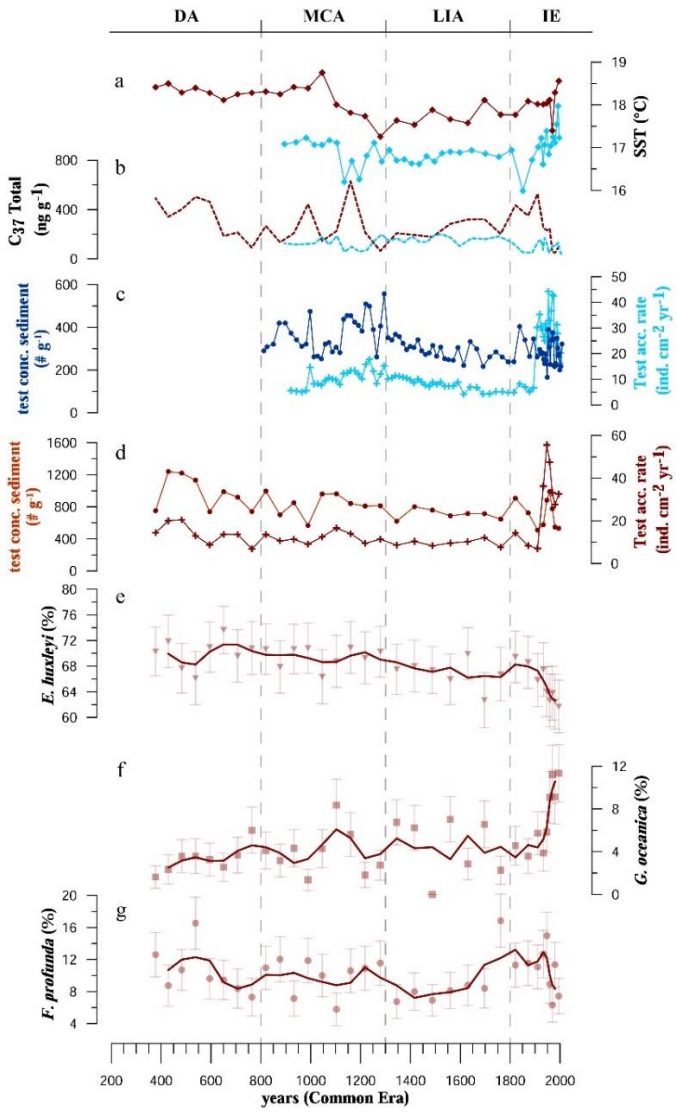

Figure 2.2: *Downcore variations of SST, surface production of calcareous organisms and relative abundances of calcareous nannoplankton taxa during the Common Era in the Alboran (red) and Balearic*

cores (blue). (a) Alkenone (Uk'37) derived SSTs. (b) Alkenone concentration of total C37. (c-d) Test accumulation rates and test concentrations per gram sediment in Balearic and Alboran cores. (e-g) Red symbols show percentage values of calcareous nannoplankton species, with 95% confidence interval of the counts indicated by the error bars. Red lines show 3-pt running average of calcareous nannoplankton species data. Duration of the Dark Age (DA), Medieval Climate Anomaly (MCA), Little Ice Age (LIA) and Industrial Era (IE) is based on estimates by Nieto-Moreno et al. (2011).

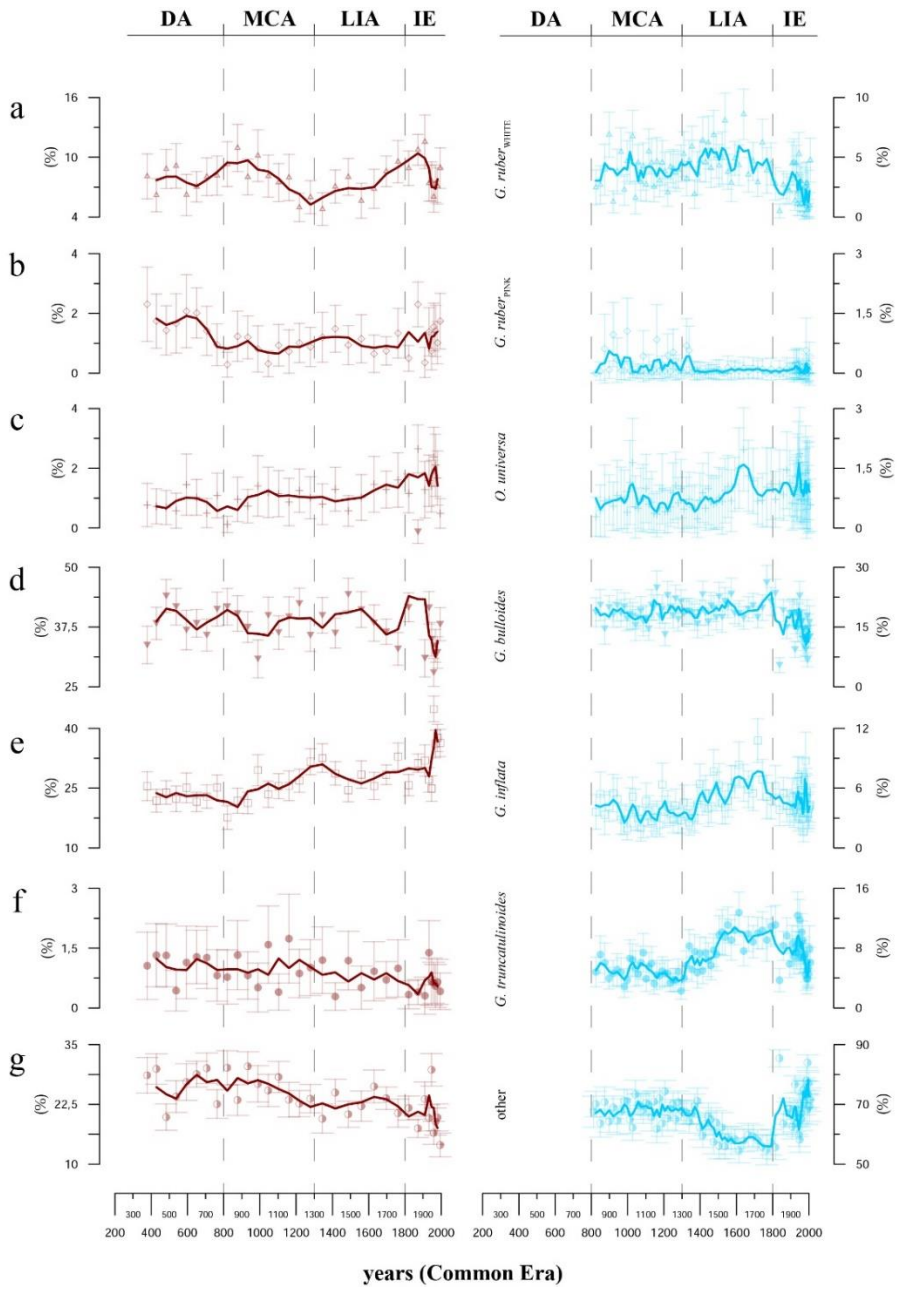

Figure 2.3: *Downcore variations of relative planktic foraminiferal species abundances (a-g) during the Common Era in the Alboran (red) and Balearic cores (blue). Symbols show percentage values of planktic*

foraminiferal species with 95% confidence interval of the counts indicated by the error bars. Solid lines indicate 3-pt running average of >150 µm size fraction of planktic foraminiferal species. Duration of the Dark Age (DA), Medieval Climate Anomaly (MCA), Little Ice Age (LIA) and Industrial Era (IE) is based on estimates by Nieto-Moreno et al. (2011)

2.4.2 Absolute changes in reconstructed SST

Data on SST and alkenone concentration of both records is summarized in Figure 2.2 and Data Set S2.4 & S2.5 (Supplementary Information). In the Balearic Sea record, SST ranged between 16.0 °C to 18.0 °C, with slightly higher SST during the MCA (17.0 °C; 895 – 1135 CE) than during the LIA (16.8 °C; 1135 -1755 CE). An SST drop to ~16.2 °C is detected between 1135 CE and 1195 CE, and to 16.0 °C around 1851 CE. The 20th century is marked by an SST increase of almost 2 °C. SST recorded in the Alboran Sea is ranging between 18.8 °C and 17.3 °C. Differences between MCA (18.4 °C; 378 – 1046 CE) and LIA (17.7 °C; 1103 – 1762 CE) are more pronounced than in the Balearic Sea. Two minimums of SST are detected at the end of the 13th century (17.3 °C) and at the end of the 1960s CE (17.4 °C). An SST warming is detected from the 1970s of up to 18.6 °C.

2.4.3 Planktic foraminiferal species abundance

Even though the time interval under investigation is comparably short, assuming little changes in climatological and oceanographic conditions, some species reveal large abundance variations and trends at both study sites, beyond the 95% confidence level errors related with counting (Fig. 2.3, Data Set S2.1 & S2.2).

In the Balearic Sea record, *G. bulloides* is the dominant target species (5.4-26.2%, on average 17.6%) followed by *G. truncatulinoides* (2.3-12.7%, on average 6.7%), *G. inflata* (1.6-10.8%, on average 4.6%) and *G. ruber*$_{\mathrm{WHITE}}$ (0.2-8.6%, on average 3.6%). The Alboran Sea record reveals *G. bulloides* (28.0-57.4%, on average 38.2%) and *G. inflata* (17.6-44.9%, on average 27.5%) as the two dominant species, followed by *G. ruber*$_{\mathrm{WHITE}}$ (4.8-11.5%, on average 7.9%). In both Balearic and Alboran records, the morphospecies *G. ruber*$_{\mathrm{SL}}$ (0.1-8.0% and 3.6-9.1%, on average 3.2% and 5.9%, respectively), which occurs mainly as “platys” and elongate morphotypes, dominates over *G. ruber*$_{\mathrm{SS}}$ (0-2.1% and 0.6-3.7%, on average 0.4% and 2.0%, respectively). Other selected species are less abundant on average (< 2%). Noteworthy, *G. bulloides*,

G. inflata and *G. truncatulinoides* show abundance fluctuations of opposite signs at their core locations over some time intervals, but also between study sites (Fig. 2.3). Due to their low relative abundances, variations in *G. ruber*$_{SS}$, *G. ruber*$_{PINK}$ and *O. universa* are not statistically significant. Only the morphospecies *G. ruber*$_{SL}$ displays significant abundance changes in both records at the Balearic Sea site during the Common Era.

To display modern planktic foraminiferal productivity during the last 30 years, the annual mean test accumulation rates for core top samples representing the time period between 1980 to 2013 CE were calculated, showing higher rates in the Alboran (30.1 ind. cm^{-2} yr^{-1}) than in the Balearic (22.5 ind. cm^{-2} yr^{-1}) record. In both cores, the gradual increase of test accumulation rates occurs within radionuclide dating. The rates of test flux per gram of sediment and the standardized test accumulation rates show accelerated declines during the 20th century at both study areas.

2.4.4 Calcareous nannoplankton species composition

Calcareous nannofossils are well preserved, indicating absence of significant dissolution phenomena. The entire assemblage of counted and identified species is available in Data Set S2.3 (Supplementary Information). Taxa do not show any significant abundance variation throughout the record, except for *Emiliania huxleyi*, *Gephyrocapsa oceanica* and *Florisphaera profunda* since the 20th century (Fig. 2.2). Most strikingly, relative abundances of *G. oceanica* triple over the past 100 years in the Alboran core and *E. huxleyi* and *F. profunda* show a continuous and gradual decrease.

2.5 Discussion

2.5.1 Age Model

Age depth-models calculated for both study sites are in good agreement with results from other studies obtained nearby (Cisneros et al., 2016; Frigola et al., 2007; Masqué et al., 2003; Moreno et al., 2012; Puig et al., 2015), further discussed in the Supplementary Information (Text S2.2). There is a rapid change in sedimentation rate from the upper (oldest ^{210}Pb date; MedSeA-S3-c1: 1925 ±4 yr CE at 5.5 cm core depth;

MedSeA-S23-c1: 1922 -8 +7 yr CE at 11.5 cm; MedSeA-S23-c3: 1926 ±7 yr CE at 11.5 cm) to the lower core section (youngest ^{14}C date; MedSeA-S3-c1: 1297 -45 +40 yr CE at 15.50 cm core depth; MedSeA-S23-c1: 1481 -39 +48 yr CE at 19.25 cm), which we attribute to changes in sediment consolidation. Due to higher overburden, deeper parts of the core experience a higher consolidation leading to lower sedimentation rates, whereas unconsolidated top core sediments have a very high sedimentation rate. Due to the lack of a high-resolution age control, sedimentation rate changes because of poor consolidation are detected by abrupt changes in our age models. Rapid changes in sedimentation rates between core parts based on high resolution ^{210}Pb dates and low resolution ^{14}C dating are also reported in other studies (Cisneros et al., 2016; Margaritelli et al., 2020a). By increasing the numbers of ^{14}C datings below the unconsolidated core part, the distortion would be partly removed, as can be seen in the study of Sicre et al. (2016). Abrupt changes in sedimentation rates may be influenced by uncertainties when measuring ^{14}C and ^{210}Pb activity, like differences in reservoir ages in seawater (Alves et al., 2018; Ascough et al., 2005; Philippsen, 2013; Siani et al., 2000; Struglia et al., 2004), carbonate tests (Barker et al., 2007; Waelbroeck et al., 2001) or vertical lead diffusion and mixing (Mekik, 2014; Nittrouer et al., 1984), which is further discussed in Supplementary Information (Text S2.2).

The poor detection of changing sedimentation rates due to sediment consolidation behavior and the uncertainties occurring when combining ^{210}Pb and ^{14}C dating techniques, are both influencing parameters which are dependent on sedimentation rate. As a result, test accumulation rates seem to be overestimated in the upper (dataset based on ^{210}Pb dating) and underestimated in the lower core part (dataset based on ^{14}C dating), causing an anomalous increase at the beginning of the 20th century (Fig. 2.2). Through standardization of both datasets, setting variation on the same scale, not the amplitude of varying test accumulation rates, but the slope between the two datasets becomes comparable. Despite the above mentioned difficulties when combining age models derived from ^{210}Pb and ^{14}C dating results, to obtain high resolution age control, we reconstructed a robust age-depth model, supported by changing parameters independent from sedimentation rate, like relative abundance of principal planktic

foraminiferal species (see 5.3.3), and alkenone-derived SST (see 5.2), which coincide with main environmental changes recorded independently.

2.5.2 SST changes over the past 1600 years

$U^{k'}_{37}$ SST estimates show good accordance in comparison to instrumental measurements (HadISST & Kaplan SST V2 data) and paleorecords (Fig. 2.4). With values ranging between 16-18 °C at the Balearic and 17-19 °C at the Alboran core site, they are generally consistent with other late Holocene $U^{k'}_{37}$ SST estimates (Cacho et al., 1999; Martrat et al., 2014; Schirrmacher et al., 2019; Sicre et al., 2016), displaying modern annual mean temperature differences at the study regions (Fig. 2.1c). Lower paleotemperatures (14-16 °C) estimated by Moreno et al. (2012) for the northwestern Mediterranean, can be explained by effects on the sedimentary alkenone signal through variability in surface production and/or differential degradation of 37:3 and 37:2 alkenones. When corrected, as done by Sicre et al. (2016) using the temperature calibration of Conte et al. (2006), SSTs coincide with estimates from our study. Alboran SST estimates are slightly lower compared to values (18.5-20 °C) obtained by Nieto-Moreno et al. (2013), but are still inside the lower range for autumn and average annual SSTs in the Alboran basin during the Holocene (Cacho et al., 1999; Pérez-Folgado et al., 2003). The core location in the Alboran Sea has a strong Atlantic influence, whereas the study area in the Balearic Sea is in close vicinity to the deep-water mass formation area, known for strong winter convection (Rohling et al., 2009; Skliris et al., 2012). Even though both areas are influenced by different meteorological and oceanographic conditions, they display similar SST trends. This suggests that both study sites are under the influence of larger-scale processes.

The prolonged pre-industrial cooling trend throughout the MCA and LIA is consistent with regional (Europe, Mediterranean Sea, and North Atlantic Ocean) and global ocean cooling from 0 CE to 1800 CE (McGregor et al., 2015). The sedimentary records reported here are in phase with climatic oscillations during the past millennium describing warmer SSTs during the MCA compared to the LIA (Lüning et al., 2019; Mann et al., 2009). Taking into account age error uncertainties, both records describe a ~ 1.0 °C cooling during the MCA-LIA transition between 1100 to

1300 CE, synchronous with the 1257 CE eruption event (Crowley & Unterman, 2013), which is associated with the onset of the LIA. The marked temperature drop below 16 °C at the Balearic core site at approximately 1851 -89 +51 yr CE could be related to the 1809 CE 'unknown' and the 1815 CE Tambora volcanic eruptions, as recorded in northeastern Mediterranean marine records (Gogou et al., 2016), marking the terminal point for the long-term cooling trend during the pre-industrial Common Era, followed by warming in the last two centuries.

With increasing SSTs starting in the 19th century, and accelerated sea surface warming during the 20th century, both cores display the temperature signal, already recorded in the Balearic (Sicre et al., 2016) and Alboran Sea (Nieto-Moreno et al., 2013), affirming pronounced 20th century warming in the western Mediterranean Sea (Lionello et al., 2006; Skliris et al., 2012; Vargas-Yáñez et al., 2010). The absence of a 20th century warming signal in cores collected at the Minorca contourite (Moreno et al., 2012) can be ascribed to a lack of age control over the past 500 years and age model extrapolation in the upper core part. Figure 2.4 shows in detail SST reconstruction in the Balearic and Alboran Sea, compared to instrumental annual mean data estimated at core locations retrieved from temperature time series average over a 5° × 5° grid from Kaplan SST V2 data and the Hadley Centre Sea Ice and Sea Surface Temperature data set (HadISST) (Kaplan et al., 1998; Rayner et al., 2003; Reynolds & Smith, 1994). Industrial SST warming starting around 1850 CE is well captured by both instrumental and proxy data, describing the two phase warming of the western Mediterranean (Lionello et al., 2006), and importantly the exact moment of warming emergence under anthropogenic pressure in most of sites globally (Abram et al., 2016). SST rise during the last two centuries is more pronounced in the Balearic (2.0 °C) than in the Alboran record (0.8 °C), accelerating during the 20th century with an SST increase of more than 1°C at both study sites. This is in good agreement with satellite-derived mean annual warming rate of 0.026 °C yr^{-1} for the western Mediterranean basin during that period (Skliris et al., 2012).

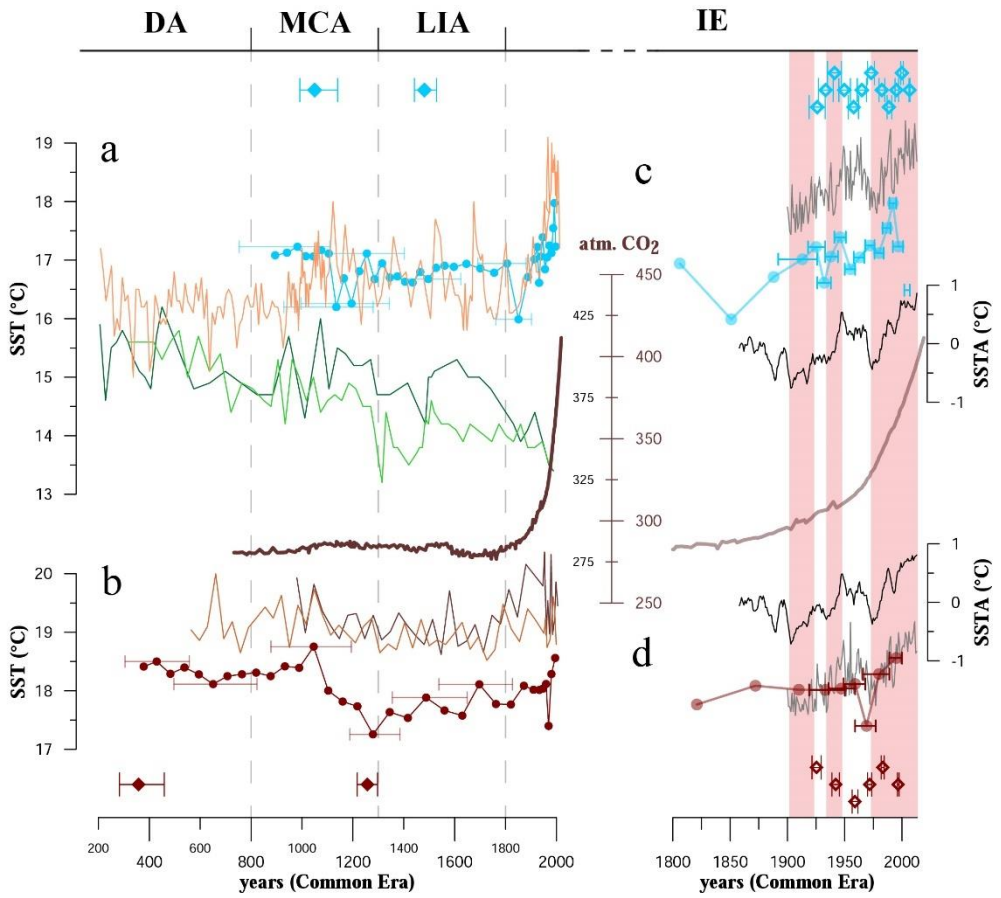

Figure 2.4: *SST records from the Balearic and Alboran Seas in comparison with nearby paleorecords and instrumental measurements with a focus on the Industrial Era. (a) Alkenone derived SST in Balearic core (blue circles). Paleotemperature records of other studies conducted in vicinity of the Balearic study site: light and dark green lines (Moreno et al., 2012); orange line (Sicre et al., 2016). (b) Alkenone derived SST in Alboran core (red circles). Paleotemperature records of other studies conducted in vicinity of the Alboran study site: light and dark brown (Nieto-Moreno et al., 2013). Industrial SST warming at the Balearic (c) and the Alboran (d) study site. Annual SST and standardized SST anomaly (SSTA), respectively, obtained through instrumental data: grey line (HadISST) and dark line (Kaplan v2) (Kaplan et al., 1998; Rayner et al., 2003; Reynolds & Smith, 1994). Red bands indicate SST warming phases derived from Kaplan and HadISST data. Blue and red circles, respectively, show alkenone derived SST in Balearic and Alboran core. Brown line shows atmospheric CO2 concentrations measured (Tans & Keeling, 2020) and reconstructed (Friedli et al., 1986). Filled and open diamonds represent 14C dates and 210Pb dates used as tie-points for age-depth model reconstruction, respectively, color coded by the corresponding core color (Alboran = red; Balearic = blue), including their associated 2σ errors. Duration of the Dark Age (DA), Medieval Climate Anomaly (MCA), Little Ice Age (LIA) and Industrial Era (IE) is based on estimates by (Nieto-Moreno et al., 2011).*

2.5.3 Planktic foraminifera

2.5.3.1 Total planktic foraminiferal production

Modern mean test accumulation rates are calculated for 1980 CE to 2013 CE to provide an average value for planktic foraminiferal productivity and to make our results comparable to previous studies conducted during the last 30 years (Bárcena et al., 2004; Mallo et al., 2017; Pujol & Grazzini, 1995; Rigual-Hernández et al., 2012). Modern mean test accumulation rates are higher at the Alboran (30.1 ind. cm^{-2} yr^{-1}) than in the Balearic (22.5 ind. cm^{-2} yr^{-1}) core site. Our findings are in accordance with results from sediment traps, deployed at water depths between 1000 and 2000 m showing that 28.6 to 35.5 ind. cm^{-2} yr^{-1} in the western Alboran Sea (Bárcena et al., 2004; Hernández-Almeida et al., 2011) and 8.2 to 15.0 ind. cm^{-2} yr^{-1} in the northwestern Mediterranean Sea (Rigual-Hernández et al., 2012), displaying different trophic conditions at the two study sites. Due to nutrient rich upwelling at the northern edge of the WAG (Fig. 2.1b), the Alboran Sea is one of the most productive marine regions in the Mediterranean (Garcia-Gorriz & Carr, 2001). The Balearic Sea is characterized by lower productivity, even if the highly dynamic character of the region with strong frontal activity (La Violette, 1990) still makes it a more productive region in the rather oligotrophic Mediterranean Sea (Stambler, 2014). Annual average chlorophyll-a values (Fig. 2.1e) derived from satellite images during the last decades show higher values in the Alboran than in the Balearic study area and support the hypothesis of a positive correlation between primary production and planktic foraminiferal standing stocks, as phytoplankton serve planktic foraminifera as a major food source (Hemleben et al., 1989; Schiebel & Hemleben, 2005).

Foraminiferal accumulation rates in the core top samples of our study were comparable to the export fluxes estimated in sediment traps (Bárcena et al., 2004; Rigual-Hernández et al., 2012) from the western Mediterranean, supporting high consistency from sinking to accumulation in the sediment bed. In addition, the high carbonate saturation horizon throughout the water column in the Mediterranean Sea, suggest carbonate dissolution being unlikely (Millero et al., 1979; A. Schneider et al., 2007).

2.5.3.2 Planktic foraminiferal assemblage composition

Planktic foraminiferal core top assemblages in the Balearic and Alboran Sea are in good agreement with recent sediment trap, plankton tow, and core top studies conducted nearby (Bárcena et al., 2004; Hernández-Almeida et al., 2011; Mallo et al., 2017; Pujol & Grazzini, 1995; Rigual-Hernández et al., 2012; Thunell, 1978). In the northwestern Mediterranean, *G. ruber*$_{\text{WHITE}}$ (including the two morphotypes), *G. ruber*$_{\text{PINK}}$ and *O. universa* are part of the summer assemblage associated with low surface productivity. *Globigerina bulloides*, *G. truncatulinoides*, and *G. inflata* are dominant from winter to spring, when cold temperatures driving winter-deep mixing and causing high surface chlorophyll-a concentrations, which stimulate planktic foraminiferal productivity and cause high export fluxes and high accumulation rates to the seafloor sediment (Rigual-Hernández et al., 2012). In the western Alboran Sea, *G. bulloides* is the dominant species during periods of high productivity in spring and fall, whereas *G. inflata* has highest relative abundances during winter and summer, characterized by stratification of the water column, reduced upwelling and less productive conditions (Bárcena et al., 2004; Kontakiotis et al., 2016).

The species composition is assumed to reflect the climatic and oceanographic differences at both study sites. *Globigerinoides ruber*$_{\text{WHITE}}$ is a surface dwelling, symbiont bearing warm water species (Bé & Tolderlund, 1971; Schiebel et al., 2002). Although it is a shallow dwelling species, it may occur at nutricline depths in less turbid oligotrophic waters (Pujol & Grazzini, 1995; Schiebel et al., 2004; Zarkogiannis et al., 2020). *Globigerinoides ruber*$_{\text{PINK}}$ seems to exhibit high sensitivity to changing SST, and to prosper only at maximum SSTs (Mallo et al., 2017). *Orbulina universa* has a high tolerance to temperature and salinity (Anderson et al., 1979; Bijma et al., 1990). As a symbiont bearing species, *O. universa* is restricted to the euphotic zone and occurs from temperate to tropical waters (Bemis et al., 2000; Hemleben et al., 1989), while in the Mediterranean Sea it proliferates by the end of summer (Pujol & Grazzini, 1995). *Globorotalia inflata* and *G. truncatulinoides* are subsurface-dwelling species, which favor mixed conditions and cool water temperatures (Hemleben et al., 1989; Pujol & Grazzini, 1995). In the Mediterranean, both species are indicators of eutrophic conditions with a deeply mixed winter ocean layer (Rigual-

Hernández et al., 2012; Rohling et al., 2004). *Globorotalia inflata* shows an opportunistic behavior in mesotrophic conditions (Chapman, 2010; Lončarić et al., 2007; Retailleau et al., 2011; Storz et al., 2009), and can be outnumbered by more opportunistic species such as *G. bulloides* in eutrophic environments. *Globigerina bulloides* thrives in high-productivity regions and is an indicator of upwelling intensity, responding to phytoplankton blooms and may outnumber species, which are adapted to less productive conditions (Conan et al., 2002; Schiebel et al., 2004; Thiede, 1975).

Higher percentages of warm water species *G. ruber*$_{SL}$ in the Alboran Sea might be explained by a narrower annual SST amplitude compared to the Balearic Sea (Fig. 2.1e), which favors the warm water species since SST is not falling below its specific temperature minimum limit of 14 °C (Bijma et al., 1990). Higher relative abundances of *G. truncatulinoides* in the Balearic Sea is of the same magnitude of those reported in the nearby Minorca Basin (Margaritelli et al., 2018). This abundance peak increases in coincidence of the Maunder Minimum event of the LIA, as in a wide portion of the central-western Mediterranean, and is due to the development of enhanced vertical mixing in winter (Margaritelli et al., 2020b). This interpretation is compatible with enhanced atmospheric circulation developed in close vicinity to the Gulf of Lion and its wind driven deep mixed conditions and/or a strong NC that may transport *G. truncatulinoides* to our study site (Fig. 2.1a). High relative abundances of *G. bulloides*, a species associated with periods of elevated primary productivity in the western Mediterranean Sea (Bárcena et al., 2004; Hernández-Almeida et al., 2011; Rigual-Hernández et al., 2012), demonstrate that the Balearic Sea is one of the most productive regions in the Mediterranean Sea (Stambler, 2014), although satellite data reveal that surface primary production may be even higher in the Alboran Basin (Fig. 2.1).

Great percentage values of non-target species in the Balearic Sea (Fig. 2.3g) are caused by high abundances of small sized species (150-250 μm; Dataset S1 & S2), dominated by *Neogloboquadrina incompta*. Its affinity to low-productive conditions with enhanced stratification of the surface water column (Schiebel & Hemleben,

2000) would explain the abundance pattern contrasting to the deep mixing indicator species *G. truncatulinoides*.

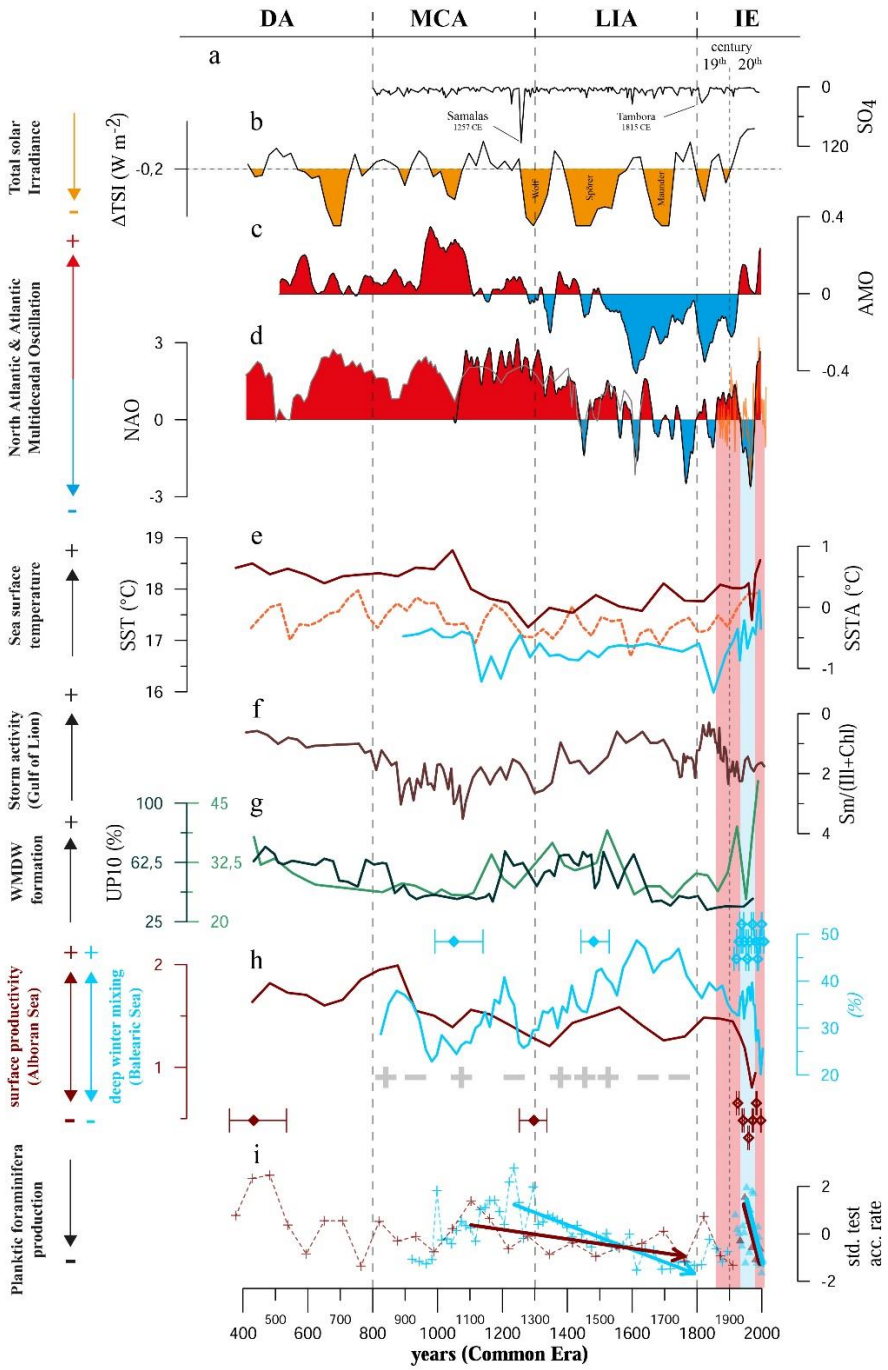

Figure 2.5: *Natural and anthropogenic forcing driving surface productivity and deep winter mixing in the western Mediterranean Sea during the Common Era expressed through planktic foraminiferal*

species composition and abundance changes. (a) Sulphate records in Antarctic and Greenland ice cores as a proxy for volcanic activity (Crowley & Unterman, 2013). (b) Total solar irradiance (TSI) based on ^{10}Be and ^{14}C data (Steinhilber et al., 2012; Steinhilber et al., 2009). Orange fillings indicate TSI periods below the mean (-0.2 W m^{-2}). (c) Reconstruction of Atlantic Multidecadal Oscillation (AMO) (Mann et al., 2009), expressed as 29 point moving average (dark line). (d) Reconstruction of North Atlantic Oscillation (NAO) through tree-ring and speleothem-based records (Trouet et al., 2009) expressed as 29 point moving average (dark line), lake sediment records as a grey line (Olsen et al., 2012) and instrumental data covering 1821 CE to 2013 CE (P. D. Jones et al., 1997) expressed as 5 point moving average (orange line). Positive and negative phases for NAO and AMO indices are highlighted as red and blue areas, above and below the mean. (e) Paleotemperature reconstruction for continental Europe as orange dashed line (Ahmed et al., 2013) and alkenone derived SST for Alboran (red) and Balearic (blue) cores. (f) Paleo storm activity in the Gulf of Lion (Sabatier et al., 2012). (g) Intensity of Western Mediterranean Deep-Water formation (WMDW), recorded through de-carbonated (green) and total (dark green) grain-size fraction (Cisneros et al., 2019). (h) Added relative abundance of G. inflata + G. truncatulinoides in the Balearic Sea (blue) as a proxy for deep winter mixing and G. bulloides versus G. inflata in the Alboran Sea (dark red) as a proxy for surface productivity. Grey plus and minus symbols indicate concurrent species composition changes at both study sites, related to (de-) and increasing phases of NAO modes on multidecadal time scales (i) Standardized total planktic foraminiferal test accumulation rate at the Alboran (red) and Balearic (blue) core sites: Crosses and dashed lines show values based on sedimentation rates rest upon ^{14}C dating. Triangles represent std. acc. rates based on sedimentation rates rest upon ^{210}Pb dating. Solid lines represent linear fit through LIA and ^{20}th century second half, respectively. Filled and open diamonds represent ^{14}C dates and ^{210}Pb dates used as tie-points for age-depth model reconstruction, respectively, color coded by the corresponding core color (Alboran = red; Balearic = blue), including their associated 2σ errors. Duration of the Dark Age (DA), Medieval Climate Anomaly (MCA), Little Ice Age (LIA) and Industrial Era (IE) is based on estimates by Nieto-Moreno et al. (2011).

2.5.3.3 Planktic foraminiferal response to natural versus anthropogenic drivers

External forcing, like variations in solar activity and the cooling effect of sulphate aerosols expelled into the atmosphere after volcanic eruptions, are thought to be main mechanisms driving climate during the last millennium (Crowley, 2000; McGregor et al., 2015). These drivers influence large scale atmospheric patterns like NAO and AMO (IPCC, 2014), which in turn are associated with changes in climate and oceanographic conditions. Synchronously, anthropogenic induced climate change is responsible for almost half of the 20th century warming (Macías et al., 2013). Figures 2.5 and 2.6 demonstrate how natural variability controls planktic foraminiferal species composition of the western Mediterranean Sea in pre-industrial times, whereas anthropogenic warming may lead to surface ocean productivity decline.

2.5.3.3.1 Natural Variability as a driver in pre-industrial times (TSI, AMO)

Decreasing solar activity revealed through increasing number and intensity of solar activity minima Maunder, Spörer and Wolf (Usoskin et al., 2016), and the more frequent occurrence of volcanic eruptions has led to a pronounced cooling since the MCA-LIA transition (Crowley & Unterman, 2013; McGregor et al., 2015).

Decreasing SSTs in the western Mediterranean are closely linked to negative AMO phases during the LIA (Lüning et al., 2019), affecting water column properties mainly during summer seasons (Marullo et al., 2011; O'Reilly et al., 2017), triggering changes in planktic foraminiferal assemblages (A. Incarbona et al., 2019). During the second phase of the LIA, relative abundances of *G. ruber*$_{\text{WHITE}}$ decrease from ~8.1% to ~0.5% in the Balearic core (Fig. 2.3a). The surface-dwelling species, favoring warm, stratified waters was probably disadvantaged by decreasing SSTs and intensified vertical mixing of the water column. As winter SSTs are quite low at present, warm times with a monthly mean of 13.2 °C in February (Fig. 2.1e), winter months are expected to be colder during the LIA, with SSTs falling below temperature tolerance of *G. ruber*$_{WHITE}$ (Bijma et al., 1990), affecting standing stocks of this species even in summer. The drop in *G. ruber*$_{WHITE}$ is synchronous with an abundance increase of *G. inflata* and *G. truncatulinoides* (Fig. 2.3), two species associated with deep-winter mixing in this region (Rigual-Hernández et al., 2012). Results are supported by former studies in the Tyrrhenian Sea with a positive response of deep dwelling species during minimum solar activity during the LIA (Lirer et al., 2014; Margaritelli et al., 2018; Margaritelli et al., 2020b; Margaritelli et al., 2016). Increasing abundances of the deep dwelling species might indicate more intense vertical mixing during winter months, delaying the spring bloom and shortening the growing season for *G. ruber*$_{WHITE}$. It is not clear if reduced light levels during solar activity minima have a direct negative impact on the symbiont bearing species, since the species uses dinoflagellates for photosymbiosis (Hemleben et al., 1989).

During the older part of the Alboran record, percentage values of the warm water species G. ruber$_{\text{WHITE}}$ are in phase with $U^{k'}_{37}$ SST estimates likely driven by variabilities in AMO (Fig. 2.5). As a main representative of the summer assemblage (Bárcena et al., 2004), proliferation of G. ruber$_{\text{WHITE}}$ is favored by higher SST during the DA, whereas lower temperatures throughout the MCA result in a relative abundance drop. A prevailing negative AMO during the LIA is not recorded in G. ruber$_{\text{WHITE}}$. Instead, it increases its stock continuously in line with $U^{k'}_{37}$ SST in the Alboran Sea.

2.5.3.3.2 Natural variability as a driver for planktic foraminiferal population dynamics in pre-industrial times (NAO)

Changes of climatologic and oceanographical conditions in the Mediterranean are closely linked to the boreal winter NAO index (Hurrell, 1995; Lionello et al., 2006; Nieto-Moreno et al., 2015; Schirrmacher et al., 2019; Tsimplis et al., 2013; Ulbrich et al., 2012), affecting phytoplankton and zooplankton communities through changes in ocean circulation and air-sea heat fluxes (Drinkwater et al., 2003), including plankton calcifier (Ausín et al., 2015; Bazzicalupo et al., 2020; Mojtahid et al., 2015). Long-term variability is displayed by planktic foraminiferal records, i.e. by ratios between indicators of eutrophic (*G. bulloides*) and deep-mixing (*G. inflata* and *G. truncatulinoides*) conditions, and the NAO and AMO (Fig. 2.5 & 2.6).

In the northwestern Mediterranean, *G. inflata* and *G. truncatulinoides* are associated with stronger winter mixing conditions (Rigual-Hernández et al., 2012). A relation between large scale atmospheric patterns and these species has been reported from the central Mediterranean Sea and is interpreted as changes in deep winter mixing (A. Incarbona et al., 2019). The flow of cold and dry air masses from continental regions into the western Mediterranean, which enhances heat loss and strengthens the NC circulation (Vignudelli et al., 1999), resulting in strong vertical mixing of water masses during WMDW formation in the Gulf of Lion during winter months (Medoc, 1970; Mertens & Schott, 1998; Rohling et al., 2009). Cold and dry northerlies and north-westerlies, better known under the names Tramontana and Mistral, in particular during a negative phase of the East Atlantic Pattern, have the potential to cause intense heat loss, affecting dense water formation (DWF) in the Gulf of Lion (Josey et al., 2011). *Globorotalia truncatulinoides* inhabit subsurface waters most of their life span and migrate to surface waters for reproduction (Hemleben et al., 1989; Schiebel & Hemleben, 2005; Schiebel et al., 2002). Deep turbulent vertical mixing combined with a thermocline breakdown during the LIA, a period characterized by more negative NAO modes, may have caused proliferation of *G. truncatulinoides* and *G. inflata* in a shallower habitat. In contrast, stronger water column stratification as a result of lower surface heat loss during positive NAO and AMO phases during the MCA (Moreno et al., 2012) would have typically caused a subsurface habitat of *G. inflata* and *G.*

truncatulinoides. During the first half of the LIA, relative abundances of *G. ruber*$_{\text{WHITE}}$ are changing along with deep dwelling species, which is contradictory since the surface-dwelling species is a key indicator for water column stratification. As part of the summer assemblage, *G. ruber*$_{\text{WHITE}}$ might have benefited by reduced surface production during LIA summer months, as reflected in test concentration and accumulation rates (Fig. 2.2 & 2.5). Intense vertical mixing during negative NAO phases might have delayed initiation of the spring bloom, shortening the growing season and decreasing phytoplankton abundance as hypothesized for regions in the North Atlantic (R. R. Dickson et al., 1988; Fromentin & Planque, 1996). In the northwestern Mediterranean Sea, katabatic wind bursts (Tramontana, Mistral) are associated with enhanced vertical mixing and reduced surface productivity (Keerthi et al., 2021). Due to its positive response to phytoplankton blooms in the northwestern Mediterranean (Rigual-Hernández et al., 2012), total planktic foraminiferal abundances, would decrease during years of intense winter mixing, resulting in enhanced relative stocks of *G. truncatulinoides* and *G. inflata*. Increasing total planktic foraminiferal stocks and low relative abundances of *G. truncatulinoides* and *G. inflata* would indicate a weakened DWF in the northwestern Mediterranean Sea. This is further supported by proxies describing the variability of paleo storm activity and deep water formation in the Northwestern Mediterranean throughout the Common Era (Cisneros et al., 2019; Sabatier et al., 2012). Prevailing negative NAO phases are associated with more intense storm activity, bringing cold katabatic winds over the Gulf of Lion and forcing intense vertical mixing and stimulating deep water formation in the northwestern Mediterranean Sea, explaining the enhanced abundances of *G. truncatulinoides* and *G. inflata* as a result of high vertical mixing.

At our study site in the western Alboran Sea, planktic foraminiferal assemblage composition is influenced by complex small-scale hydrographic conditions associated with NAO modes. On top of the multicentennial variation between MCA and LIA as described in the previous paragraph, selected species show a multidecadal variability (Fig. 2.5; plus and minus signs) in both records associated with changes in NAO modes. The in-phase pattern between the ratio of *G. bulloides* versus *G. inflata* in the Alboran record and the relative abundance changes of *G. truncatulinoides* and *G.*

inflata in the Balearic core, is one of the most striking features of the record. As illustrated in Figure 2.6, productivity changes in the Alboran Sea are strongly linked to DWF in the Gulf of Lion, both related to NAO variability (Fig. 2.5). Stronger WMDW formation results in deficit in surface water masses in the western Mediterranean Sea, which is compensated by stronger Atlantic surface water inflow through the SoG (Macías et al., 2016). This leads to higher velocities of the AJ, flowing in a northward direction along the Iberian Peninsula coast. Together with prevailing westerlies, this atmospheric and hydrographic concurrence is associated with highly fertile, nutrient rich coastal upwelling. A poor DWF with less pronounced westerlies would weaken the AJ, streaming further southward along the northern African coast, resulting in further offshore upwelling characterized by less fertile surface water conditions (Macías et al., 2008; Macías et al., 2007; Sarhan et al., 2000). Seasonal sediment trap data in the Alboran Sea (Bárcena et al., 2004) support the relation between Atlantic water inflow and planktic foraminiferal surface production. Specifically, G. *bulloides* is associated to high surface production and *G. inflata* is an indicator for less productive conditions. We suppose that a continuous strong AJ during times towards more positive NAO phases favors the occurrence of *G. bulloides* in the Alboran Sea as a result of high surface primary productivity, whereas a weak AJ during periods of decreasing NAO modes makes the Alboran Sea more meso- to oligotrophic, thus favoring *G. inflata* over *G. bulloides*.

The strong link between DWF in the Gulf of Lion and surface productivity in the Alboran Sea (Fig. 2.6) and its see-saw pattern related to NAO variability was previously described in Holocene marine records (Ausín et al., 2015; Bazzicalupo et al., 2020). There is still uncertainty as to which NAO mode is associated with reinforced WMDW formation and related surface productivity in the Alboran Sea. When looking at the multicenntenial variability described by *G. truncatulinoides* and *G. inflata* of the Balearic record, our data corroborate the assumption of Ausín et al. (2015) relating a negative NAO to enhanced northwesterlies and a strong WMDW formation, which is further supported by paleoenvironmental records covering the Late Holocene (Cacho et al., 2000; Schirrmacher et al., 2019). In contrast, Bazzicalupo et al. (2020) suggest that throughout the Holocene positive NAO phases

were associated with strong northwesterlies which strengthen DWF and increase surface productivity in the Alboran basin, which is in accordance with the abundance changes on multidecadal time scales, which are in phase at both study sites (Fig. 2.5h). Recent hydrographic studies close to our core location support the hypothesis of Bazzicalupo et al. (2020) since upwelling intensity increased due to stronger westerly winds and an enhanced Atlantic Water inflow (Fenoglio-Marc et al., 2013; Vargas-Yáñez et al., 2008), thus enhancing productivity during the Dark Age and MCA (Nieto-Moreno et al., 2013). However, according to our data, the hypothesis of Bazzicalupo et al. (2020) may be applied to explain the multidecadal NAO variabilities during the Common Era, whereas findings of Ausín et al. (2015) are in good agreement with (paleo-) climatic and (paleo-) oceanographic processes stated above.

Additionally, the following reason may complicate a straightforward relation between western Mediterranean deep-water formation, Alboran Sea productivity and NAO variability. The main driver of WMDW formation could have changed from air-sea heat exchange during the MCA and LIA to buoyancy loss due to more arid climates during IE (Cisneros et al., 2019), explaining higher water fluxes through the Strait of Gibraltar during positive NAO indices (Fenoglio-Marc et al., 2013). Our findings do not contradict Mid-Pleistocene records, relating NAO+ phases to enhanced Alboran upwelling intensity and primary production (González-Lanchas et al., 2020), since they describe NAO phases with millennial cyclicity, whereas our cores cover higher temporal resolution. Additionally, complex interannual hydrographic variability (Peliz et al., 2013) relocating the high productive upwelling zones on a small spatial scale (Macías et al., 2008; Sarhan et al., 2000) and causing great interannual variability in the seasonal cycle of algal biomass (Bosc et al., 2004; D'Ortenzio & Ribera d'Alcalà, 2009) makes the Alboran Sea a challenging research site to study surface productivity changes (Bárcena et al., 2004; Mallo et al., 2017).

2.5.3.3.3 Anthropogenic warming as main driver in post-industrial times

In the Balearic and Alboran seas, a decrease of planktic foraminiferal production, test accumulation rates, and a rapid changing species assemblage are indicating an

unprecedented reduction of WMDW formation and surface primary productivity during the 20th century. This is the first evidence of significant changes in planktic foraminiferal assemblages other than a geographical displacement of assemblages in the oceans and took place before the oldest survey used by Jonkers et al. (2019). Particularly, the drop of *G. bulloides* relative to *G. inflata* in the Alboran Sea over a period of low NAO indices during the first half of the 20th century, reveals depleting surface primary productivity, corroborated by decreasing alkenone concentrations recorded in the Alboran core at this time (Fig. 2.2b). In the Balearic Sea, declining abundances of *G. truncatulinoides* and *G. bulloides* during the second half of the 20th century, indicating reduced vertical mixing and lower surface productivity (Fig. 2.3 & 5h). During the same time period, SST shows unprecedented warming (Ahmed et al., 2013), as recorded in $U^{k'}_{37}$ SST estimates of both cores (discussed in 5.2) and more positive AMO phases (Fig. 2.5). These findings suggest that the western Mediterranean Sea became more oligotrophic during the 20th century, as a result of anthropogenically induced SST warming and vertical stratification of the surface water column. Primary productivity depends on light, and nutrient supply affected by stratification of the water column mostly driven by temperature (Longhurst, 1995). Higher SSTs increase near surface stratification inhibiting vertical mixing. Consequently, less nutrients are transported to the upper ocean causing less fertilized surface conditions (Behrenfeld et al., 2006). Lower primary production levels favor the proliferation of *G. inflata* over the high productivity indicator species *G. bulloides* (Fig. 2.5h). As the decrease in primary production cascades through the food web, total planktic foraminiferal abundance declines at 1953 ± 5 in the Balearic and at 1947 ± 3 CE in the Alboran Sea, manifested in decreases of test accumulation rates 10X and 25X faster than during the LIA respectively (Fig. 2.5i). This is in agreement with decreasing foraminiferal fluxes in the western Mediterranean Sea, when comparing plankton tow studies carried out from the late 1980s (Mallo et al., 2017; Pujol & Grazzini, 1995), and decreasing surface chlorophyll-a concentrations at both study sites during the last two decades (Fig. 2.1e).

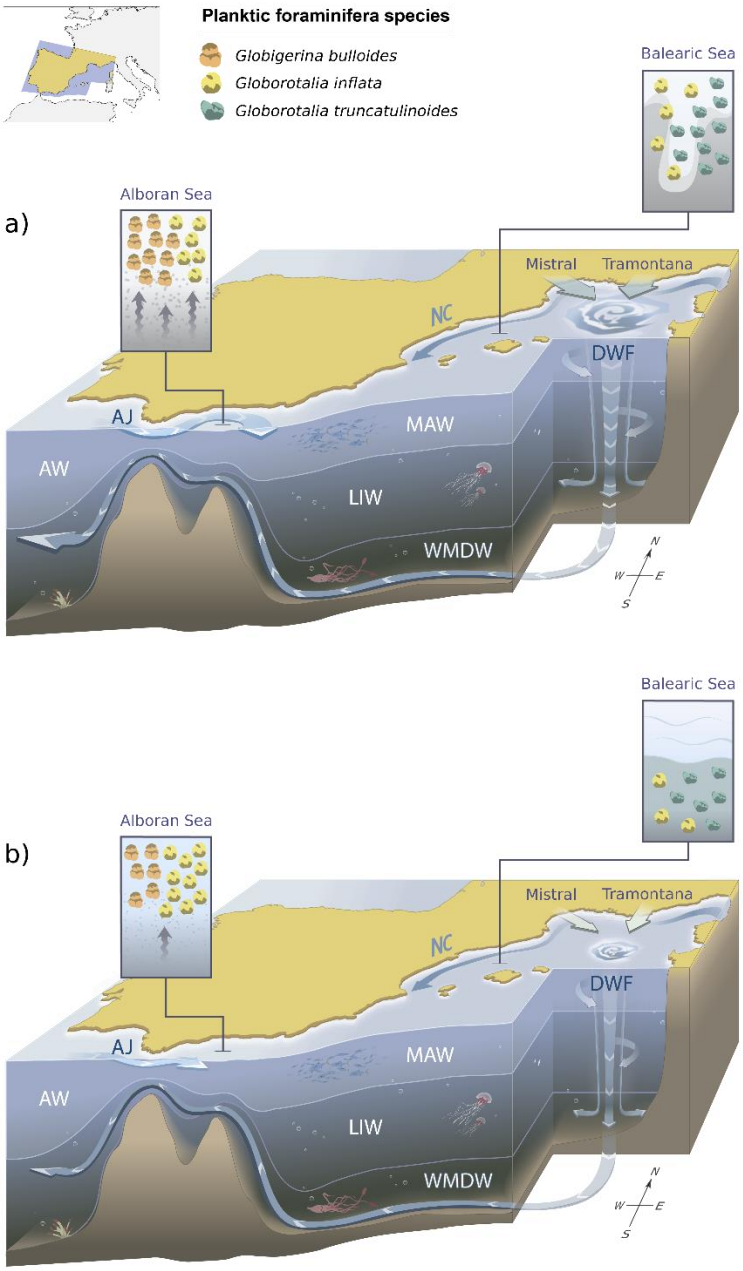

Figure 2.6: *Western Mediterranean circulation pattern and interaction with planktic foraminiferal community as explained in the text. (a) Enhanced northwesterly winds, deep water formation, strong Atlantic inflow inducing upwelling and increasing relative abundance of G. bulloides over G. inflata in the Alboran Sea, and G. inflata and G. truncatulinoides in the Balearic Sea. (b) Weakened northwesterly winds and deep water formation, lowering Atlantic inflow and reducing upwelling, increasing relative abundance of G. inflata over G. bulloides in the Alboran Sea, and decreasing percentages of G. inflata and G. truncatulinoides in the Balearic Sea (Figure by Jagoba Malumbres-Olarte).*

These results differ from biogeochemical models and historical data suggesting an overall increase of surface primary productivity during the last century (D. G. Boyce et al., 2014; Macías et al., 2014). Marine productivity models show a positive trend taking the whole productive layer reaching depths of 200 m into account (von Schuckmann et al., 2020), whereas surface chlorophyll-a concentrations derived from satellites (Fig. 2.1) just represent the primary productivity of the upper surface layer. Surface dwellers as *G. bulloides* (Rebotim et al., 2017) respond to productivity changes in the upper surface layer. This would explain the low planktic foraminiferal summer production, despite the fact that summer is the most productive season in the Mediterranean Sea when considering the entire productive layer (von Schuckmann et al., 2020).

Interestingly, *G. ruber*$_{\text{WHITE}}$ does not capture any warming signal at the beginning of the IE, but describing an abundance drop at both study sites. Negative excursions of *G. ruber*$_{\text{WHITE}}$ during the same time period are detected at other regions in the western Mediterranean (Lirer et al., 2014; Margaritelli et al., 2016), suggesting a possible human overprint, manifested in changes of nutrient cycling in coastal areas. The onset of the Modern Warm Period starting around 1950 CE is characterized by a recovery of the warm water species, visible in both records.

Coccolithophore assemblages in the Alboran Sea core also testify a drastic environmental change since the IE. In the modern ocean, *Emiliania huxleyi* is the most common coccolithophore species, an opportunistic and r-selected taxon that rapidly responds to upper ocean nutrient supply (Young, 1994), and in the Alboran Sea the recent decrease in abundance suggests an overall decrease in productivity (Fig 2.2e). In the western Mediterranean, *Gephyrocpasa oceanica* is identified as a tracer of Atlantic surface water inflow through the Gibraltar Strait (Incarbona et al., 2008a; Knappertsbusch, 1993; Oviedo et al., 2015) and has indicated that the inflow of a sustained surface Atlantic water mass has increased in recent time, as a consequence of enhanced DWF (Nieto-Moreno et al. (2015), contradicting planktic foraminiferal composition changes in the western Mediterranean (Fig. 2.5h). In the temperate Northeastern Atlantic, *G. oceanica* has a clear affinity for oligotrophic warm waters

(Bollmann, 1997; Ziveri et al., 2004) as suggested by the recent increase in abundance in our record (Fig. 2.2f). The opposite abundance changes of *E. huxleyi* and *G. oceanica* described in our record, can be interpreted as a response to decreased nutrient availability in the western Alboran Sea (Bárcena et al., 2004). *Florisphaera profunda* abundance is used generally to infer nutricline dynamics and productivity (Luc Beaufort et al., 1997; Grelaud et al., 2012; Incarbona et al., 2008b; Molfino & McIntyre, 1990). However, a recent review points out that in the Mediterranean Sea, except for the Sicily Channel, the relationship with productivity levels is not clearly established (Hernández-Almeida et al., 2019). In particular, previous studies had shown that *F. profunda* can have different dynamics of deep production (Stoll et al., 2007) and this seems the case for the slight decrease of this taxa recorded in our core in recent years (Fig. 2.2 g). In summary, we interpret *G. oceanica* abundance increases and *E. huxleyi* decreases in the top layer of the Alboran Sea sediment core as a reduction in surface productivity, which agrees with changes in planktic foraminiferal composition (Fig. 2.5). Remarkably, this study provides the first evidence of a distinct ecological modification in Mediterranean coccolithophore assemblages since industrial anthropogenic greenhouse gas emission.

2.6 Conclusion

We found that during pre-industrial times, planktic foraminiferal assemblages were strongly related to variabilities in NAO and AMO influenced by changes in solar irradiation. Positive NAO modes prevailed during the MCA and led to a weakened DWF in the Gulf of Lion. A predominant negative NAO during the LIA is associated with intense, cool northwesterly winds, reinforcing WMDW formation. A multidecadal variability is overlaying multicentennial variation, reflected in the species composition of both records showing lower surface productivity in the Alboran because of reduced DWF in the Gulf of Lion during times of declining NAO modes, and vice versa. The discrepancy between multidecadal and multicentennial responses of planktic foraminifera during the Common Era may not explain which NAO mode is associated with reinforced DWF in the Gulf of Lion and related surface productivity in the western Alboran Sea. The pre-industrial signal of natural variability controlling the species composition and indicating sea surface productivity,

is superimposed by anthropogenic warming during the 20th century. Increasing SSTs and enhanced vertical stratification since the second half of the last century has reduced marine surface productivity and resulted in a decrease of planktic foraminiferal production in the western Mediterranean Sea. Our results are supported by alkenone derived SST records at both sites showing an unprecedented increase of SST in the Anthropocene since about 1850 CE, which is remarkably in good accordance with instrumental data presenting 20th century warming and regional/global SST reconstructions. In pre-industrial times, both cores display warmer and colder sea surface conditions respectively during the MCA and the LIA, which is consistent with previous studies covering the Common Era.

Planktic foraminiferal assemblage composition is characteristic of climatic and oceanographic conditions prevailing at both study sites. Differences in total abundances mirror the distinct trophic conditions in the Balearic and Alboran seas. Relative abundances of *G. inflata* plus *G. truncatulinoides* might be used as a proxy for deep water formation intensity in the northwestern Mediterranean. Changing relative abundance between *G. bulloides* and *G. inflata* may be indicative of changes in the hydrographic conditions of the Alboran Gyre system driving surface ocean primary productivity.

Further investigations are needed to assess the effects of sea warming and changes in productivity on key marine planktic organisms and test production for the last centuries at different locations in the Mediterranean Sea, in particular since the semi-enclosed basin is known to be highly vulnerable and sensitive to alterations of the global climate. Further work is also required to better understand the mechanisms of deep-water formation in the entire Mediterranean Sea, including the eastern basin and the effects of large atmospheric patterns like NAO and AMO, to better predict changes in MTHC under anthropogenic climate change.

2.7 Supplementary Material

The supplementary information contains three text boxes, four figures, two tables and three datasets. Text S2.1 provides complementary information on water mass

properties in the western Mediterranean Sea. Text S2.2 discusses the anomalies in sedimentation rate changes arising by combining two different dating methods based on ^{14}C and ^{210}Pb. Text S2.3 describes the age-depth model development of core MedSea-S23-c3 we used for reconstructing the SST in the Balearic Sea. Figure S2.1, S2.3 and S2.4 showing the age depth model reconstructed by combining a ^{210}Pb based CF:CS model and Bayesian model using two ^{14}C dates for each core. The activity profile of total ^{210}Pb concentration comparing cores from both study sites is depicted in Figure S2.2. Table S2.2 and S2.3 show data regarding the construction of the age models. Dataset 1, 2 and 3 containing information about sample properties, planktic foraminiferal and calcareous nannoplankton counts and alkenone results used for reconstructing SST.

2.7.1 Complementary description of study areas in the western Mediterranean Sea (Text S2.1)

At the surface, fresh Atlantic Water (AW) flowing through the Strait of Gibraltar (SoG) forms two anticyclonic gyres in the Alboran Sea (Gascard & Richez, 1985). Mixing of AW with saltier Mediterranean Water (MW) produces Modified Atlantic Water (MAW), which flows along the north African coast and divides into two branches at the Strait of Sicily. The stronger current is entering the eastern basin where it forms the Levantine Intermediate Water (LIW) and later the Eastern Mediterranean Deep Water (EMDW), and one weaker branch continuing through the Tyrrhenian Sea northwestwards along the south European coast following the cyclonic surface circulation of the Western Mediterranean Sea (Millot, 1999; Schroeder et al., 2008). In the northwestern Mediterranean (Gulf of Lion), Western Mediterranean Deep Water (WMDW) is formed through cold katabatic airflows during winter. LIW spreads as a subsurface flow towards the west while mixing with regional winter mixed-layer water masses, known as Mediterranean Intermediate Water (MIW). The warm and salty MIW flows at subsurface through the SoG into the North Atlantic (Rohling et al., 2009).

2.7.2 Age model discussion: changes in sedimentary rates (Text S2.2)

Mass accumulation rate (MAR) of core MedSea-S3-c1 is in agreement with those results obtained in several sediment cores collected in the Alboran Sea (Masqué et al., 2003). In particular, ^{210}Pb inventory, supported ^{210}Pb, surface ^{210}Pb and MAR are in agreement with two sediment cores (ALB-1, ALB-2) collected close to our sampling station. MAR and sedimentation rate (SR) derived from ^{210}Pb measurements for MedSea-S23-c1 are in the range of results obtained in the submarine canyon system offshore Barcelona (Puig et al., 2015). SR derived from radiocarbon dates are in good agreement with studies close to the continental slope north of Menorca (Cisneros et al., 2016; Frigola et al., 2007; Moreno et al., 2012). The accordance with other sediment cores from the same area emphasizes the representativeness of our results and supports the accuracy of the age-depth model based on ^{210}Pb and ^{14}C.

When calibrating ^{14}C dates, we assume the global average marine reservoir age (R(t) = 400 yr) of surface ocean waters (Reimer et al., 2013), however, values vary as a function of time and geographical location (Ascough et al., 2005). In the Mediterranean Sea, reservoir ages vary over the entire basin, within a range between 240 to 660 years. Reservoir ages of ^{14}C close to the Balearic core location (MedSeA-S23-c1) might be higher than expected (R(t)St6: 485 ± 35; R(t)St12: 480 ± 55), whereas the reservoir age in the east (R(t)St18: 655 ± 35) varies highly in contrast to the value in the west (R(t)St25: 280 ± 35) of the Alboran core location (Siani et al., 2000).

There is a clear discrepancy between the ^{210}Pb and ^{14}C derived sedimentation rates that is commonly a consequence of physical and chemical alterations in sediments. Vertical lead diffusion and mixing as a result of physical processes or bioturbation in the upper sediment layers might bias estimations of mean sedimentation rate based on ^{210}Pb activity profiles towards maximum values (Nittrouer et al., 1984). Particularly in high productivity areas like the northern edge of the Western Alboran Gyre (WAG), occurrence of bioturbation effects might be high. Increasing bulk density with core depth results in higher estimations for ^{210}Pb derived sedimentation rates, when values presented in length per time (cm yr^{-1}) rather than mass flux (g cm^{-2} yr^{-1}).

Different ^{14}C concentrations and residence time amongst different reservoirs (Alves et al., 2018), reworking and erosion of sediments (Mekik, 2014), differences in shell morphology (Barker et al., 2007) and ecology (Waelbroeck et al., 2001) can lead to age offsets among planktic foraminiferal tests of the same sediment horizon of a given core. High amounts of ancient, dissolved carbon in river systems can alter the reservoir age of carbon shells in marine sediment from coastal sites (Philippsen, 2013). The northwestern Mediterranean Sea is characterized by the highest annual river discharges of the entire western Mediterranean basin (Struglia et al., 2004). The near-coast Balearic core site with its location in an area of high freshwater input, make it likely that hardwater effects had enhanced the reservoir age at the Balearic core site. Both the Balearic and the Alboran Sea are under the influence of the North Atlantic Oscillation (NAO). Negative NAO phases lead to less pronounced westerly winds and higher precipitation over the west Mediterranean Sea (Hurrell, 1995), so higher river runoff might increase the freshwater reservoir effect at both sites. Less freshwater input and enhanced ^{14}C renewal in the surface water masses due to dry climate and intensification of westerlies over both core sites as a result of a positive NAO mode, would decrease the reservoir age as reported in Siani et al. (2000). The multidecadal variability of the NAO (Ortega et al., 2015) could highly influence the radiocarbon age determination at both core sites. Morphological and ecological differences between species cause interspecific age offsets. *G. inflata* features robust shells more resistant to dissolution than *G. bulloides* or *G. ruber*, the latter two species mainly used for radiocarbon dating (source). *Globorotalia inflata* on average lives deeper in the water column than the afore mentioned species. Sturdier tests tend to be older than fragile shells (Barker et al., 2007) and deeper dwelling species likely incorporate older carbonate into their shells than surface dwellers (Waelbroeck et al., 2001). According to that, the reservoir age of *G. inflata* might be older than the applied global average of 400 yrs., even though sedimentation rates and bottom water corrosiveness at both core sites should prevent age offsets (Barker et al., 2007).

The changes in sedimentation rate at 5.5 cm depth (1933 CE) in core MedSeA-S3-c1 (Alboran Sea) and at depth 12.5 cm (1901 CE) in core MedSeA-S23-c1 (Balearic Sea) might be overestimated. Exaggerated changes in sedimentation rate result from a

maximum mean sedimentation rate in the upper core part, which is based on ^{210}Pb activity profiles and underestimated sedimentation rates for the lower core part, which is based on radiocarbon dates affected by reservoir age effects. Since the modelled age accuracy is of fundamental importance for the interpretation of past environmental parameters, changes in the amplitude of age uncertainties with depth need to be considered. While the first 100 yr are subjected to a relatively accurate ^{210}Pb age-model, age uncertainties are higher for older core sections. Therefore, the environmental analysis carried out in this study will emphasize the younger history of the sediment record (approx. last 150 years), when the paleo-environmental interpretation includes less uncertainties.

2.7.3 Age-depth model reconstruction of core MedSeA-S23-c3 (Text S2.3)

For reconstructing the age-depth model of MedSeA-S23-c3, we combined the ^{210}Pb ages for the upper 11.5 cm, calculated on basis of the CF:CS model applied on the ^{210}Pb activity profile of the core, with two radiocarbon dates obtained for the lower core part of MedSeA-S23-c1 (see tie points in table S2.2). Since both cores were collected in the same Multicore deployment and ^{210}Pb activity profiles show high similarity (Figure S2.2), we assume that sedimentation history of both cores is comparable. The low ^{210}Pb activity concentration in the top sample, might be indicative for enhanced bioturbation and/or vertical diffusion making measurements of other parameters less reliable. Based on this assumption, we excluded the last data point in the SST record of the Balearic Sea.

2.7.4 Figures

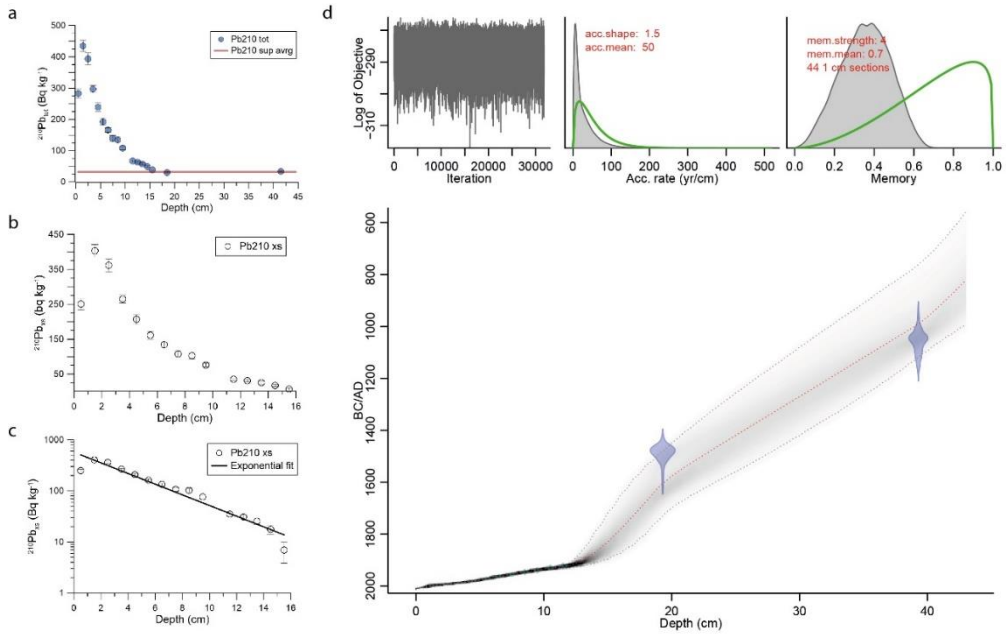

***Figure S2.1**: Age-depth model for the Balearic Sea core (MedSeA-S23-c3). reconstructed by combining a ^{210}Pb based CF:CS model and Bayesian model using two ^{14}C dates retrieved from planktic foraminiferal shells. (a) Activity profile of total ^{210}Pb concentration (blue dots) with red horizontal line representing the supported ^{210}Pb activity; (b) Activity profile of excess ^{210}Pb (open circles); (c) activity profile of excess ^{210}Pb plotted against logarithmic y-axis and exponentially fitted by non-linear least square fit (dark line). Vertical and horizontal error bars representing 1σ uncertainties and (d) Lower panel: Depth-age model (red line, single best model) based on two calibrated ^{14}C (transparent blue) and twelve ^{210}Pb dates (transparent green). 95% confidence interval is marked by grey stippled line, while darker greys areas inside confidence interval significate more likely calendar ages. Upper left panel: MCMC iterations. Upper middle panel: prior (green curve) and posterior (grey histogram) distribution of the accumulation rate. Upper right panel: prior (green curve) and posterior (grey histogram) distribution of the memory. Important to note: ^{14}C ages are derived from S23_core1.*

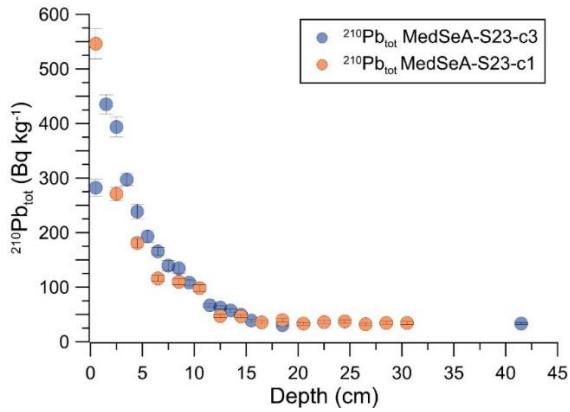

***Figure S2.2**: Activity profile of total ^{210}Pb concentration of core MedSeA-S23-c3 (blue dots) and MedSeA-S23-c1 (orange dots). Error bars represent 1σ uncertainties.*

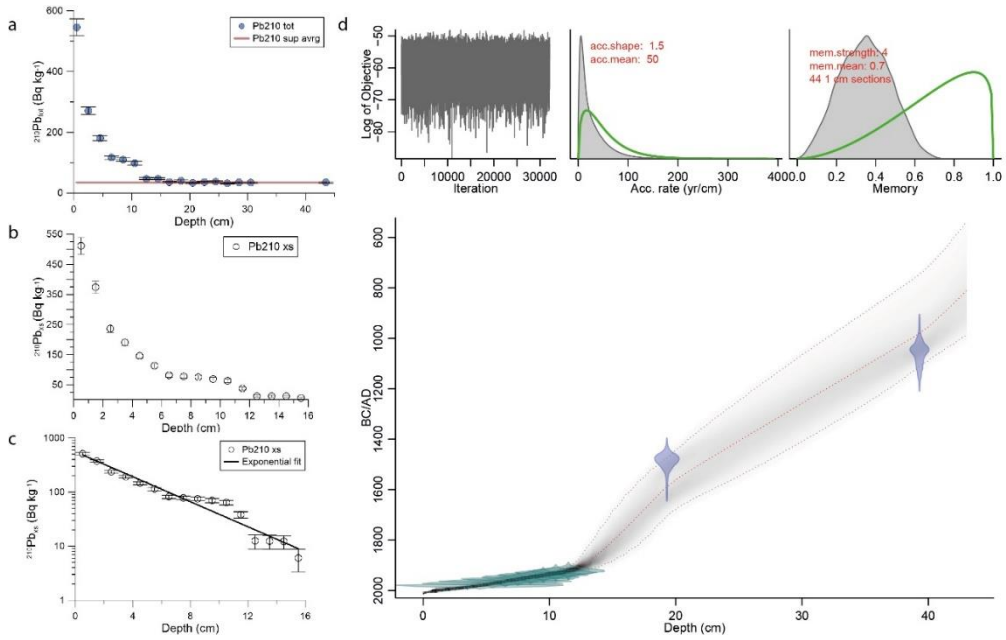

Figure S2.3: *Age-depth model for the Balearic Sea core (MedSeA-S23-c1). Reconstructed by combining a ^{210}Pb based CF:CS model and Bayesian model using two ^{14}C dates retrieved from planktic foraminiferal shells. (a) Activity profile of total ^{210}Pb concentration (blue dots) with red horizontal line representing the supported ^{210}Pb activity; (b) Activity profile of excess ^{210}Pb (open circles); (c) activity profile of excess ^{210}Pb plotted against logarithmic y-axis and exponentially fitted by non-linear least square fit (dark line). Vertical and horizontal error bars representing 1σ uncertainties. (d) Lower panel: Depth-age model (red line, single best model) based on two calibrated ^{14}C (transparent blue) and twelve ^{210}Pb dates (transparent green). 95% confidence interval is marked by grey stippled line, while darker greys areas inside confidence interval means more likely calendar ages. Upper left panel: MCMC iterations. Upper middle panel: prior (green curve) and posterior (grey histogram) distribution of the accumulation rate. Upper right panel: prior (green curve) and posterior (grey histogram) distribution of the memory.*

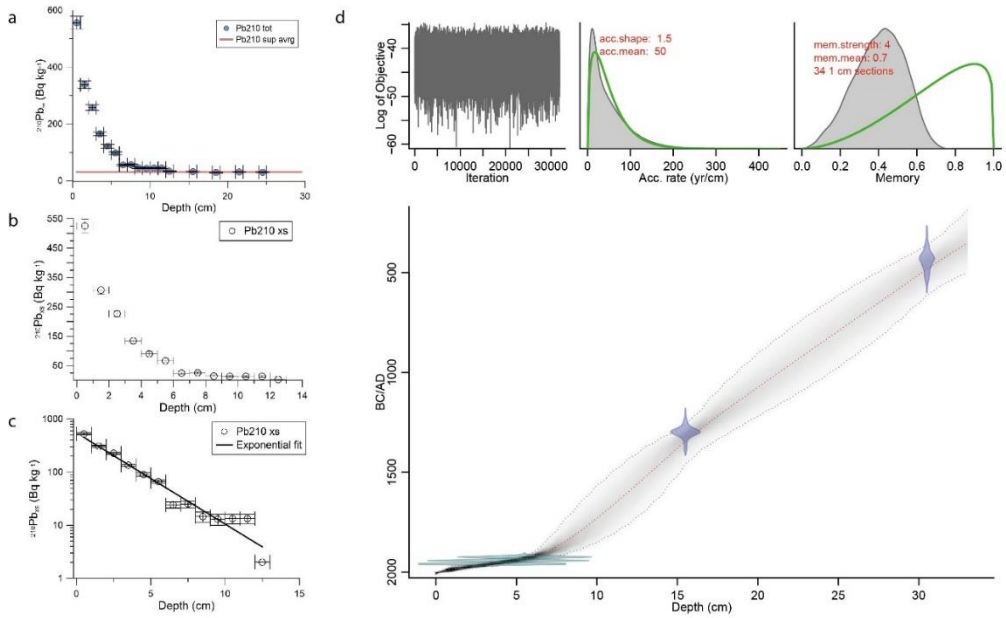

Figure S2.4: *Age-depth model for the Alboran Sea core (MedSeA-S3-c1). Reconstructed by combining a ^{210}Pb based CF:CS model and Bayesian model using two ^{14}C dates retrieved from planktic foraminiferal shells. (a) Activity profile of total ^{210}Pb concentration (blue dots) with red horizontal line representing the supported ^{210}Pb activity; (b) Activity profile of excess ^{210}Pb (open circles); (c) activity profile of excess ^{210}Pb plotted against logarithmic y-axis and exponentially fitted by non-linear least square fit (dark line). Vertical and horizontal error bars representing 1σ uncertainties and (d) Lower panel: Depth-age model (red line, single best model) based on two calibrated ^{14}C (transparent blue) and six ^{210}Pb dates (transparent green). 95% confidence interval is marked by grey stippled line, while darker greys areas inside confidence interval means more likely calendar ages. Upper left panel: MCMC iterations. Upper middle panel: prior (green curve) and posterior (grey histogram) distribution of the accumulation rate. Upper right panel: prior (green curve) and posterior (grey histogram) distribution of the memory.*

2.7.5 Tables

Table S2.1*: Core depth, mean sedimentation rates (SR) and mean time resolution (TR) of all cores according to final age-depth model*

Core	Depth [cm]	Mean SR [cm·kyr^{-1}]	Mean TR [yr·cm^{-1}]
MedSeA-S3-c1	0 -5.5	79.48	12.58
	6.5 - 15.5	17.38	57.54
	16.5 - 30.5	17.54	57.01
	31.5 - 33.0	19.42	51.50
	core mean	**33.45**	**29.89**
MedSeA-S23-c1	0 -12.5	127.76	7.83
	13 - 19	21.87	45.72
	19.5 -39.0	32.96	30.34
	39.5 - 43	19.79	50.53
	core mean	**50.60**	**19.76**
MedSeA-S23-c3	*0 -12.5*	*138.00*	*7.25*
	13 - 19	*21.79*	*45.89*
	19.5 -39.0	*32.53*	*30.74*
	39.5 - 43	*22.82*	*43.82*
	core mean	***53.79***	***18.59***

Table S2.2: *Tie points used on each core to construct age models with their attendant errors through Bayesian statistics in Figure S2.1, S2.3, S2.4.*

Core	Mean depth [cm]	Method	Ages [years CE]	Age-uncertainties interval [years CE]
MedSeA-S3-c1	0.5	^{210}Pb	1997	1996 - 1997
	1.5	^{210}Pb	1983	1982 - 1985
	2.5	^{210}Pb	1972	1970 - 1974
	3.5	^{210}Pb	1959	1957 - 1961
	4.5	^{210}Pb	1942	1939 - 1945
	5.5	^{210}Pb	1925	1921 - 1929
	15.5	^{14}C (calibrated)	1297	1252 - 1337
	30.5	^{14}C (calibrated)	433	358 - 534
MedSeA-S23-c1	0.5	^{210}Pb	2006	2006 - 2007
	1.5	^{210}Pb	1999	1998 - 2000
	2.5	^{210}Pb	1994	1993 - 1996
	3.5	^{210}Pb	1987	1985 - 1989
	4.5	^{210}Pb	1981	1978 - 1983

	5.5	^{210}Pb	1971	1968 - 1974
	6.5	^{210}Pb	1963	1958 - 1967
	7.5	^{210}Pb	1955	1950 - 1960
	8.5	^{210}Pb	1946	1941 - 1952
	9.5	^{210}Pb	1938	1931 - 1944
	10.5	^{210}Pb	1929	1923 - 1936
	11.5	^{210}Pb	1922	1914 - 1929
	19.25	^{14}C (calibrated)	1481	1442 - 1529
	39.25	^{14}C (calibrated)	1050	992 - 1140
MedSeA-S23-c3	0.5	^{210}Pb	2007	2006 - 2007
	1.5	^{210}Pb	2000	1999 - 2001
	2.5	^{210}Pb	1995	1994 - 1997
	3.5	^{210}Pb	1989	1987 - 1991
	4.5	^{210}Pb	1982	1980 - 1985
	5.5	^{210}Pb	1973	1970 - 1976
	6.5	^{210}Pb	1965	1961 - 1969
	7.5	^{210}Pb	1958	1953 - 1962
	8.5	^{210}Pb	1950	1945 - 1955
	9.5	^{210}Pb	1941	1935 - 1947
	10.5	^{210}Pb	1933	1927 - 1940
	11.5	^{210}Pb	1926	1919 - 1933
	19.25	tie point (MedSeA-S23-c1)	1481	1442 - 1529
	39.25	tie point (MedSeA-S23-c1)	1050	992 - 1140

2.7.6 Data Availability

Supplementary data regarding data set S2.1 to S2.5 can be found online at https://doi.org/10.1016/j.gloplacha.2021.103549.

CHAPTER 3

3 Anthropogenic acidification of the Mediterranean Sea drives decreased calcification

Abstract

Anthropogenic CO_2 emissions cause ocean acidification and warming leading to enhanced stratification and associated changes in marine productivity. Although marine calcifiers are extensively studied, the response of these key organisms to the combined effects of climate change stressors on decadal to centennial timescales is insufficiently understood as yet. Here, we present almost 2000 foraminiferal test size normalized weight (SNW) measurements of the species *Globigerinoides elongatus* and *Globigerina bulloides* alongside other multi-proxy data from three high-resolution western Mediterranean sediment cores, to investigate the calcification response to CO_2-induced environmental change. We conclude that anthropogenic CO_2 impairs foraminiferal calcification. We observe a basin wide SNW decrease with an enhanced uptake of anthropogenic CO_2 by Mediterranean surface waters as evidenced by decreasing planktic foraminiferal $\delta^{13}C$ (Suess Effect) and decreasing pH derived from boron isotopes ($\delta^{11}B$). Rising sea surface temperatures (SSTs) and changes in biological productivity, inferred from alkenone concentrations and test accumulation rates, do little to alleviate decreasing SNW resulting from acidification. Our results show that the effects of anthropogenic CO_2 on ocean carbonate chemistry will drive ongoing reduction of marine biogenic calcification and alter marine ecosystems even in high alkalinity systems like the Mediterranean Sea, with knock-on implications for ecosystem deterioration in a more acidified global ocean.

Chapter based on: Pallacks, S., Ziveri, P., Schiebel, R., Vonhof, H., Rae, J., Littley, E., . . . Martrat, B. ((under revision)). Anthropogenic acidification of the Mediterranean Sea drives decreased calcification. Communications Earth & Environment.

3.1 Introduction

Since the onset of the Industrial Revolution, human-induced climate change has rapidly modified the Earth system with notable impacts on the oceans. Rapidly increasing atmospheric CO_2 concentrations have resulted in global surface ocean pH decline of approximately 0.1 units compared to pre-industrial levels (Jacobson, 2005), impacting the calcification process of marine calcifiers (Kroeker et al., 2013; Orr et al., 2005). Since the mid-19th century, enhanced CO_2 emissions have also contributed to global ocean surface warming by 0.76 ± 0.16 K between 1904 and 2016 (Abram et al., 2016; NOAA National Centers for Environmental Information, 2021). In the second half of the 20th century, anthropogenically induced warming has also intensified vertical ocean stratification (Li et al., 2020), leading to changes in nutrient cycling and depletion of surface marine productivity (Behrenfeld et al., 2006). These alterations of pH, temperature, and food availability are each assumed to influence the calcification rates of critical calcifying taxa such as planktic foraminifera (Marshall et al., 2013; Weinkauf et al., 2016, references therein), but their response to the combination of these factors is still unclear.

The Mediterranean is a primary climate change hot-spot that shows amplified climate responses to global change (Cramer et al., 2018; Giorgi, 2006), making it a key region to investigate the response of marine ecosystems to human-induced changes of the chemical, physical, and biological environment. Due to its high alkalinity and the short residence times of its water bodies, the Mediterranean Sea is expected to have an exceptionally high uptake rate of anthropogenic carbon (A. Schneider et al., 2010; A. Schneider et al., 2007; Touratier & Goyet, 2009). Both annual mean surface air temperature and sea surface temperature (SST) have accelerated in the Mediterranean region compared to the global average since 1880 CE (Cramer et al., 2018). The recent SST warming at a rate of 0.35 K per decade (Shaltout & Omstedt, 2014), may result in thermally induced stratification and decreasing biological productivity (Pallacks et al., 2021).

Comprehensive, multi-decadal monitoring of plankton communities started in 1931 (Richardson et al., 2006), while time series measurements of seawater carbonate

chemistry (Bates et al., 2014) and surface ocean productivity (Madrid, 1978) began only in the late 20th century. As a result, observational time series are too short to reasonably attribute changes in the ocean's biological productivity to anthropogenically driven climate change (Henson et al., 2010). Laboratory experiments give important clues on how calcifying plankton copes with rapid climate change, but it remains difficult to capture the complex natural environment in a laboratory setting. Paleo-reconstructions of plankton calcification and accompanying records of environmental conditions can address these issues, providing records going back to pre-industrial times which could capture the impact of changing physical and chemical conditions on the marine ecosystem.

Here, we provide radiocarbon and radionuclide-dated, high-resolution marine proxy records from three locations in the western Mediterranean Sea (Figure 3.1), covering the transition from the pre-Industrial (pre-IE) to Industrial Era (IE), starting from about 1800 CE. With these we investigate the basin-wide, interspecies (*Globigerinoides elongatus* and *Globigerina bulloides*) response of planktic foraminiferal calcification (represented by the measured SNW) to warming, acidification, and variations in primary productivity, reconstructed using a suite of paleo proxies, over the onset of the Industrial Revolution. We show an unprecedented basin wide SNW decrease of 18% to 34% in the species *G. elongatus*, and 7% to 35% in *G. bulloides* over the 20th century. Enhanced uptake of anthropogenic CO_2 by Mediterranean surface waters as shown by decreasing planktic foraminiferal $\delta^{13}C$ (Suess Effect) and decreasing pH derived from boron isotopes ($\delta^{11}B$), brings us to the conclusion that anthropogenic CO_2 impairs foraminiferal calcification.

3.2 Results and Discussion

3.2.1 Human induced sea surface warming and productivity changes in the western Mediterranean

The western Mediterranean Sea is a hotspot of rising SST, at a rate above the global average (Pisano et al., 2020), and anthropogenically-driven productivity changes during the IE (Pallacks et al., 2021). Warming of western Mediterranean surface waters over the 20th century is shown by alkenone derived SST data and (HadISST)

satellite time series observations (Figures 3.2a, 3.3c). A mid-20th century cooling period by > 1 K in the Mediterranean from the end of the 1940s to the end of the 1980s is confirmed, as seen in other western Mediterranean paleotemperature records (Lionello et al., 2006; Pallacks et al., 2021). This cooling episode is followed by rapid warming over the last 20 years. Any offsets between instrumental and paleorecords might be due to low data coverage for SST calibrations in the central Mediterranean (Text S3.1). Indeed, while the Strait of Sicily alkenone record indicates warming just above average over the last two decades, other recently published paleorecords in the Alboran and Balearic Sea (Pallacks et al., 2021) consistently show accelerated 20th century sea surface warming (Figure 3.2a), with unprecedented warming rates at present in the Mediterranean Sea (Marriner et al., 2022). High sea surface warming rates at our sites confirm a rapid, anthropogenically induced sea surface warming in the western Mediterranean.

Accelerated anthropogenic climate change has altered marine productivity in the Mediterranean Sea, as reflected by plankton community changes (Pallacks et al., 2021). The sedimentation rate of planktic foraminiferal tests is positively related to primary productivity (Schiebel, 2002), while alkenone concentrations are closely related to phytoplankton biomass (Raja & Rosell-Melé, 2021). Both foraminiferal tests and alkenones thus serve as proxies of changes in past ocean productivity and reflect surface productivity levels at all three study sites (Text S3.1). In the Strait of Sicily, test accumulation rates decrease between the 1850s and 1940s, then increase rapidly, which, alongside increasing C_{37} alkenone concentrations, indicates enhanced productivity during the second half of the 20th century (Figure 3.2b). Biogeochemical model results (Macías et al., 2014) and historical records (D. G. Boyce et al., 2014), confirm productivity increase in Mediterranean surface waters during the 20th century, and suggest enhanced anthropogenic nitrate and phosphate loads as the main driver of surface water eutrophication. In contrast, a decrease in productivity is observed in the Alboran and Balearic records during the second half of the 20th century (Figure 3.2b). At these sites, enhanced stratification through 20th century SST increase likely explain surface productivity losses, which are also recorded through changes in planktic foraminiferal species composition (Pallacks et al., 2021). Our results and previous

studies thus show regionally distinctive patterns of 20th century productivity changes for the western Mediterranean.

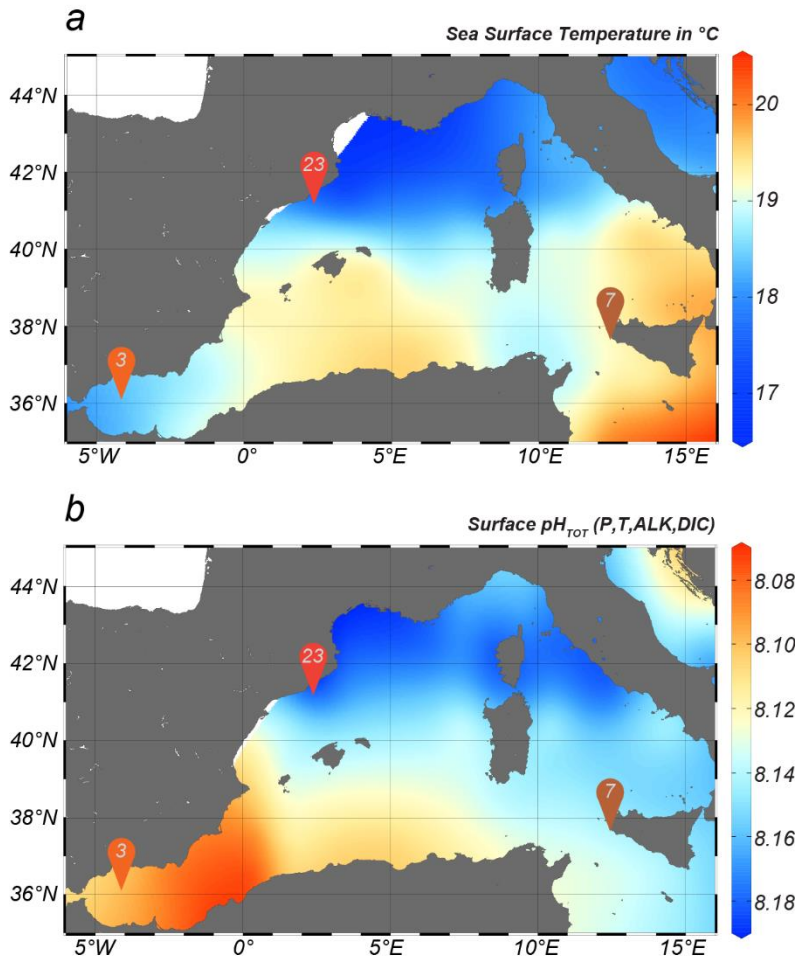

Figure 3.1: *Station map of the western Mediterranean produced in Ocean Data View (Schlitzer, 2019) indicating core locations: MedSeA-S3-c1 (Alboran Sea; 3), MedSeA-S23-c1 (Balearic Sea; 23), MedSeA-S7-c2 (Strait of Sicily; 23). (a) Western Mediterranean SSTs from World Ocean Atlas 2018 (Garcia et al., 2019). (b) Sea surface pH based on a global gridded dataset covering the period 1982–2020 (Gregor & Gruber, 2021).*

3.2.2 Anthropogenic CO_2 intrusion into western Mediterranean waters recorded by planktic foraminiferal test chemistry

The $\delta^{13}C$ and $\delta^{11}B$ signatures of planktic foraminiferal tests provide sensitive tracers of anthropogenic carbon uptake and acidification of the western Mediterranean Sea. While fluctuations in carbonate chemistry, productivity, and hydrography may modulate the carbon isotope signal, these influences are relatively small compared to

the change in the isotopic composition of ambient seawater due to the input of low $\delta^{13}C$ CO_2 from fossil fuel burning (the Suess Effect) (Eide et al., 2017; Mellon et al., 2019; Quay et al., 1992), making $\delta^{13}C$ a good tracer for natural versus anthropogenic environmental changes.

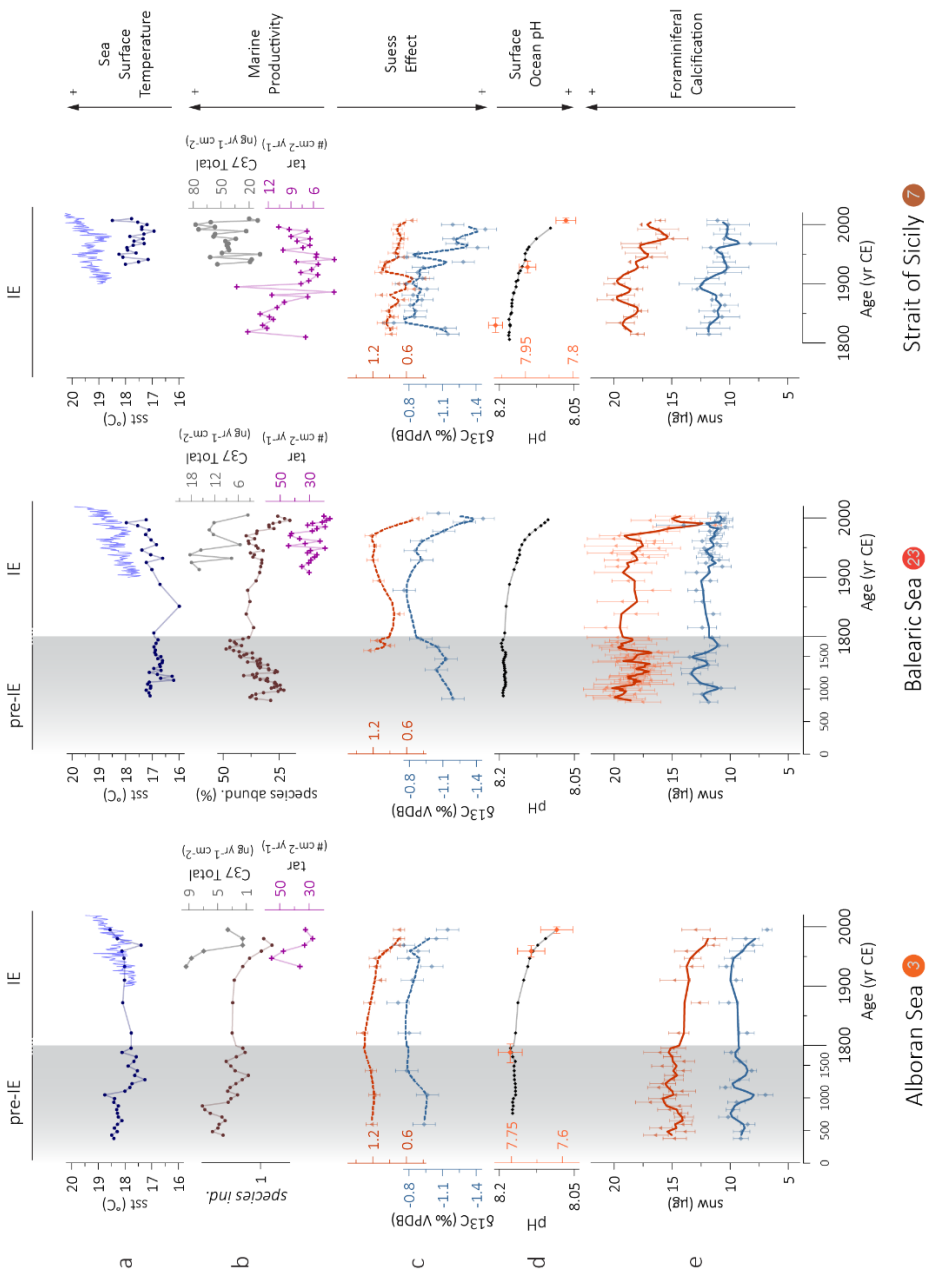

***Figure 3.2**: Changing environmental parameters at three core locations (Alboran and Balearic Seas, Strait of Sicily) in the western Mediterranean Sea during the Common Era (a) Sea surface temperature*

(SST) changes derived from alkenones (dark blue line) and the HadISST data set (light blue line). (b) Marine surface productivity represented by total test accumulation rate (purple line), alkenone concentration (grey symbols), and species composition (G. bulloides versus G. inflata) and species abundance (G. inflata + G. truncatulinoides) changes (brown line) (Pallacks et al., 2021) (c) Suess effect displayed through $\delta^{13}C$ (‰ VPDB) signature measured in planktic foraminiferal tests of G. elongatus (red dashed line) and G. bulloides (blue dashed line) with error bars indicating 0.1 ‰ uncertainty (1SD level) and displayed as 3 point running average. (d) Surface ocean pH estimated with CO2SYS (black line- see methods) and boron isotope measurements (Orange symbols) in tests of G. elongatus (Alboran Sea) and G. ruber albus (Strait of Sicily). (e) Planktic foraminiferal calcification expressed as size normalized weight (SNW) for G. elongatus (red) and G. bulloides (blue). Grey shaded area in Alboran and Balearic time series represents the pre Industrial Era, prior to 1800 CE with a compressed time axis.

We use the two morphotypes of planktic foraminiferal species *Globigerinoides elongatus* (syn. *Globigerinoides ruber* white sensu lato) and *G. ruber albus* (syn. *G. ruber* white sensu stricto) as well as *Globigerina bulloides* to evaluate environmental alterations in the upper water column, as they are surface mixed layer dwellers (Pujol & Grazzini, 1995). As *G. bulloides* thrives in late winter / early spring and *G. ruber* in late spring / summer (Bárcena et al., 2004; Rigual-Hernández et al., 2012), we also cover most of the seasonal change in sea surface temperature and primary productivity.

At all three sites analyzed here, *G. elongatus* and *G. bulloides* show a notable $\delta^{13}C$ drop during the IE, against a backdrop of pre-industrial natural variability (Figures 3.2c and 3d), which we refer to here as negative anthropogenic carbon isotope excursions (nCIEs). nCIEs show most marked decreases during the latter half of the 20th century with a mean amplitude of −0.60‰ and range between −1.24‰ and −0.14‰ (Figure S3.1). We attribute these nCIEs to the increase of the surface ocean concentration of anthropogenic CO_2 (Gruber et al., 1999). The measured decline of $\delta^{13}C$ in our foraminiferal tests during the second half of the 20th century describes a more pronounced Suess Effect signal when compared with results from the Northwest Atlantic (range = −0.174‰ to −0.757‰; weighted average = −0.45‰) (Mellon et al., 2019).

Ocean uptake of anthropogenic CO_2 increases hydrogen ion (H^+) concentrations and hence lowers pH (Caldeira & Wickett, 2003). Boron isotope ratios of tests of *G. ruber albus* and *G. elongatus* reveal a notable pH decline in the Alboran Sea of −0.14 units between 1697 and 1995 CE, which is in accordance with previous estimates over the

industrial period ranging from −0.06 to −0.16 units (Hassoun et al., 2022), and also notable ocean acidification in the Strait of Sicily, with reconstructed pH decreasing by 0.22 units from 1830 to 2007 CE. These results are largely consistent with the acidification expected from anthropogenic CO_2 invasion (Figure S3.2), which we calculate by assuming equilibrium between surface waters and the atmosphere alongside modern alkalinity and observed SST change at each site (see Methods); we note that absolute pH values from $\delta^{11}B$ are lower than recent pH levels (Figures 3.2d) measured in the Mediterranean Sea (Álvarez et al., 2014; Flecha et al., 2019; Jiménez-López et al., 2021; Kapsenberg et al., 2017; Marcellin Yao et al., 2016), a feature that is discussed in more detail in the supplements (Text S3.2). Slightly enhanced acidification in the Strait of Sicily might be caused by enhanced vertical mixing during the second half of the 20th century, transporting low-pH Mediterranean intermediate waters to the surface (Hassoun et al., 2015) as indicated through enhanced productivity and SST cooling compared to other sites (Figure 3.2a,b). Measurements reveal recent pH decreases between 0.0009 yr^{-1} and 0.0036 pH units yr^{-1} in the Alboran Sea (Flecha et al., 2019) and between 0.0013 yr^{-1} and 0.0030 pH units yr^{-1} in the North Western Mediterranean (Kapsenberg et al., 2017; Marcellin Yao et al., 2016), which exceed the global average trend of 0.0017 ± 0.0002 pH units yr^{-1} (Gehlen et al., 2020). The rate of pre-industrial to modern pH decline is well-reflected by our boron isotope derived values and corroborated by CO2SYS model estimates (Figure S3.2), suggesting acceleration of ocean acidification in western Mediterranean surface waters during the 20th century.

Whilst the nCIEs primarily reflect uptake of isotopically light CO_2 in the surface ocean, falling $[CO_3^{2-}]$ and pH levels tend to increase $\delta^{13}C$ in foraminiferal tests (Spero et al., 1997), and could thus dampen the Suess Effect driven nCIE signal we observe. Based on laboratory and field data (Bijma et al., 1999; Peeters et al., 2002; Spero et al., 1997), western Mediterranean pH and $[CO_3^{2-}]$ changes since 1900 are estimated to account for approximately 0.24‰ to 0.33‰ (*G. ruber)* and 0.48‰ (*G. bulloides)* of $\delta^{13}C$ test changes (Table S3.1). Ambient water temperature changes have a minimal, negative effect on $\delta^{13}C$ in foraminiferal tests (Peeters et al., 2002; Schiebel & Hemleben, 2017), accounting for −0.12 ‰ in *G. bulloides* tests, when basing

estimations upon SST warming rates in the western Mediterranean (Table S3.1). Variability in upwelling strength and biological productivity can also influence $\delta^{13}C$ in calcite tests at the species scale (Peeters et al., 2002), as can algal or bacterial symbionts, which change the microenvironment of planktic foraminifera near the test surface impacting their $\delta^{13}C$ signal (Bird et al., 2017; Köhler-Rink & Kühl, 2005; Spero, 1992). Strong pH and SST changes, differential upwelling, and productivity patterns at our three study sites are thought on the whole to slightly counter the Suess Effect and attenuate the full magnitude of the signal of decreasing $\delta^{13}C$ in our planktic foraminiferal tests (Eide et al., 2017).

We conclude that the input of isotopically light anthropogenic CO_2 in the surface ocean has caused nCIEs during the IE in both *G. bulloides* and *G. elongatus* in the western Mediterranean Sea. At the same time, enhanced CO_2 uptake by the ocean drives acidification, as indicated by boron isotope measurements and model estimates, attenuating the Suess Effect signal. Sea surface warming, upwelling, and changes in marine surface production during the 20th century have minor attenuating influences on the $\delta^{13}C$ signal.

3.2.3 Anthropogenic impacts on planktic foraminiferal calcification

Size normalized weight (SNW) is a useful tool for understanding the differential response of planktic foraminifera to climate change stressors like ocean warming, acidification, and productivity changes. SNW provides a normalized measure of chamber wall thickness and density, reflecting carbonate production and preservation of planktic foraminiferal tests (Schiebel & Hemleben, 2017), and is used as a proxy for past $[CO_3^{2-}]$ (Marshall et al., 2013; Osborne et al., 2016), though has also been suggested to provide a potential proxy for growth rate in planktic and benthic foraminifera (Dong et al., 2022; Keul et al., 2013). Although secondary influences such as physico-chemical conditions of ambient seawater, and autecological properties can influence SNW, these do not seem to prevent the application of the proxy (Beer et al., 2010b; Weinkauf et al., 2016). We found that SNW of *G. elongatus* and *G. bulloides* decreased at all three stations throughout the last 200 yr., unprecedented against the backdrop of our ~1500 yr. long records in the Alboran and

Balearic Seas (Figures 3.2e; 3.3f). Basin-wide relative SNW loss during the 20th century in *G. elongatus* ranges from 18% to 34% and in *G. bulloides* from 7% to 35% (Figure S3.3).

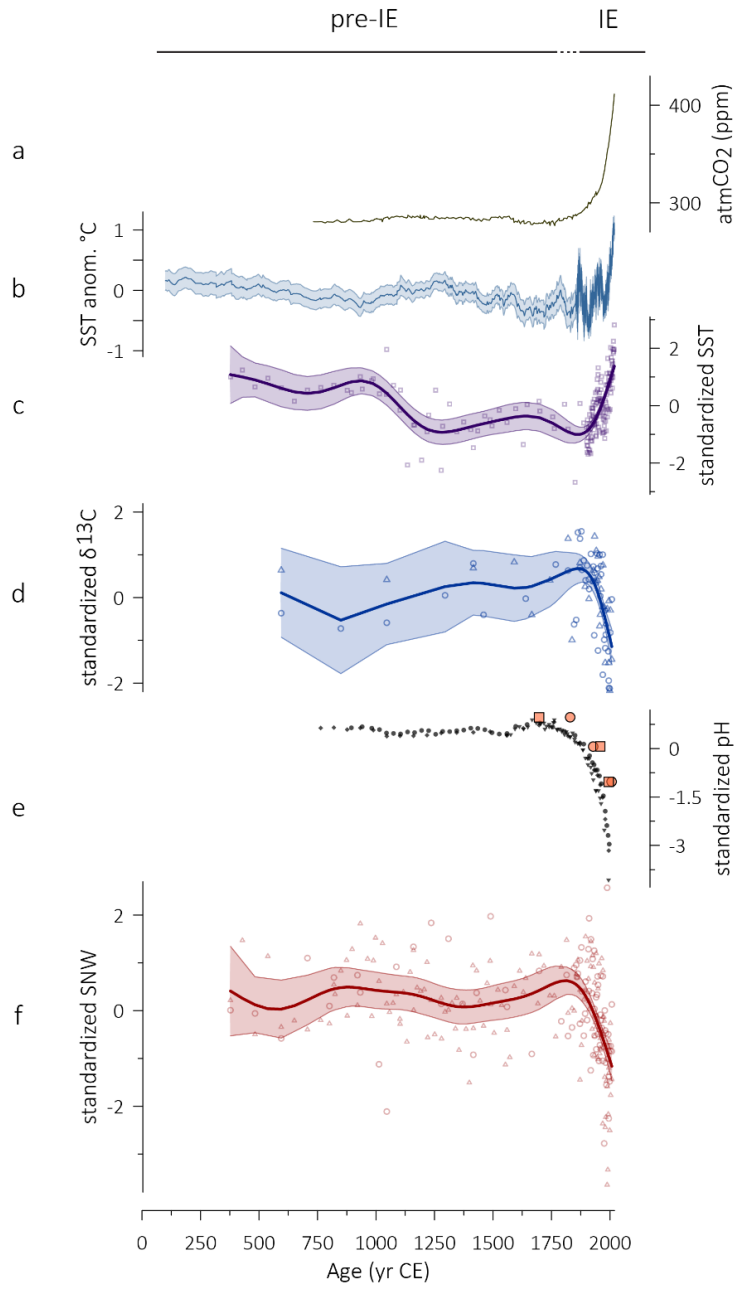

Figure 3.3: *Changing western Mediterranean biogeochemistry over the last 2000 years driven by enhanced anthropogenic CO_2 emissions. (a) Atmospheric CO_2 concentrations derived from measured (Tans & Keeling, 2020) and reconstructed (Bauska et al., 2015; Friedli et al., 1986) records. (b) Stack*

of Mediterranean Sea Surface Temperature (SST) anomalies (blue line) with light blue shading indicating the 68% Confidence Interval (Marriner et al., 2022). (c) Generalized additive model (GAM) fit (purple line) of standardized SST data (purple open squares) including alkenone derived SST and calculated mean from HadISST for each location. Purple shading indicates 95% Confidence Interval. (d) GAM fit (dark blue line) to standardized $\delta^{13}C$ results comprising G. elongatus (blue triangles) and G. bulloides (blue circles) of all three stations, blue transparent ribbon indicates 95% confidence interval. (e) Standardized pH values (black symbols) estimated through CO2SYS for Alboran Sea (diamonds), Balearic Sea (full circles) and Strait of Sicily (triangles). Standardized pH values derived from boron isotope measurements (orange symbols) in G. ruber albus at Strait of Sicily (circles), and in G. elongatus at the Alboran Sea (squares). (f) GAM fit (dark red line) to standardized size normalized weights (SNW) of G. elongatus (red triangles) and G. bulloides (red circles) of all three stations, red transparent ribbon indicating 95% confidence interval.

Decreasing ocean pH and [CO_3^{2-}] due to enhanced CO_2 uptake from the atmosphere can impede the biological precipitation of carbonate tests (Doney et al., 2009), depending on the species-specific response. Commonly, *G. elongatus* and *G. bulloides* reduce their test calcite mass with lower [CO_3^{2-}], calcite saturation (Ω), and pH, shown by numerous studies based on sediment and water samples, sediment trap time series, as well as culture experiments (C. V. Davis et al., 2017; Marshall et al., 2013; Moy et al., 2009; Osborne et al., 2016). Despite this, in the natural environment, it is important to consider the combined influence of the various environmental drivers on planktic foraminiferal calcification, with studies using cultures, sediment traps, plankton nets and marine sediments attributing SNW changes to surface ocean carbonate chemistry, alongside temperature and productivity (Aldridge et al., 2012; Beer et al., 2010b; Marshall et al., 2013; Moy et al., 2009; Naik et al., 2011; Osborne et al., 2016; Todd et al., 2020; Weinkauf et al., 2016).

Sea surface warming decreases the solubility of atmospheric CO_2, elevating [CO_3^{2-}] in surface water, while higher temperature can also foster enzymatic activity, resulting in faster growth rates and enhanced calcification rates (Spero et al., 1991). Both effects cause an increase in planktic foraminiferal SNW, a relationship observed in our target species in a number of earlier studies (Aldridge et al., 2012; C. V. Davis et al., 2017; Gonzalez-Mora et al., 2008; Marshall et al., 2013; Osborne et al., 2016; Weinkauf et al., 2016). Sea surface warming in the western Mediterranean, as shown in our records (Figures 3.2a; 3.3c), should have enhanced SNW in both species over the IE if temperature were the leading influence. The negative correlation between SST and SNW of *G. elongatus* and *G. bulloides* at all three study sites during the IE, is indicative of an overriding effect of declining [CO_3^{2-}] due to anthropogenic carbon

input during the last 150 yr, masking any small opposing effect of temperature changes. Although temperature rise may have somewhat dampened the decrease in SNW, our results substantiate the dominat role of [CO_3^{2-}] decline due to ocean acidification as the main driver of test calcite production.

Marine primary productivity in surface waters is assumed to influence test calcite production and therefore SNW (Mallo et al., 2017; Weinkauf et al., 2016). Test calcification is energy demanding (de Nooijer et al., 2014), as greater food availability could allow foraminifera to allocate more energy to it. Chlorophyll *a* concentrations may serve as a proxy for marine primary productivity and food availability, as phytoplankton is considered to be the basis of planktic foraminiferal alimentation (Hemleben et al., 1989; Schiebel & Hemleben, 2005). However, the relationship between marine primary productivity and SNW for our targeted species varies according to interspecific and intraspecific diversity and thus different calcification responses to changing trophic conditions. Previous studies detect weak positive / negative correlations between chlorophyll *a* and SNW for symbiont-barren *G. bulloides* / symbiont bearing *G. elongatus* in the Atlantic Ocean (Aldridge et al., 2012; Weinkauf et al., 2016), while a reverse correlation is observed for those species in the Mediterranean Sea (Mallo et al., 2017). Evidence for a minor effect of varying productivity on the calcification response of planktic foraminifera is given by the fact that, despite opposing productivity signals during the second half of the 20th century (Figure 3.2b), we see consistent SNW decreases in both species at all three stations (Figures 3.2e; 3.3f).

Changes of the chemical test microenvironment due to photosynthetic activity also influences calcification of planktic foraminifera (Köhler-Rink & Kühl, 2005). Higher photosynthetic activity increases pH and reduces CO_2 concentrations near the shell, resulting in enhanced calcification rates (Spero, 1992). If enhanced stratification led to enhanced light availability during the 20th century, this would likely have increased SNW of planktic foraminiferal species associated with symbionts capable of performing photosynthesis, though this effect is evidently masked by the dominant role of [CO_3^{2-}] on calcification. Diagenetic processes can bias the significance of SNW

as a proxy for planktic foraminiferal calcification, as dissolution / precipitation of carbonates on tests might be interpreted as reduced / enhanced mass of planktic foraminiferal shells. Across all three western Mediterranean records (Figure 3.1), scanning electron microscope (SEM) images (Plate S3.1-S3.3) of both species *G. bulloides* and *G. elongatus* show approximately the same degree of dissolution from top to bottom core depth with minor surface corrosion and breakup of the surface layer structure of the test wall (Dittert & Henrich, 2000; Regenberg et al., 2013). Therefore, calcite saturation level of subsurface to bottom waters at the three core sites are expected to not have significantly changed, and weight loss of settling tests in the deep water column as discussed by Schiebel et al. (2007) may have been the same over the entire time interval discussed here. As western Mediterranean deep and bottom waters are supersaturated with regard to calcite (Álvarez et al., 2014; Millero et al., 1979; A. Schneider et al., 2007), dissolution at the sediment pore water interface is unlikely. The post-sapropel (<6 kyrs) western Mediterranean is a mesotrophic sea with limited changes and overall decreasing biological productivity over the past 150 years (Jimenez-Espejo et al., 2008; Pallacks et al., 2021). Accordingly, supra-lysoclinical dissolution as well as corrosive porewater conditions, which may infer post depositional test weight reduction in surface seafloor sediments through decomposing organic matter can be assumed absent (Tachikawa et al., 2008). This is in line with previous sediment trap and core top studies from the western Mediterranean Sea, reporting no signs of dissolution in fossil planktic foraminifera assemblages (Bárcena et al., 2004; Béjard et al., 2023; Rigual-Hernández et al., 2012). In contrast, early diagenetic calcite coating is reported for both species from core top samples at certain sites in the western and central Mediterranean Sea (Sabbatini et al., 2011; Van Raden et al., 2011). However, no signs of diagenetic overgrowth and secondary precipitated inorganic carbonates (e.g., inorganic calcite crusts, inorganic calcite crystals, overgrown pores) are present in the tests of *G. elongatus* and *G. bulloides* from the three core sites analyzed here (Plate S3.1-S3.3). Accordingly, due to the constant mild surface etching dissolution of similar magnitude of all tests observed across all three records, the relative foraminiferal SNW changes at the three core sites are expected

to result from changes in biogenic calcification at the sea surface rather than diagenetic processes during sedimentation.

Driven by industrial carbon dioxide emissions, enhanced anthropogenic CO_2 penetration into the western Mediterranean Sea and resulting reductions in pH and $[CO_3^{2-}]$ are shown to be the key drivers of planktic foraminiferal SNW loss during the 20th century (Figures 3.3a-f, S3.2). Reduced SNW of similar magnitude during the 20th century have been observed in the tropical Atlantic, Southern Ocean, the California Current System, and the western Mediterranean Sea, showing similar amplitudes of relative calcification decrease (Béjard et al., 2023; A. N. Davis et al., 2019; Moy et al., 2009; Osborne et al., 2020). Sea surface warming, productivity and solar activity changes are assumed to play only a negligible role, with rising SST and solar irradiance maxima potentially slightly attenuating the impact of anthropogenic CO_2 on planktic foraminiferal SNW. Accordingly, different oceanographic settings at the three selected core sites are responsible for the variability in 20th SNW trends (Text S3.3), while the effects of diagenetic processes biasing the planktic foraminiferal SNW signal can be ruled out.

3.3 Conclusion

Accelerated anthropogenically-induced surface water pH decline in the western Mediterranean Sea is confirmed by boron isotopes and drives decreasing SNW of planktic foraminiferal tests. Negative carbon isotope excursions during the IE in tests of the planktic foraminifera species *G. elongatus* and *G. bulloides* display the signal of the Suess Effect – the anthropogenic CO_2-driven shift to lower $\delta^{13}C$ – and highlight the influence of anthropogenic emissions as the most important driver of foraminiferal calcite mass decline. Alkenone-derived SST and instrumental temperature records show unprecedented anthropogenic sea surface warming, that potentially mitigates this effect slightly. This basin-wide, interspecies multiproxy approach, covering multidecadal to centennial time scales, thus yields a much-needed high-confidence, low-variability assessment of the impacts of anthropogenic climate change on key marine species, in a critically sensitive region.

3.4 Methods

3.4.1 Material

The study is based on high resolution multicore records collected in the central and western Mediterranean Sea with a MC400-Multicorer system during the MedSeA cruise (Mediterranean Sea Acidification in a changing climate) on 2nd May to 2nd June 2013 onboard the R/V Àngeles Alvariño. Core sampling of MedSeA-S3-c1 and MedSeA-S23-c1 was previously described in (Pallacks et al., 2021). MedSeA-S7-c2 was retrieved in the Strait of Sicily (Lat. 37.7080° N, Long. 12.40553° E) at a water depth of 263 m, with a core length of 46.5 cm, sliced every centimeter.

3.4.2 Age Model development

Age models of cores MedSeA-S3-c1 and MedSeA-S23-c1 were estimated through a combination of radiocarbon and radionuclide dating, previously described in (Pallacks et al., 2021). The age model of MedSeA-S7-c2 (Table S3.2; Text S3.4) was estimated through radionuclide analysis, determining total ^{210}Pb activity by measuring its alpha-emitter daughter nuclide ^{210}Po, following the methodology described in (Sánchez-Cabeza et al., 1998). ^{209}Po was added as an internal tracer, before sample aliquots of 200–300 mg were totally digested in acid media by using an analytical microwave oven and Po isotopes plated on silver discs in HCl 1N at 70° C while stirring for 8 h. Po emissions were subsequently counted through α-spectrometers equipped with low background silicon surface barrier (SSB) detectors (EG&G Ortec) for $4x10^5$ seconds. The difference between total ^{210}Pb and the constant ^{210}Pb at depth describes the concentration of excess ^{210}Pb, which was used to estimate maximum mean sediment accumulation rates and the age-depth model by applying the Constant Flux : Constant Sedimentation (CF:CS) model (Krishnaswamy et al., 1971; Robbins, 1978). The activities of ^{137}Cs (661 keV) were determined by γ spectrometry in a coaxial high-purity Ge detector (EG&G Ortec) calibrated with the SRM-4276 solution standard supplied by the National Institute of Standards and Technology. The quality of the results determined by gamma and alpha spectrometry was evaluated by participation in IAEA proficiency tests and continuous analysis of certified and replicate materials.

3.4.3 Planktic foraminifera

Samples were dried at 60° C for approximately 24 hours to obtain dry bulk sediment mass. After washing over a 63 µm screen using distilled Elix water, the size fraction larger than 63 µm was oven dried at 60° C for 1−2 hours. Samples were dry sieved and divided by a riffle splitter (comparable to an ASC Sample Microsplitter, ASC Scientific) at the chosen size fractions: 150–250 µm, 250–315 µm, and > 315 µm. Total test accumulation rate was obtained by counting of more than 300 specimens in the >150 µm size fraction in all samples.

Taxonomic analysis of planktic foraminiferal tests was performed on core MedSeA-S7-c2 by visual identification using a binocular stereo microscope (magnification 10x–20x) and a bifurcated illuminator. Classification of foraminiferal target species was based on (Schiebel & Hemleben, 2017), distinguishing between *Globigerina bulloides* (d'Orbigny 1826) and the two morphotypes of *Globigerinoides ruber* (d'Orbigny 1839), *Globigerinoides elongatus* and *G. ruber albus* (Morard et al., 2019).

3.4.4 Size Normalized Weight

In order to obtain the calcite mass of planktic foraminiferal tests, a size related measure of test wall thickness and density – the Size Normalized Weight (SNW) – was obtained, which can be calculated by means of Eq. (1):

$$SNW = C + \frac{C \times (100 - \frac{100}{B} \times A)}{100}$$

Where C is the species average mass (µg) for each sample, A represents the average minimum Feret diameter (µm) for each sample and B is the average minimum Feret diameter (µm) of all specimens of one species of all samples. The equation (Eq. 1) includes the term to account for the relative SNW changes of the same species. Our methodology for measuring SNW is based on the sieve-based weight (SBW) technique, however, our approach also integrates measurements of individual test sizes in SNW estimations, a parameter used for the measurement-based weight (MBW) technique (Beer et al., 2010a). All specimens of a single sample are weighed

together, while the average test size per sample is calculated by the minimum Feret diameter of each individual specimen. The SNW average standard error for each station (Alboran Sea: 7.0%; Balearic Sea: 8.3%; Strait of Sicily: 8.6%) is below the methodological 11% error reported by Beer et al. (2010a). Narrowing down the size fraction of analyzed tests to 250–315 µm ensured sufficient numbers of adult specimens which are large enough for SNW measurements. By applying the test weight size-normalization technique described above, we were able to factor out size related mass changes, mainly influenced by temperature variations.

SNW was determined for *G. elongatus* and *G. bulloides*. Bulk population measurements were performed on as many tests as available but not more than 10 and at least two specimens per sample per species, representing a total of 1,990 analyzed tests out of 224 samples included in this dataset. Selected tests were free of visible clay particles or organic matter and abnormally formed specimens were excluded from analysis. We weighed selected specimens together by triplicate with a Sartorius CP2P microbalance at Universitat Autònoma de Barcelona (UAB) and a Mettler Toledo XP6U Ultra Micro Balance at Max Planck Institute for Chemistry (MPIC) in Mainz, Germany, in environmentally controlled weighing rooms. Tests were positioned umbilical side up, photographed with a Canon EOS 650 D camera device attached to a Leica Z16 AP0 at UAB and with an Olympus UC90 attached to an Olympus SZY16 stereoscope at MPIC to measure the minimum Feret diameter of each individual test, using the software ImageJ 1.53k (C. A. Schneider et al., 2012) and Olympus Stream Essentials 2.1. After measuring mean weight and mean minimum Feret diameter we calculated SNW for each sample using Eq. (1).

3.4.5 Biomarkers

Alkenones (heptatriaconta-8E,15E,22E-trie2-one and heptatriaconta-15E,22E-die2-one) of core MedSeA-S7-c2 were extracted from sediments, purified using organic solvents and quantified with a Varian gas chromatograph Model 450 equipped with a septum programmable injector, flame ionization detector and a CPSIL-5 CB column (coated with 100% dimethyl siloxane; film thickness of 0.12 µm; L(m) * ID(mm) * OD(mm): 50 * 0.32 * 0.45). Hydrogen was the carrier gas (2.5 mL min− 1).

Concentrations were determined using n-hexatriacontane ($CH_3(CH_2)_{34}CH_3$) as an internal standard. Absolute concentration errors were below 10% (resolution between the alkenones from 1.5 to 1.7). Reproducibility tests showed that uncertainty in the $U^{k'}_{37}$ determination is lower than 0.015 (ca. 0.5 °C) (Cacho et al., 1999; Martrat et al., 2004; Martrat et al., 2014; Pallacks et al., 2021, this study) confirming the precision of the paleothermometry tool (Eglinton et al., 2001). SST reconstructions were based on the global calibration of Conte et al. (2006), with a standard error on surface sediments at 1.1 °C.

3.4.6 Stable isotope measurements

For chemical analysis, adult specimens were selected from a narrow size range (250−315µm) to minimize uncertainty in paleoceanographic interpretation due to vital effects, following suggestions by Spero and Lea (1996).

3.4.6.1 3.4.6.1 $\delta^{13}C$ and $\delta^{18}O$

Bulk population measurements, including 5−10 specimens per species sample, were performed on *G. elongatus* and *G. bulloides*. Sample weight was determined through a Mettler Toledo XP6U Ultra Micro Balance at MPIC. Selected tests were crushed and soaked in ultrapure water (Milli-Q), before ultrasonication for up to 20 seconds, to remove clay contamination.

Samples were analyzed on a Thermo Delta V mass spectrometer equipped with a GASBENCH preparation device. ~8−50 µg of $CaCO_3$ sample, placed in a He-filled 4.5 ml exetainer vial was digested in water-free H_3PO_4 at a temperature of 70 °C. Subsequently the CO_2-He gas mixture was transported to the GASBENCH in Helium carrier gas. In the GASBENCH, water vapor and various gaseous compounds were separated from the He-CO_2 mixture prior to sending it to the mass spectrometer in nine separate peaks. Isotope values of these individual peaks were averaged and reported as $\delta^{13}C$ and $\delta^{18}O$ relative to V-PDB. A total of 20 replicates of two in-house $CaCO_3$ standards were analyzed in each run of 55 samples. $CaCO_3$ standard weights were chosen so that they span the entire range of sample weights of the samples. After correction of isotope effects related to sample size the reproducibility of these standards is typically better than 0.1 ‰ (1SD) for $\delta^{18}O$ and 0.1 ‰ (1SD) for $\delta^{13}C$.

Samples of 8 to 3µg of $CaCO_3$ were analyzed on the same equipment using a cold trap technique that analyzes the entire sample in one single peak (Fiebig et al., 2005; Vonhof et al., 2020). With this setting, 30 $CaCO_3$ standards were analyzed in each run of 30 samples. $CaCO_3$ standard weights were chosen so that they span the entire range of sample weights of the samples. Reproducibility of these <8 µg standards with the cold trap technique, after sample size correction, is typically better than 0.1 ‰ (1SD) for $\delta^{18}O$ and 0.1 ‰ (1SD) for $\delta^{13}C$.

3.4.6.2 $\delta^{11}B$

For boron isotope analysis, samples of *G. ruber* (250−315 µm) were prepared in a class 100 clean lab at the University of St Andrews STAiG laboratories. The two morphotypes of the species were analyzed separately. Samples were first crushed between two glass slides before transferring to acid cleaned centrifuge tubes in preparation for clay removal by ultrasonication. This was followed by oxidative cleaning in 1% hydrogen peroxide buffered with 0.1 M NH_4OH and a weak acid leach in 0.0005 M distilled HNO_3 according to established protocols (Barker et al., 2003; J. W. B. Rae et al., 2011). After addition of 100 µl boron-free Milli-Q, samples were dissolved by incremental addition of 0.5 M distilled HNO_3 (total volume of acid per sample 30−50 µl). A 5% cut of the dissolved sample was analyzed by ICP-MS for a suite of trace elements (Table S3.3) including Mg/Ca on an Agilent 8900 following Foster (2008) and J. W. B. Rae et al. (2011) with the addition of trace hydrofluoric acid in the wash to improve washout (Zeebe & Rae, 2020). Samples were run alongside matrix-matched bracketing and consistency standards to monitor long-term instrument reproducibility which is reported at 95% confidence (2SD). Low Al/Ca in all samples confirms the absence of residual clays. Elevated Mn/Ca was recorded in one sample but it does not display elevated Mg/Ca or any other anomalous trace element or isotopic signal.

After trace element analysis, a few samples with low boron concentrations, as determined from B/Ca, meant it was necessary to combine adjacent dissolved samples in MedSeA-S7-c2 core in order to reduce $\delta^{11}B$ uncertainty (Table S3.4). Boron was isolated from the sample matrix using boron-specific Amberlite IRA 743 resin (Kiss,

1988; Lemarchand et al., 2002) using a batch method. For this technique, 2 ml centrifuge tubes containing 50 µl of resin were pre-cleaned by addition and removal of 1 ml 0.5M HNO_3 (repeated 3 times) and 1ml boron-free Milli-Q (repeated twice) and then pre-conditioned with 100 µl 0.1M ammonium acetate buffer at pH 8.5. Before loading, the sample was first buffered to pH 5 with 0.1M ammonium acetate. After pipetting onto the resin, the tubes were agitated on a VWR mini vortex and the solution pipetted off after the resin settled. Following rinses with boron free Milli-Q water, the concentrated sample was eluted in 500 µl 0.5M distilled HNO_3 and the boron isotopic composition analyzed by MC-ICPMS with sample-standard bracketing against NIST 951 according to methods described by (Foster, 2008; J. W. B. Rae et al., 2011). Addition of Hydrofluoric acid at 0.3 M helped to improve washout and reduce boron evaporation (Zeebe & Rae, 2020). Matrix matched carbonate consistency standards were run alongside samples to monitor reproducibility which is ± 0.23 ‰ (2SD).

3.4.7 pH Calculations

3.4.7.1 CO2SYS

To estimate unknown variables in the seawater marine carbonate system, we used the CO2SYS program (version 2.0) (Lewis & Wallace, 1998; Pierrot et al., 2006). Through a set of given input conditions (e.g., temperature, salinity, atm. CO_2 concentration), this program can estimate the remaining unknown variables of a two "master" carbonate system (TA, DIC, pH, pCO_2). We estimated surface ocean pH and carbonate ion concentrations for the three study sites, using seawater pCO_2 and total alkalinity (TA). TA was assumed constant over the last century, accounting for 2400 µmol/kgSW in the Alboran Sea (Cossarini et al., 2015), 2478 µmol/kgSW in the Strait of Sicily (A. Schneider et al., 2007), and 2550 µmol/kgSW in the Balearic Sea (Gemayel et al., 2015). Surface seawater pCO_2 was derived from temperature, salinity and pressure dependent solubility coefficient (K_0) following the formulation of Weiss (1974) and atmospheric CO_2 measurements from an interpolated stack including the Mauna Loa time series (Tans & Keeling, 2020) and reconstructed CO_2 concentrations (Bauska et al., 2015; Friedli et al., 1986). Time-specific K_0 values were determined as input conditions for down core calculations using surface pressure, SST and salinity

for each study location. SST was based on alkenone ($U^{k'}_{37}$) derived paleo estimates at each study location (Incarbona et al., 2016; Pallacks et al., 2021) and salinity was defined as the constant mean (1950–2019 CE) of Hadley EN4 (version EN.4.2.2) subsurface salinity objective analysis (Good et al., 2013). Constants for our CO2SYS carbonate system estimations were the dissociation constant (K_1 and K_2) defined by (Mehrbach et al., 1973), refitted to seawater scale by (A. G. Dickson & Millero, 1987), the dissociation constants K_{HSO4} and K_B according to (A. G. Dickson, 1990), and the chlorinity relationship and boron concentration based on (Uppstrom, 1974).

3.4.7.2 Boron isotope transformation

To calculate pH, the $\delta^{11}B$ of *G. ruber albus* and *G. elongatus* was first converted to seawater $\delta^{11}B_{borate}$ using the calibration of (Henehan et al., 2013) for the 250−300 µm size fraction:

$$\delta^{11}B_{borate} = (\delta^{11}B_{foram} - 9.52 \pm 1.51)/(0.60 \pm 0.08)$$

The boric acid dissociation constant is determined by both salinity and temperature and thus calculated pH can be susceptible to variations in these assigned values. Salinity was set at modern levels (37 PSU) for the region and temperature was calculated from Mg/Ca using the species specific calibration for *G. ruber* from (W. R. Gray et al., 2018).

$$Mg/Ca = 0.97 \pm 0.50 \times \exp(0.063 \pm 0.019 \times T)$$

The pH derived from Mg/Ca temperatures were compared to those from temperatures determined from Hadley, $U^{k'}_{37}$ and $\delta^{18}O$ SST in (Table S3.4). A sample depth of 25 m was given to approximate the upper habitation depth of the species below the sea surface (Pujol & Grazzini, 1995).

3.4.8 Statistical analysis

3.4.8.1 General additive model

Statistical analysis has been performed using the statistical software R (R Core Team, 2023). General additive models (GAM) have been used in paleoenvironmental time series as a superior alternative tool to conventional statistical trend estimations

(Simpson, 2018). We used a GAM to better show the basin wide, interspecies specific change in SNW and $\delta^{13}C$, and western Mediterranean SST changes. The complex, non-linear GAM fits as a smoothed function, which allows us to identify the period of significant SNW, $\delta^{13}C$ and SST change based on proper accounting for model uncertainty. The general and applied mathematical form of the general additive model can be described as:

$$y_i = \beta_0 + f(x_i) + \varepsilon_i \text{ where } \varepsilon_i \sim N(0, \sigma^2)$$

$$SNW = 4.081e^{-15} + 6.997 + \varepsilon_i \text{ where } \varepsilon_i \sim N(0, \sigma^2)$$

$$\delta^{13}C = 0.02111 + 6.238 + \varepsilon_i \text{ where } \varepsilon_i \sim N(0, \sigma^2)$$

$$SST = -0.02993 + 8.033 + \varepsilon_i \text{ where } \varepsilon_i \sim N(0, \sigma^2)$$

SNW and $\delta^{13}C$ values were standardized and merged, combining *G. bulloides* and *G. elongatus* at all three stations. Standardized SST is based on alkenone measurements and the calculated mean from HadISST dataset across the three stations. Uncertainty in the estimated model fits were addressed through 95% confidence intervals, after confirming gaussian error distribution via histogram plot, Q-Q plot and Kolmogorov-Smirnov test for standardized datasets of SNW (p-value=0.5501), $\delta^{13}C$ (p-value=0.1738) and SST (p-value=0.7126). Additionally, a GAM fit was applied (Wood, 2011), by means of the the *mgcv* package (version 1.8.42). To avoid under smoothing of the fit, the smoothing term was calculated using restricted maximum likelihood (Reiss & Todd Ogden, 2009; Wood et al., 2016).

3.4.8.2 Regression analysis

To quantify changes of SNW and $\delta^{13}C$ during the 20th century, linear regression analysis was applied including all available data points post 1900 CE. Estimations of SNW and $\delta^{13}C$ (negative anthropogenic carbon isotope excursions; nCIEs) change are defined by the difference between 1900 CE and 2013 CE, based on the regression model accounting for statistical significance (Figure S3.1, S3.2). To determine statistically significant relationships between the explanatory variable (SNW) and the independent variables (productivity based on species composition and abundance

changes, SST based on alkenone and HadISST data sets, pH calculated from pCO_2 and total alkalinity on CO2SYS, $\delta^{13}C$ based on carbon isotopes) we performed multiple linear regression analysis for time windows prior (pre-Industrial Era) and post 1800 CE (Industrial Era). To generate evenly spaced time series, we standardized data for each station and parameter before combining station data for each parameter by interpolating non-linear GAM fits (method see above) using generalized cross-validation (GCV) method for smoothing parameter estimation to avoid over smoothing of the fit. Goodness of the fit for each parameter is shown through deviance explained (Table S3.5). Due to high collinearity, we have removed $\delta^{13}C$ from the multiple linear regression model prior 1800 CE, and pH from the model including data post 1800 CE. Both parameters are highly correlated particularly during the Industrial Era as the $\delta^{13}C$ signals mirrors the input of anthropogenic CO_2, resulting in pH decrease (see discussion). The conditions of application required for the multiple linear regression analysis have been verified by using *performance* package (version 0.10.3). It can be assumed that there is no Multicollinearity since all parameters included in the model show a Variance Inflation Factor (VIF) below ten. Information on multiple linear regression models and their significance values can be found in the supplementary material (Table S3.6-3.7), confirming a significant correlation between independent parameters and the explanatory variable, and substantiating the effect of ocean acidification on SNW.

3.5 Supplementary Material

3.5.1 Alkenone derived SST: mid-20th century cooling and recent warming trends (Text S3.1)

The mid-20th century cooling in the Mediterranean (Lionello et al., 2006), is observed through instrumental measurements (HadISST) and Mediterranean paleorecords (Pallacks et al., 2021; this study) at the three study sites. The global surface temperature decline between 1940 and 1975 CE, is supposed to be a consequence of global dimming as a result of enhanced natural and anthropogenic sulfate emissions during that time (Hegerl et al., 2018; Rasool & Schneider, 1971), and is well captured by the alkenone derived SST measurements in the Strait of Sicily. The shift of the

warming onset by around five years, might be due to age model uncertainty or the higher specific heat capacity of water, resulting in faster warming of the atmosphere than the oceans. Additionally, the alkenone derived warming of 0.048 K yr^{-1} at the Strait of Sicily is within error of warming rates observed for the entire Mediterranean (0.041 ± 0.006 K yr^{-1}, as seen by satellite datasets covering the time period from 1982 to 2018 CE (Pisano et al., 2020), or slightly higher than warming rates derived by globally available products such as the HadISST datasets (0.014 K yr^{-1} for the Strait of Sicily from 1993 to 2011). The offset between instrumental and alkenone derived SST of approximately 1.5 K, might be caused by calibration uncertainty, given that data coverage is low in the central and eastern Mediterranean (Conte et al., 2006), though the main trends are reproduced.

To further explore the results, test accumulation rates of foraminifera and alkenone concentrations are compared. Test accumulation rate in the Strait of Sicily ranges between 3 to 16 (# cm^{-2} yr^{-1}), which is slightly lower than in the Balearic (16 to 44 # cm^{-2} yr^{-1}) and Alboran (28 to 56 # cm^{-2} yr^{-1}) records (Pallacks et al., 2021), reflecting differences in surface chlorophyll-a values at the three study sites (Figures 3.2b; Table S3.8). Average alkenone concentration rates are highest in the Strait of Sicily (42.72 ng yr^{-1} cm^{-2}), compared to the Balearic (12.24 ng yr^{-1} cm^{-2}) and Alboran Sea record (5.26 ng yr^{-1} cm^{-2}). It suggests diverse productivity patterns between the three sites, in line with test accumulation rates. Higher values in the Strait of Sicily might be explained by the shallow core location (depth: 263m), in comparison with the deeper Balearic and Alboran sites (depths: 1156m and 1137m, respectively) as alkenone concentrations decrease with depth in the water column (Müller & Fischer, 2001; Yamamoto et al., 2007).

3.5.2 $\delta^{11}B$ derived pH in the Strait of Sicily and Alboran Sea (Text S3.2)

Analyzed *G. ruber albus* tests in the Strait of Sicily core (8.045 ± 0.022 (1830 CE) to 7.82 ± 0.031 (2007 CE), show slightly lower modern pH values compared to direct measurements (pH = ~7.95) conducted close by in 2011 (Álvarez et al., 2014; Hassoun et al., 2015). Also, results derived from *G. elongatus* tests in the Alboran core (7.75 ± 0.035 (1697 CE) to 7.62 ± 0.047 (1995 CE)), show significantly lower pH values,

when compared to recent measurements (7.95 ± 0.04) in that area (Flecha et al., 2019; Hassoun et al., 2015; Jiménez-López et al., 2021). This could be explained by foraminiferal vital effects. The offset from seawater and foraminiferal carbonate is not constant (Foster & Rae, 2016; James W. B. Rae, 2018), as foraminifera manipulate pH within their microenvironment (Glas et al., 2012; Toyofuku et al., 2017), influencing the pH signature in planktic foraminifera tests. Alternatively, while lower pH values recorded in *G. ruber* carbonate cannot be explained by differences in habitat depth of each morphospecies, offsets with direct measurements could be linked to vertical transport of deeper water depleted in pH. The Alboran core site is situated in an upwelling cell (Garcia-Gorriz & Carr, 2001), transporting bottom water, low in pH and carbonate ion concentration, to the surface. Surface carbonate chemistry is also influenced by Atlantic water inflow. Modern pH values as low as 7.75 have been measured in upwelling regions on the California shelf (Chan et al., 2017; Feely et al., 2008) or on the East Australian shelf where pH dropped by 0.12 units during upwelling events in a matter of hours (Schulz et al., 2019). However, pH levels of Mediterranean bottom waters as well as Atlantic inflow are not low enough to explain the offsets between directly measured and reconstructed pH values (Flecha et al., 2019; Jiménez-López et al., 2021).

3.5.3 Species specific size normalized weight (SNW) variability across stations (Text S3.3)

The basin wide 20th century SNW drop in the western Mediterranean across all stations (Alboran and Balearic Sea, Strait of Sicily) and species (*G. bulloides* and *G. elongatus*) is consistent, although the amplitude of reported trends show some variability. Differences in planktic foraminiferal calcification response to CO_2 changes are associated with differences in oceanographic settings and species ecology. The lowest species average SNW (Figure S3.4) and the most pronounced 20th century SNW loss (Figure S3.3, -29.9%) are reported in the Alboran Sea core. Here, low pH and carbonate ion concentrations (Figure S3.2), due to enhanced upwelling and Atlantic water influence (see discussion Text S3.2), can be suggested to be the main driver for the strongest SNW loss among the three stations (C. V. Davis et al., 2017; Marshall et al., 2013; Moy et al., 2009; Osborne et al., 2016). High sea

surface temperatures and productivity increase during 20th century might be responsible for a moderate SNW decline in the Strait of Sicily (Figure S3.3; -12.8%), as enhanced temperature and productivity can increase foraminiferal SNW (Aldridge et al., 2012; C. V. Davis et al., 2017; Gonzalez-Mora et al., 2008; Mallo et al., 2017; Marshall et al., 2013; Osborne et al., 2016; Weinkauf et al., 2016), thus mitigating SNW decrease in the Strait of Sicily. The species average SNW change is less distinctive in *G. bulloides* (-17.0%) than in *G. elongatus* (-25.2%). The latter lives and calcifies closer to the sea surface (Rebotim et al., 2017; Stainbank et al., 2019), thus it might be more affected by CO_2 ingress into surface waters. Stronger influence of anthropogenic CO_2 for shallower dwelling species is also indicated through the carbon isotope signature of their tests (*G. elongatus*: -0.68 ‰; *G. bulloides* -0.51 ‰; Figure S3.1). This is also supported by less pronounced SNW declines of *G. bulloides* at the Strait of Sicily and Balearic Sea stations, as subsurface pH is higher at inner western Mediterranean regions compared to the Alboran Sea which is influenced by inflow of low pH Atlantic water (Álvarez et al., 2014; Cossarini et al., 2015; Flecha et al., 2019; Gemayel et al., 2015; A. Schneider et al., 2007).

3.5.4 Results and discussion: Age Model MedSeA-S7-c2 at Strait of Sicily (Text S3.4)

Concentrations of $^{210}Pb_{tot}$ decrease with core depth, reaching a constant average value ($^{210}Pb_{sup}$) of ~20 ± 2 Bq kg-1 at ~25-26 cm core depth (Table S3.4). Applying the CF:CS model, we estimate a maximum mean mass accumulation rate (MAR) of 0.16 ± 0.010 g cm^{-2} yr^{-1} and a sedimentation rate (SR) of 0.25 ± 0.02 cm yr^{-1}. The age model presented in this study considers that the MAR and SR obtained during the 20th century using the ^{210}Pb technique can be extrapolated to the 19th century.

The $^{210}Pb_{tot}$ of the topmost sediment layer (259 ± 16 Bq kg^{-1}) is in range with results from other cores collected off-shore the coast of southern Sicily, ranging between 66 to 596 Bq kg^{-1} (Hassen et al., 2019; Incarbona et al., 2016). Our results are in good accordance with Holocene MAR and SR based on ^{210}Pb (Hassen et al., 2019; Incarbona et al., 2016) and radiocarbon dates (Cacho et al., 2001; Titschack et al., 2016). The higher sedimentation rates at our study site can be explained by shallower

water depth, as an inverse correlation between water depth and sedimentation rates is observed in the Mediterranean Sea (Hassen et al., 2019; Zuo et al., 1997).

The robustness of the age-model is further supported through changing parameters independent from sedimentation rate, as alkenone derived SST and the instrumental temperature record (HadISST; Figure 3.2a), which coincides with main temperature changes recorded independently. In addition, the ^{137}Cs measurement (Table S3.2) of the sediments, as a marker of the record of the nuclear testing program of the 1960s and the 1986 Chernobyl accident (Garcia-Orellana et al., 2009), showed a nearly perfect agreement with the dates obtained through ^{210}Pb. Therefore, the accordance with other sediment cores from the same area and the validation through independent parameters SST and ^{137}Cs, emphasizes the representativeness of our results and supports the accuracy of the CF:CS chronology based on ^{210}Pb.

3.5.5 Figures

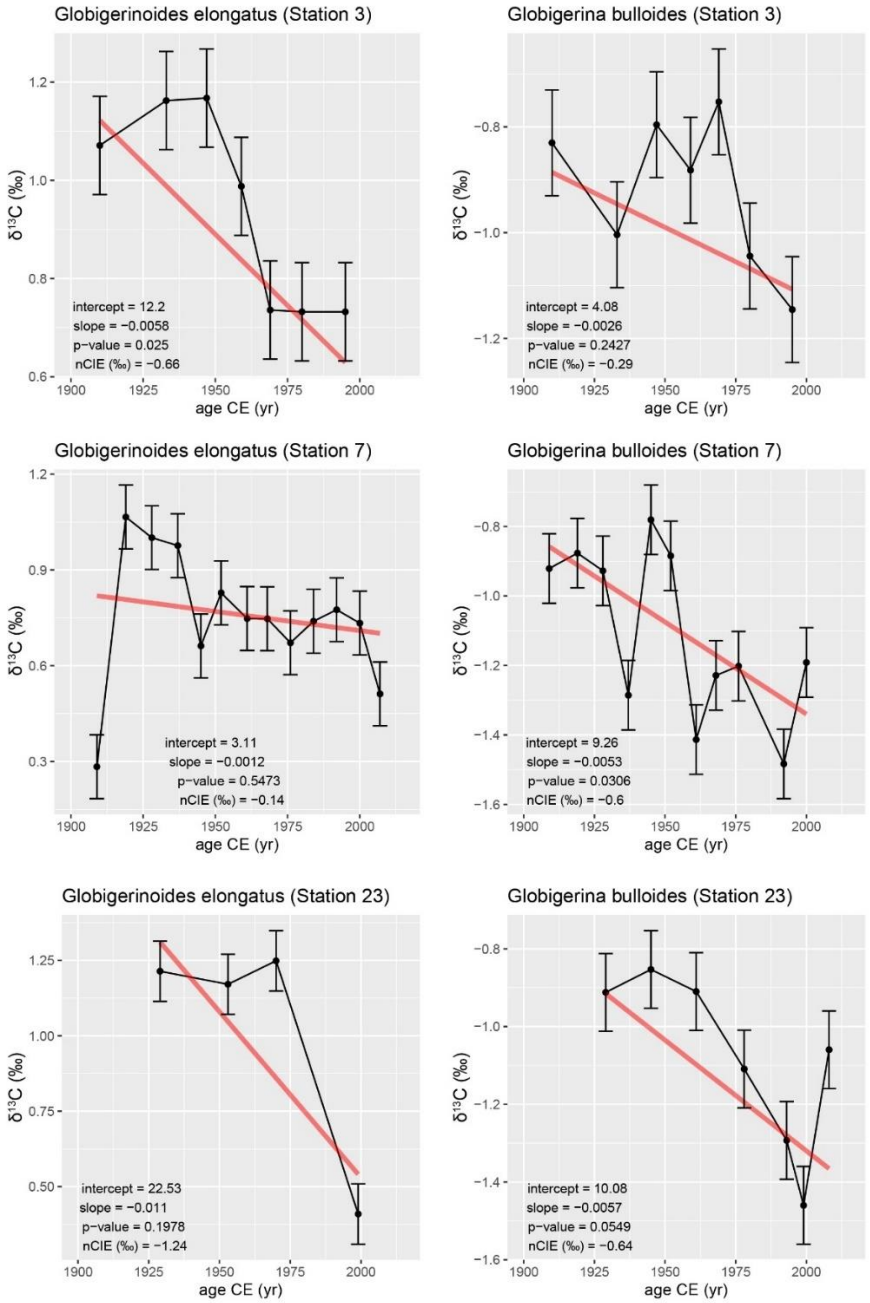

Figure S3.1: *Negative anthropogenic carbon isotope excursions (nCIE) in planktic foraminiferal tests at three Stations in the western Mediterranean Sea for G. elongatus (left) and G. bulloides (right) during the 20th century with error bars indicating 0.1 ‰ uncertainty (1SD level). A linear regression model (red line) is used to calculate nCIEs during the time period from 1900 CE to 2013 CE. Beside $\delta^{13}C$ changes, the intercept, slope and p-value of the regression model are shown. Station 3: Alboran Sea, Station 7: Strait of Sicily, Station 23: Balearic Sea.*

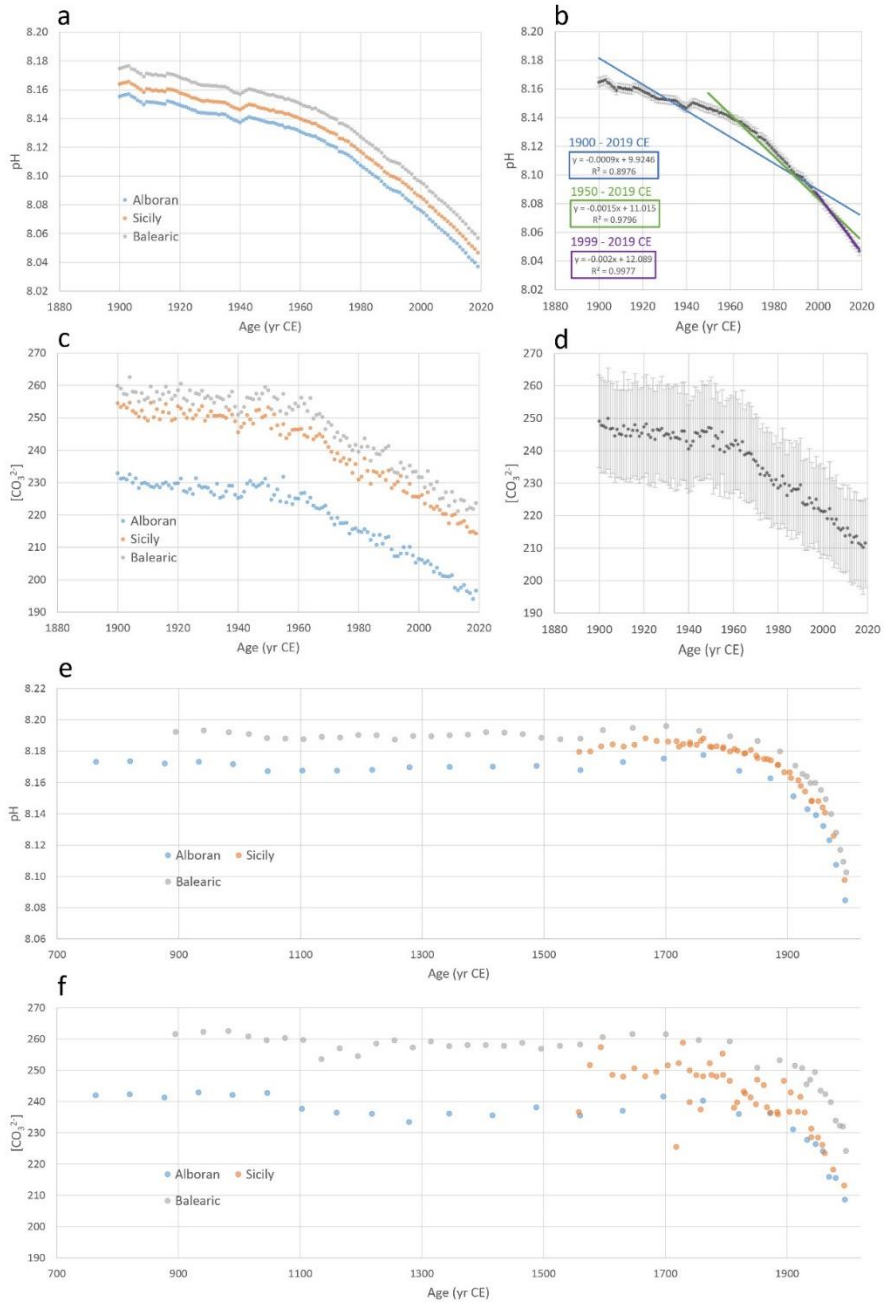

Figure S3.2: *Estimated changes in western Mediterranean surface water carbonate chemistry performed by CO2SYS program (version 2.0), assuming equilibration between surface seawater with constant alkalinity and atmospheric CO_2 (see Methods). (a,c,e,f) pH and [CO_3^{2-}] values for Alboran Sea (blue), Strait of Sicily (orange), Balearic Sea (grey). (b,d)Mean values for all three stations, error bars represented by standard deviations. Linear trends calculated for time periods 1900–2019 CE (blue); 1950–2019 CE (green), 1999–2019 CE (purple). (a-d) Estimates based on sea surface temperatures (SST) derived from HadISST data set; (e,f) Estimates based on alkenone derived SSTs (Incarbona et al., 2016; Pallacks et al., 2021).*

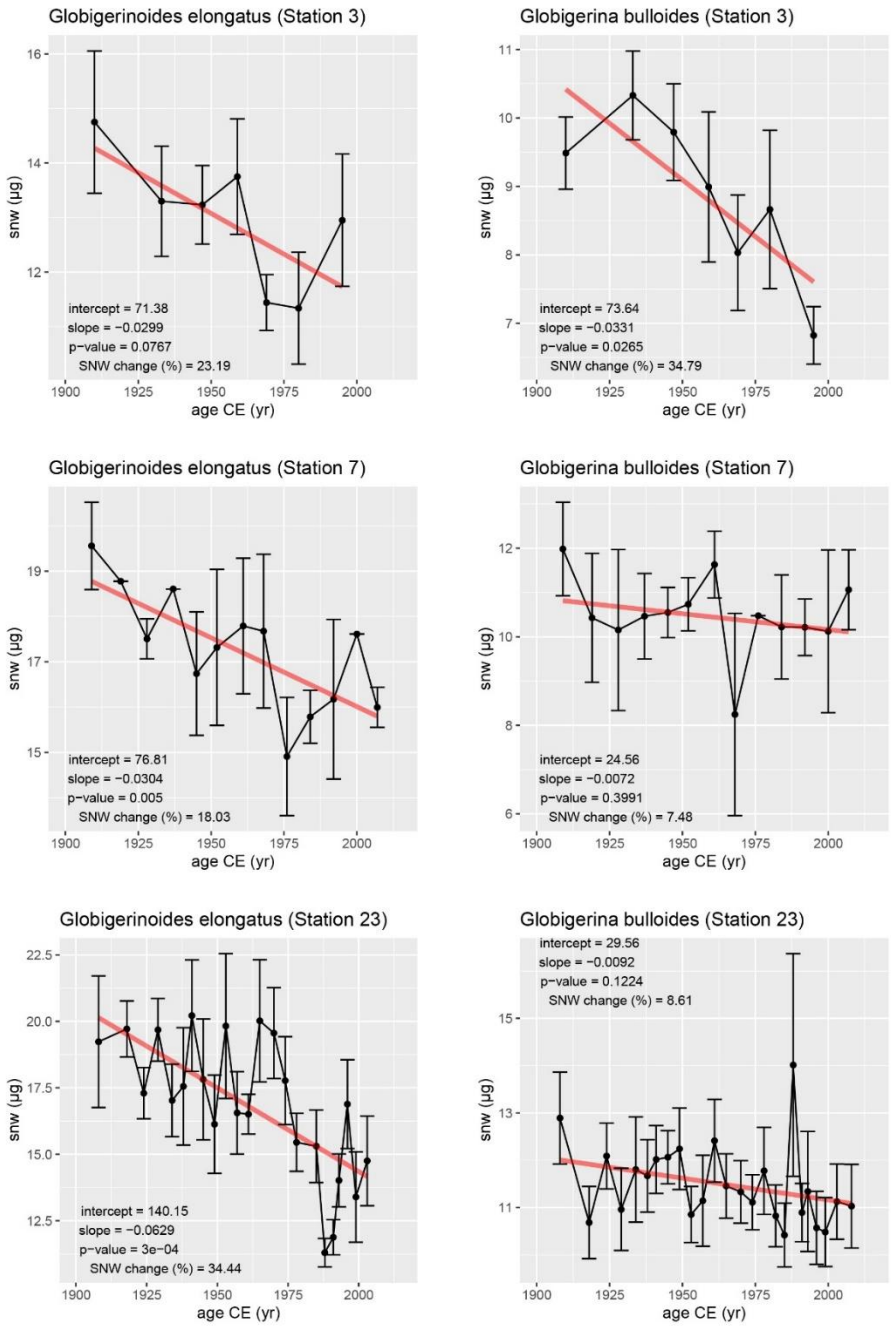

Figure S3.3: *20th century size normalized weight (SNW; µg) changes in planktic foraminiferal tests at three Stations in the western Mediterranean Sea for G. elongatus (left) and G. bulloides (right). A linear regression model (red line) is used to calculate 20th century SNW change during the time period from 1900 CE to 2013 CE. Beside SNW changes, the intercept, slope and p-value of the regression model are shown. Station 3: Alboran Sea, Station 7: Strait of Sicily, Station 23: Balearic Sea.*

Figure S3.4: *Boxplots of average size normalized weight (SNW) at each station for Globigerinoides elongatus (left) and Globigerina bulloides (right).*

3.5.6 Tables

Table S3.1*: Carbon chemistry and temperature effect on $\delta^{13}C$ of planktic foraminifera tests in the western Mediterranean Sea. Mean pH, $[CO_3^{2-}]$ and temperature changes from 1900 to 2019 yr CE are calculated based on CO2SYS estimates and HadISST records at all three stations. Species specific impacts on $\delta^{13}C$ of planktic foraminifera tests estimated by equations derived from laboratory culture and field experiments (Bemis et al., 2000; Bijma et al., 1999; Peeters et al., 2002; Spero et al., 1997).*

parameter		dataset	time period (yr. CE)	western Mediterranean	effect on $\delta^{13}C$		references
					G. bulloides	*G. elongatus*	
pH		*CO2SYS*	*1900-2019*	*-0.11*	*0.48 ± 0.03‰*	*0.24 ± 0.01 ‰ to 0.33 ± 0.02‰*	Peeters et al. (2002) Spero et al. (1997)
$[CO_3^{2-}]$	*µmol kg^{-1}*	*CO2SYS*		*37.1 ± 2.0*			Bijma et al. (1999)
SST	*°C*	*HadISST*	*1900 - 2019*	*1.10 ± 0.12*	*-0.11 ± 0.01‰*	*n.a.*	Bemis et al. (2000)

***Table S3.2**: Age controls for core MedSeA-S7-c2 (Strait of Sicily). Age model is derived through ^{210}PB and ^{137}Cs profiles. Ages for each sample depth are estimated by CF:CS model (see methods).*

Sample ID	section depth			density	^{210}Pb			^{137}Cs			Age		
	center	bottom	top		Total			Total					
		(cm)		(g cm^{-3})	(Bq kg^{-1})			(Bq kg^{-1})			(yr CE)		
MedSeA-St7-core2_0.5	0.5	0	1	0.39	258.7	±	16.0				2010	±	1
MedSeA-St7-core2_1.5	1.5	1	2	0.47	186.9	±	7.8				2007	±	1
MedSeA-St7-core2_2.5	2.5	2	3	0.51	204.9	±	9.1				2004	±	1
MedSeA-St7-core2_3.5	3.5	3	4	0.57	180.4	±	9.4				2000	±	1
MedSeA-St7-core2_4.5	4.5	4	5	0.51	197.7	±	8.0				1996	±	1
MedSeA-St7-core2_5.5	5.5	5	6	0.57	204.1	±	8.2	2.8	±	0.8	1992	±	1
MedSeA-St7-core2_6.5	6.5	6	7	0.52	188.7	±	9.9	4.4	±	0.3	1989	±	2
MedSeA-St7-core2_7.5	7.5	7	8	0.64	129.6	±	6.5	4.9	±	1.4	1984	±	2
MedSeA-St7-core2_8.5	8.5	8	9	0.62	118.7	±	5.9	4.2	±	1.0	1980	±	2
MedSeA-St7-core2_9.5	9.5	9	10	0.54	115.8	±	4.4	4.5	±	0.3	1976	±	2
MedSeA-St7-core2_10.5	10.5	10	11	0.59	110.8	±	6.8	3.8	±	1.2	1972	±	3
MedSeA-St7-core2_11.5	11.5	11	12	0.57	108.1	±	6.1	4.0	±	0.2	1968	±	3
MedSeA-St7-core2_12.5	12.5	12	13	0.55	119.0	±	4.5	3.2	±	0.2	1965	±	3
MedSeA-St7-core2_13.5	13.5	13	14	0.56	80.3	±	4.7	2.4	±	0.9	1961	±	3
MedSeA-St7-core2_14.5	14.5	14	15	0.60	76.7	±	4.5	1.9	±	0.9	1957	±	4
MedSeA-St7-core2_15.5	15.5	15	16	0.62	75.4	±	3.4	1.7	±	0.9	1952	±	4
MedSeA-St7-core2_16.5	16.5	16	17	0.41	59.5	±	3.7				1950	±	4
MedSeA-St7-core2_17.5	17.5	17	18	0.64	57.5	±	3.5				1945	±	4
MedSeA-St7-core2_18.5	18.5	18	19	0.61	42.5	±	2.3				1941	±	5
MedSeA-St7-core2_19.5	19.5	19	20	0.64	43.7	±	2.5				1937	±	5
MedSeA-St7-core2_20.5	20.5	20	21	0.55	40.5	±	2.0				1933	±	5
MedSeA-St7-core2_21.5	21.5	21	22	0.70	39.6	±	2.3				1928	±	6
MedSeA-St7-core2_22.5	22.5	22	23	0.59	36.0	±	2.0				1924	±	6
MedSeA-St7-core2_23.5	23.5	23	24	0.69	28.5	±	1.7				1919	±	6
MedSeA-St7-core2_24.5	24.5	24	25	0.63	27.9	±	1.6				1915	±	6
MedSeA-St7-core2_25.5	25.5	25	26	0.82	21.6	±	1.8				1909	±	7
MedSeA-St7-core2_26.5	26.5	26	27	0.56							1905	±	7
MedSeA-St7-core2_27.5	27.5	27	28	0.75							1900	±	7
MedSeA-St7-core2_28.5	28.5	28	29	0.76							1895	±	8
MedSeA-St7-core2_29.5	29.5	29	30	0.58							1891	±	8
MedSeA-St7-core2_30.5	30.5	30	31	0.68							1886	±	8
MedSeA-St7-core2_31.5	31.5	31	32	0.76							1881	±	9
MedSeA-St7-core2_32.5	32.5	32	33	0.50							1878	±	9
MedSeA-St7-core2_33.5	33.5	33	34	0.66							1873	±	9
MedSeA-St7-core2_34.5	34.5	34	35	0.58							1869	±	9
MedSeA-St7-core2_35.5	35.5	35	36	0.76							1864	±	10
MedSeA-St7-core2_36.5	36.5	36	37	0.64							1860	±	10
MedSeA-St7-core2_37.5	37.5	37	38	0.79							1854	±	10
MedSeA-St7-core2_38.5	38.5	38	39	0.75							1849	±	11
MedSeA-St7-core2_39.5	39.5	39	40	0.73							1844	±	11
MedSeA-St7-core2_40.5	40.5	40	41	0.65							1840	±	11
MedSeA-St7-core2_41.5	41.5	41	42	0.84							1834	±	12
MedSeA-St7-core2_42.5	42.5	42	43	0.58							1830	±	12
MedSeA-St7-core2_43.5	43.5	43	44	0.67							1825	±	12
MedSeA-St7-core2_44.5	44.5	44	45	0.90							1819	±	13
MedSeA-St7-core2_45.5	45.5	45	46	0.66							1815	±	13
MedSeA-St7-core2_46.5	46.5	46	47	0.67	19.5	±	1.2				1810	±	13

Table S3.3: *Trace element data for Station 3 (Alboran Sea) and Station 7 (Strait of Sicily) measured in planktic foraminiferal calcite tests of Globigerinoides elongatus and Globigerinoides ruber albus. Sample depths and specimens are the same as analyzed for boron isotopes.*

Station	3			7						
Depth (cm)	0.5	3.5	10.5	0.5	1.5	2.5	20.5	21.5	22.5	42.5
Age (yr CE)	1995	1959	1697	2010	2007	2004	1933	1928	1924	1830
Foraminifera species	*Globigerinoides elongatus*			*Globigerinoides ruber alba*						
Li/Ca (µmol/mol)	15.86	16.73	15.89	19.03	22.69	18.71	19.71	19.52	16.49	16.64
B/Ca (µmol/mol)	123.99	119.89	117.89	121.97	118.09	107.88	125.71	114.21	109.79	107.17
Na/Ca (mmol/mol)	6.17	6.37	6.53	6.77	6.59	6.42	6.67	6.62	6.65	6.47
Mg/Ca (mmol/mol)	2.61	2.76	2.87	2.83	3.29	2.42	2.65	2.93	2.57	2.75
Al/Ca (µmol/mol)	1.88	1.86	1.29	2.62	2.23	8.08	0.96	-0.02	0.89	-0.61
Mn/Ca (µmol/mol)	56.62	95.58	158.38	33.03	30.76	42.31	31.82	31.28	28.62	50.90
Sr/Ca (mmol/mol)	1.37	1.38	1.39	1.41	1.40	1.39	1.40	1.41	1.38	1.40
Cd/Ca (µmol/mol)	0.02	0.01	0.00	0.01	0.00	0.01	0.01	0.00	0.01	0.01
Ba/Ca (µmol/mol)	0.91	1.00	1.06	0.90	0.98	8.39	1.02	1.04	1.04	1.14
Nd/Ca (µmol/mol)	0.69	0.80	0.80	0.34	0.26	0.38	0.33	0.32	0.27	0.21
U/Ca (nmol/mol)	8.94	9.55	14.86	5.15	5.93	7.16	5.75	5.72	5.20	7.00

Table S3.4: *Comparison of pH estimations based on different temperature reconstructions. Mg/Ca temperatures using the W. R. Gray et al. (2018) calibration (this study), HadISST after Reynolds and Smith (1994) (Pallacks et al., 2021; this study), alkenone SST (Pallacks et al., 2021; this study), $\delta^{18}O$ SST for G. elongatus and G. bulloides calculated bayfoxr package, providing a global core top calibration (Malevich et al., 2019). Station 3: Alboran Sea, Station 7: Strait of Sicily.*

Station		3	3	3	7	7	7
Depth (cm)		0.5	3.5	10.5	0.5-2.5	20.5-22.5	42.5
Age (yr CE)		1995	1959	1697	2007	1928	1830
Mg/Ca	(°C)	*15.7*	*16.6*	*17.2*	*17.0*	*16.0*	*16.5*
	pH	*7.6*	*7.7*	*7.8*	*7.8*	*7.9*	*8.0*
	stdev	*0.0*	*0.0*	*0.0*	*0.0*	*0.0*	*0.0*
HadISST	(°C)	*18.8*	*18.3*	*n.a.*	*19.8*	*19.5*	*n.a.*
	pH	*7.6*	*7.7*	*n.a.*	*7.8*	*7.9*	*n.a.*
	stdev	*0.0*	*0.0*	*n.a.*	*0.0*	*0.0*	*n.a.*
alkenone	(°C)	*18.6*	*18.1*	*18.1*	*17.9*	*18.0*	*n.a.*
	pH	*7.6*	*7.7*	*7.7*	*7.8*	*7.9*	*n.a.*
	stdev	*0.0*	*0.0*	*0.0*	*0.0*	*0.0*	*n.a.*
$\delta^{18}O$ *G.elongatus*	(°C)	*17.3*	*17.2*	*n.a.*	*14.0*	*12.1*	*n.a.*
	pH	*7.6*	*7.7*	*n.a.*	*7.9*	*8.0*	*n.a.*
	stdev	*0.0*	*0.0*	*n.a.*	*0.0*	*0.0*	*n.a.*

Table S3.5: *Goodness of the GAM fit for each interpolated parameter indicated by deviance explained.*

	Deviance explained (%)	
	prior 1800 CE	past 1800 CE
pH	96.9	83.0
SST	55.9	69.9
Productivity	24.7	28.5
$\delta^{13}C$	46.5	66.2
SNW	43.1	64.7

Table S3.6: *Information on multiple linear regression model post 1800 CE including their significance levels.*

Parameter	Coefficient	SE	t value	p
(Intercept)	-0.24	0.02	-11.61	***
Productivity	0.20	0.06	3.70	***
SST	-0.39	0.05	-8.24	***
$\delta^{13}C$	0.54	0.02	23.33	***

Model: SNW = (Productivity $*$ 0.20) - (SST $*$ 0.39) + ($\delta^{13}C * 0.54$)

F-statistic: 751.2 on 3 and 173 DF, p-value: > 2.2e-16

R2: 0.9287; adjusted R2: 0.9275

significance code: <0.0001***; <0.001**; <0.01*

Table S3.7: *Information on multiple linear regression model prior 1800 CE including their significance levels.*

Parameter	Coefficient	SE	t value	p
(Intercept)	0.12	0.03	3.62	***
Productivity	0.02	0.01	2.08	*
SST	0.25	0.01	39.6	***
$\delta^{13}C$	0.41	0.06	7.3	***

Model: SNW = (Productivity $*$ 0.02) - (SST $*$ 0.25) + (pH $*$ 0.41)

F-statistic: 850.3 on 3 and 1033 DF, p-value: > 2.2e-16

R2: 0.7118; adjusted R2: 0.7109

significance code: <0.0001***; <0.001**; <0.01*

Table S3.8: *Alkenone raw data in core MedSeA-S7-c2 (Strait of Sicily). From the left: depth (cm below the seafloor); total planktic foraminiferal test accumulation rate (tests cm^{-2} yr^{-1}) in >150µm fraction; heptatriaconta-8E,15E,22E-trie2-one [C37:3me (ng g^{-1})] and heptatriaconta-15E,22E-die2-one [C37:2me (ng g^{-1})], long chain alkenone; $U^{k'}_{37}$, proxy indicator of sea surface temperature; SST (°C) derived from the relative proportion of the later ($U^{k'}_{37}$); SST estimation by using the calibration of Conte et al. (2006) including integrated production temperature SST = $(-0.957+54.293*(U^{k'}_{37})-52.894*(U^{k'}_{37})\text{^}2+28.321*(U^{k'}_{37})\text{^}3)$, coretop global, 1–30ºC, n=567, R2=0.97; error ±1.1°C (SST in °C).*

depth (cm)	test acc. rate (# cm^{-2} yr^{-1})	C37:3me (ng/g)	C37:2me (ng/g)	UK'37	SST (°C)
0.5	6480	91.3321	114.9540	0.5573	17.7736
1.5	11700	37.1372	53.5772	0.5906	18.4932
2.5	9040	216.4820	261.1089	0.5467	17.5440
3.5		253.6348	286.9932	0.5309	17.1955
4.5	10620	203.2673	238.3512	0.5397	17.3908
5.5	9220	240.5492	282.1828	0.5398	17.3930
6.5	6860	85.8433	92.6097	0.5190	16.9318
7.5		164.6264	190.2852	0.5361	17.3122
8.5	8980	163.8900	208.7534	0.5602	17.8374
9.5	6440	116.7335	135.6453	0.5375	17.3412
10.5	8200	136.7178	169.2247	0.5531	17.6837
11.5		137.2470	158.3447	0.5357	17.3021
12.5	6480	141.9070	176.6236	0.5545	17.7135
13.5	7390	131.6130	171.1601	0.5653	17.9482
14.5	10060	119.5989	154.7963	0.5641	17.9228
15.5		143.1633	174.6133	0.5495	17.6044
16.5	5580	33.8953	46.6279	0.5791	18.2450
17.5	5660	164.0459	219.4922	0.5723	18.0989
18.5	3220	53.2697	59.8389	0.5290	17.1555
19.5	8260	53.6401	64.3113	0.5452	17.5116
20.5	5370	169.5989	222.9050	0.5679	18.0043
21.5		n.a.	n.a.	n.a.	n.a.
22.5	6250	n.a.	n.a.	n.a.	n.a.
23.5	7690	n.a.	n.a.	n.a.	n.a.
24.5	5440	n.a.	n.a.	n.a.	n.a.
25.5		n.a.	n.a.	n.a.	n.a.
26.5	6620	n.a.	n.a.	n.a.	n.a.
27.5	7670	n.a.	n.a.	n.a.	n.a.
28.5	16210	n.a.	n.a.	n.a.	n.a.
29.5		n.a.	n.a.	n.a.	n.a.
30.5	3270	n.a.	n.a.	n.a.	n.a.
31.5	11530	n.a.	n.a.	n.a.	n.a.
32.5	6750	n.a.	n.a.	n.a.	n.a.
33.5		n.a.	n.a.	n.a.	n.a.
34.5	9870	n.a.	n.a.	n.a.	n.a.
35.5		n.a.	n.a.	n.a.	n.a.
36.5	10830	n.a.	n.a.	n.a.	n.a.
37.5		n.a.	n.a.	n.a.	n.a.
38.5	13110	n.a.	n.a.	n.a.	n.a.
39.5	11860	n.a.	n.a.	n.a.	n.a.
40.5	11340	n.a.	n.a.	n.a.	n.a.
41.5		n.a.	n.a.	n.a.	n.a.
42.5	12760	n.a.	n.a.	n.a.	n.a.
43.5	12180	n.a.	n.a.	n.a.	n.a.
44.5	14740	n.a.	n.a.	n.a.	n.a.
45.5		n.a.	n.a.	n.a.	n.a.
46.5	7050	n.a.	n.a.	n.a.	n.a.

Table S3.9: *Size normalized weight (SNW) raw data in core MedSeA-S3-c1 (Alboran Sea) analyzed in G. elongatus and G. bulloides. From the left: depth (cm below the sea floor); mean and standard deviation of planktic foraminiferal test mass (µg), minimum ferret (µm), and SNW (µg); N equals number of analyzed tests per sample depth.*

depth	mass				minimum feret				snw				N	
(cm)	(µg)				(µm)				(µg)					
	G.elong		*G.bull*		*G.elong*		*G.bull*		*G.elong*		*G.bull*		*G.elong*	*G.bull*
	mean	stdev	mean	stdev	mean	stdev	mean	stdev	mean	stdev	mean	stdev		
0.5	12.88	0.21	6.55	0.10	297.45	23.08	306.45	14.24	12.95	1.21	6.82	0.42	10	10
1.5	11.38	0.15	8.93	0.58	300.23	23.15	329.51	22.71	11.34	1.03	8.66	1.16	10	10
2.5	11.40	0.10	7.48	0.15	297.96	10.72	296.41	25.19	11.44	0.51	8.03	0.84	10	10
3.5	13.23	0.15	9.83	0.58	287.33	18.81	347.21	21.97	13.75	1.06	8.99	1.10	10	10
4.5	13.12	0.06	9.50	0.26	296.36	14.85	309.97	13.84	13.23	0.72	9.79	0.71	10	10
5.5	12.80	0.10	10.80	0.00	287.35	19.60	333.75	20.98	13.30	1.01	10.33	0.65	10	10
6.5	14.43	0.06	9.30	0.20	292.44	24.71	313.41	10.69	14.75	1.31	9.49	0.53	10	10
7.5	12.62	0.12	10.60	0.00	298.75	14.72	334.07	27.64	12.63	0.74	10.13	0.84	10	10
8.5	14.03	0.25	8.15	0.00	290.46	12.39	304.24	21.86	14.43	0.87	8.55	0.61	10	10
9.5	14.58	0.06			292.46	19.66			14.90	1.06			10	
10.5	15.82	0.12	9.83	0.06	295.09	24.11	317.43	17.58	16.02	1.43	9.91	0.61	10	10
11.5	15.62	0.06			310.83	14.65			15.00	0.76			10	
12.5	13.71	0.00	8.93	0.12	293.34	19.17	311.81	14.78	13.97	0.91	9.16	0.56	7	10
13.5	16.52	0.12			311.10	15.79			15.85	0.92			10	
14.5	13.67	0.06	8.02	0.06	291.23	11.93	314.29	13.96	14.02	0.63	8.16	0.42	10	10
15.5	14.67	0.06			295.39	15.07			14.84	0.82			10	
16.5	14.98	0.06	9.17	0.21	301.73	15.47	317.96	21.77	14.85	0.82	9.22	0.84	10	10
17.5	15.93	0.06			301.27	20.04			15.81	1.11			10	
18.5	16.13	0.06	10.37	0.06	298.92	17.15	318.44	12.55	16.14	0.98	10.41	0.47	10	10
19.5	13.93	0.15			294.58	20.64			14.14	1.15			10	
20.5	14.82	0.06	6.83	0.15	301.60	21.27	313.48	22.69	14.69	1.09	6.97	0.66	10	10
21.5	16.17	0.15			304.73	19.41			15.86	1.16			10	
22.5	17.43	0.15	9.57	0.15	308.88	21.08	323.49	20.81	16.86	1.30	9.46	0.76	10	10
23.5	15.03	0.12			312.38	19.31			14.36	1.00			10	
24.5	15.25	0.10	9.70	0.00	299.95	18.70	317.56	18.96	15.20	1.05	9.77	0.58	10	10
25.5	14.33	0.06			300.98	11.47			14.24	0.60			10	
26.5	14.03	0.06	10.92	0.23	299.98	16.38	341.56	20.21	13.99	0.82	10.18	0.82	10	10
27.5	14.30	0.10			300.51	18.63			14.23	0.98			10	
28.5	13.95	0.10	8.47	0.06	296.69	13.45	318.65	21.20	14.06	0.74	8.50	0.63	10	10
29.5	16.75	0.00			312.84	18.79			15.97	0.96			10	
30.5	13.72	0.06	9.23	0.15	295.93	16.48	327.26	20.52	13.86	0.83	9.02	0.71	10	10
31.5	16.40	0.00			298.95	19.37			16.40	1.06			10	
32.5	15.48	0.06	9.27	0.21	312.59	20.06	326.03	15.78	14.78	1.00	9.09	0.65	10	10

Table S3.10: *Size normalized weight (SNW) raw data in core MedSeA-S23-c1 (Balearic Sea) analyzed in G. elongatus and G. bulloides. From the left: depth (cm below the sea floor); mean and standard deviation of planktic foraminiferal test mass (µg), minimum ferret (µm), and SNW (µg); N equals number of analyzed tests per sample depth.*

depth (cm)	mass (µg)				minimum feret (µm)				snw (µg)				N	
	G.elong		*G.bull*		*G.elong*		*G.bull*		*G.elong*		*G.bull*		*G.elong*	*G.bull*
	mean	stdev	mean	stdev	mean	stdev	mean	stdev	mean	stdev	mean	stdev		
0.25	17.20	0.10	10.33	0.02	315.56		296.07	23.26			11.03	0.88		5
0.75	13.93	0.45	10.81	0.10	289.27	23.72	308.23	19.30	14.75	1.69	11.13	0.80	2	5
1.25	12.76	0.46	9.87	0.01	291.26	26.50	297.64	20.43	13.39	1.70	10.48	0.73	5	10
1.75	15.18	0.36	10.21	0.02	277.49	20.89	306.10	21.74	16.88	1.67	10.57	0.77	5	10
2.25	13.30	0.10	11.09	0.08	290.35	18.43	310.37	32.48	14.02	1.00	11.34	1.27	5	5
2.75	11.26	0.32	10.24	0.07	290.05	7.86	297.14	14.79	11.88	0.66	10.89	0.62	3	6
3.25	10.47	0.10	14.05	0.41	284.77	10.75	318.21	44.29	11.30	0.53	14.01	2.35	3	2
3.75	13.06	0.06	10.22	0.03	264.32	22.45	311.21	19.25	15.30	1.37	10.42	0.67	3	10
4.25	10.60	0.26	10.37	0.06	292.38		303.45	16.45			10.82	0.65		8
4.75	18.03	0.06	11.07	0.05	333.77	22.52	297.25	21.87	15.45	1.09	11.77	0.92	2	6
5.25	17.32	0.25	11.11	0.00	296.51	23.27	317.47	16.51	17.77	1.65	11.11	0.58	3	10
5.75	19.25	0.31	11.04	0.02	298.65	21.36	309.17	17.58	19.56	1.71	11.33	0.66	5	10
6.25	20.08	0.40	11.26	0.00	302.87	28.75	311.80	18.48	20.02	2.30	11.45	0.68	5	10
6.75	15.63	0.15	12.56	0.03	289.79	10.27	321.21	21.90	16.51	0.75	12.41	0.87	5	10
7.25	15.57	0.61	10.98	0.02	288.19	15.68	312.79	26.51	16.56	1.55	11.14	0.96	5	10
7.75	19.01	0.93	10.40	0.14	292.73	25.89	303.59	12.52	19.82	2.72	10.85	0.59	5	10
8.25	15.97	0.10	12.50	0.00	299.95	32.53	323.88	22.75	16.13	1.85	12.24	0.86	3	10
8.75	18.17	0.84	12.21	0.01	306.53	24.99	321.30	14.78	17.82	2.27	12.06	0.56	5	10
9.25	19.87	0.12	11.77	0.10	298.35	29.25	310.76	15.79	20.21	2.10	12.02	0.72	5	10
9.75	16.63	0.15	12.12	0.02	289.91	33.78	329.18	21.07	17.55	2.21	11.67	0.77	5	10
10.25	16.10	0.26	11.76	0.01	289.54	18.41	316.33	29.47	17.03	1.36	11.80	1.11	5	10
10.75	19.99	0.12	10.71	0.05	305.65	16.52	309.90	23.24	19.68	1.18	10.96	0.87	5	10
11.25	16.78	0.06	12.05	0.04	295.48	15.46	316.46	17.05	17.30	0.96	12.09	0.69	4	10
11.75	20.02	0.17	10.58	0.04	305.56	13.64	314.38	21.14	19.71	1.05	10.68	0.76	5	9
12.25	18.39	0.31	13.67	0.01	292.15	32.75	335.52	25.02	19.23	2.48	12.89	0.97	5	10
12.75	19.00	0.10	12.33	0.03	304.71	21.22	333.16	17.11	18.78	1.41	11.72	0.63	5	10
13.25	15.65	0.51	13.66	0.01	287.66	17.61	334.44	18.37	16.68	1.57	12.93	0.72	5	10
13.75	20.29	0.35	12.78	0.02	313.17	30.19	327.22	17.94	19.28	2.19	12.39	0.70	5	9
14.25	16.92	0.10	11.54	0.00	286.84	28.56	319.39	17.03	18.10	1.91	11.46	0.62	5	10
14.75	19.99	0.06	12.37	0.02	294.09	25.49	316.14	31.11	20.73	1.86	12.42	1.24	5	10
15.25	19.49	0.55	11.76	0.04	299.98	31.67	322.24	17.56	19.69	2.64	11.58	0.67	5	10
15.75	15.29	0.40			277.39	18.25			17.01	1.57			5	
16.25	18.17	0.12			297.23	27.15			18.58	1.82			5	
16.75	19.49	0.06			299.43	15.40			19.73	1.07			5	
17.25	17.80				296.26	31.56			18.28	1.95			5	
17.75	20.94	0.17	11.01	0.05	309.94	23.65	318.13	21.42	20.20	1.71	10.98	0.78	5	9
18.25	19.72	0.26			307.34	27.88			19.26	2.01			5	
18.75	19.15	0.23			297.67	19.60			19.54	1.52			5	
19.25	19.67	0.23			310.25	20.08			18.95	1.45			5	
19.75	16.55	0.26			306.73	28.23			16.21	1.75			4	
20.25	16.73	0.06	11.83	0.35	309.46	20.65	308.98	14.47	15.92	1.12	12.15	0.93	10	10
20.75	19.13	0.42	14.00	0.17	305.02	14.13			18.22	1.24			10	
21.25	19.30	0.35	11.73	0.29	304.27	26.55			18.81	1.98			10	
21.75	18.63	0.06	12.40	0.10	322.10	34.06			17.15	1.87			10	
22.25	19.27	0.23	14.10	0.53	305.03	24.53	331.05	21.69	18.25	1.69	13.49	1.39	10	10
22.75	21.63	0.25	13.27	0.25	328.64	17.12			19.06	1.21			10	
23.25	18.57	0.25	13.80	0.26	309.02	21.75			17.42	1.46			10	
23.75	18.60	0.26	12.33	0.31	295.77	18.24			18.39	1.40			10	

	mean	stdev	mean	stdev	mean	stdev	mean	stdev	mean	stdev	mean	stdev		
24.25	20.23	0.15	11.90	0.36	296.08	25.97	312.14	12.29	19.55	1.86	12.10	0.84	10	10
24.75	19.00	0.20	14.00	0.20	292.93	28.26			19.75	2.11			10	
25.25	15.40	0.17	13.41	0.22	292.27	16.36			15.23	1.02			10	
25.75	17.63	0.32			294.65	20.81			17.30	1.54			10	
26.25	18.67	0.31	12.50	0.17	299.35	22.10	332.78	18.70	18.23	1.64	11.89	0.83	10	10
26.75	16.17	0.38			289.06	18.84			16.49	1.46			10	
27.25	17.60	0.20			291.28	18.72			17.31	1.31			10	
27.75	19.10	0.26			296.91	15.57			18.30	1.21			10	
28.25	18.03	0.25	13.67	0.25	290.77	17.21	330.93	23.68	18.03	1.32	13.08	1.18	10	10
28.75	17.77	0.21			292.25	19.46			17.96	1.41			10	
29.25	17.70	0.26			298.18	18.55			16.93	1.31			10	
29.75	19.30	0.17			299.05	21.24								
30.25	16.70	0.10			290.64	18.01			17.09	1.16			10	
30.75	19.70	0.10	13.57	0.15	311.73	18.21	321.93	16.11	18.40	1.17	13.37	0.82	10	10
31.25	16.93	0.12			285.85	29.95			16.98	1.89			10	
31.75	18.83	0.21			287.53	20.20			18.82	1.53			10	
32.25	18.33	0.49			290.23	17.49			18.76	1.64			10	
32.75	18.70	0.10			294.91	22.79			18.89	1.56			10	
33.25	18.63	0.12	11.53	0.23	295.95	17.52			18.03	1.18			10	
33.75	19.73	0.25			297.43	27.71			19.50	2.06			10	
34.25	17.20	0.44			290.49	15.97			16.81	1.35			10	
34.75	19.87	0.15			307.87	18.21			18.73	1.25			10	
35.25	17.10	0.36			287.75	23.96			17.69	1.85			10	
35.75	19.03	0.06	12.33	0.31	297.51	25.56	311.27	18.76	18.63	1.66	12.57	1.07	10	10
36.25	17.85	0.36			278.04	46.90			18.30	3.45			9	
36.75	19.03	0.38			304.82	11.86			17.95	1.06			10	
37.25	20.22	0.11			286.39	78.62								
37.75	21.50	0.10			296.91	15.57			20.60	1.18			10	
38.25	19.57	0.15	12.63	0.15	296.69	21.60	363.63	36.65	19.14	1.54	10.79	1.22	10	10
38.75	21.67	0.29			307.55	23.05			20.81	1.84			10	
39.25	18.27	0.40			293.31	14.63			17.79	1.28			10	
39.75	20.73	0.40			300.32	8.63			20.00	0.96			10	
40.25	21.63	0.23			290.50	67.62								
40.75	19.00	0.36	12.73	0.15	299.14	25.60	325.25	16.02	18.21	1.90	12.42	0.76	10	10
41.25	21.43	0.21			304.47	27.98			20.38	2.07			10	
41.75	19.87	0.23			291.87	24.19			19.95	1.89			10	
42.25	18.47	0.51			282.05	24.41			19.55	2.23			10	
42.75	17.6667	0.05774			278.76	14.83			18.64	1.05			10	
43.25	16.8667	0.15275	12.0333	0.15275	286.21	22.79	322.07	17.07	17.51	1.55	11.86	0.78	10	8

Table S3.11: *Size normalized weight (SNW) raw data in core MedSeA-S7-c2 (Strait of Sicily) analyzed in G. elongatus and G. bulloides. From the left: depth (cm below the sea floor); mean and standard deviation of planktic foraminiferal test mass (µg), minimum ferret (µm), and SNW (µg); N equals number of analyzed tests per sample depth.*

depth	mass				minimum feret				snw				N	
(cm)	(µg)				(µm)				(µg)					
	G.elong		*G.bull*		*G.elong*		*G.bull*		*G.elong*		*G.bull*		*G.elong*	*G.bull*
	mean	stdev	mean	stdev	mean	stdev	mean	stdev	mean	stdev	mean	stdev		
1.50	15.82	0.58	10.90	1.00	298.14	24.37	306.34	22.77	15.99	0.44	11.06	0.90	10	10
3.50	17.50	0.00	9.93	1.53	299.59	18.08	305.03	16.51	17.61	0.00	10.12	1.84	10	10
5.50	16.02	2.08	10.08	0.58	298.56	22.72	306.92	18.55	16.17	1.76	10.21	0.64	10	10
7.50	15.07	0.58	10.52	1.15	287.16	19.46	319.68	20.35	15.78	0.58	10.22	1.18	10	10
9.50	14.55	1.00	10.65	0.00	294.09	13.70	316.03	22.54	14.91	1.30	10.48	0.00	10	10
11.50	17.58	2.31	7.95	1.73	299.95	24.93	299.38	14.12	17.68	1.70	8.25	2.28	10	10
13.50	16.93	1.53	11.75	1.00	286.28	20.10	314.13	25.84	17.79	1.50	11.63	0.75	10	10
15.50	17.13	1.53	10.67	0.58	298.31	17.18	308.98	19.96	17.32	1.72	10.73	0.60	10	10
17.50	16.68	1.15	10.42	0.58	300.55	16.12	307.00	21.15	16.74	1.36	10.55	0.57	10	10
19.50	18.40	0.00	10.13	1.15	298.16	11.83	300.80	24.15	18.61	0.00	10.46	0.96	10	10
21.50	17.57	0.58	10.12	1.53	302.58	24.33	309.84	16.79	17.51	0.44	10.15	1.82	10	10
23.50	18.95	0.00	10.50	1.00	304.29	19.34	313.11	11.27	18.78	0.00	10.43	1.46	10	10
25.50	19.55	1.00	12.43	1.15	301.40	20.44	322.22	22.52	19.56	0.96	11.98	1.05	10	10
27.50	19.85	1.00	12.15	2.00	299.88	21.68	305.07	20.89	19.96	0.90	12.38	1.98	10	10
29.50	18.63	0.58	12.73	0.58	311.63	21.84	309.20	25.64	18.01	0.51	12.80	0.44	10	10
31.50	19.62	1.15	10.88	1.53	304.83	19.18	314.94	30.79	19.40	1.18	10.74	0.78	10	10
33.50	20.23	1.15	12.15	0.00	303.54	16.44	327.02	19.93	20.10	1.35	11.52	0.00	10	10
35.50	18.57	0.58	10.38	1.15	306.10	24.35	309.65	20.38	18.29	0.44	10.43	1.17	10	10
37.50	17.87	0.58	11.10	1.00	304.73	18.35	304.65	13.92	17.68	0.62	11.32	1.33	10	10
39.50	19.52	0.58	10.77	1.53	316.26	18.91	313.76	20.72	18.56	0.60	10.67	1.53	10	10
41.50	19.90	1.00	11.72	1.15	308.56	15.59	311.80	26.38	19.44	1.21	11.68	0.84	10	10
43.50	19.50	0.00	12.30	2.00	308.96	24.86	322.11	22.08	19.02	0.00	11.86	1.87	10	10
45.50	17.98	0.58	11.55	1.00	301.81	19.19	304.22	19.35	17.97	0.59	11.80	1.07	10	10

Table S3.12: *Carbon isotope ($\delta^{13}C$) data on VPDB scale with a δ13C uncertainty of 0.1 permille (1SD level) for all three stations analyzed in G. elongatus and G. bulloides calcite tests. From the left: depth (cm below the sea floor); corrected mean values and standard deviation; n number of tests analyzed per sample depth.*

Alboran Sea (Station 3)					Strait of Sicily (Station 7)					Balearic Sea (Station 23)				
depth (cm)	$\delta^{13}C$ (‰)		n-tested		depth (cm)	$\delta^{13}C$ (‰)		n-tested		depth (cm)	$\delta^{13}C$ (‰)		n-tests	
	G.elong corr	*G.bull* corr	*G.elong*	*G.bull*		*G.elong* corr	*G.bull* corr	*G.elong*	*G.bull*		*G.elong* corr	*G.bull* corr	*G.elong*	*G.bull*
0.50	0.73	-1.15	10	10	1.50	0.51		9		0.25		-1.06		10
1.50	0.73	-1.04	10	10	3.50	0.73	-1.19	10	10	1.25	0.41	-1.46	5	10
2.50	0.74	-0.75	10	10	5.50	0.78	-1.48	6	8	2.25		-1.29		10
3.50	0.99	-0.88	10	10	7.50	0.74		10		4.75		-1.11		10
4.50	1.17	-0.80	10	10	9.50	0.67	-1.20	9	5	5.75	1.25		5	
5.50	1.16	-1.00	10	10	11.50	0.75	-1.23	10	10	6.25				
6.50	1.07	-0.83	10	10	13.50	0.75	-1.41	10	10	6.75		-0.91		10
7.50	1.26	-0.70	10	10	15.50	0.83	-0.88	9	10	7.25				
8.50	1.39	-0.80	10	10	17.50	0.66	-0.78	10	10	7.75	1.17		5	
14.50	1.23	-0.78	10	10	19.50	0.98	-1.29	10	6	8.75		-0.85		10
20.50	1.17	-0.97	10	10	21.50	1.00	-0.93	10	10	10.75	1.21	-0.91	5	11
28.50	1.22	-0.94	10	10	23.50	1.07	-0.88	10	9	12.75	1.11		5	
					25.50	0.28	-0.92	10	2	13.25		-0.75		10
					27.50	0.75	-0.78	10	10	14.25	0.75		5	
					29.50	0.47	-0.96	10	10	15.75		-0.90		10
					31.50	1.05	-0.84	10	9	16.25	1.15		5	
					33.50	0.66	-0.92	10	10	17.75	0.92		5	
					35.50	0.81	-0.81	10	10	18.25		-1.06		11
					37.50	0.95	-0.86	10	9	19.25	1.27		5	
					39.50	0.85	-0.85	10	10	23.25		-1.13		10
					41.50	1.02	-0.66	10	5	28.75		-1.04		10
					43.50	0.87	-1.12	10	9	42.25		-1.19		9
					45.50	0.88	-1.15	10	10					

3.5.7 Plates

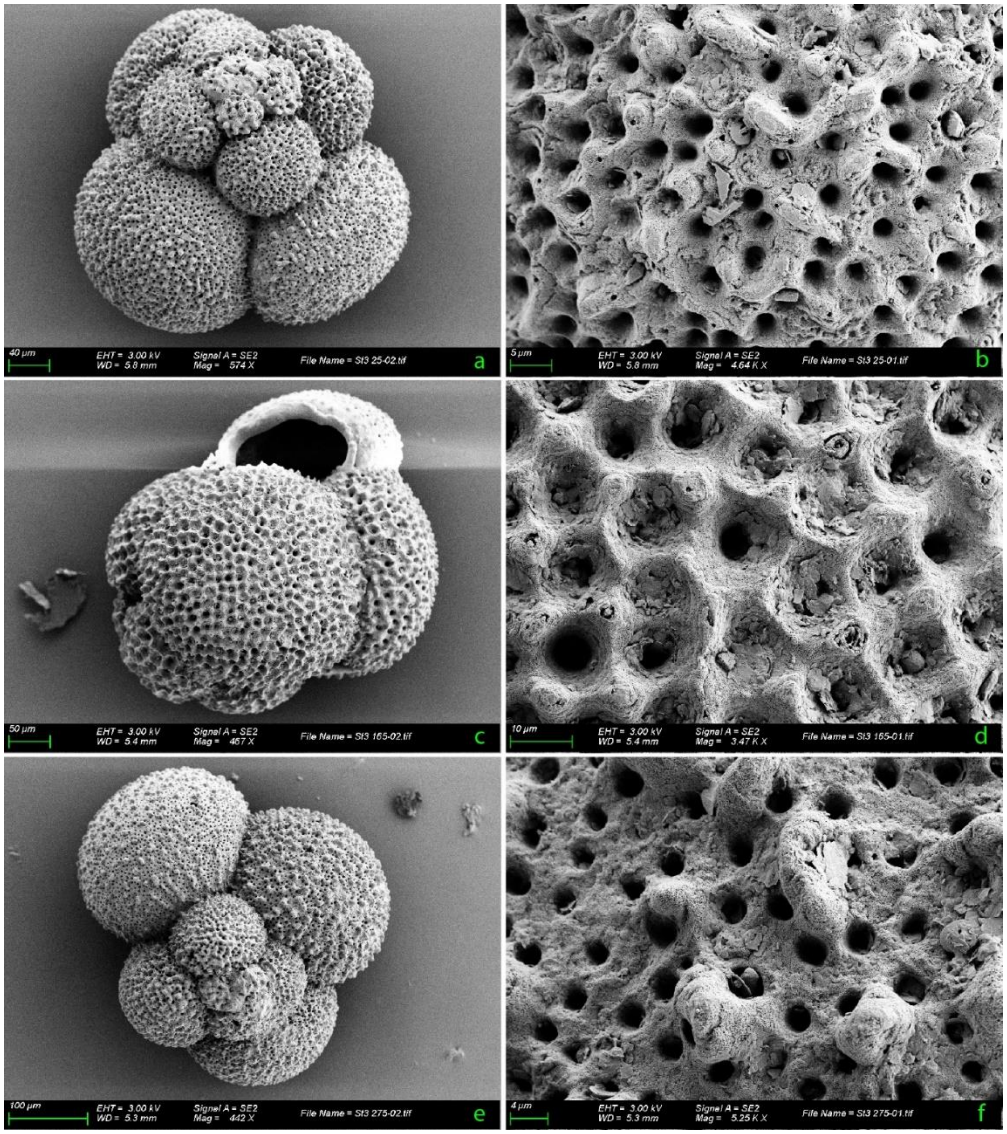

Plate S3.1: *Scanning electron microscope images of fossil planktic foraminifera of core Station 3 (Alboran Sea). (a,b) Globigerina bulloides at 2.5cm core depth (1969 yr CE); (c,d) Globigerinoides elongatus at 16.5 cm core depth (1279 yr CE); (e,f) Globigerina bulloides at 27.5 cm core depth (651 yr CE).*

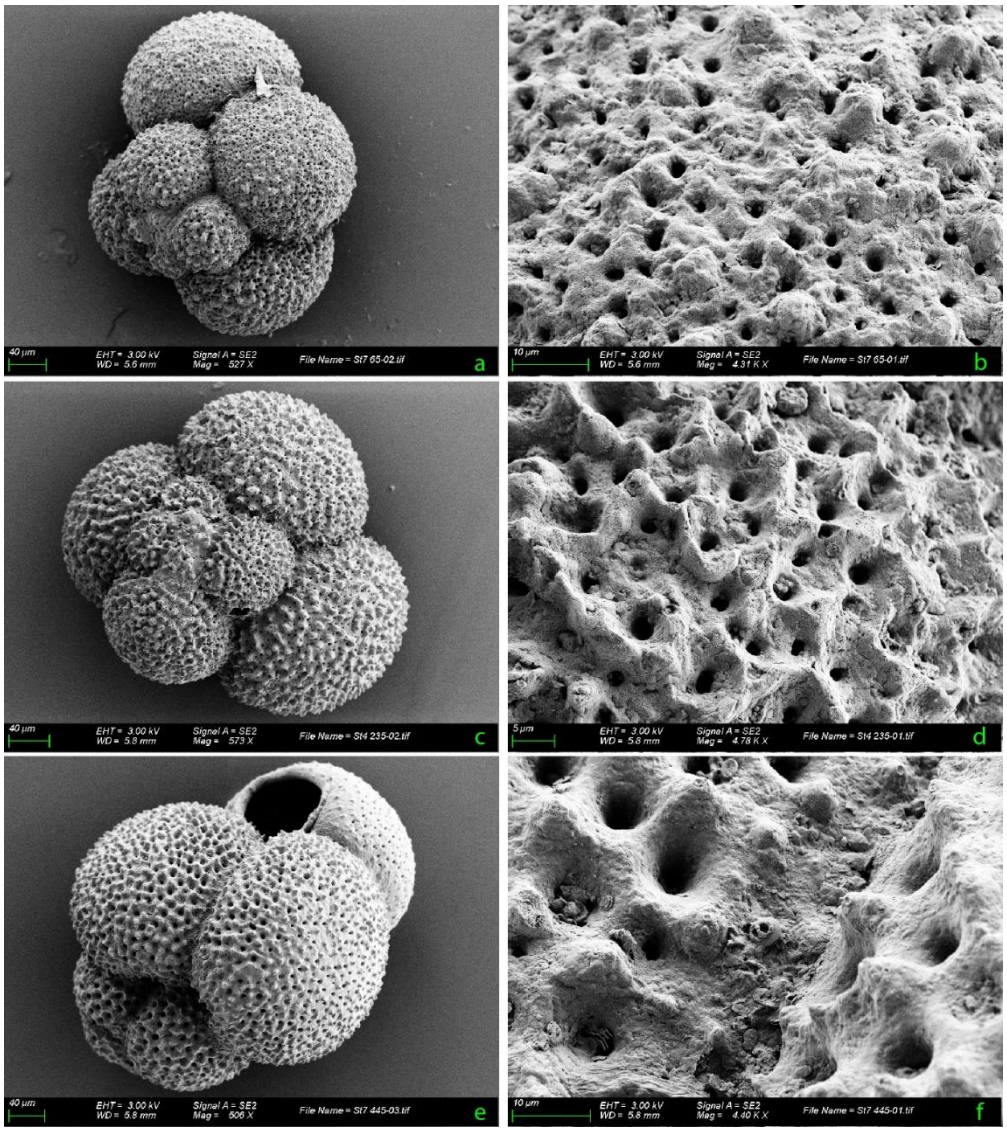

Plate S3.2: *Scanning electron microscope images of fossil planktic foraminifera of core Station 7 (Strait of Sicily). (a,b) Globigerina bulloides at 6.5 cm core depth (1989 yr CE); (c,d) Globigerina bulloides at 23.5 cm core depth (1919 yr CE); (e,f) Globigerinoides elongatus at 44.5 cm core depth (1819 yr CE).*

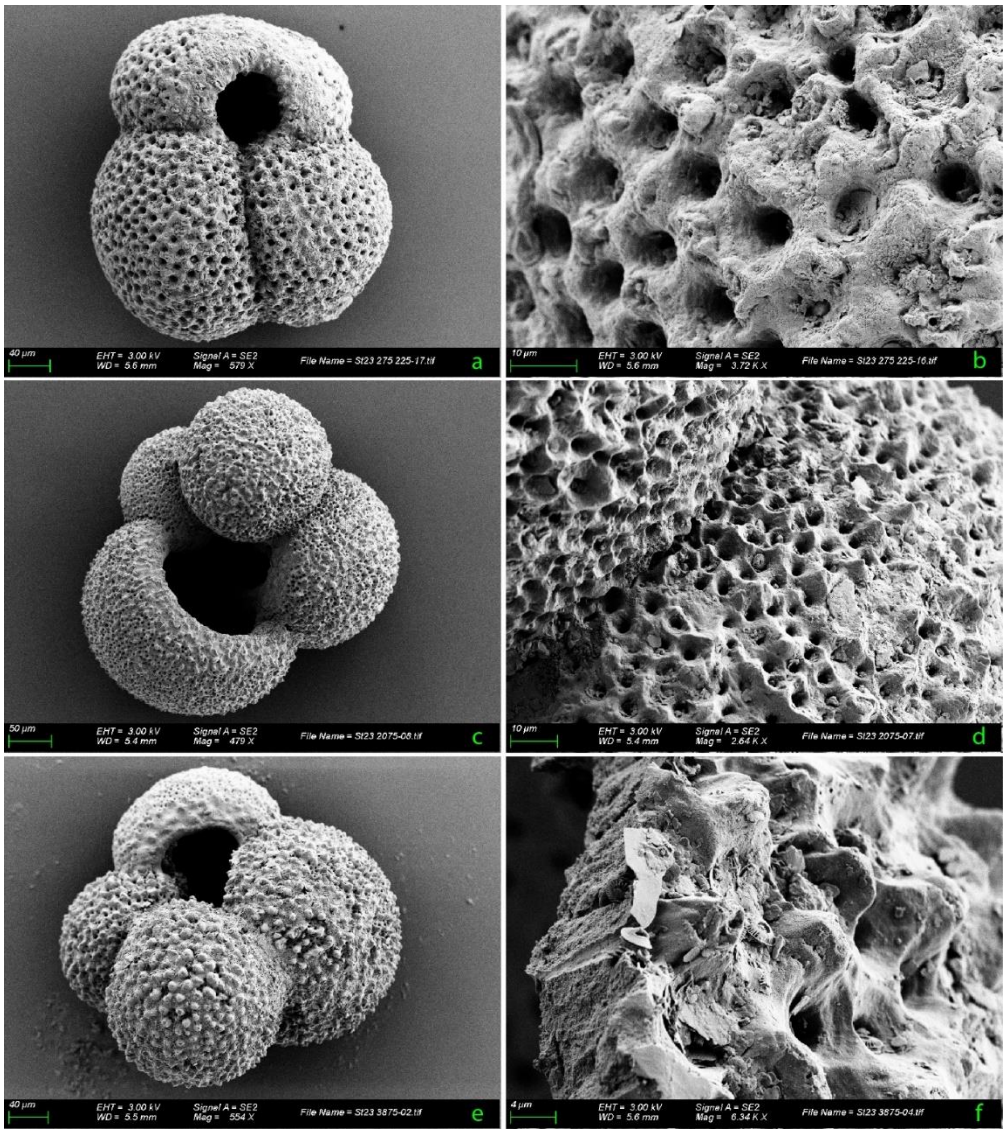

Plate S3.3: *Scanning electron microscope images of fossil planktic foraminifera of core Station 23 (Balearic Sea). (a,b) Globigerinoides elongatus at 2.25/2.75 cm core depth (1992 yr CE); (c,d) Globigerina bulloides at 20.75 cm core depth (1537 yr CE); (e,f) Globigerina bulloides at 38.75 cm core depth (998 yr CE).*

3.5.8 Data Availability

The dataset used in this study is publicly available online for download at PANGAEA Data Publisher (https://doi.pangaea.de/10.1594/PANGAEA.955015).

CHAPTER 4

4 Ocean deoxygenation linked to ancient midwater fish decline

Abstract

Mesopelagic fish are integral to ocean food webs (Catul et al., 2011; Hunt et al., 2015), and play an important role in carbon transport through their vertical migration behavior (Saba et al., 2021). Ocean deoxygenation caused by anthropogenic warming is hypothesized to pose severe threats to mesopelagic fauna, by enhancing physical stress and changing prey-predator relationships (Gilly et al., 2013; Koslow et al., 2011; Wishner et al., 2013), but the degree to which this interacts with other drivers of fish abundance is unclear. Here we use otolith-records from Mediterranean sediment cores to show near absence of mesopelagic fish abundance between 7 and 11 kyr ago, concurrent with high productivity and low oxygenation of mid-depth waters. At these times, fish species adapted to the epipelagic habitat including European anchovy (*Engraulis encrasicolus*) and Silvery lightfish (*Maurolicus muelleri*), dominate the otolith record. After reoxygenation, mesopelagic fish abundance increases by a factor of ~3, with Lanternfish (Myctophidae) being the most dominant family from the middle-Holocene to present times. Our results provide evidence for the important role of Oxygen Minimum Zone dynamics in shaping fish communities, a key ongoing process expected to intensify over the coming centuries (Bindoff et al., 2019; Keeling et al., 2010; Shaffer et al., 2009). A decline of mesopelagic fish abundance could have major impacts on marine fisheries, marine conservation, ocean food web structure and carbon storage capacity with long-lasting, adverse knock-on effects for structure and functioning of global marine ecosystem services.

4.1 Introduction

Ocean deoxygenation through the intensification, expansion and shoaling of Oxygen Minimum Zones (OMZs) is thought to pose a serious threat to mesopelagic fish communities (Koslow et al., 2011). OMZs are associated with the mesopelagic zone, hence they occur usually at midwater depth, where oxygen saturation is at its lowest, limiting macrofaunal life (Gilly et al., 2013). A global expansion, intensification, and shoaling of OMZs has been documented over the last several decades related to anthropogenic climate change (Bindoff et al., 2019; Bograd et al., 2008; Helm et al., 2011; Ito et al., 2017; Schmidtko et al., 2017; Stramma et al., 2008; Whitney et al., 2007). In addition, ocean models project further decline of oxygen levels to continue during the next decades (Bindoff et al., 2019; Bopp et al., 2013; Keeling et al., 2010; Shaffer et al., 2009). Intensified oxygen loss enhances hypoxic stress on marine organisms, leading to negative physiological effects on biological performance, including survival, abundance and reproduction (Breitburg et al., 2018; Claireaux & Chabot, 2019; Sampaio et al., 2021), with fish being particularly sensitive to hypoxia (Vaquer-Sunyer & Duarte, 2008). Lanternfish are key players of the mesopelagic community, being the most common and abundant family accounting for 75% of mesopelagic fish biomass (Catul et al., 2011). Lanternfish are diel vertical migrators (DVM), feeding at the surface during nighttime. At dawn, they migrate down to the mesopelagic zone to escape visual predation and to hide in oxygen deprived waters during the day (Barham, 1966; Klevjer et al., 2016). Although adapted to hypoxic conditions (Catul et al., 2011; Seibel, 2011), Lanternfish are likely impaired by prolonged hypoxia within a vertically expanded OMZ core (Wishner et al., 2013). Shoaling OMZs cause vertical compression of their nighttime habitat and upward shift of their daytime habitat into the lower edge of the euphotic zone, which enhances exposure to visual predators with negative consequences for Lanternfish overall abundances (D. Bianchi et al., 2013; Koslow et al., 2011; Netburn & Koslow, 2015; Seibel & Wishner, 2019).

The potential decline of mesopelagic fish under expanded ocean hypoxia has major implications for ocean productivity. The mesopelagic zone forms major parts of

Earth's total biosphere, providing habitat to mesopelagic fish with an estimated biomass of 11 to 15 billion tons only between 40° N and 40° S (Irigoien et al., 2014), which is around two orders of magnitude higher than world fisheries and aquaculture production in 2020, which is estimated at 178 million tons (FAO, 2022). As most mesopelagic fish are a reliable source for essential amino acids and nutritive proteins (Koizumi et al., 2014; Seo et al., 1998), they are an important resource to supply aquaculture and nutraceutical markets (St. John et al., 2016), and could be a potentially new nutritional resource to sustainably feed the world. Mesopelagic fish inherit a central role in the marine food web, thus being of high importance for trophodynamics (Catul et al., 2011; Eduardo et al., 2021; Hunt et al., 2015). Due to their great biomass and vertical migrating behavior, they are important contributors to the marine carbon cycle (Davison et al., 2013; Saba et al., 2021). Owing to their fundamental functions for marine conservation, commercial fishery and biogeochemical cycling, a decline in mesopelagic fish abundance would have severe ecological and socioeconomic implications (Daniel G. Boyce et al., 2020). However, the effects of OMZ expansion and intensification on mesopelagic communities are still under debate, as their biological response to the combined effects of deoxygenation and other environmental stressors seems to be complicated (Claireaux & Chabot, 2019; Koslow et al., 2019). Apart from oxygen saturation, other parameters like ocean temperature (Proud et al., 2017; Salvatteci et al., 2022) and primary productivity (Davison et al., 2013; Irigoien et al., 2014) also play an important role for mesopelagic fish dynamics, and how species and communities adapt to long-term environmental variability (W. A. Jones & Checkley, 2019).

The Eastern Mediterranean Sea is an ideal study area to investigate fish community response to changing ocean oxygen levels, as oceanographic conditions have alternated between a well oxygenated and a hypoxic water column throughout the last 13.5 million years (Rohling et al., 2015). Repeated climatic changes lead to higher organic matter preservation in sediments due to low oxygen availability and higher organic fluxes to the sea floor, causing the formation of dark, organic-rich sedimentary deposits, called sapropels. The most recent Sapropel S1 was formed between 9.8-5.7 kyr BP (subsequently abbreviated kyr) (De Lange et al., 2008), and

is subject to our investigations. Here we show that changes in ocean oxygen levels are associated with Holocene mesopelagic fish dynamics, by using a high-resolution (38.6 a cm^{-1}) marine record of fossil fish ear bones (otoliths), collected in a "Kasten Lot" core from the central western Aegean Sea (Figure 4.1c; see Methods), a study region being notable for Sapropel S1 deposits (Casford et al., 2007; Kontakiotis et al., 2016). Total fish abundance is estimated by otolith accumulation rates (OAR). To evaluate fish community changes, we identified 82% of all otoliths at least to the family level.

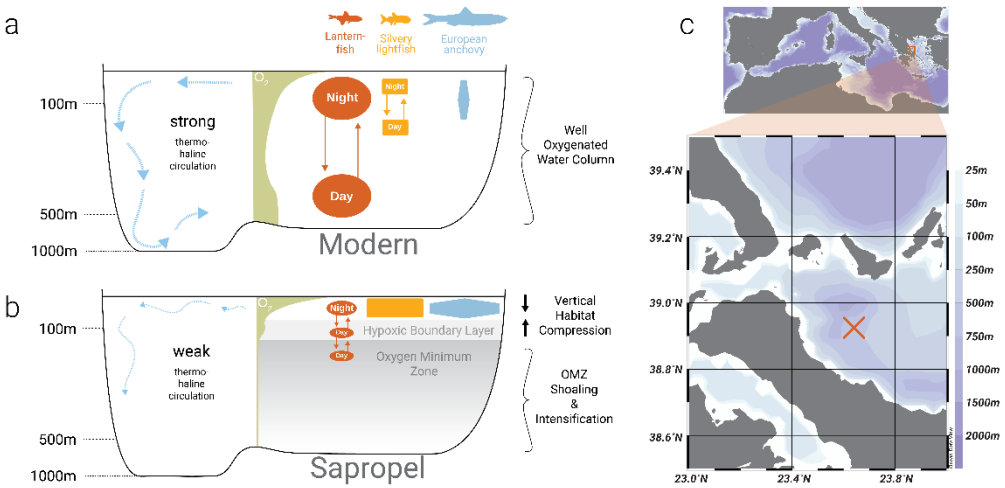

Figure 4.1: *(a-b) Two hypothetical schemes describing oceanographic 2-component system during Sapropel deposition and Younger Holocene at our core location in the central west Aegean Sea, and the ecological response of our target fish to changing oxygen concentration levels; adapted from previous studies (Koslow et al., 2011; Rohling et al., 2015; Seibel & Wishner, 2019). (c) Ocean data view bathymetry map (Schlitzer, 2019) of study area and M144 KC5-6 core location (red cross).*

4.2 Results and Discussion

4.2.1 Eastern Mediterranean Holocene fish dynamics

Total otolith variability and fish family dynamics throughout the last ~10.5 kyr in the central western Aegean is expressed as OARs and relative abundances (Figure 4.2b, S4.1; Table S4.1). Previous to S1 deposition, mean $_{tot}$OARs are low (3.4 otoliths m^{-2} yr^{-1}) and species composition is dominated by the Silvery lightfish (*Maurolicus muelleri*; 39.7%) a mesopelagic fish species belonging to the family of Sternoptychidae. European anchovy (*Engraulis encrasicolus*), an epipelagic forage fish belonging to the family of Engraulidae, accounts for 8.6% of otolith flux. Otoliths belonging to the mesopelagic Lanternfish family (Myctophidae) make up 31.6%.

During sapropel deposition in the early Holocene (Table S4.1), mean $_{tot}$OARs increase slightly (4.9 otoliths m^{-2} yr^{-1}) together with changes in species composition. The Silvery lightfish (42.4%) still dominates the record. Abundances of the European anchovy increase up to 17.7%, while Lanternfish decline to 14.0%. Otoliths from the Gadidae (4.8%) and Gonostomatidae (2.9%) form minor parts of the sapropel fauna, and species of both families have been found living in meso- to bathypelagic depths. Between ~7 to ~3 kyr BP mean OAR increases by ~3x over sapropel otolith production to 15.9 (otoliths m^{-2} yr^{-1}) and reaches a peak of 33.6 (otoliths m^{-2} yr^{-1}) at 3.66 kyr BP dominated by Lanternfish (81.0%). We identified a total of 12 Lanternfish species (Plates 4.1-4.2) without remarkable composition changes throughout the Middle to Late Holocene. After 3 kyr, there is a marked drop in average $_{tot}$OAR to 9.79 (otoliths m^{-2} yr^{-1}) but no change in the overall fish assemblage.

The Lanternfish species composition is similar to recent fossil assemblages (Lin et al., 2017) and modern fish catches (Kapelonis et al., 2019; Somarakis et al., 2011) from the Mediterranean Sea, highlighting the representativeness of our findings. The dominance of Lanternfish in the Middle to Late Holocene otolith record is in accordance with previous studies of marine sediments from the Western Atlantic (Elder et al., 1996), the Eastern Atlantic (Lin et al., 2016), the Eastern Pacific (W. A. Jones & Checkley, 2019), the Red Sea (Lin et al., 2018) and the Mediterranean Sea (Cartes et al., 2017; Lin et al., 2017). Fish catch data and acoustic backscatter analysis (Irigoien et al., 2014; Pauly et al., 2021) corroborate the dominance of Lanternfish in the modern ocean in terms of biomass and species diversity (Catul et al., 2011). Accordingly, the predominance of Lanternfish in the central western Aegean otolith record appears to reflect actual trends of the global mesopelagic fish fauna.

4.2.2 Ocean deoxygenation in the ancient Eastern Mediterranean Sea

Between 9.33 and 6.87 kyr BP, the low $_{tot}$OAR and reduced abundances of Lanternfish may indicate deterioration of the mesopelagic fish habitat during sapropel S1 deposition (Figure 4.2b). The near absence of Lanternfish suggests that in the Aegean Sea their daytime habitat between 250m and 650m water depth (Kapelonis et al., 2021) became uninhabitable. By comparison, the shallow habitats of the Silvery

lightfish (daytime habitat: 75–275m) and the European anchovy (day-/nighttime habitat: 0–180m) (Giannoulaki et al., 2013; Kapelonis et al., 2021; Stein et al., 1998) may have allowed both species to avoid the expansion of anoxic midwater conditions. The sporadic presence of otoliths (Figure S4.1) belonging to deep-sea fish of the families Gonostomatidae and Gadidae (Priede, 2017) argue against constantly euxinic midwater conditions, which are defined through a raised level of free hydrogen sulfides (H_2S), and are lethal to most metazoans including marine fish (Bagarinao & Vetter, 1989; Riesch et al., 2015).

Numerical model and paleoceanographic data on the distribution and intensity of the sapropel conditions support our inference that hypoxic waters shoaled, and oxygen depletion intensified in the early Holocene. During S1 formation large parts of the Eastern Mediterranean Sea have been associated with anoxic mid- to bottom waters (Rohling et al., 2015; Rohling et al., 2000; Schmiedl et al., 2010), including the central western Aegean Sea (Casford et al., 2007; Kontakiotis, 2016). Enhanced freshwater runoff and reduced evaporation due to abundant precipitation in the eastern Mediterranean region (Kallel et al., 1997; Rohling & Hilgen, 1991) intensified vertical stratification in surface waters, impairing deep water formation and leading to oxygen depleted mid- to bottom waters (Stratford et al., 2000). Sapropel layers are rare in sediment cores recovered from less than ~80 to ~125m (Perissoratis & Piper, 1992; Rohling et al., 2015) while cores from greater depths have well developed sapropel deposits. The presence of sapropel deposits over a wide depth range but not in near surface cores suggests that the water column was severely anoxic below the wind-mixed surface ocean. Despite proxy evidence for enhanced hydrogen sulfide (H_2S) concentrations in the Eastern Mediterranean basin during previous interglacial sapropel phases (Benkovitz et al., 2020; Chiu et al., 2022; Rohling et al., 2006), we do not assume bottom to midwater euxinia to be present at our study site, as otoliths of deep-sea fish and benthic foraminifera (personal communication: Oliver Friedrich) occur throughout the S1 deposit. This is in line with previous studies reporting mild euxinic bottom water conditions only at considerably deeper sites compared to our study region (Andersen et al., 2020; Azrieli-Tal et al., 2014; Slomp et al., 2004).

While mid- to bottom waters became more uninhabitable due to lower oxygen levels, a shallow OMZ and elevated riverine nutrient runoff are thought to have stimulated surface ocean productivity (Rohling et al., 2015; Schmiedl et al., 2010). There is comprehensive microfossil and geochemical proxy evidence from the Eastern Mediterranean Sea for high downward fluxes of organic matter to the seabed during S1 formation (Castradori, 1993; Filippidi & De Lange, 2019; Higgins et al., 2010; Alessandro Incarbona et al., 2019; Sachs & Repeta, 1999; Thomson et al., 2004). Planktic foraminiferal accumulation rates (Figure 4.2d) provide evidence for enhanced surface production at our study site during S1, as planktic foraminiferal standing stocks are positively related to primary production (Hemleben et al., 1989; Schiebel & Hemleben, 2005). This is in agreement with planktic foraminiferal species composition changes, indicating eutrophic surface conditions during S1 close to our core location (Kontakiotis, 2016). However, the ocean production spiked during the central western Aegean sapropel phase and may have altered midwater habitats by changes in nutrient inventories, the types of food available to mesopelagic fish or the composition of microbially-generated dissolved gasses.

4.2.3 Low mesopelagic fish production beneath a highly productive surface ocean

Lanternfish nearly disappear within the sapropel, likely reflecting the changed ecology of a newly anoxic ocean basin (Figure 4.2b, S4.1e). Lanternfish feed at the surface during night and hide in oxygen deprived mid-waters during day. Their thin bodies, enhanced respiratory surface area, blood pigments and respiratory proteins, and reduced activity to suppress metabolic activity are thought to be physiological and behavioral adaptation strategies to low oxygen environments at midwater depth (Catul et al., 2011; Seibel, 2011). However, adaptation response of Lanternfish to changing oxygen levels seems to be species specific (Lopes et al., 2013), and might depend on their development stage (Maas et al., 2014). Studies in the OMZs of Arabian Sea (Kinzer et al., 1993), Red Sea (Dypvik & Kaartvedt, 2013) and eastern tropical Pacific (Maas et al., 2014) report avoidance of low oxygen waters by several Lanternfish species. Lanternfish which retain their daytime habitat depth regardless of extremely

low oxygen conditions, must transit longer through uninhabitable (anoxic) environments (Wishner et al., 2013), with potentially negative effects on their physiology. In highly anoxic ocean environments like the Black Sea, the mesopelagic fish community is entirely absent. We assume that the vast majority of Lanternfish was not able to cope with intensified low oxygen levels at mesopelagic depth, despite possible oxygen adaptation strategies of some species.

The surface ocean continued to be well oxygenated during sapropel deposition, as seen in the fish community. Silvery lightfish dominates the fish assemblage during S1 deposition (Figure 4.2b, S4.1d), likely reflecting their ability to exploit near surface habitats above the OMZ. In the Gulf of Corinth, a semi-enclosed subbasin in the Eastern Mediterranean, Silvery lightfish inhabit shallow daytime habitats living a few meters above the seabed along the continental shelf at approximately 75–275m water depth, still residing at the surface during night (Kapelonis et al., 2019). To better cope with enhanced predator pressure, the species is known for changing from diel vertical migration to schooling behavior at the surface when exposed to illuminated summer nights in northern high latitudes (Stein et al., 1998). Both a shallower habitat and better adaptation strategies to avoid predation in the epipelagic zone, presumably made the Silvery lightfish less susceptible to an intensification and shoaling of the OMZ during S1 deposition, while still benefiting from enhanced productivity at the surface.

High epipelagic fish production during the sapropel is also indicated by the increase in abundance of European anchovy (Figure 4.2b, S4.1c). These fish thrive in oceanic systems characterized by strong, shallow OMZs and high surface productivity, as reported from the modern Black Sea (Capet et al., 2018; FAO, 2018) and from paleorecords off the coast of Peru (Salvatteci et al., 2019). A shoaling OMZ in the Peruvian upwelling system is hypothesized to change plankton structure with benefits for anchovy populations (Bertrand et al., 2011). This is in agreement with enhanced planktic foraminiferal accumulation rates during S1 formation (Figure 4.2d), indicating higher primary production. Accordingly, we presume that increasing surface ocean primary productivity cascaded up the trophic ladder and stimulated

epipelagic fish production as recorded in our European anchovy and Silvery lightfish otolith record. At the same time, epipelagic predators benefitted from the shoaling OMZs, which enhanced mesopelagic prey availability in surface waters (Stewart et al., 2014).

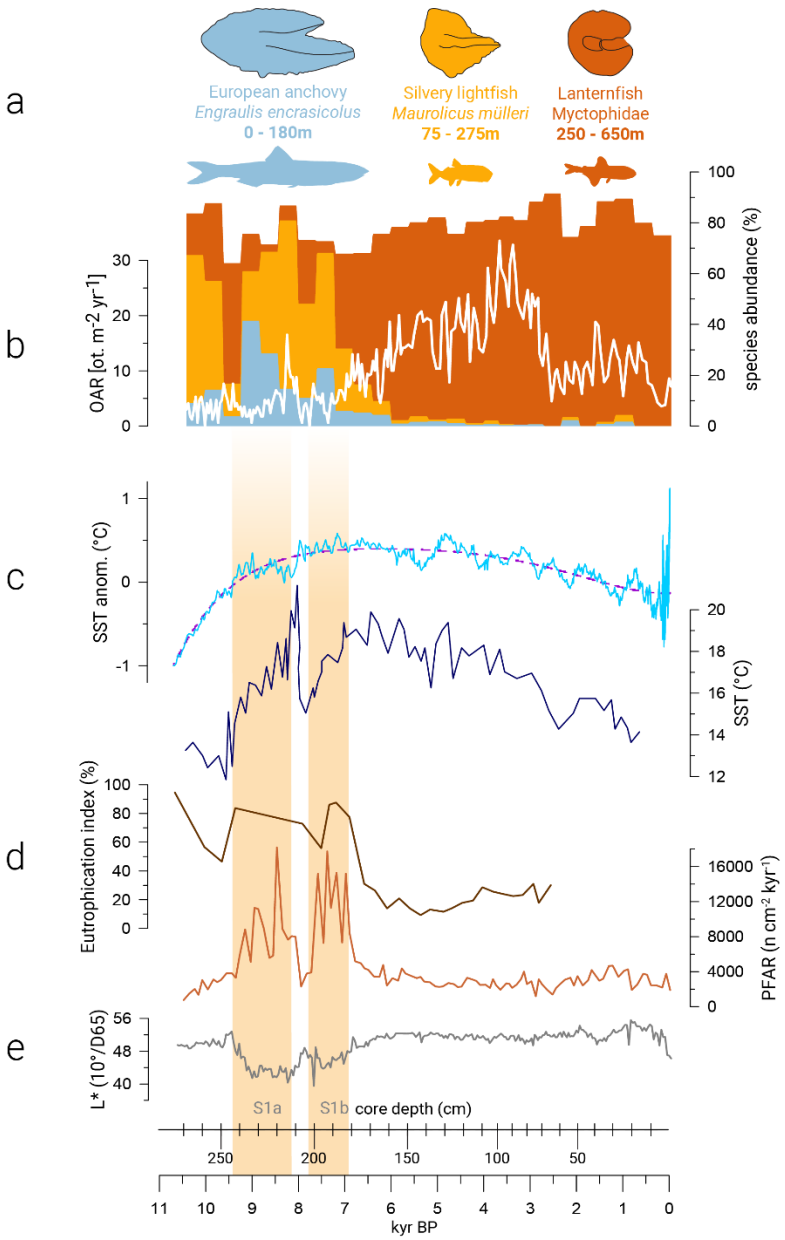

Figure 4.2: *Paleo fish composition changes in the central west Aegean Sea throughout the last 10.5 kyr retrieved from a fossil otoliths record (core: M144 KC5-6). (a) Sketches of most common fish species:*

European anchovy (Engraulis encrasicolus;, blue), Silvery lightfish (Maurolicus mülleri, orange); and species (here: Hygophum benoiti as an example) of the family: Lanternfish (Myctophidae, red) with typical daytime habitat depth indicated. (b) Relative abundance of the most common fish species/family as cumulative stacked area plot of 10cm bins. White trend line shows total otolith accumulation rates (OARs). (c) Stack of Sea Surface Temperature (SST) anomaly [°C] changes in the Mediterranean throughout the Holocene (Marriner et al., 2022), and SST [°C] variability close to our study site from core SK-1 (Kontakiotis, 2016). (d) Productivity changes in the central west Aegean Sea shown by Eutrophication index from core SK-1 (Kontakiotis, 2016), and planktic foraminiferal test accumulation rates (this study). (e) M144 KC5-6 sediment surface color scanning. Light brownish bands represent Sapropel S1a and S1b.

4.2.4 Mid- to Late Holocene recovery of the mesopelagic fish assemblage

The oceanographic shift happening in the eastern Mediterranean during the middle - Holocene (Kontakiotis, 2016; Kuhnt et al., 2008; Marriner et al., 2022; Rohling et al., 2015), a period around 7 to 5 kyr ago, sets stage for a substantial transformation of the mesopelagic fish community in the central western Aegean Sea (Figure 4.2b-d). With the end of S1 deposition, anoxic mid- to deep waters were displaced by well oxygenated conditions, allowing Lanternfish to occupy the mesopelagic zone and avoid predators in the surface ocean. Aside from basin reoxygenation, sea surface temperature (SST) and productivity are an important secondary driver for mesopelagic fish dynamics (Davison et al., 2013; Irigoien et al., 2014; W. A. Jones & Checkley, 2019; Koslow et al., 2019; Olivar et al., 2022; Salvatteci et al., 2022), and help explain Lanternfish population changes in the eastern Mediterranean Sea.

Higher temperatures enhance metabolic rates and therefore growth and reproduction (Jennings et al., 2008), including the mid-water fish community (Proud et al., 2017). Lanternfish remain in the epipelagic zone as larvae before beginning diel migration as adults (Maas et al., 2014; Sassa et al., 2004). High mid-Holocene SSTs of nearly 20 °C (Figure 4.2c) would have enhanced growth rates of larvae, boosting Lanternfish biomass. As marine fish is able to adapt their habitat depth to thermal regime changes (Freitas et al., 2016; Freitas et al., 2021), higher deep-water temperatures in the Mediterranean would allow Lanternfish to move deeper during the day to increase avoidance of predators. The combination of reduced predation and elevated growth rate in a warmer, better oxygenated ocean may explain the mid-Holocene recovery of the Lanternfish population. In the reverse manner, colder oceans lead to reduced growth and a shallower habitat depth of Lanternfish, causing low overall abundances prior to S1 formation and their decline around 3 kyr (Figure 4.2b). However, the

anticorrelation between Lanternfish abundance and planktic foraminiferal accumulation rate (PFAR) reported in our record (Figure 4.2b,d) disagrees with previous observation describing a positive correlation between primary production and mesopelagic fish abundance (Davison et al., 2013; Irigoien et al., 2014; Olivar et al., 2022), and emphasizes that the complexity of the marine food web structure is likely insufficiently understood as yet.

4.2.5 Sapropel S1 analog for future OMZs and its implications

In the future, models suggest that global OMZs will intensify and expand, shifting the upper hypoxic boundary layer closer towards the sea surface (Bindoff et al., 2019; Bopp et al., 2013; Keeling et al., 2010; Shaffer et al., 2009), affecting the mesopelagic fauna, as their vertical habitat depth range is mainly controlled by oxygen levels (D. Bianchi et al., 2013; Klevjer et al., 2016; Maas et al., 2014; Netburn & Koslow, 2015). Shoaling of daytime habitat and vertical compression of nighttime habitat, have been hypothesized to alter prey-predator relationships with negative impacts on the mesopelagic fish community (Koslow et al., 2011). The near absence of Lanternfish during sapropel formation suggests that habitat compression occurred during the sapropel in agreement with Koslow's model (Figure 4.1a-b). However, Koslow et al. (2019) reports that the correlation between mesopelagic fish and oxygen broke down when ocean temperatures became warmer, resulting in an increase of mesopelagic warm water species including Lanternfish. The community composition of mesopelagic fish can shift toward taxa better adapted to more intense, shallower OMZs, as substantiated in our study by the replacement of Lanternfish by the Silvery lightfish being the dominant species during S1 formation. Koslow et al. (2019) in agreement with our observations show that the model of Koslow et al. (2011) is not universal, and mechanisms controlling the marine food structure are more complex than a simple correlation between oxygen and abundance of mesopelagic fish. However, the sapropel period in the eastern Mediterranean may have been particularly hostile to life in the mesopelagic zone, as shown by the near absence of fossil otoliths during S1 deposition, possibly caused through the development of severe photic zone

anoxia. Additional to the effects of ocean hypoxia, it is likely that changes in the marine food web architecture have favored epipelagic over mesopelagic fish.

Unprecedented ocean warming is projected to drive shoaling and intensification of OMZs in the future, with unknown consequences for pelagic ecosystems. Our findings suggest an increase of mesopelagic fish abundances with future ocean warming. However, it is also likely that beyond a certain point, which might be above 20°C SST warming at our study area, thermally driven stratification and reduced solubility cause such severe ocean deoxygenation, that the relation with temperature breaks up. Not till then oxygen levels become the main driver on population dynamics, with dramatic consequences for the mesopelagic fish community. Therefore, the S1 record might help to project the pelagic fish community in a highly deoxygenated global ocean.

4.3 Methods

4.3.1 Material

The study is based on Core M144 KC 5-6, collected with a Kasten Corer system (appendix in Gersonde, 2012) at 559.2m water depth in the central western Aegean Sea (38°55.545'N; 23°38.684'E) during cruise M144 from December 2017 to January 2018 on board *R/V Meteor* (Pross et al., 2021). Sapropel phases are identified through dark shaded bands (Figure S4.2, Table S4.2). The 345 cm long, 30 cm x 30 cm Kasten Core is subsampled into cores A and B, each core representing the top 272 cm and a surface area of 14.5 cm x 14.5 cm, sliced every 1 cm. The 0.5 cm thick walls of the Plexiglas boxes used for subsampling result in three missing samples at depths 100.5 cm, 101.5 cm and 202 cm. We obtain bulk sediment mass after drying each 1 cm slice at 50-60°C for approximately three weeks until samples reach constant dry weight. Dry samples are washed over a 125 µm screen, before drying them at 50-60°C for about 24h. Dry bulk density for each sample is calculated through dividing dry bulk sediment mass by sample volume.

4.3.2 Age Model

Six radiocarbon dates (^{14}C) are obtained from different depths of the upper core part (Table S4.3), measured in planktic foraminifera (*Globigerinoides ruber* white) tests, isolated from the 250 to 315 µm fraction. Analysis is performed by using accelerator mass spectrometry (AMS) at the NOSAMS facility at Woods Hole Oceanographic Institution (Volkman et al., 1995). Radiocarbon ages are calibrated to calendar ages by using CALIB REV8.2 program in conjunction with the Marine20 radiocarbon calibration curve allowing for the globally averaged mixed-layer reservoir age (Heaton et al., 2020; Stuiver & Reimer, 1993). Ages are reported with 2σ uncertainty. We calculate the age depth model through linear inter- and extrapolation using the given 14C calendar ages (Figure S4.3). Sedimentation rate ranges from 31.4 to 23.2 cm kyr^{-1}, which is in good accordance with sedimentation rates of Holocene records from the central Aegean Sea varying between 8.6 and 58.5 cm kyr^{-1} (Casford et al., 2007).

4.3.3 Otoliths

After dry sieving over a >250 µm screen, we isolate all otoliths and otolith fragments from the coarse size fraction and archive them on micropaleontological slides. Otolith count and identification is performed on both cores A and B, with lower resolution between 0.5cm and 151.5cm, and highest resolution between 152.5cm and 272.5cm. A binocular stereo microscope (magnification 10x – 20x) and a bifurcated illuminator is used to undertake counting and taxonomic analysis.

Otolith accumulation rates (OAR, otoliths m^{-2} yr^{-1}) are estimated by dividing raw otolith counts by dry bulk sediment mass (g^{-1}), and further multiply with sediment accumulation rate (cm yr^{-1}) and dry bulk density (g cm^{-3}) of each sample and multiplied by ten.

Identification of otoliths to the lowest taxonomic level is based on an automatic taxon identification software (Parisi-Baradad et al., 2010), web database (Lombarte et al., 2006), and otolith catalogs from the Mediterranean region (Lin et al., 2018; Tuset et

al., 2008). We classified a total number of 3273 otoliths into one of six groups: the families Myctophidae, Sternoptychidae, Engraulidae, Gadidae, and Gonostomatidae, representing the most common taxa of the otolith record, and Other. Within the five families, the following species are identified: Myctophidae: *Benthosema glaciale, Ceratoscopelus maderensis, Diaphus holti, Electrona risso, Hygophum benoiti, Hygophum hygomii, Lampanyctus crocodilus, Lampanyctus pusillus, Lobianchia dofleini, Myctophum punctatum, Notoscopelus elongatus, Symbolophorus veranyi*; Sternoptychidae: *Argyropelecus hemigymnus, Maurolicus muelleri*; Engraulidae: *Engraulis encrasicolus*; Gadidae: *Gadiculus argenteus, Micromesistius poutassou*. Otoliths we cannot identify due to deficient preservation and/or missing modern analog we classify under unidentified. Unidentified and identified otoliths not belonging to one of the target families are grouped into Other (Figure S4.1; Table 4.4-4.5). Color images for each target species are taken with reflected light and a black background using a Canon EOS 650 D camera device attached to a Leica Z16 AP0 at UAB laboratory facilities, to produce a reference catalog (Plates 4.1–4.3) and to perform automated taxon identification through the AFORO software (Parisi-Baradad et al., 2010).

Relative abundance records for the six groups are smoothed by calculating the mean values for 10 cm bins (Figure 4.1b; S4.1). Mean values regarding sapropel phases are calculated for otolith relative abundance and otolith accumulation rate (OAR) for each target family (Table S4.1).

4.3.4 Planktic foraminifera

For calculation of planktic foraminiferal accumulation rates (PFAR), a total of 108 samples were taken from Core M144 5-6 in a sample resolution of 2–4 cm. All sediment samples were initially dried and weighed before being disaggregated in distilled water and washed through a 63 µm sieve. Planktic foraminiferal counts are based on the >125 µm size fraction. If more than 250-300 specimens were present in a single sample, representative splits of the sample material were counted. Planktic foraminiferal counts (PFAR) are then recalculated for the entire sample. PFAR were calculated following Herguera and Berger (1991):

$$PFAR = F \times LSR \times DBS\ [n\ cm^{-2}\ kyr^{-1}]$$

where F is the planktic foraminifera abundance (n g^{-1}), LSR is the linear sedimentation rate (cm kyr^{-1}) and DBS is the dry bulk sediment (g cm^{-3}) (g = grams of dry sediment).

4.3.5 Color scanning

A MINOLTA CM-700d hand-held spectrophotometer was used combined with a CM-A178 target mask (Ø 8 mm, with plate) to color scan M144 KC5-6 each cm downcore on board. Sediment surface was cleaned and covered air-bubble-free with apolyethylene foil before scanning. Color data were reported in the CIELAB space using the L*a*b* system. To calibrate the spectrophotometer, a Konica Minolta White Calibration Cap CM-A177 and Zero Calibration Box CM-A182 were used. Spectral reflectance was measured over a wavelength spectrum from 400 to 700 nm. The L* and a* values were used to define sapropel phases (Table S4.4-4.6).

4.4 Supplementary Material

4.4.1 Figures

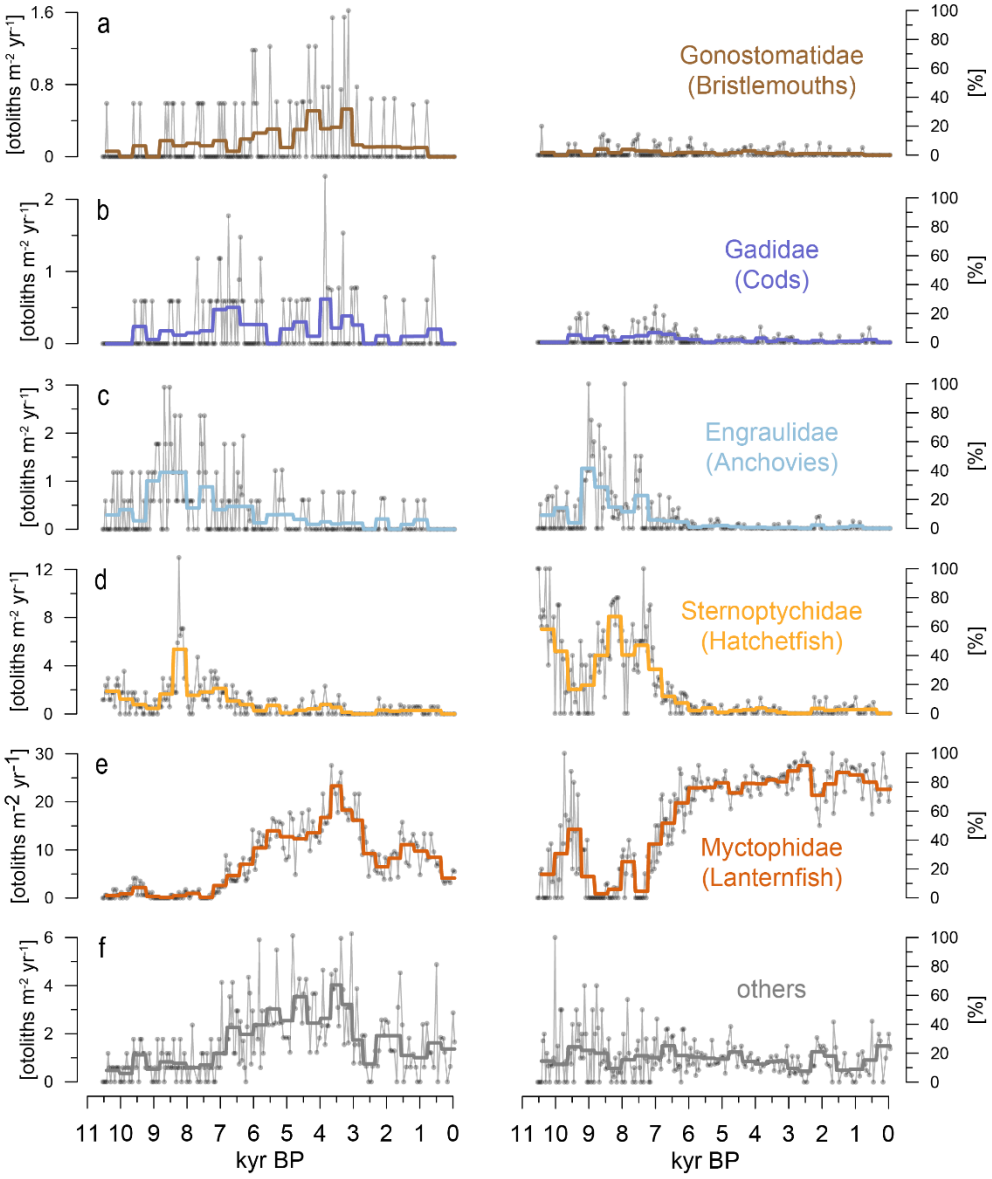

Figure S4.1: *Downcore variation of fossil otolith abundances (a-f) during the last 10.5 kyr in the central western Aegean Sea. Data represents the most common families of the otolith record, and others, shown as otolith accumulation rates (otoliths m^{-2} yr^{-1}; OAR) and relative abundances (%). Color coded lines are average values calculated for 10 cm bins.*

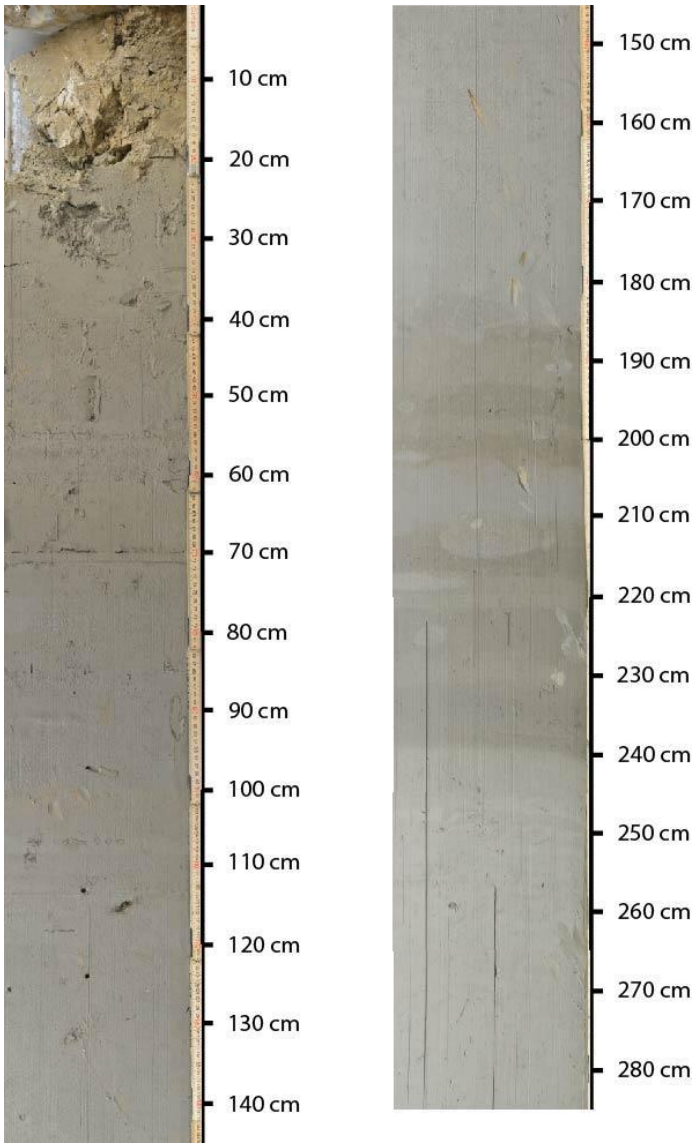

Figure S4.2: *Image of core M144 KC5-6 with core depth (cm). Darker bands identified as Sapropel layers.*

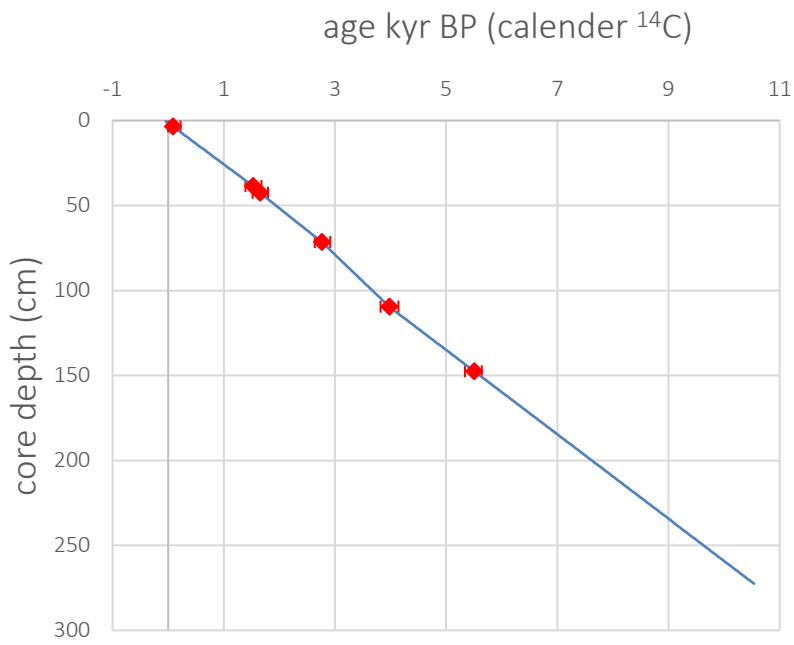

Figure S4.3: *Age-depth model derived through inter-/extrapolation of ^{14}C calendar ages.*

4.4.2 Tables

Table S4.1: *Mean otolith relative abundances (%) and -accumulation rates (otoliths m^{-2} yr^{-1}) for each sapropel phase.*

	Pre-S1	S1			Post-S1
		S1a	S1b	Interruption	
	% (ot.$m^{-2}yr^{-1}$)	% (ot.$m^{-2}yr^{-1}$)	% (ot.$m^{-2}yr^{-1}$)	% (ot.$m^{-2}yr^{-1}$)	% (ot.$m^{-2}yr^{-1}$)
Engraulidae	8.6 *(0.30)*	17.7 *(0.89)* 22.4 *(1.03)*	12.9 *(0.68)*	13.6 *(0.51)*	1.4 *(0.19)*
Gadidae	1.2 *(0.04)*	4.8 *(0.22)* 3.2 *(0.15)*	6.5 *(0.34)*	0.0 *(0.00)*	1.5 *(0.21)*
Myctophidae	31.6 *(1.08)*	14.0 *(0.64)* 8.0 *(0.37)*	20.0 *(1.04)*	25.0 *(0.93)*	77.2 *(11.11)*
Gonostomatidae	1.7 *(0.06)*	2.9 *(0.13)* 2.0 *(0.09)*	3.8 *(0.20)*	0.0 *(0.00)*	1.3 *(0.19)*
Sternoptychidae	40.8 *(1.40)*	44.2 *(2.17)* 48.4 *(2.23)*	40.0 *(2.08)*	43.2 *(1.60)*	3.0 *(0.41)*
Other	16.1 *(0.55)*	16.4 *(0.79)* 16.0 *(0.74)*	16.8 *(0.87)*	18.2 *(0.68)*	15.6 *(2.19)*
Total	-- (3.43)	-- (4.85) -- *(4.61)*	-- *(3.71)*	-- *(5.20)*	-- (14.31)

Table S4.2: *Definition of Sapropel phases through visual analysis of darker bands (see Figure S4.2). Owing to its high organic content, the Sapropel S1 layer can be identified visually by its darker color, and can be further subdivided into S1a and S1b, as the color shading displays an interruption attributed to an arid climate interlude around ~8.2 kyr BP in the Mediterranean region (Rohling et al., 2015).*

Sapropel phase	Core depth (cm)	Age (kyr BP)
Post-S1	0.5 - 180.5	-45 - 6835
S1b	181.5 - 203.5	6875 - 7761
S1-Interruption	204.5 - 210.5	7801 - 8043
S1a	211.5 - 242.5	8083 - 9331
Pre-S1	243.5 - 272.5	9371 - 10539

Table S4.3: *Uncalibrated and calibrated 14C dates of core M144 KC5-6. Calibration to calendar years AD (Median Probability), including 95.4 age error, through Marine20 radiocarbon calibration curve (Heaton et al., 2020; Stuiver & Reimer, 1993).*

depth (cm)	age ^{14}C uncalib. (yr)	age error	age ^{14}C calib. (yr AD)	2σ minus	2σ plus	species
3.5	620	20	1,866	1,727	1,950	*G. ruber* white
38.5	2120	20	425	272	561	*G. ruber* white
42.5	2230	20	299	154	432	*G. ruber* white
71.5	3130	25	-814	-964	-687	*G. ruber* white
109.5	4110	25	-2,026	-2,192	-1,870	*G. ruber* white
147.5	5330	25	-3,556	-3,691	-3,389	*G. ruber* white

Table S4.4: *M144 KC5-6 data used in the study from 0.5-99.5cm core depth. From left to right: Core ID, sample depth, sample mean age, dry bulk weight (DBD), dry bulk density (DBS), sedimentation rate; Total otolith count, concentration and accumulation rate; core color scan; planktic foraminiferal accumulation rate (PFAR).*

Core Data								Total Otolith Abundance (>250um)			Color scan	Planktic Foram
core	bottom	top	depth	mean age	DBW	DBD	sr	count	conc.	OAR	L*	PFAR
		(cm)		(kyr BP)	(g)	(g cm^{-3})	(cm kyr^{-1})	(#)	(# g^{-1})	(# cm^{-2} kyr^{-1})	(10°/D65)	(n cm^{-2} kyr^{-1})
M144 KC5-6 A&B	0	1	0.5	-0.05	141.08	0.34	23.18	13	0.09	7.17	46.20	1898.81
M144 KC5-6 A&B	1	2	1.5	0.00	120.97	0.30	23.18	15	0.12	8.62	46.91	n.a.
M144 KC5-6 A&B	2	3	2.5	0.04	117.98	0.29	23.18	n.a.	n.a.	n.a.	47.06	3763.42
M144 KC5-6 A&B	3	4	3.5	0.08	126.93	0.33	24.29	6	0.05	3.82	51.48	n.a.
M144 KC5-6 A&B	4	5	4.5	0.13	141.93	0.35	24.29	n.a.	n.a.	n.a.	51.43	2191.81
M144 KC5-6 A&B	5	6	5.5	0.17	132.86	0.33	24.29	6	0.05	3.60	53.25	n.a.
M144 KC5-6 A&B	6	7	6.5	0.21	141.26	0.35	24.29	n.a.	n.a.	n.a.	49.42	n.a.
M144 KC5-6 A&B	7	8	7.5	0.25	143.88	0.36	24.29	7	0.05	4.28	52.06	2424.98
M144 KC5-6 A&B	8	9	8.5	0.29	132.71	0.33	24.29	9	0.07	5.41	52.53	n.a.
M144 KC5-6 A&B	9	10	9.5	0.33	140.54	0.35	24.29	n.a.	n.a.	n.a.	50.85	n.a.
M144 KC5-6 A&B	10	11	10.5	0.37	159.53	0.40	24.29	12	0.08	7.39	54.08	2456.07
M144 KC5-6 A&B	11	12	11.5	0.41	179.50	0.44	24.29	n.a.	n.a.	n.a.	54.52	n.a.
M144 KC5-6 A&B	12	13	12.5	0.45	178.20	0.44	24.29	13	0.07	7.82	53.85	3645.25
M144 KC5-6 A&B	13	14	13.5	0.50	190.90	0.48	24.29	19	0.10	11.58	52.97	n.a.
M144 KC5-6 A&B	14	15	14.5	0.54	195.20	0.48	24.29	n.a.	n.a.	n.a.	53.73	3769.60
M144 KC5-6 A&B	15	16	15.5	0.58	182.60	0.45	24.29	20	0.11	11.99	52.97	n.a.
M144 KC5-6 A&B	16	17	16.5	0.62	214.10	0.53	24.29	n.a.	n.a.	n.a.	53.94	n.a.
M144 KC5-6 A&B	17	18	17.5	0.66	190.80	0.48	24.29	25	0.13	15.14	54.11	2572.66
M144 KC5-6 A&B	18	19	18.5	0.70	188.40	0.47	24.29	16	0.08	9.64	54.10	n.a.
M144 KC5-6 B	19	20	19.5	0.74	65.60	0.35	24.29	n.a.	n.a.	n.a.	55.13	n.a.
M144 KC5-6 A&B	20	21	20.5	0.78	195.28	0.49	24.29	19	0.10	11.54	54.89	1912.01
M144 KC5-6 A&B	21	22	21.5	0.83	212.80	0.52	24.29	n.a.	n.a.	n.a.	55.60	n.a.
M144 KC5-6 A&B	22	23	22.5	0.87	194.42	0.49	24.29	24	0.12	14.58	49.54	4274.81
M144 KC5-6 A&B	23	24	23.5	0.91	206.90	0.51	24.29	21	0.10	12.54	54.39	n.a.
M144 KC5-6 A&B	24	25	24.5	0.95	190.10	0.48	24.29	n.a.	n.a.	n.a.	54.44	4096.04
M144 KC5-6 A&B	25	26	25.5	0.99	205.40	0.51	24.29	9	0.04	5.43	53.79	n.a.
M144 KC5-6 A&B	26	27	26.5	1.03	232.80	0.58	24.29	n.a.	n.a.	n.a.	53.08	n.a.
M144 KC5-6 A&B	27	28	27.5	1.07	215.30	0.53	24.29	20	0.09	11.96	53.04	3396.53
M144 KC5-6 A&B	28	29	28.5	1.11	216.20	0.54	24.29	21	0.10	12.63	52.66	n.a.
M144 KC5-6 A	29	30	29.5	1.15	124.60	0.59	24.29	n.a.	n.a.	n.a.	52.55	n.a.
M144 KC5-6 A&B	30	31	30.5	1.20	219.29	0.52	24.29	27	0.12	15.60	53.26	4678.97
M144 KC5-6 A&B	31	32	31.5	1.24	215.40	0.54	24.29	n.a.	n.a.	n.a.	52.43	n.a.
M144 KC5-6 A&B	32	33	32.5	1.28	212.90	0.53	24.29	20	0.09	12.12	51.87	4647.88
M144 KC5-6 A&B	33	34	33.5	1.32	225.20	0.56	24.29	15	0.07	9.09	51.60	n.a.
M144 KC5-6 A&B	34	35	34.5	1.36	219.20	0.56	24.29	n.a.	n.a.	n.a.	50.44	n.a.
M144 KC5-6 A&B	35	36	35.5	1.40	215.60	0.54	24.29	13	0.06	7.96	51.23	3194.45
M144 KC5-6 A&B	36	37	36.5	1.44	230.30	0.57	24.29	n.a.	n.a.	n.a.	50.49	n.a.
M144 KC5-6 A&B	37	38	37.5	1.48	231.90	0.58	24.29	23	0.10	13.91	50.82	2964.33
M144 KC5-6 A&B	38	39	38.5	1.53	227.51	0.57	31.75	23	0.10	18.15	50.50	n.a.
M144 KC5-6 A&B	39	40	39.5	1.56	227.70	0.56	31.75	n.a.	n.a.	n.a.	49.61	n.a.
M144 KC5-6 A&B	40	41	40.5	1.59	245.24	0.58	31.75	25	0.10	18.87	50.92	n.a.
M144 KC5-6 A&B	41	42	41.5	1.62	222.10	0.58	31.75	n.a.	n.a.	n.a.	51.28	3919.90
M144 KC5-6 A&B	42	43	42.5	1.65	249.75	0.59	26.06	12	0.05	7.44	51.18	4193.93
M144 KC5-6 A&B	43	44	43.5	1.69	235.30	0.59	26.06	14	0.06	9.14	52.30	n.a.
M144 KC5-6 A&B	44	45	44.5	1.73	235.70	0.59	26.06	n.a.	n.a.	n.a.	52.04	3022.46
M144 KC5-6 A&B	45	46	45.5	1.77	245.10	0.61	26.06	18	0.07	11.61	51.43	n.a.
M144 KC5-6 A&B	46	47	46.5	1.80	241.70	0.60	26.06	n.a.	n.a.	n.a.	52.51	n.a.
M144 KC5-6 A&B	47	48	47.5	1.84	282.30	0.69	26.06	16	0.06	10.25	52.77	2426.31
M144 KC5-6 A&B	48	49	48.5	1.88	249.50	0.62	26.06	9	0.04	5.85	53.22	n.a.
M144 KC5-6 A&B	49	50	49.5	1.92	259.90	0.64	26.06	n.a.	n.a.	n.a.	53.26	n.a.
M144 KC5-6 A&B	50	51	50.5	1.96	248.88	0.59	26.06	16	0.06	9.91	54.27	3485.21
M144 KC5-6 A&B	51	52	51.5	2.00	253.90	0.63	26.06	n.a.	n.a.	n.a.	52.47	n.a.
M144 KC5-6 A&B	52	53	52.5	2.03	250.64	0.62	26.06	18	0.07	11.62	53.07	2409.63
M144 KC5-6 A&B	53	54	53.5	2.07	253.27	0.63	26.06	12	0.05	7.73	52.22	n.a.
M144 KC5-6 A&B	54	55	54.5	2.11	263.78	0.66	26.06	n.a.	n.a.	n.a.	51.61	3301.78
M144 KC5-6 A&B	55	56	55.5	2.15	259.93	0.64	26.06	13	0.05	8.36	51.71	n.a.
M144 KC5-6 A&B	56	57	56.5	2.19	257.94	0.64	26.06	n.a.	n.a.	n.a.	51.56	n.a.
M144 KC5-6 A&B	57	58	57.5	2.23	258.50	0.64	26.06	18	0.07	11.61	52.51	3085.00
M144 KC5-6 A	58	59	58.5	2.27	255.41	0.63	26.06	9	0.04	5.82	51.34	n.a.
M144 KC5-6 A&B	59	60	59.5	2.30	133.62	0.64	26.06	n.a.	n.a.	n.a.	51.97	n.a.
M144 KC5-6 A&B	60	61	60.5	2.34	264.53	0.65	26.06	11	0.04	7.05	52.77	2534.70
M144 KC5-6 A&B	61	62	61.5	2.38	261.70	0.65	26.06	n.a.	n.a.	n.a.	51.47	n.a.
M144 KC5-6 A&B	62	63	62.5	2.42	264.20	0.65	26.06	16	0.06	10.30	52.51	2134.48
M144 KC5-6 A&B	63	64	63.5	2.46	264.10	0.65	26.06	15	0.06	9.65	52.23	n.a.
M144 KC5-6 A&B	64	65	64.5	2.50	263.80	0.65	26.06	n.a.	n.a.	n.a.	51.40	1384.08
M144 KC5-6 A&B	65	66	65.5	2.53	270.10	0.67	26.06	7	0.03	4.51	51.37	n.a.
M144 KC5-6 A&B	66	67	66.5	2.57	262.90	0.65	26.06	n.a.	n.a.	n.a.	52.08	n.a.
M144 KC5-6 A&B	67	68	67.5	2.61	265.60	0.66	26.06	19	0.07	12.24	51.59	1909.36
M144 KC5-6 A&B	68	69	68.5	2.65	267.30	0.66	26.06	26	0.10	16.70	51.58	n.a.
M144 KC5-6 A&B	69	70	69.5	2.69	287.29	0.68	26.06	n.a.	n.a.	n.a.	51.97	n.a.
M144 KC5-6 A&B	70	71	70.5	2.73	270.20	0.67	26.06	17	0.06	10.93	51.91	2577.88
M144 KC5-6 B	71	72	71.5	2.76	126.60	0.65	31.35	n.a.	n.a.	n.a.	52.76	n.a.
M144 KC5-6 A&B	72	73	72.5	2.80	272.70	0.67	31.35	17	0.06	13.14	51.96	3125.28
M144 KC5-6 A&B	73	74	73.5	2.83	268.90	0.66	31.35	30	0.11	23.21	51.90	n.a.
M144 KC5-6 A&B	74	75	74.5	2.86	273.40	0.67	31.35	n.a.	n.a.	n.a.	51.31	1183.89
M144 KC5-6 A&B	75	76	75.5	2.89	270.30	0.67	31.35	28	0.10	21.68	51.44	n.a.
M144 KC5-6 A&B	76	77	76.5	2.92	268.80	0.66	31.35	n.a.	n.a.	n.a.	50.68	n.a.
M144 KC5-6 A&B	77	78	77.5	2.96	270.50	0.67	31.35	31	0.11	23.93	51.50	2904.55
M144 KC5-6 A&B	78	79	78.5	2.99	277.60	0.68	31.35	23	0.08	17.75	52.03	n.a.
M144 KC5-6 A&B	79	80	79.5	3.02	289.60	0.69	31.35	n.a.	n.a.	n.a.	49.43	n.a.
M144 KC5-6 A&B	80	81	80.5	3.05	277.86	0.68	31.35	32	0.12	24.64	51.15	2578.48
M144 KC5-6 A&B	81	82	81.5	3.08	279.30	0.69	31.35	n.a.	n.a.	n.a.	50.49	n.a.
M144 KC5-6 A&B	82	83	82.5	3.11	278.20	0.69	31.35	28	0.10	21.63	50.29	4013.20
M144 KC5-6 B	83	84	83.5	3.15	121.40	0.63	31.35	12	0.10	19.44	50.72	n.a.
M144 KC5-6 A&B	84	85	84.5	3.18	282.60	0.70	31.35	n.a.	n.a.	n.a.	49.79	3170.43
M144 KC5-6 A&B	85	86	85.5	3.21	283.20	0.70	31.35	27	0.10	20.82	50.65	n.a.
M144 KC5-6 A&B	86	87	86.5	3.24	280.80	0.69	31.35	n.a.	n.a.	n.a.	51.13	n.a.
M144 KC5-6 A&B	87	88	87.5	3.27	273.80	0.68	31.35	29	0.11	22.44	50.61	2518.28
M144 KC5-6 A&B	88	89	88.5	3.31	271.00	0.66	31.35	35	0.13	26.83	51.94	n.a.
M144 KC5-6 A&B	89	90	89.5	3.34	265.28	0.65	31.35	n.a.	n.a.	n.a.	51.05	n.a.
M144 KC5-6 A&B	90	91	90.5	3.37	289.93	0.69	31.35	44	0.15	32.81	50.51	2152.08
M144 KC5-6 A&B	91	92	91.5	3.40	272.95	0.67	31.35	n.a.	n.a.	n.a.	51.78	n.a.
M144 KC5-6 A&B	92	93	92.5	3.43	282.24	0.69	31.35	38	0.13	29.30	51.80	2613.60
M144 KC5-6 A&B	93	94	93.5	3.47	274.47	0.68	31.35	28	0.10	21.64	51.71	n.a.
M144 KC5-6 A&B	94	95	94.5	3.50	275.69	0.68	31.35	n.a.	n.a.	n.a.	50.93	2663.76
M144 KC5-6 A&B	95	96	95.5	3.53	271.67	0.67	31.35	34	0.13	26.32	50.77	n.a.
M144 KC5-6 A&B	96	97	96.5	3.56	275.64	0.68	31.35	n.a.	n.a.	n.a.	51.46	n.a.
M144 KC5-6 A&B	97	98	97.5	3.59	284.21	0.70	31.35	36	0.13	27.77	51.50	n.a.
M144 KC5-6 A&B	98	99	98.5	3.63	282.37	0.69	31.35	37	0.13	28.51	51.98	1936.37
M144 KC5-6 A&B	99	100	99.5	3.66	413.34	0.98	-0.27	45	0.11	-0.29	52.31	n.a.

Table S4.5: *M144 KC5-6 data used in the study from 100.5-199.5cm core depth. From left to right: Core ID, sample depth, sample mean age, dry bulk weight (DBD), dry bulk density (DBS), sedimentation rate; Total otolith count, concentration and accumulation rate; core color scan; planktic foraminiferal accumulation rate (PFAR).*

	Core Data							Total Otolith Abundance (>250um)			Color scan	Planktic Foram
core	bottom	top	depth	mean age	DBW	DBD	sr	count	conc.	OAR	L*	PFAR
		(cm)		(kyr BP)	(g)	(g cm^{-3})	(cm kyr^{-1})	(#)	(# g^{-1})	(# cm^{-2} kyr^{-1})	(10^3/D65)	(n cm^{-2} kyr^{-1})
M144 KC5-6 A&B	100	101	100.5	3.69	265.35	0.63	31.35	n.a.	n.a.	n.a.	n.a.	n.a.
M144 KC5-6 A&B	101	102	101.5	3.72	260.06	0.64	31.35	n.a.	n.a.	n.a.	n.a.	2478.15
M144 KC5-6 A&B	102	103	102.5	3.75	264.13	0.65	31.35	27	0.10	20.89	51.26	n.a.
M144 KC5-6 A&B	103	104	103.5	3.78	260.84	0.65	31.35	24	0.09	18.70	51.55	3150.36
M144 KC5-6 A&B	104	105	104.5	3.82	272.80	0.67	31.35	n.a.	n.a.	n.a.	51.05	n.a.
M144 KC5-6 A&B	105	106	105.5	3.85	268.90	0.66	31.35	28	0.10	21.65	50.46	n.a.
M144 KC5-6 A&B	106	107	106.5	3.88	268.97	0.66	31.35	n.a.	n.a.	n.a.	49.97	2142.05
M144 KC5-6 A&B	107	108	107.5	3.91	265.20	0.65	31.35	37	0.14	28.64	51.05	n.a.
M144 KC5-6 A&B	108	109	108.5	3.94	259.57	0.65	31.35	21	0.08	16.36	50.72	n.a.
M144 KC5-6 A&B	109	110	109.5	3.98	270.97	0.67	24.84	n.a.	n.a.	n.a.	51.13	2502.80
M144 KC5-6 A&B	110	111	110.5	4.02	278.80	0.68	24.84	22	0.08	13.35	51.73	n.a.
M144 KC5-6 A&B	111	112	111.5	4.06	283.70	0.70	24.84	n.a.	n.a.	n.a.	51.33	2479.69
M144 KC5-6 A&B	112	113	112.5	4.10	286.60	0.71	24.84	23	0.08	14.07	51.32	n.a.
M144 KC5-6 A&B	113	114	113.5	4.14	279.70	0.69	24.84	30	0.11	18.36	51.91	2932.71
M144 KC5-6 A&B	114	115	114.5	4.18	279.70	0.69	24.84	n.a.	n.a.	n.a.	50.92	n.a.
M144 KC5-6 A&B	115	116	115.5	4.22	277.50	0.68	24.84	35	0.13	21.40	50.86	n.a.
M144 KC5-6 A&B	116	117	116.5	4.26	282.80	0.70	24.84	n.a.	n.a.	n.a.	52.12	3091.66
M144 KC5-6 A&B	117	118	117.5	4.30	289.80	0.71	24.84	19	0.07	11.64	51.91	n.a.
M144 KC5-6 A&B	118	119	118.5	4.34	279.22	0.69	24.84	39	0.14	23.86	51.58	n.a.
M144 KC5-6 A&B	119	120	119.5	4.38	290.00	0.71	24.84	n.a.	n.a.	n.a.	52.08	3306.25
M144 KC5-6 A&B	120	121	120.5	4.42	313.90	0.77	24.84	28	0.09	17.07	51.47	n.a.
M144 KC5-6 A&B	121	122	121.5	4.46	311.50	0.76	24.84	n.a.	n.a.	n.a.	50.80	2296.89
M144 KC5-6 A&B	122	123	122.5	4.50	315.30	0.77	24.84	31	0.10	18.88	50.76	n.a.
M144 KC5-6 A&B	123	124	123.5	4.54	300.90	0.74	24.84	38	0.13	23.18	51.41	2233.31
M144 KC5-6 A&B	124	125	124.5	4.58	305.20	0.75	24.84	n.a.	n.a.	n.a.	51.55	n.a.
M144 KC5-6 A&B	125	126	125.5	4.62	294.80	0.73	24.84	29	0.10	17.76	50.91	n.a.
M144 KC5-6 A&B	126	127	126.5	4.66	137.50	0.70	24.84	n.a.	n.a.	n.a.	51.94	2567.11
M144 KC5-6 A&B	127	128	127.5	4.70	318.60	0.76	24.84	29	0.09	17.13	52.09	n.a.
M144 KC5-6 A&B	128	129	128.5	4.74	302.09	0.74	24.84	13	0.04	7.91	52.13	n.a.
M144 KC5-6 A&B	129	130	129.5	4.78	307.60	0.76	24.84	n.a.	n.a.	n.a.	51.16	2702.22
M144 KC5-6 A&B	130	131	130.5	4.82	290.00	0.71	24.84	37	0.13	22.49	51.82	n.a.
M144 KC5-6 A&B	131	132	131.5	4.86	287.63	0.71	24.84	n.a.	n.a.	n.a.	51.21	2312.78
M144 KC5-6 A&B	132	133	132.5	4.90	286.46	0.71	24.84	33	0.12	20.21	51.92	n.a.
M144 KC5-6 A&B	133	134	133.5	4.94	294.32	0.72	24.84	17	0.06	10.39	51.72	2265.10
M144 KC5-6 A&B	134	135	134.5	4.98	295.46	0.73	24.84	n.a.	n.a.	n.a.	52.33	n.a.
M144 KC5-6 A&B	135	136	135.5	5.02	299.43	0.74	24.84	17	0.06	10.38	52.32	n.a.
M144 KC5-6 A&B	136	137	136.5	5.06	293.03	0.72	24.84	n.a.	n.a.	n.a.	52.15	2312.78
M144 KC5-6 A&B	137	138	137.5	5.10	300.53	0.74	24.84	22	0.07	13.44	52.24	n.a.
M144 KC5-6 A&B	138	139	138.5	5.14	301.32	0.75	24.84	31	0.10	19.14	52.59	n.a.
M144 KC5-6 A&B	139	140	139.5	5.18	297.80	0.73	24.84	n.a.	n.a.	n.a.	52.03	2797.59
M144 KC5-6 A&B	140	141	140.5	5.22	310.70	0.76	24.84	32	0.10	19.52	51.82	n.a.
M144 KC5-6 A&B	141	142	141.5	5.26	309.20	0.76	24.84	n.a.	n.a.	n.a.	51.82	2857.20
M144 KC5-6 A&B	142	143	142.5	5.30	314.70	0.77	24.84	31	0.10	18.90	51.53	n.a.
M144 KC5-6 A&B	143	144	143.5	5.34	299.70	0.74	24.84	34	0.11	20.75	50.12	3401.62
M144 KC5-6 A&B	144	145	144.5	5.39	307.70	0.76	24.84	n.a.	n.a.	n.a.	52.63	n.a.
M144 KC5-6 A&B	145	146	145.5	5.43	302.51	0.72	24.84	34	0.11	20.08	51.97	n.a.
M144 KC5-6 A&B	146	147	146.5	5.47	277.10	0.68	24.84	n.a.	n.a.	n.a.	51.47	3258.56
M144 KC5-6 A&B	147	148	147.5	5.51	293.80	0.72	24.84	27	0.09	16.51	52.15	n.a.
M144 KC5-6 A&B	148	149	148.5	5.55	318.24	0.76	24.84	24	0.08	14.18	52.49	n.a.
M144 KC5-6 A&B	149	150	149.5	5.59	290.30	0.71	24.84	n.a.	n.a.	n.a.	52.32	3512.89
M144 KC5-6 A&B	150	151	150.5	5.63	318.24	0.76	24.84	25	0.08	14.77	52.29	n.a.
M144 KC5-6 A&B	151	152	151.5	5.67	300.20	0.71	24.84	n.a.	n.a.	n.a.	52.27	3783.11
M144 KC5-6 A&B	152	153	152.5	5.71	306.22	0.73	24.84	24	0.08	14.18	51.44	n.a.
M144 KC5-6 A&B	153	154	153.5	5.75	315.61	0.75	24.84	24	0.08	14.18	51.48	4379.19
M144 KC5-6 A&B	154	155	154.5	5.79	300.37	0.71	24.84	22	0.07	12.99	50.97	n.a.
M144 KC5-6 A&B	155	156	155.5	5.83	298.04	0.71	24.84	34	0.11	20.08	52.35	n.a.
M144 KC5-6 A&B	156	157	156.5	5.87	293.39	0.70	24.84	24	0.08	14.18	51.63	2972.44
M144 KC5-6 A&B	157	158	157.5	5.91	266.56	0.63	24.84	22	0.08	12.99	51.30	n.a.
M144 KC5-6 A&B	158	159	158.5	5.95	266.19	0.63	24.84	17	0.06	10.04	51.01	n.a.
M144 KC5-6 A&B	159	160	159.5	5.99	282.90	0.67	24.84	17	0.06	10.04	51.52	3258.56
M144 KC5-6 A&B	160	161	160.5	6.03	269.75	0.64	24.84	32	0.12	18.90	52.29	n.a.
M144 KC5-6 A&B	161	162	161.5	6.07	322.76	0.77	24.84	18.21	0.06	10.76	51.21	2408.16
M144 KC5-6 A&B	162	163	162.5	6.11	354.77	0.84	24.84	23.41	0.07	13.83	51.48	n.a.
M144 KC5-6 A&B	163	164	163.5	6.15	378.37	0.90	24.84	20.09	0.05	11.87	51.63	4776.58
M144 KC5-6 A&B	164	165	164.5	6.19	357.88	0.85	24.84	10.65	0.03	6.29	51.49	n.a.
M144 KC5-6 A&B	165	166	165.5	6.23	274.78	0.65	24.84	7.08	0.03	4.18	51.72	n.a.
M144 KC5-6 A&B	166	167	166.5	6.27	317.36	0.75	24.84	9.34	0.03	5.52	50.88	3401.62
M144 KC5-6 A&B	167	168	167.5	6.31	276.27	0.66	24.84	23.51	0.09	13.89	51.05	n.a.
M144 KC5-6 A&B	168	169	168.5	6.35	287.13	0.68	24.84	17.04	0.06	10.06	50.76	n.a.
M144 KC5-6 A&B	169	170	169.5	6.39	296.30	0.70	24.84	20	0.07	11.81	50.53	3449.31
M144 KC5-6 A&B	170	171	170.5	6.43	284.50	0.68	24.84	15.95	0.06	9.42	49.27	n.a.
M144 KC5-6 A&B	171	172	171.5	6.47	276.06	0.66	24.84	15.55	0.06	9.18	50.27	4212.29
M144 KC5-6 A&B	172	173	172.5	6.51	319.25	0.76	24.84	16	0.05	9.45	49.04	n.a.
M144 KC5-6 A&B	173	174	173.5	6.55	324.42	0.77	24.84	9	0.03	5.32	49.22	4379.19
M144 KC5-6 A&B	174	175	174.5	6.59	336.95	0.80	24.84	14	0.04	8.27	49.18	n.a.
M144 KC5-6 A&B	175	176	175.5	6.63	315.36	0.75	24.84	19	0.06	11.22	49.10	n.a.
M144 KC5-6 A&B	176	177	176.5	6.67	325.39	0.77	24.84	11	0.03	6.50	48.78	4967.32
M144 KC5-6 A&B	177	178	177.5	6.71	317.61	0.76	24.84	22	0.07	12.99	50.54	n.a.
M144 KC5-6 A&B	178	179	178.5	6.75	346.29	0.82	24.84	16	0.05	9.45	51.46	n.a.
M144 KC5-6 A&B	179	180	179.5	6.79	330.99	0.79	24.84	14	0.04	8.27	47.92	5173.96
M144 KC5-6 A&B	180	181	180.5	6.83	322.31	0.77	24.84	22	0.07	12.99	47.70	n.a.
M144 KC5-6 A&B	181	182	181.5	6.87	299.50	0.71	24.84	13	0.04	7.68	48.06	8392.78
M144 KC5-6 A&B	182	183	182.5	6.92	311.00	0.74	24.84	12	0.04	7.09	46.48	n.a.
M144 KC5-6 A&B	183	184	183.5	6.96	333.68	0.79	24.84	16	0.05	9.45	44.89	15196.03
M144 KC5-6 A&B	184	185	184.5	7.00	329.00	0.78	24.84	8	0.02	4.73	47.81	n.a.
M144 KC5-6 A&B	185	186	185.5	7.04	333.50	0.79	24.84	10	0.03	5.91	46.50	n.a.
M144 KC5-6 A&B	186	187	186.5	7.08	264.96	0.63	24.84	11	0.04	6.50	46.26	7327.79
M144 KC5-6 A&B	187	188	187.5	7.12	324.87	0.77	24.84	11	0.03	6.50	45.81	n.a.
M144 KC5-6 A&B	188	189	188.5	7.16	343.62	0.82	24.84	8	0.02	4.73	46.00	n.a.
M144 KC5-6 A&B	189	190	189.5	7.20	288.80	0.69	24.84	7	0.02	4.13	46.58	15291.40
M144 KC5-6 A&B	190	191	190.5	7.24	318.77	0.76	24.84	7	0.02	4.13	44.02	n.a.
M144 KC5-6 A&B	191	192	191.5	7.28	294.80	0.70	24.84	10	0.03	5.91	45.23	11285.75
M144 KC5-6 A&B	192	193	192.5	7.32	317.11	0.75	24.84	6	0.02	3.54	44.78	n.a.
M144 KC5-6 A&B	193	194	193.5	7.36	347.38	0.83	24.84	1	0.00	0.59	44.01	17739.29
M144 KC5-6 A&B	194	195	194.5	7.40	326.86	0.78	24.84	4	0.01	2.36	43.70	n.a.
M144 KC5-6 A&B	195	196	195.5	7.44	354.27	0.84	24.84	4	0.01	2.36	44.13	n.a.
M144 KC5-6 A&B	196	197	196.5	7.48	214.97	0.51	24.84	10	0.05	5.91	46.31	7280.10
M144 KC5-6 A&B	197	198	197.5	7.52	381.36	0.91	24.84	7	0.02	4.13	46.32	n.a.
M144 KC5-6 A&B	198	199	198.5	7.56	328.72	0.78	24.84	9	0.03	5.32	48.98	n.a.
M144 KC5-6 A&B	199	200	199.5	7.60	278.89	0.66	24.84	8	0.03	4.73	39.55	n.a.

Table S4.6: *M144 KC5-6 data used in the study from 200.5-272.5cm core depth. From left to right: Core ID, sample depth, sample mean age, dry bulk weight (DBD), dry bulk density (DBS), sedimentation rate; Total otolith count, concentration and accumulation rate; core color scan; planktic foraminiferal accumulation rate (PFAR).*

	Core Data							otal Otolith Abundance (>250un			Color scan	Planktic Foram
core	bottom	top	depth	mean age	DBW	DBD	sr	count	conc.	OAR	L*	PFAR
		(cm)		(kyr BP)	(g)	(g cm^{-3})	(cm kyr^{-1})	(#)	(# g^{-1})	(# cm^{-2} kyr^{-1})	(10°/D65)	(n cm^{-2} kyr^{-1})
M144 KC5-6 A&B	200	201	200.5	7.64	324.44	0.77	24.84	10	0.03	5.91	46.37	15186.94
M144 KC5-6 A&B	201	202	201.5	7.68	494.88	1.18	24.84	13	0.03	7.68	47.11	n.a.
M144 KC5-6 A&B	202	203	202.5	7.72	0.00	0.00	24.84	n.a.	n.a.	n.a.	46.32	3910.27
M144 KC5-6 A&B	203	204	203.5	7.76	343.20	0.82	24.84	2	0.01	1.18	47.93	n.a.
M144 KC5-6 A&B	204	205	204.5	7.80	366.88	0.87	24.84	5	0.01	2.95	48.84	n.a.
M144 KC5-6 A&B	205	206	205.5	7.84	317.78	0.76	24.84	7	0.02	4.13	47.33	3783.11
M144 KC5-6 A&B	206	207	206.5	7.88	324.08	0.77	24.84	6	0.02	3.54	47.59	n.a.
M144 KC5-6 A&B	207	208	207.5	7.92	335.40	0.80	24.84	1	0.00	0.59	44.21	n.a.
M144 KC5-6 A&B	208	209	208.5	7.96	317.37	0.75	24.84	3	0.01	1.77	44.09	2296.89
M144 KC5-6 A&B	209	210	209.5	8.00	331.99	0.79	24.84	7	0.02	4.13	44.50	n.a.
M144 KC5-6 A&B	210	211	210.5	8.04	293.67	0.70	24.84	15	0.05	8.86	42.06	7995.40
M144 KC5-6 A&B	211	212	211.5	8.08	284.10	0.68	24.84	10	0.04	5.91	43.49	n.a.
M144 KC5-6 A&B	212	213	212.5	8.12	326.69	0.78	24.84	15	0.05	8.86	41.55	8066.93
M144 KC5-6 A&B	213	214	213.5	8.16	336.85	0.80	24.84	15	0.04	8.86	40.29	n.a.
M144 KC5-6 A&B	214	215	214.5	8.20	320.43	0.76	24.84	18	0.06	10.63	43.90	n.a.
M144 KC5-6 A&B	215	216	215.5	8.24	390.11	0.93	24.84	28	0.07	16.54	42.92	7653.65
M144 KC5-6 A&B	216	217	216.5	8.28	341.92	0.81	24.84	13	0.04	7.68	43.05	n.a.
M144 KC5-6 A&B	217	218	217.5	8.32	400.88	0.95	24.84	4	0.01	2.36	44.39	n.a.
M144 KC5-6 A&B	218	219	218.5	8.36	373.72	0.89	24.84	8	0.02	4.73	42.33	8885.54
M144 KC5-6 A&B	219	220	219.5	8.40	361.66	0.86	24.84	10	0.03	5.91	41.63	n.a.
M144 KC5-6 A&B	220	221	220.5	8.45	415.49	0.99	24.84	10	0.02	5.91	41.94	18184.37
M144 KC5-6 A&B	221	222	221.5	8.49	493.31	1.17	24.84	11	0.02	6.50	41.62	n.a.
M144 KC5-6 A&B	222	223	222.5	8.53	316.03	0.75	24.84	9	0.03	5.32	43.67	5825.67
M144 KC5-6 A&B	223	224	223.5	8.57	338.45	0.80	24.84	7	0.02	4.13	43.71	n.a.
M144 KC5-6 A&B	224	225	224.5	8.61	293.89	0.70	24.84	4	0.01	2.36	43.39	n.a.
M144 KC5-6 A&B	225	226	225.5	8.65	405.07	0.96	24.84	8	0.02	4.73	43.83	5563.40
M144 KC5-6 A&B	226	227	226.5	8.69	304.61	0.72	24.84	7	0.02	4.13	43.03	n.a.
M144 KC5-6 A&B	227	228	227.5	8.73	325.20	0.77	24.84	8	0.02	4.73	44.47	n.a.
M144 KC5-6 A&B	228	229	228.5	8.77	326.55	0.78	24.84	3	0.01	1.77	44.46	8933.23
M144 KC5-6 A&B	229	230	229.5	8.81	323.82	0.77	24.84	3	0.01	1.77	41.88	n.a.
M144 KC5-6 A&B	230	231	230.5	8.85	380.66	0.91	24.84	5	0.01	2.95	41.68	11158.59
M144 KC5-6 A&B	231	232	231.5	8.89	296.43	0.70	24.84	6	0.02	3.54	43.11	n.a.
M144 KC5-6 A&B	232	233	232.5	8.93	407.96	0.97	24.84	4	0.01	2.36	41.41	11301.65
M144 KC5-6 A&B	233	234	233.5	8.97	349.28	0.83	24.84	5	0.01	2.95	42.96	n.a.
M144 KC5-6 A&B	234	235	234.5	9.01	382.83	0.91	24.84	1	0.00	0.59	44.27	n.a.
M144 KC5-6 A&B	235	236	235.5	9.05	430.32	1.02	24.84	5	0.01	2.95	43.28	5118.33
M144 KC5-6 A&B	236	237	236.5	9.09	305.37	0.73	24.84	3	0.01	1.77	46.41	n.a.
M144 KC5-6 A&B	237	238	237.5	9.13	333.80	0.79	24.84	3	0.01	1.77	46.72	n.a.
M144 KC5-6 A&B	238	239	238.5	9.17	352.04	0.84	24.84	6	0.02	3.54	46.26	8821.96
M144 KC5-6 A&B	239	240	239.5	9.21	311.53	0.74	24.84	3	0.01	1.77	49.85	n.a.
M144 KC5-6 A&B	240	241	240.5	9.25	328.91	0.78	24.84	6	0.02	3.54	47.06	5770.04
M144 KC5-6 A&B	241	242	241.5	9.29	346.67	0.82	24.84	5	0.01	2.95	48.11	n.a.
M144 KC5-6 A&B	242	243	242.5	9.33	341.61	0.81	24.84	7	0.02	4.13	50.16	3298.30
M144 KC5-6 A&B	243	244	243.5	9.37	360.70	0.86	24.84	6	0.02	3.54	52.82	n.a.
M144 KC5-6 A&B	244	245	244.5	9.41	385.10	0.92	24.84	13	0.03	7.68	52.33	n.a.
M144 KC5-6 A&B	245	246	245.5	9.45	449.38	1.07	24.84	5	0.01	2.95	51.94	3799.01
M144 KC5-6 A&B	246	247	246.5	9.49	405.67	0.96	24.84	5	0.01	2.95	52.10	n.a.
M144 KC5-6 A&B	247	248	247.5	9.53	364.13	0.87	24.84	8	0.02	4.73	49.76	n.a.
M144 KC5-6 A&B	248	249	248.5	9.57	383.30	0.91	24.84	10	0.03	5.91	48.91	3814.90
M144 KC5-6 A&B	249	250	249.5	9.61	405.83	0.97	24.84	13	0.03	7.68	49.25	n.a.
M144 KC5-6 A&B	250	251	250.5	9.65	400.06	0.95	24.84	8	0.02	4.73	50.57	3043.97
M144 KC5-6 A&B	251	252	251.5	9.69	362.22	0.86	24.84	7	0.02	4.13	49.56	n.a.
M144 KC5-6 A&B	252	253	252.5	9.73	327.35	0.78	24.84	1	0.00	0.59	50.05	2805.54
M144 KC5-6 A&B	253	254	253.5	9.77	523.68	1.25	24.84	8	0.02	4.73	50.99	n.a.
M144 KC5-6 A&B	254	255	254.5	9.81	443.16	1.05	24.84	4	0.01	2.36	49.89	n.a.
M144 KC5-6 A&B	255	256	255.5	9.85	485.67	1.15	24.84	2	0.00	1.18	49.22	3107.56
M144 KC5-6 A&B	256	257	256.5	9.89	393.88	0.94	24.84	8	0.02	4.73	50.05	n.a.
M144 KC5-6 A&B	257	258	257.5	9.93	386.96	0.92	24.84	4	0.01	2.36	50.41	n.a.
M144 KC5-6 A&B	258	259	258.5	9.98	366.21	0.87	24.84	7	0.02	4.13	49.76	1963.08
M144 KC5-6 A&B	259	260	259.5	10.02	435.39	1.04	24.84	0	0.00	0.00	49.95	n.a.
M144 KC5-6 A&B	260	261	260.5	10.06	386.88	0.92	24.84	6	0.02	3.54	49.96	3043.97
M144 KC5-6 A&B	261	262	261.5	10.10	387.20	0.92	24.84	9	0.02	5.32	49.91	n.a.
M144 KC5-6 A&B	262	263	262.5	10.14	482.68	1.15	24.84	8	0.02	4.73	50.16	1351.11
M144 KC5-6 A&B	263	264	263.5	10.18	396.23	0.94	24.84	1	0.00	0.59	49.42	n.a.
M144 KC5-6 A&B	264	265	264.5	10.22	357.03	0.85	24.84	9	0.03	5.32	49.15	n.a.
M144 KC5-6 A&B	265	266	265.5	10.26	405.12	0.96	24.84	5	0.01	2.95	48.70	2018.72
M144 KC5-6 A&B	266	267	266.5	10.30	318.43	0.76	24.84	2	0.01	1.18	48.65	n.a.
M144 KC5-6 A&B	267	268	267.5	10.34	324.33	0.77	24.84	3	0.01	1.77	49.47	n.a.
M144 KC5-6 A&B	268	269	268.5	10.38	334.38	0.80	24.84	7	0.02	4.13	49.21	1486.22
M144 KC5-6 A&B	269	270	269.5	10.42	328.90	0.78	24.84	5	0.02	2.95	49.32	n.a.
M144 KC5-6 A&B	270	271	270.5	10.46	327.55	0.78	24.84	6	0.02	3.54	49.55	735.16
M144 KC5-6 A&B	271	272	271.5	10.50	391.29	0.93	24.84	2	0.01	1.18	49.35	n.a.
M144 KC5-6 A&B	272	273	272.5	10.54	300.78	0.72	24.84	2	0.01	1.18	49.50	n.a.

Table S4.7: *M144 KC5-6 data used in the study from 0.5-99.5cm core depth. Core depth; Taxa otolith count, concentration and accumulation rate.*

Core Data	Engraulidae			Gadidae						Myctophidae			Gonostomatidae			Sternoptychidae						Rest		
	E. encrasicolus			*G. argenteus*			*M. poutassou*									A. hemigymnus			M. mülleri					
depth	count	OAR	relative	count	OAR	relative	count	OAR	relative	count	OAR	relative	count	OAR	relative	count	OAR	relative	count	OAR	relative	count	OAR	relative
(cm)	(#)	(# cm^{-2} kyr^{-1})	(%)	(#)	(# cm^{-2} kyr^{-1})	(%)	(#)	(# cm^{-2} kyr^{-1})	(%)	(#)	(# cm^{-2} kyr^{-1})	(%)	(#)	(# cm^{-2} kyr^{-1})	(%)	(#)	(# cm^{-2} kyr^{-1})	(%)	(#)	(# cm^{-2} kyr^{-1})	(%)	(#)	(# cm^{-2} kyr^{-1})	(%)
0.5	0.00	0.00	0.00	0.00	0.00	0.00	0.00	0.00	0.00	10.00	5.51	76.92	0.00	0.00	0.00	0.00	0.00	0.00	0.00	0.00	0.00	3.00	1.65	23.08
1.5	0.00	0.00	0.00	0.00	0.00	0.00	0.00	0.00	0.00	10.00	5.74	66.67	0.00	0.00	0.00	0.00	0.00	0.00	0.00	0.00	0.00	5.00	2.87	33.33
2.5	n.a.	n.a.	n.a.	n.a.	n.a.	n.a.	n.a.	n.a.	n.a.	n.a.	n.a.	n.a.	n.a.	n.a.	n.a.	n.a.	n.a.	n.a.	n.a.	n.a.	n.a.	n.a.	n.a.	n.a.
3.5	0.00	0.00	0.00	0.00	0.00	0.00	0.00	0.00	0.00	5.00	3.18	83.33	0.00	0.00	0.00	0.00	0.00	0.00	0.00	0.00	0.00	1.00	0.64	16.67
4.5	n.a.	n.a.	n.a.	n.a.	n.a.	n.a.	n.a.	n.a.	n.a.	n.a.	n.a.	n.a.	n.a.	n.a.	n.a.	n.a.	n.a.	n.a.	n.a.	n.a.	n.a.	n.a.	n.a.	n.a.
5.5	0.00	0.00	0.00	0.00	0.00	0.00	0.00	0.00	0.00	6.00	3.60	100.00	0.00	0.00	0.00	0.00	0.00	0.00	0.00	0.00	0.00	0.00	0.00	0.00
6.5	n.a.	n.a.	n.a.	n.a.	n.a.	n.a.	n.a.	n.a.	n.a.	n.a.	n.a.	n.a.	n.a.	n.a.	n.a.	n.a.	n.a.	n.a.	n.a.	n.a.	n.a.	n.a.	n.a.	n.a.
7.5	0.00	0.00	0.00	0.00	0.00	0.00	0.00	0.00	0.00	5.00	3.06	71.43	0.00	0.00	0.00	0.00	0.00	0.00	0.00	0.00	0.00	2.00	1.22	28.57
8.5	0.00	0.00	0.00	0.00	0.00	0.00	0.00	0.00	0.00	6.00	3.60	66.67	0.00	0.00	0.00	0.00	0.00	0.00	0.00	0.00	0.00	3.00	1.80	33.33
9.5	n.a.	n.a.	n.a.	n.a.	n.a.	n.a.	n.a.	n.a.	n.a.	n.a.	n.a.	n.a.	n.a.	n.a.	n.a.	n.a.	n.a.	n.a.	n.a.	n.a.	n.a.	n.a.	n.a.	n.a.
10.5	0.00	0.00	0.00	0.00	0.00	0.00	0.00	0.00	0.00	9.00	5.54	75.00	0.00	0.00	0.00	0.00	0.00	0.00	0.00	0.00	0.00	3.00	1.85	25.00
11.5	n.a.	n.a.	n.a.	n.a.	n.a.	n.a.	n.a.	n.a.	n.a.	n.a.	n.a.	n.a.	n.a.	n.a.	n.a.	n.a.	n.a.	n.a.	n.a.	n.a.	n.a.	n.a.	n.a.	n.a.
12.5	0.00	0.00	0.00	0.00	0.00	0.00	0.00	0.00	0.00	12.00	7.22	92.31	0.00	0.00	0.00	1.00	0.60	7.69	0.00	0.00	0.00	0.00	0.00	0.00
13.5	0.00	0.00	0.00	0.00	0.00	0.00	0.00	0.00	0.00	11.00	6.70	57.89	0.00	0.00	0.00	0.00	0.00	0.00	0.00	0.00	0.00	8.00	4.88	42.11
14.5	n.a.	n.a.	n.a.	n.a.	n.a.	n.a.	n.a.	n.a.	n.a.	n.a.	n.a.	n.a.	n.a.	n.a.	n.a.	n.a.	n.a.	n.a.	n.a.	n.a.	n.a.	n.a.	n.a.	n.a.
15.5	0.00	0.00	0.00	2.00	1.20	10.00	0.00	0.00	0.00	16.00	9.59	80.00	0.00	0.00	0.00	1.00	0.60	5.00	0.00	0.00	0.00	1.00	0.60	5.00
16.5	n.a.	n.a.	n.a.	n.a.	n.a.	n.a.	n.a.	n.a.	n.a.	n.a.	n.a.	n.a.	n.a.	n.a.	n.a.	n.a.	n.a.	n.a.	n.a.	n.a.	n.a.	n.a.	n.a.	n.a.
17.5	0.00	0.00	0.00	0.00	0.00	0.00	0.00	0.00	0.00	22.00	13.33	88.00	0.00	0.00	0.00	1.00	0.61	4.00	0.00	0.00	0.00	2.00	1.21	8.00
18.5	0.00	0.00	0.00	0.00	0.00	0.00	0.00	0.00	0.00	14.00	8.43	87.50	0.00	0.00	0.00	0.00	0.00	0.00	0.00	0.00	0.00	2.00	1.20	12.50
19.5	n.a.	n.a.	n.a.	n.a.	n.a.	n.a.	n.a.	n.a.	n.a.	n.a.	n.a.	n.a.	n.a.	n.a.	n.a.	n.a.	n.a.	n.a.	n.a.	n.a.	n.a.	n.a.	n.a.	n.a.
20.5	0.00	0.00	0.00	0.00	0.00	0.00	0.00	0.00	0.00	13.00	7.90	68.42	1.00	0.61	5.26	0.00	0.00	0.00	0.00	0.00	0.00	5.00	3.04	26.32
21.5	n.a.	n.a.	n.a.	n.a.	n.a.	n.a.	n.a.	n.a.	n.a.	n.a.	n.a.	n.a.	n.a.	n.a.	n.a.	n.a.	n.a.	n.a.	n.a.	n.a.	n.a.	n.a.	n.a.	n.a.
22.5	1.00	0.61	4.17	0.00	0.00	0.00	0.00	0.00	0.00	22.00	13.37	91.67	0.00	0.00	0.00	0.00	0.00	0.00	0.00	0.00	0.00	1.00	0.61	4.17
23.5	0.00	0.00	0.00	0.00	0.00	0.00	0.00	0.00	0.00	17.00	10.15	80.95	0.00	0.00	0.00	0.00	0.00	0.00	0.00	0.00	0.00	4.00	2.39	19.05
24.5	n.a.	n.a.	n.a.	n.a.	n.a.	n.a.	n.a.	n.a.	n.a.	n.a.	n.a.	n.a.	n.a.	n.a.	n.a.	n.a.	n.a.	n.a.	n.a.	n.a.	n.a.	n.a.	n.a.	n.a.
25.5	0.00	0.00	0.00	0.00	0.00	0.00	0.00	0.00	0.00	8.00	4.83	88.89	0.00	0.00	0.00	0.00	0.00	0.00	1.00	0.60	11.11	0.00	0.00	0.00
26.5	n.a.	n.a.	n.a.	n.a.	n.a.	n.a.	n.a.	n.a.	n.a.	n.a.	n.a.	n.a.	n.a.	n.a.	n.a.	n.a.	n.a.	n.a.	n.a.	n.a.	n.a.	n.a.	n.a.	n.a.
27.5	1.00	0.60	5.00	0.00	0.00	0.00	0.00	0.00	0.00	18.00	10.76	90.00	0.00	0.00	0.00	0.00	0.00	0.00	1.00	0.60	5.00	0.00	0.00	0.00
28.5	0.00	0.00	0.00	0.00	0.00	0.00	0.00	0.00	0.00	19.00	11.43	90.48	0.00	0.00	0.00	0.00	0.00	0.00	1.00	0.60	4.76	1.00	0.60	4.76
29.5	n.a.	n.a.	n.a.	n.a.	n.a.	n.a.	n.a.	n.a.	n.a.	n.a.	n.a.	n.a.	n.a.	n.a.	n.a.	n.a.	n.a.	n.a.	n.a.	n.a.	n.a.	n.a.	n.a.	n.a.
30.5	0.00	0.00	0.00	0.00	0.00	0.00	0.00	0.00	0.00	23.00	13.29	85.19	1.00	0.58	3.70	1.00	0.58	3.70	0.00	0.00	0.00	2.00	1.16	7.41
31.5	n.a.	n.a.	n.a.	n.a.	n.a.	n.a.	n.a.	n.a.	n.a.	n.a.	n.a.	n.a.	n.a.	n.a.	n.a.	n.a.	n.a.	n.a.	n.a.	n.a.	n.a.	n.a.	n.a.	n.a.
32.5	0.00	0.00	0.00	0.00	0.00	0.00	0.00	0.00	0.00	19.00	11.52	95.00	0.00	0.00	0.00	0.00	0.00	0.00	0.00	0.00	0.00	1.00	0.61	5.00
33.5	0.00	0.00	0.00	0.00	0.00	0.00	0.00	0.00	0.00	11.00	6.67	73.33	0.00	0.00	0.00	1.00	0.61	6.67	0.00	0.00	0.00	3.00	1.82	20.00
34.5	n.a.	n.a.	n.a.	n.a.	n.a.	n.a.	n.a.	n.a.	n.a.	n.a.	n.a.	n.a.	n.a.	n.a.	n.a.	n.a.	n.a.	n.a.	n.a.	n.a.	n.a.	n.a.	n.a.	n.a.
35.5	0.00	0.00	0.00	0.00	0.00	0.00	0.00	0.00	0.00	12.00	7.35	92.31	0.00	0.00	0.00	0.00	0.00	0.00	0.00	0.00	0.00	1.00	0.61	7.69
36.5	n.a.	n.a.	n.a.	n.a.	n.a.	n.a.	n.a.	n.a.	n.a.	n.a.	n.a.	n.a.	n.a.	n.a.	n.a.	n.a.	n.a.	n.a.	n.a.	n.a.	n.a.	n.a.	n.a.	n.a.
37.5	1.00	0.60	4.35	1.00	0.60	4.35	0.00	0.00	0.00	20.00	12.10	86.96	0.00	0.00	0.00	0.00	0.00	0.00	1.00	0.60	4.35	0.00	0.00	0.00
38.5	0.00	0.00	0.00	0.00	0.00	0.00	0.00	0.00	0.00	20.00	15.78	86.96	0.00	0.00	0.00	0.00	0.00	0.00	0.00	0.00	0.00	3.00	2.37	13.04
39.5	n.a.	n.a.	n.a.	n.a.	n.a.	n.a.	n.a.	n.a.	n.a.	n.a.	n.a.	n.a.	n.a.	n.a.	n.a.	n.a.	n.a.	n.a.	n.a.	n.a.	n.a.	n.a.	n.a.	n.a.
40.5	0.00	0.00	0.00	0.00	0.00	0.00	0.00	0.00	0.00	18.00	13.59	72.00	0.00	0.00	0.00	1.00	0.75	4.00	0.00	0.00	0.00	6.00	4.53	24.00
41.5	n.a.	n.a.	n.a.	n.a.	n.a.	n.a.	n.a.	n.a.	n.a.	n.a.	n.a.	n.a.	n.a.	n.a.	n.a.	n.a.	n.a.	n.a.	n.a.	n.a.	n.a.	n.a.	n.a.	n.a.
42.5	0.00	0.00	0.00	0.00	0.00	0.00	0.00	0.00	0.00	7.00	4.34	58.33	0.00	0.00	0.00	0.00	0.00	0.00	0.00	0.00	0.00	5.00	3.10	41.67
43.5	0.00	0.00	0.00	0.00	0.00	0.00	0.00	0.00	0.00	14.00	9.14	100.00	0.00	0.00	0.00	0.00	0.00	0.00	0.00	0.00	0.00	0.00	0.00	0.00
44.5	n.a.	n.a.	n.a.	n.a.	n.a.	n.a.	n.a.	n.a.	n.a.	n.a.	n.a.	n.a.	n.a.	n.a.	n.a.	n.a.	n.a.	n.a.	n.a.	n.a.	n.a.	n.a.	n.a.	n.a.
45.5	0.00	0.00	0.00	0.00	0.00	0.00	0.00	0.00	0.00	15.00	9.67	83.33	1.00	0.64	5.56	0.00	0.00	0.00	0.00	0.00	0.00	2.00	1.29	11.11
46.5	n.a.	n.a.	n.a.	n.a.	n.a.	n.a.	n.a.	n.a.	n.a.	n.a.	n.a.	n.a.	n.a.	n.a.	n.a.	n.a.	n.a.	n.a.	n.a.	n.a.	n.a.	n.a.	n.a.	n.a.
47.5	0.00	0.00	0.00	0.00	0.00	0.00	0.00	0.00	0.00	14.00	8.97	87.50	0.00	0.00	0.00	0.00	0.00	0.00	0.00	0.00	0.00	2.00	1.28	12.50
48.5	0.00	0.00	0.00	0.00	0.00	0.00	0.00	0.00	0.00	6.00	3.90	66.67	0.00	0.00	0.00	1.00	0.65	11.11	0.00	0.00	0.00	2.00	1.30	22.22
49.5	n.a.	n.a.	n.a.	n.a.	n.a.	n.a.	n.a.	n.a.	n.a.	n.a.	n.a.	n.a.	n.a.	n.a.	n.a.	n.a.	n.a.	n.a.	n.a.	n.a.	n.a.	n.a.	n.a.	n.a.
50.5	0.00	0.00	0.00	0.00	0.00	0.00	0.00	0.00	0.00	12.00	7.44	75.00	0.00	0.00	0.00	0.00	0.00	0.00	0.00	0.00	0.00	4.00	2.48	25.00
51.5	n.a.	n.a.	n.a.	n.a.	n.a.	n.a.	n.a.	n.a.	n.a.	n.a.	n.a.	n.a.	n.a.	n.a.	n.a.	n.a.	n.a.	n.a.	n.a.	n.a.	n.a.	n.a.	n.a.	n.a.
52.5	0.00	0.00	0.00	1.00	0.65	5.56	0.00	0.00	0.00	13.00	8.39	72.22	0.00	0.00	0.00	0.00	0.00	0.00	0.00	0.00	0.00	4.00	2.58	22.22
53.5	1.00	0.64	8.33	0.00	0.00	0.00	0.00	0.00	0.00	6.00	3.87	50.00	1.00	0.64	8.33	1.00	0.64	8.33	0.00	0.00	0.00	3.00	1.93	25.00
54.5	n.a.	n.a.	n.a.	n.a.	n.a.	n.a.	n.a.	n.a.	n.a.	n.a.	n.a.	n.a.	n.a.	n.a.	n.a.	n.a.	n.a.	n.a.	n.a.	n.a.	n.a.	n.a.	n.a.	n.a.
55.5	1.00	0.64	7.69	0.00	0.00	0.00	0.00	0.00	0.00	8.00	5.14	61.54	0.00	0.00	0.00	0.00	0.00	0.00	0.00	0.00	0.00	4.00	2.57	30.77
56.5	n.a.	n.a.	n.a.	n.a.	n.a.	n.a.	n.a.	n.a.	n.a.	n.a.	n.a.	n.a.	n.a.	n.a.	n.a.	n.a.	n.a.	n.a.	n.a.	n.a.	n.a.	n.a.	n.a.	n.a.
57.5	0.00	0.00	0.00	0.00	0.00	0.00	0.00	0.00	0.00	14.00	9.03	77.78	0.00	0.00	0.00	1.00	0.65	5.56	1.00	0.65	5.56	2.00	1.29	11.11
58.5	0.00	0.00	0.00	0.00	0.00	0.00	0.00	0.00	0.00	8.00	5.18	88.89	0.00	0.00	0.00	0.00	0.00	0.00	0.00	0.00	0.00	1.00	0.65	11.11
59.5	n.a.	n.a.	n.a.	n.a.	n.a.	n.a.	n.a.	n.a.	n.a.	n.a.	n.a.	n.a.	n.a.	n.a.	n.a.	n.a.	n.a.	n.a.	n.a.	n.a.	n.a.	n.a.	n.a.	n.a.
60.5	0.00	0.00	0.00	0.00	0.00	0.00	0.00	0.00	0.00	9.00	5.77	81.82	0.00	0.00	0.00	0.00	0.00	0.00	0.00	0.00	0.00	2.00	1.28	18.18
61.5	n.a.	n.a.	n.a.	n.a.	n.a.	n.a.	n.a.	n.a.	n.a.	n.a.	n.a.	n.a.	n.a.	n.a.	n.a.	n.a.	n.a.	n.a.	n.a.	n.a.	n.a.	n.a.	n.a.	n.a.
62.5	0.00	0.00	0.00	0.00	0.00	0.00	0.00	0.00	0.00	15.00	9.66	93.75	0.00	0.00	0.00	0.00	0.00	0.00	0.00	0.00	0.00	1.00	0.64	6.25
63.5	0.00	0.00	0.00	0.00	0.00	0.00	0.00	0.00	0.00	14.00	9.01	93.33	1.00	0.64	6.67	0.00	0.00	0.00	0.00	0.00	0.00	0.00	0.00	0.00
64.5	n.a.	n.a.	n.a.	n.a.	n.a.	n.a.	n.a.	n.a.	n.a.	n.a.	n.a.	n.a.	n.a.	n.a.	n.a.	n.a.	n.a.	n.a.	n.a.	n.a.	n.a.	n.a.	n.a.	n.a.
65.5	0.00	0.00	0.00	0.00	0.00	0.00	0.00	0.00	0.00	7.00	4.51	100.00	0.00	0.00	0.00	0.00	0.00	0.00	0.00	0.00	0.00	0.00	0.00	0.00
66.5	n.a.	n.a.	n.a.	n.a.	n.a.	n.a.	n.a.	n.a.	n.a.	n.a.	n.a.	n.a.	n.a.	n.a.	n.a.	n.a.	n.a.	n.a.	n.a.	n.a.	n.a.	n.a.	n.a.	n.a.
67.5	0.00	0.00	0.00	0.00	0.00	0.00	0.00	0.00	0.00	18.00	11.60	94.74	0.00	0.00	0.00	0.00	0.00	0.00	0.00	0.00	0.00	1.00	0.64	5.26
68.5	0.00	0.00	0.00	0.00	0.00	0.00	0.00	0.00	0.00	23.00	14.77	88.46	0.00	0.00	0.00	0.00	0.00	0.00	0.00	0.00	0.00	3.00	1.93	11.54
69.5	n.a.	n.a.	n.a.	n.a.	n.a.	n.a.	n.a.	n.a.	n.a.	n.a.	n.a.	n.a.	n.a.	n.a.	n.a.	n.a.	n.a.	n.a.	n.a.	n.a.	n.a.	n.a.	n.a.	n.a.
70.5	0.00	0.00	0.00	0.00	0.00	0.00	0.00	0.00	0.00	14.00	9.00	82.35	0.00	0.00	0.00	0.00	0.00	0.00	0.00	0.00	0.00	3.00	1.93	17.65
71.5	n.a.	n.a.	n.a.	n.a.	n.a.	n.a.	n.a.	n.a.	n.a.	n.a.	n.a.	n.a.	n.a.	n.a.	n.a.	n.a.	n.a.	n.a.	n.a.	n.a.	n.a.	n.a.	n.a.	n.a.
72.5	0.00	0.00	0.00	0.00	0.00	0.00	0.00	0.00	0.00	16.00	12.37	94.12	0.00	0.00	0.00	0.00	0.00	0.00	0.00	0.00	0.00	1.00	0.77	5.88
73.5	0.00	0.00	0.00	0.00	0.00	0.00	0.00	0.00	0.00	28.00	21.66	93.33	0.00	0.00	0.00	0.00	0.00	0.00	0.00	0.00	0.00	2.00	1.55	6.67
74.5	n.a.	n.a.	n.a.	n.a.	n.a.	n.a.	n.a.	n.a.	n.a.	n.a.	n.a.	n.a.	n.a.	n.a.	n.a.	n.a.	n.a.	n.a.	n.a.	n.a.	n.a.	n.a.	n.a.	n.a.
75.5	0.00	0.00	0.00	1.00	0.77	3.57	0.00	0.00	0.00	21.00	16.26	75.00	1.00	0.77	3.57	0.00	0.00	0.00	0.00	0.00	0.00	5.00	3.87	17.86
76.5	n.a.	n.a.	n.a.	n.a.	n.a.	n.a.	n.a.	n.a.	n.a.	n.a.	n.a.	n.a.	n.a.	n.a.	n.a.	n.a.	n.a.	n.a.	n.a.	n.a.	n.a.	n.a.	n.a.	n.a.
77.5	0.00	0.00	0.00	1.00	0.77	3.23	0.00	0.00	0.00	28.00	21.62	90.32	0.00	0.00	0.00	0.00	0.00	0.00	0.00	0.00	0.00	2.00	1.54	6.45
78.5	1.00	0.77	4.35	0.00	0.00	0.00	0.00	0.00	0.00	21.00	16.21	91.30	0.00	0.00	0.00	0.00	0.00	0.00	0.00	0.00	0.00	1.00	0.77	4.35
79.5	n.a.	n.a.	n.a.	n.a.	n.a.	n.a.	n.a.	n.a.	n.a.	n.a.	n.a.	n.a.	n.a.	n.a.	n.a.	n.a.	n.a.	n.a.	n.a.	n.a.	n.a.	n.a.	n.a.	n.a.
80.5	0.00	0.00	0.00	1.00	0.77	3.13	0.00	0.00	0.00	23.00	17.71	71.88	0.00	0.00	0.00	0.00	0.00	0.00	0.00	0.00	0.00	8.00	6.16	25.00
81.5	n.a.	n.a.	n.a.	n.a.	n.a.	n.a.	n.a.	n.a.	n.a.	n.a.	n.a.	n.a.	n.a.	n.a.	n.a.	n.a.	n.a.	n.a.	n.a.	n.a.	n.a.	n.a.	n.a.	n.a.
82.5	0.00	0.00	0.00	0.00	0.00	0.00	0.00	0.00	0.00	24.00	18.54	85.71	0.00	0.00	0.00	0.00	0.00	0.00	0.00	0.00	0.00	4.00	3.09	14.29
83.5	0.00	0.00	0.00	0.00	0.00	0.00	0.00	0.00	0.00	10.00	16.20	83.33	1.00	1.62	8.33	0.00	0.00	0.00	0.00	0.00	0.00	1.00	1.62	8.33
84.5	n.a.	n.a.	n.a.	n.a.	n.a.	n.a.	n.a.	n.a.	n.a.	n.a.	n.a.	n.a.	n.a.	n.a.	n.a.	n.a.	n.a.	n.a.	n.a.	n.a.	n.a.	n.a.	n.a.	n.a.
85.5	0.00	0.00	0.00	0.00	0.00	0.00	0.00	0.00	0.00	23.00	17.74	85.19	0.00	0.00	0.00	0.00	0.00	0.00	0.00	0.00	0.00	4.00	3.08	14.81
86.5	n.a.	n.a.	n.a.	n.a.	n.a.	n.a.	n.a.	n.a.	n.a.	n.a.	n.a.	n.a.	n.a.	n.a.	n.a.	n.a.	n.a.	n.a.	n.a.	n.a.	n.a.	n.a.	n.a.	n.a.
87.5	0.00	0.00	0.00	0.00	0.00	0.00	0.00	0.00	0.00	24.00	18.57	82.76	2.00	1.55	6.90	1.00	0.77	3.45	0.00	0.00	0.00	2.00	1.55	6.90
88.5	1.00	0.77	2.86	0.00	0.00	0.00	0.00	0.00	0.00	27.00	20.70	77.14	0.00	0.00	0.00	0.00	0.00	0.00	0.00	0.00	0.00	7.00	5.37	20.00
89.5	n.a.	n.a.	n.a.	n.a.	n.a.	n.a.	n.a.	n.a.	n.a.	n.a.	n.a.	n.a.	n.a.	n.a.	n.a.	n.a.	n.a.	n.a.	n.a.	n.a.	n.a.	n.a.	n.a.	n.a.
90.5	0.00	0.00	0.00	0.00	0.00	0.00	0.00	0.00	0.00	35.00	26.10	79.55	1.00	0.75	2.27	0.00	0.00	0.00	0.00	0.00	0.00	8.00	5.96	18.18
91.5	n.a.	n.a.	n.a.	n.a.	n.a.	n.a.	n.a.	n.a.	n.a.	n.a.	n.a.	n.a.	n.a.	n.a.	n.a.	n.a.	n.a.	n.a.	n.a.	n.a.	n.a.	n.a.	n.a.	n.a.
92.5	1.00	0.77	2.63	0.00	0.00	0.00	0.00	0.00	0.00	31.00	23.90	81.58	0.00	0.00	0.00	2.00	1.54	5.26	0.00	0.00	0.00	4.00	3.08	10.53
93.5	0.00	0.00	0.00	0.00	0.00	0.00	0.00	0.00	0.00	23.00	17.77	82.14	0.00	0.00	0.00	0.00	0.00	0.00	1.00	0.77	3.57	4.00	3.09	14.29
94.5	n.a.	n.a.	n.a.	n.a.	n.a.	n.a.	n.a.	n.a.	n.a.	n.a.	n.a.	n.a.	n.a.	n.a.	n.a.	n.a.	n.a.	n.a.	n.a.	n.a.	n.a.	n.a.	n.a.	n.a.
95.5	0.00	0.00	0.00	0.00	0.00	0.00	0.00	0.00	0.00	28.00	21.68	82.35	0.00	0.00	0.00	0.00	0.00	0.00	0.00	0.00	0.00	6.00	4.64	17.65
96.5	n.a.	n.a.	n.a.	n.a.	n.a.	n.a.	n.a.	n.a.	n.a.	n.a.	n.a.	n.a.	n.a.	n.a.	n.a.	n.a.	n.a.	n.a.	n.a.	n.a.	n.a.	n.a.	n.a.	n.a.
97.5	0.00	0.00	0.00	0.00	0.00	0.00	0.00	0.00	0.00	30.00	23.14	83.33	0.00	0.00	0.00	1.00	0.77	2.78	0.00	0.00	0.00	5.00	3.86	13.89
98.5	0.00	0.00	0.00	0.00	0.00	0.00	0.00	0.00	0.00	30.00	23.11	81.08	2.00	1.54	5.41	0.00	0.00	0.00	0.00	0.00	0.00	5.00	3.85	13.51
99.5	0.00	0.00	0.00	1.00	0.75	2.22	0.00	0.00	0.00	37.00	27.59	82.22	0.00	0.00	0.00	1.00	0.75	2.22	0.00	0.00	0.00	6.00	4.47	13.33

Table S4.8: *M144 KC5-6 data used in the study from 99.5-199.5cm core depth. Core depth; Taxa otolith count, concentration and accumulation rate.*

Core Data	Engraulidae			Gadidae						Myctophidae			Gonostomatidae			Sternoptychidae						Rest		
	E. encrasicolus			*G. argenteus*			*M. poutassou*									A. hemigymnus			M. mülleri					
depth	count	OAR	relative	count	OAR	relative	count	OAR	relative	count	OAR	relative	count	OAR	relative	count	OAR	relative	count	OAR	relative	count	OAR	relative
(cm)	(#)	(# cm^{-2} kyr^{-1})	(%)	(#)	(# cm^{-2} kyr^{-1})	(%)	(#)	(# cm^{-2} kyr^{-1})	(%)	(#)	(# cm^{-2} kyr^{-1})	(%)	(#)	(# cm^{-2} kyr^{-1})	(%)	(#)	(# cm^{-2} kyr^{-1})	(%)	(#)	(# cm^{-2} kyr^{-1})	(%)	(#)	(# cm^{-2} kyr^{-1})	(%)
100.5	n.a.	n.a.	n.a.	n.a.	n.a.	n.a.	n.a.	n.a.	n.a.	n.a.	n.a.	n.a.	n.a.	n.a.	n.a.	n.a.	n.a.	n.a.	n.a.	n.a.	n.a.	n.a.	n.a.	n.a.
101.5	n.a.	n.a.	n.a.	n.a.	n.a.	n.a.	n.a.	n.a.	n.a.	n.a.	n.a.	n.a.	n.a.	n.a.	n.a.	n.a.	n.a.	n.a.	n.a.	n.a.	n.a.	n.a.	n.a.	n.a.
102.5	0.00	0.00	0.00	0.00	0.00	0.00	1.00	0.77	3.70	22.00	17.02	81.48	1.00	0.77	3.70	0.00	0.00	0.00	0.00	0.00	0.00	3.00	2.32	11.11
103.5	0.00	0.00	0.00	0.00	0.00	0.00	0.00	0.00	0.00	20.00	15.58	83.33	0.00	0.00	0.00	0.00	0.00	0.00	1.00	0.78	4.17	3.00	2.34	12.50
104.5	n.a.	n.a.	n.a.	n.a.	n.a.	n.a.	n.a.	n.a.	n.a.	n.a.	n.a.	n.a.	n.a.	n.a.	n.a.	n.a.	n.a.	n.a.	n.a.	n.a.	n.a.	n.a.	n.a.	n.a.
105.5	0.00	0.00	0.00	3.00	2.32	10.71	0.00	0.00	0.00	20.00	15.47	71.43	0.00	0.00	0.00	2.00	1.55	7.14	1.00	0.77	3.57	2.00	1.55	7.14
106.5	n.a.	n.a.	n.a.	n.a.	n.a.	n.a.	n.a.	n.a.	n.a.	n.a.	n.a.	n.a.	n.a.	n.a.	n.a.	n.a.	n.a.	n.a.	n.a.	n.a.	n.a.	n.a.	n.a.	n.a.
107.5	1.00	0.77	2.70	0.00	0.00	0.00	0.00	0.00	0.00	28.00	21.67	75.68	1.00	0.77	2.70	1.00	0.77	2.70	0.00	0.00	0.00	6.00	4.64	16.22
108.5	0.00	0.00	0.00	0.00	0.00	0.00	0.00	0.00	0.00	18.00	14.03	85.71	0.00	0.00	0.00	0.00	0.00	0.00	0.00	0.00	0.00	3.00	2.34	14.29
109.5	n.a.	n.a.	n.a.	n.a.	n.a.	n.a.	n.a.	n.a.	n.a.	n.a.	n.a.	n.a.	n.a.	n.a.	n.a.	n.a.	n.a.	n.a.	n.a.	n.a.	n.a.	n.a.	n.a.	n.a.
110.5	0.00	0.00	0.00	0.00	0.00	0.00	0.00	0.00	0.00	19.00	11.53	86.36	0.00	0.00	0.00	0.00	0.00	0.00	0.00	0.00	0.00	3.00	1.82	13.64
111.5	n.a.	n.a.	n.a.	n.a.	n.a.	n.a.	n.a.	n.a.	n.a.	n.a.	n.a.	n.a.	n.a.	n.a.	n.a.	n.a.	n.a.	n.a.	n.a.	n.a.	n.a.	n.a.	n.a.	n.a.
112.5	0.00	0.00	0.00	0.00	0.00	0.00	0.00	0.00	0.00	21.00	12.85	91.30	0.00	0.00	0.00	0.00	0.00	0.00	0.00	0.00	0.00	2.00	1.22	8.70
113.5	0.00	0.00	0.00	0.00	0.00	0.00	0.00	0.00	0.00	21.00	12.85	70.00	2.00	1.22	6.67	1.00	0.61	3.33	0.00	0.00	0.00	6.00	3.67	20.00
114.5	n.a.	n.a.	n.a.	n.a.	n.a.	n.a.	n.a.	n.a.	n.a.	n.a.	n.a.	n.a.	n.a.	n.a.	n.a.	n.a.	n.a.	n.a.	n.a.	n.a.	n.a.	n.a.	n.a.	n.a.
115.5	0.00	0.00	0.00	0.00	0.00	0.00	0.00	0.00	0.00	26.00	15.89	74.29	0.00	0.00	0.00	2.00	1.22	5.71	1.00	0.61	2.86	6.00	3.67	17.14
116.5	n.a.	n.a.	n.a.	n.a.	n.a.	n.a.	n.a.	n.a.	n.a.	n.a.	n.a.	n.a.	n.a.	n.a.	n.a.	n.a.	n.a.	n.a.	n.a.	n.a.	n.a.	n.a.	n.a.	n.a.
117.5	0.00	0.00	0.00	0.00	0.00	0.00	0.00	0.00	0.00	16.00	9.80	84.21	1.00	0.61	5.26	0.00	0.00	0.00	0.00	0.00	0.00	2.00	1.22	10.53
118.5	1.00	0.61	2.56	0.00	0.00	0.00	1.00	0.61	2.56	30.00	18.35	76.92	2.00	1.22	5.13	0.00	0.00	0.00	0.00	0.00	0.00	5.00	3.06	12.82
119.5	n.a.	n.a.	n.a.	n.a.	n.a.	n.a.	n.a.	n.a.	n.a.	n.a.	n.a.	n.a.	n.a.	n.a.	n.a.	n.a.	n.a.	n.a.	n.a.	n.a.	n.a.	n.a.	n.a.	n.a.
120.5	0.00	0.00	0.00	1.00	0.61	3.57	0.00	0.00	0.00	20.00	12.19	71.43	0.00	0.00	0.00	0.00	0.00	0.00	0.00	0.00	0.00	7.00	4.27	25.00
121.5	n.a.	n.a.	n.a.	n.a.	n.a.	n.a.	n.a.	n.a.	n.a.	n.a.	n.a.	n.a.	n.a.	n.a.	n.a.	n.a.	n.a.	n.a.	n.a.	n.a.	n.a.	n.a.	n.a.	n.a.
122.5	1.00	0.61	3.23	0.00	0.00	0.00	0.00	0.00	0.00	23.00	14.01	74.19	1.00	0.61	3.23	0.00	0.00	0.00	0.00	0.00	0.00	6.00	3.66	19.35
123.5	1.00	0.61	2.63	1.00	0.61	2.63	0.00	0.00	0.00	29.00	17.69	76.32	1.00	0.61	2.63	0.00	0.00	0.00	2.00	1.22	5.26	4.00	2.44	10.53
124.5	n.a.	n.a.	n.a.	n.a.	n.a.	n.a.	n.a.	n.a.	n.a.	n.a.	n.a.	n.a.	n.a.	n.a.	n.a.	n.a.	n.a.	n.a.	n.a.	n.a.	n.a.	n.a.	n.a.	n.a.
125.5	0.00	0.00	0.00	0.00	0.00	0.00	0.00	0.00	0.00	21.00	12.86	72.41	0.00	0.00	0.00	0.00	0.00	0.00	1.00	0.61	3.45	7.00	4.29	24.14
126.5	n.a.	n.a.	n.a.	n.a.	n.a.	n.a.	n.a.	n.a.	n.a.	n.a.	n.a.	n.a.	n.a.	n.a.	n.a.	n.a.	n.a.	n.a.	n.a.	n.a.	n.a.	n.a.	n.a.	n.a.
127.5	0.00	0.00	0.00	1.00	0.59	3.45	0.00	0.00	0.00	21.00	12.40	72.41	1.00	0.59	3.45	0.00	0.00	0.00	0.00	0.00	0.00	6.00	3.54	20.69
128.5	0.00	0.00	0.00	0.00	0.00	0.00	0.00	0.00	0.00	8.00	4.87	61.54	0.00	0.00	0.00	0.00	0.00	0.00	0.00	0.00	0.00	5.00	3.04	38.46
129.5	n.a.	n.a.	n.a.	n.a.	n.a.	n.a.	n.a.	n.a.	n.a.	n.a.	n.a.	n.a.	n.a.	n.a.	n.a.	n.a.	n.a.	n.a.	n.a.	n.a.	n.a.	n.a.	n.a.	n.a.
130.5	0.00	0.00	0.00	0.00	0.00	0.00	0.00	0.00	0.00	27.00	16.41	72.97	0.00	0.00	0.00	0.00	0.00	0.00	0.00	0.00	0.00	10.00	6.08	27.03
131.5	n.a.	n.a.	n.a.	n.a.	n.a.	n.a.	n.a.	n.a.	n.a.	n.a.	n.a.	n.a.	n.a.	n.a.	n.a.	n.a.	n.a.	n.a.	n.a.	n.a.	n.a.	n.a.	n.a.	n.a.
132.5	0.00	0.00	0.00	1.00	0.61	3.03	0.00	0.00	0.00	29.00	17.76	87.88	1.00	0.61	3.03	0.00	0.00	0.00	0.00	0.00	0.00	2.00	1.22	6.06
133.5	0.00	0.00	0.00	0.00	0.00	0.00	0.00	0.00	0.00	14.00	8.56	82.35	0.00	0.00	0.00	0.00	0.00	0.00	0.00	0.00	0.00	3.00	1.83	17.65
134.5	n.a.	n.a.	n.a.	n.a.	n.a.	n.a.	n.a.	n.a.	n.a.	n.a.	n.a.	n.a.	n.a.	n.a.	n.a.	n.a.	n.a.	n.a.	n.a.	n.a.	n.a.	n.a.	n.a.	n.a.
135.5	0.00	0.00	0.00	0.00	0.00	0.00	0.00	0.00	0.00	13.00	7.94	76.47	0.00	0.00	0.00	0.00	0.00	0.00	1.00	0.61	5.88	3.00	1.83	17.65
136.5	n.a.	n.a.	n.a.	n.a.	n.a.	n.a.	n.a.	n.a.	n.a.	n.a.	n.a.	n.a.	n.a.	n.a.	n.a.	n.a.	n.a.	n.a.	n.a.	n.a.	n.a.	n.a.	n.a.	n.a.
137.5	1.00	0.61	4.55	1.00	0.61	4.55	0.00	0.00	0.00	17.00	10.38	77.27	0.00	0.00	0.00	0.00	0.00	0.00	0.00	0.00	0.00	3.00	1.83	13.64
138.5	2.00	1.23	6.45	0.00	0.00	0.00	0.00	0.00	0.00	25.00	15.43	80.65	0.00	0.00	0.00	0.00	0.00	0.00	0.00	0.00	0.00	4.00	2.47	12.90
139.5	n.a.	n.a.	n.a.	n.a.	n.a.	n.a.	n.a.	n.a.	n.a.	n.a.	n.a.	n.a.	n.a.	n.a.	n.a.	n.a.	n.a.	n.a.	n.a.	n.a.	n.a.	n.a.	n.a.	n.a.
140.5	1.00	0.61	3.13	0.00	0.00	0.00	0.00	0.00	0.00	26.00	15.86	81.25	0.00	0.00	0.00	0.00	0.00	0.00	1.00	0.61	3.13	4.00	2.44	12.50
141.5	n.a.	n.a.	n.a.	n.a.	n.a.	n.a.	n.a.	n.a.	n.a.	n.a.	n.a.	n.a.	n.a.	n.a.	n.a.	n.a.	n.a.	n.a.	n.a.	n.a.	n.a.	n.a.	n.a.	n.a.
142.5	0.00	0.00	0.00	0.00	0.00	0.00	0.00	0.00	0.00	21.00	12.81	67.74	1.00	0.61	3.23	0.00	0.00	0.00	0.00	0.00	0.00	9.00	5.49	29.03
143.5	2.00	1.22	5.88	0.00	0.00	0.00	0.00	0.00	0.00	26.00	15.87	76.47	0.00	0.00	0.00	2.00	1.22	5.88	0.00	0.00	0.00	4.00	2.44	11.76
144.5	n.a.	n.a.	n.a.	n.a.	n.a.	n.a.	n.a.	n.a.	n.a.	n.a.	n.a.	n.a.	n.a.	n.a.	n.a.	n.a.	n.a.	n.a.	n.a.	n.a.	n.a.	n.a.	n.a.	n.a.
145.5	0.00	0.00	0.00	0.00	0.00	0.00	0.00	0.00	0.00	28.00	16.54	82.35	0.00	0.00	0.00	0.00	0.00	0.00	2.00	1.18	5.88	4.00	2.36	11.76
146.5	n.a.	n.a.	n.a.	n.a.	n.a.	n.a.	n.a.	n.a.	n.a.	n.a.	n.a.	n.a.	n.a.	n.a.	n.a.	n.a.	n.a.	n.a.	n.a.	n.a.	n.a.	n.a.	n.a.	n.a.
147.5	0.00	0.00	0.00	0.00	0.00	0.00	0.00	0.00	0.00	20.00	12.23	74.07	2.00	1.22	7.41	0.00	0.00	0.00	0.00	0.00	0.00	5.00	3.06	18.52
148.5	0.00	0.00	0.00	0.00	0.00	0.00	0.00	0.00	0.00	18.00	10.63	75.00	0.00	0.00	0.00	1.00	0.59	4.17	1.00	0.59	4.17	4.00	2.36	16.67
149.5	n.a.	n.a.	n.a.	n.a.	n.a.	n.a.	n.a.	n.a.	n.a.	n.a.	n.a.	n.a.	n.a.	n.a.	n.a.	n.a.	n.a.	n.a.	n.a.	n.a.	n.a.	n.a.	n.a.	n.a.
150.5	0.00	0.00	0.00	0.00	0.00	0.00	0.00	0.00	0.00	20.00	11.81	80.00	0.00	0.00	0.00	0.00	0.00	0.00	0.00	0.00	0.00	5.00	2.95	20.00
151.5	n.a.	n.a.	n.a.	n.a.	n.a.	n.a.	n.a.	n.a.	n.a.	n.a.	n.a.	n.a.	n.a.	n.a.	n.a.	n.a.	n.a.	n.a.	n.a.	n.a.	n.a.	n.a.	n.a.	n.a.
152.5	0.00	0.00	0.00	0.00	0.00	0.00	0.00	0.00	0.00	22.00	12.99	91.67	0.00	0.00	0.00	0.00	0.00	0.00	0.00	0.00	0.00	2.00	1.18	8.33
153.5	0.00	0.00	0.00	0.00	0.00	0.00	0.00	0.00	0.00	18.00	10.63	75.00	0.00	0.00	0.00	0.00	0.00	0.00	0.00	0.00	0.00	6.00	3.54	25.00
154.5	0.00	0.00	0.00	1.00	0.59	4.55	1.00	0.59	4.55	18.00	10.63	81.82	0.00	0.00	0.00	0.00	0.00	0.00	1.00	0.59	4.55	1.00	0.59	4.55
155.5	1.00	0.59	2.94	0.00	0.00	0.00	0.00	0.00	0.00	23.00	13.58	67.65	0.00	0.00	0.00	0.00	0.00	0.00	0.00	0.00	0.00	10.00	5.91	29.41
156.5	0.00	0.00	0.00	0.00	0.00	0.00	0.00	0.00	0.00	20.00	11.81	83.33	0.00	0.00	0.00	1.00	0.59	4.17	0.00	0.00	0.00	3.00	1.77	12.50
157.5	1.00	0.59	4.55	0.00	0.00	0.00	1.00	0.59	4.55	15.00	8.86	68.18	1.00	0.59	4.55	0.00	0.00	0.00	0.00	0.00	0.00	4.00	2.36	18.18
158.5	0.00	0.00	0.00	0.00	0.00	0.00	0.00	0.00	0.00	10.00	5.91	58.82	2.00	1.18	11.76	0.00	0.00	0.00	1.00	0.59	5.88	4.00	2.36	23.53
159.5	0.00	0.00	0.00	0.00	0.00	0.00	0.00	0.00	0.00	13.00	7.68	76.47	1.00	0.59	5.88	0.00	0.00	0.00	1.00	0.59	5.88	2.00	1.18	11.76
160.5	0.00	0.00	0.00	0.00	0.00	0.00	0.00	0.00	0.00	24.00	14.18	75.00	2.00	1.18	6.25	0.00	0.00	0.00	1.00	0.59	3.13	5.00	2.95	15.63
161.5	1.00	0.59	5.49	0.00	0.00	0.00	0.00	0.00	0.00	13.85	8.18	76.06	0.00	0.00	0.00	0.12	0.07	0.66	2.00	1.18	10.98	1.24	0.73	6.81
162.5	0.29	0.17	1.24	0.00	0.00	0.00	0.00	0.00	0.00	13.53	7.99	57.80	0.29	0.17	1.24	0.88	0.52	3.76	2.18	1.29	9.31	6.24	3.69	26.66
163.5	0.71	0.42	3.53	0.00	0.00	0.00	0.00	0.00	0.00	9.19	5.43	45.74	0.00	0.00	0.00	0.00	0.00	0.00	2.82	1.67	14.04	7.37	4.35	36.68
164.5	0.00	0.00	0.00	0.00	0.00	0.00	0.00	0.00	0.00	6.78	4.00	63.66	0.00	0.00	0.00	0.00	0.00	0.00	0.00	0.00	0.00	3.87	2.29	36.34
165.5	0.00	0.00	0.00	0.00	0.00	0.00	0.00	0.00	0.00	6.08	3.59	85.88	0.00	0.00	0.00	0.00	0.00	0.00	1.00	0.59	14.12	0.00	0.00	0.00
166.5	0.00	0.00	0.00	0.00	0.00	0.00	0.00	0.00	0.00	8.34	4.93	89.29	0.00	0.00	0.00	0.00	0.00	0.00	0.00	0.00	0.00	1.00	0.59	10.71
167.5	3.29	1.94	13.99	1.00	0.59	4.25	0.00	0.00	0.00	14.05	8.30	59.76	1.00	0.59	4.25	1.00	0.59	4.25	0.29	0.17	1.23	2.88	1.70	12.25
168.5	1.21	0.71	7.10	1.00	0.59	5.87	0.00	0.00	0.00	11.62	6.86	68.19	0.00	0.00	0.00	1.00	0.59	5.87	0.71	0.42	4.17	1.50	0.89	8.80
169.5	1.50	0.89	7.50	1.75	1.03	8.75	0.00	0.00	0.00	11.75	6.94	58.75	0.00	0.00	0.00	0.00	0.00	0.00	0.00	0.00	0.00	5.00	2.95	25.00
170.5	0.00	0.00	0.00	1.25	0.74	7.84	0.00	0.00	0.00	11.42	6.75	71.60	0.00	0.00	0.00	0.00	0.00	0.00	1.78	1.05	11.16	1.50	0.89	9.40
171.5	2.00	1.18	12.86	0.00	0.00	0.00	0.00	0.00	0.00	7.33	4.33	47.14	0.00	0.00	0.00	0.00	0.00	0.00	1.22	0.72	7.85	5.00	2.95	32.15
172.5	1.00	0.59	6.25	0.00	0.00	0.00	1.00	0.59	6.25	6.00	3.54	37.50	0.00	0.00	0.00	1.00	0.59	6.25	2.00	1.18	12.50	5.00	2.95	31.25
173.5	0.00	0.00	0.00	0.00	0.00	0.00	0.00	0.00	0.00	6.00	3.54	66.67	1.00	0.59	11.11	0.00	0.00	0.00	0.00	0.00	0.00	2.00	1.18	22.22
174.5	3.00	1.77	21.43	1.00	0.59	7.14	0.00	0.00	0.00	6.00	3.54	42.86	0.00	0.00	0.00	0.00	0.00	0.00	2.00	1.18	14.29	2.00	1.18	14.29
175.5	0.00	0.00	0.00	0.00	0.00	0.00	1.00	0.59	5.26	7.00	4.13	36.84	0.00	0.00	0.00	0.00	0.00	0.00	4.00	2.36	21.05	7.00	4.13	36.84
176.5	0.00	0.00	0.00	0.00	0.00	0.00	0.00	0.00	0.00	6.00	3.54	54.55	0.00	0.00	0.00	0.00	0.00	0.00	1.00	0.59	9.09	4.00	2.36	36.36
177.5	1.00	0.59	4.55	0.00	0.00	0.00	0.00	0.00	0.00	12.00	7.09	54.55	0.00	0.00	0.00	0.00	0.00	0.00	2.00	1.18	9.09	7.00	4.13	31.82
178.5	1.00	0.59	6.25	2.00	1.18	12.50	1.00	0.59	6.25	7.00	4.13	43.75	0.00	0.00	0.00	0.00	0.00	0.00	2.00	1.18	12.50	3.00	1.77	18.75
179.5	0.00	0.00	0.00	0.00	0.00	0.00	0.00	0.00	0.00	10.00	5.91	71.43	0.00	0.00	0.00	0.00	0.00	0.00	1.00	0.59	7.14	3.00	1.77	21.43
180.5	0.00	0.00	0.00	0.00	0.00	0.00	0.00	0.00	0.00	15.00	8.86	68.18	0.00	0.00	0.00	3.00	1.77	13.64	1.00	0.59	4.55	3.00	1.77	13.64
181.5	3.00	1.77	23.08	0.00	0.00	0.00	0.00	0.00	0.00	4.00	2.36	30.77	1.00	0.59	7.69	0.00	0.00	0.00	3.00	1.77	23.08	2.00	1.18	15.38
182.5	0.00	0.00	0.00	0.00	0.00	0.00	0.00	0.00	0.00	6.00	3.54	50.00	0.00	0.00	0.00	2.00	1.18	16.67	1.00	0.59	8.33	3.00	1.77	25.00
183.5	1.00	0.59	6.25	0.00	0.00	0.00	0.00	0.00	0.00	4.00	2.36	25.00	1.00	0.59	6.25	0.00	0.00	0.00	3.00	1.77	18.75	7.00	4.13	43.75
184.5	0.00	0.00	0.00	1.00	0.59	12.50	1.00	0.59	12.50	4.00	2.36	50.00	0.00	0.00	0.00	0.00	0.00	0.00	1.00	0.59	12.50	1.00	0.59	12.50
185.5	0.00	0.00	0.00	2.00	1.18	20.00	0.00	0.00	0.00	2.00	1.18	20.00	1.00	0.59	10.00	0.00	0.00	0.00	2.00	1.18	20.00	3.00	1.77	30.00
186.5	0.00	0.00	0.00	0.00	0.00	0.00	0.00	0.00	0.00	4.00	2.36	36.36	0.00	0.00	0.00	0.00	0.00	0.00	5.00	2.95	45.45	2.00	1.18	18.18
187.5	2.00	1.18	18.18	0.00	0.00	0.00	0.00	0.00	0.00	2.00	1.18	18.18	0.00	0.00	0.00	1.00	0.59	9.09	3.00	1.77	27.27	3.00	1.77	27.27
188.5	0.00	0.00	0.00	0.00	0.00	0.00	0.00	0.00	0.00	2.00	1.18	25.00	0.00	0.00	0.00	1.00	0.59	12.50	5.00	2.95	62.50	0.00	0.00	0.00
189.5	1.00	0.59	14.29	0.00	0.00	0.00	0.00	0.00	0.00	1.00	0.59	14.29	0.00	0.00	0.00	0.00	0.00	0.00	5.00	2.95	71.43	0.00	0.00	0.00
190.5	1.00	0.59	14.29	0.00	0.00	0.00	0.00	0.00	0.00	2.00	1.18	28.57	0.00	0.00	0.00	1.00	0.59	14.29	2.00	1.18	28.57	1.00	0.59	14.29
191.5	0.00	0.00	0.00	0.00	0.00	0.00	0.00	0.00	0.00	0.00	0.00	0.00	0.00	0.00	0.00	0.00	0.00	0.00	6.00	3.54	60.00	4.00	2.36	40.00
192.5	0.00	0.00	0.00	1.00	0.59	16.67	0.00	0.00	0.00	1.00	0.59	16.67	0.00	0.00	0.00	0.00	0.00	0.00	3.00	1.77	50.00	1.00	0.59	16.67
193.5	0.00	0.00	0.00	0.00	0.00	0.00	0.00	0.00	0.00	0.00	0.00	0.00	0.00	0.00	0.00	0.00	0.00	0.00	1.00	0.59	100.00	0.00	0.00	0.00
194.5	0.00	0.00	0.00	0.00	0.00	0.00	0.00	0.00	0.00	0.00	0.00	0.00	0.00	0.00	0.00	0.00	0.00	0.00	2.00	1.18	50.00	2.00	1.18	50.00
195.5	2.00	1.18	50.00	0.00	0.00	0.00	0.00	0.00	0.00	0.00	0.00	0.00	0.00	0.00	0.00	0.00	0.00	0.00	2.00	1.18	50.00	0.00	0.00	0.00
196.5	4.00	2.36	40.00	0.00	0.00	0.00	0.00	0.00	0.00	0.00	0.00	0.00	0.00	0.00	0.00	0.00	0.00	0.00	5.00	2.95	50.00	1.00	0.59	10.00
197.5	1.00	0.59	14.29	0.00	0.00	0.00	1.00	0.59	14.29	0.00	0.00	0.00	1.00	0.59	14.29	0.00	0.00	0.00	2.00	1.18	28.57	2.00	1.18	28.57
198.5	3.00	1.77	33.33	0.00	0.00	0.00	0.00	0.00	0.00	0.00	0.00	0.00	1.00	0.59	11.11	0.00	0.00	0.00	3.00	1.77	33.33	2.00	1.18	22.22
199.5	4.00	2.36	50.00	0.00	0.00	0.00	0.00	0.00	0.00	0.00	0.00	0.00	0.00	0.00	0.00	0.00	0.00	0.00	4.00	2.36	50.00	0.00	0.00	0.00

Table S4.9: *M144 KC5-6 data used in the study from 200.5-272.5cm core depth. Core depth; Taxa otolith count, concentration and accumulation rate.*

Core Data	Engraulidae			Gadidae						Myctophidae			Gonostomatidae			Sternoptychidae						Rest		
	E. encrasicolus			*G. argenteus*			*M. poutassou*									A. hemigymnus			M. mülleri					
depth	count	OAR	relative	count	OAR	relative	count	OAR	relative	count	OAR	relative	count	OAR	relative	count	OAR	relative	count	OAR	relative	count	OAR	relative
(cm)	(#)	(# cm^{-2} kyr^{-1})	(%)	(#)	(# cm^{-2} kyr^{-1})	(%)	(#)	(# cm^{-2} kyr^{-1})	(%)	(#)	(# cm^{-2} kyr^{-1})	(%)	(#)	(# cm^{-2} kyr^{-1})	(%)	(#)	(# cm^{-2} kyr^{-1})	(%)	(#)	(# cm^{-2} kyr^{-1})	(%)	(#)	(# cm^{-2} kyr^{-1})	(%)
200.5	2.00	1.18	20.00	0.00	0.00	0.00	0.00	0.00	0.00	3.00	1.77	30.00	1.00	0.59	10.00	0.00	0.00	0.00	3.00	1.77	30.00	1.00	0.59	10.00
201.5	0.00	0.00	0.00	1.00	0.59	7.69	0.00	0.00	0.00	2.00	1.18	15.38	1.00	0.59	7.69	0.00	0.00	0.00	8.00	4.73	61.54	1.00	0.59	7.69
202.5	n.a.	n.a.	n.a.	n.a.	n.a.	n.a.	n.a.	n.a.	n.a.	n.a.	n.a.	n.a.	n.a.	n.a.	n.a.	n.a.	n.a.	n.a.	n.a.	n.a.	n.a.	n.a.	n.a.	n.a.
203.5	0.00	0.00	0.00	0.00	0.00	0.00	0.00	0.00	0.00	0.00	0.00	0.00	0.00	0.00	0.00	0.00	0.00	0.00	0.00	0.00	0.00	2.00	1.18	100.00
204.5	0.00	0.00	0.00	0.00	0.00	0.00	0.00	0.00	0.00	2.00	1.18	40.00	0.00	0.00	0.00	1.00	0.59	20.00	1.00	0.59	20.00	1.00	0.59	20.00
205.5	1.00	0.59	14.29	0.00	0.00	0.00	0.00	0.00	0.00	2.00	1.18	28.57	0.00	0.00	0.00	0.00	0.00	0.00	0.00	0.00	0.00	4.00	2.36	57.14
206.5	1.00	0.59	16.67	0.00	0.00	0.00	0.00	0.00	0.00	1.00	0.59	16.67	0.00	0.00	0.00	0.00	0.00	0.00	3.00	1.77	50.00	1.00	0.59	16.67
207.5	1.00	0.59	100.00	0.00	0.00	0.00	0.00	0.00	0.00	0.00	0.00	0.00	0.00	0.00	0.00	0.00	0.00	0.00	0.00	0.00	0.00	0.00	0.00	0.00
208.5	0.00	0.00	0.00	0.00	0.00	0.00	0.00	0.00	0.00	1.00	0.59	33.33	0.00	0.00	0.00	0.00	0.00	0.00	1.00	0.59	33.33	1.00	0.59	33.33
209.5	1.00	0.59	14.29	0.00	0.00	0.00	0.00	0.00	0.00	2.00	1.18	28.57	0.00	0.00	0.00	0.00	0.00	0.00	4.00	2.36	57.14	0.00	0.00	0.00
210.5	2.00	1.18	13.33	0.00	0.00	0.00	0.00	0.00	0.00	3.00	1.77	20.00	0.00	0.00	0.00	0.00	0.00	0.00	9.00	5.32	60.00	1.00	0.59	6.67
211.5	1.00	0.59	10.00	0.00	0.00	0.00	0.00	0.00	0.00	2.00	1.18	20.00	0.00	0.00	0.00	1.00	0.59	10.00	4.00	2.36	40.00	2.00	1.18	20.00
212.5	1.00	0.59	6.67	0.00	0.00	0.00	0.00	0.00	0.00	0.00	0.00	0.00	1.00	0.59	6.67	0.00	0.00	0.00	12.00	7.09	80.00	1.00	0.59	6.67
213.5	2.00	1.18	13.33	0.00	0.00	0.00	0.00	0.00	0.00	1.00	0.59	6.67	0.00	0.00	0.00	0.00	0.00	0.00	12.00	7.09	80.00	0.00	0.00	0.00
214.5	4.00	2.36	22.22	0.00	0.00	0.00	0.00	0.00	0.00	0.00	0.00	0.00	0.00	0.00	0.00	0.00	0.00	0.00	11.00	6.50	61.11	3.00	1.77	16.67
215.5	2.00	1.18	7.14	1.00	0.59	3.57	0.00	0.00	0.00	2.00	1.18	7.14	0.00	0.00	0.00	0.00	0.00	0.00	22.00	12.99	78.57	1.00	0.59	3.57
216.5	1.00	0.59	7.69	1.00	0.59	7.69	0.00	0.00	0.00	0.00	0.00	0.00	0.00	0.00	0.00	0.00	0.00	0.00	10.00	5.91	76.92	1.00	0.59	7.69
217.5	1.00	0.59	25.00	0.00	0.00	0.00	0.00	0.00	0.00	0.00	0.00	0.00	0.00	0.00	0.00	0.00	0.00	0.00	3.00	1.77	75.00	0.00	0.00	0.00
218.5	4.00	2.36	50.00	0.00	0.00	0.00	0.00	0.00	0.00	0.00	0.00	0.00	0.00	0.00	0.00	0.00	0.00	0.00	3.00	1.77	37.50	1.00	0.59	12.50
219.5	2.00	1.18	20.00	0.00	0.00	0.00	0.00	0.00	0.00	0.00	0.00	0.00	1.00	0.59	10.00	0.00	0.00	0.00	4.00	2.36	40.00	3.00	1.77	30.00
220.5	2.00	1.18	20.00	1.00	0.59	10.00	0.00	0.00	0.00	1.00	0.59	10.00	1.00	0.59	10.00	0.00	0.00	0.00	4.00	2.36	40.00	1.00	0.59	10.00
221.5	3.00	1.77	27.27	1.00	0.59	9.09	0.00	0.00	0.00	1.00	0.59	9.09	0.00	0.00	0.00	0.00	0.00	0.00	5.00	2.95	45.45	1.00	0.59	9.09
222.5	5.00	2.95	55.56	1.00	0.59	11.11	0.00	0.00	0.00	0.00	0.00	0.00	0.00	0.00	0.00	0.00	0.00	0.00	1.00	0.59	11.11	2.00	1.18	22.22
223.5	1.00	0.59	14.29	0.00	0.00	0.00	0.00	0.00	0.00	0.00	0.00	0.00	1.00	0.59	14.29	0.00	0.00	0.00	4.00	2.36	57.14	1.00	0.59	14.29
224.5	0.00	0.00	0.00	0.00	0.00	0.00	0.00	0.00	0.00	0.00	0.00	0.00	0.00	0.00	0.00	0.00	0.00	0.00	2.00	1.18	50.00	2.00	1.18	50.00
225.5	3.00	1.77	37.50	0.00	0.00	0.00	0.00	0.00	0.00	0.00	0.00	0.00	1.00	0.59	12.50	0.00	0.00	0.00	3.00	1.77	37.50	1.00	0.59	12.50
226.5	5.00	2.95	71.43	0.00	0.00	0.00	0.00	0.00	0.00	0.00	0.00	0.00	0.00	0.00	0.00	0.00	0.00	0.00	2.00	1.18	28.57	0.00	0.00	0.00
227.5	0.00	0.00	0.00	0.00	0.00	0.00	0.00	0.00	0.00	0.00	0.00	0.00	0.00	0.00	0.00	0.00	0.00	0.00	5.00	2.95	62.50	3.00	1.77	37.50
228.5	0.00	0.00	0.00	0.00	0.00	0.00	0.00	0.00	0.00	0.00	0.00	0.00	0.00	0.00	0.00	0.00	0.00	0.00	1.00	0.59	33.33	2.00	1.18	66.67
229.5	1.00	0.59	33.33	0.00	0.00	0.00	0.00	0.00	0.00	0.00	0.00	0.00	0.00	0.00	0.00	0.00	0.00	0.00	1.00	0.59	33.33	1.00	0.59	33.33
230.5	3.00	1.77	60.00	0.00	0.00	0.00	0.00	0.00	0.00	0.00	0.00	0.00	0.00	0.00	0.00	0.00	0.00	0.00	2.00	1.18	40.00	0.00	0.00	0.00
231.5	3.00	1.77	50.00	0.00	0.00	0.00	0.00	0.00	0.00	0.00	0.00	0.00	0.00	0.00	0.00	0.00	0.00	0.00	0.00	0.00	0.00	3.00	1.77	50.00
232.5	3.00	1.77	75.00	0.00	0.00	0.00	0.00	0.00	0.00	0.00	0.00	0.00	0.00	0.00	0.00	0.00	0.00	0.00	1.00	0.59	25.00	0.00	0.00	0.00
233.5	2.00	1.18	40.00	0.00	0.00	0.00	0.00	0.00	0.00	0.00	0.00	0.00	0.00	0.00	0.00	0.00	0.00	0.00	2.00	1.18	40.00	1.00	0.59	20.00
234.5	1.00	0.59	100.00	0.00	0.00	0.00	0.00	0.00	0.00	0.00	0.00	0.00	0.00	0.00	0.00	0.00	0.00	0.00	0.00	0.00	0.00	0.00	0.00	0.00
235.5	2.00	1.18	40.00	0.00	0.00	0.00	0.00	0.00	0.00	2.00	1.18	40.00	0.00	0.00	0.00	0.00	0.00	0.00	0.00	0.00	0.00	1.00	0.59	20.00
236.5	1.00	0.59	33.33	0.00	0.00	0.00	0.00	0.00	0.00	0.00	0.00	0.00	0.00	0.00	0.00	0.00	0.00	0.00	1.00	0.59	33.33	1.00	0.59	33.33
237.5	0.00	0.00	0.00	0.00	0.00	0.00	0.00	0.00	0.00	1.00	0.59	33.33	0.00	0.00	0.00	0.00	0.00	0.00	0.00	0.00	0.00	2.00	1.18	66.67
238.5	2.00	1.18	33.33	0.00	0.00	0.00	0.00	0.00	0.00	2.00	1.18	33.33	0.00	0.00	0.00	0.00	0.00	0.00	1.00	0.59	16.67	1.00	0.59	16.67
239.5	0.00	0.00	0.00	0.00	0.00	0.00	0.00	0.00	0.00	1.00	0.59	33.33	0.00	0.00	0.00	0.00	0.00	0.00	1.00	0.59	33.33	1.00	0.59	33.33
240.5	0.00	0.00	0.00	1.00	0.59	16.67	0.00	0.00	0.00	1.00	0.59	16.67	0.00	0.00	0.00	1.00	0.59	16.67	2.00	1.18	33.33	1.00	0.59	16.67
241.5	1.00	0.59	20.00	1.00	0.59	20.00	0.00	0.00	0.00	1.00	0.59	20.00	0.00	0.00	0.00	0.00	0.00	0.00	0.00	0.00	0.00	2.00	1.18	40.00
242.5	0.00	0.00	0.00	0.00	0.00	0.00	0.00	0.00	0.00	5.00	2.95	71.43	0.00	0.00	0.00	0.00	0.00	0.00	0.00	0.00	0.00	2.00	1.18	28.57
243.5	0.00	0.00	0.00	1.00	0.59	16.67	0.00	0.00	0.00	1.00	0.59	16.67	0.00	0.00	0.00	0.00	0.00	0.00	1.00	0.59	16.67	3.00	1.77	50.00
244.5	2.00	1.18	15.38	0.00	0.00	0.00	0.00	0.00	0.00	6.00	3.54	46.15	1.00	0.59	7.69	0.00	0.00	0.00	1.00	0.59	7.69	3.00	1.77	23.08
245.5	0.00	0.00	0.00	0.00	0.00	0.00	0.00	0.00	0.00	4.00	2.36	80.00	0.00	0.00	0.00	0.00	0.00	0.00	1.00	0.59	20.00	0.00	0.00	0.00
246.5	0.00	0.00	0.00	0.00	0.00	0.00	0.00	0.00	0.00	1.00	0.59	20.00	0.00	0.00	0.00	0.00	0.00	0.00	2.00	1.18	40.00	2.00	1.18	40.00
247.5	0.00	0.00	0.00	0.00	0.00	0.00	0.00	0.00	0.00	7.00	4.13	87.50	0.00	0.00	0.00	0.00	0.00	0.00	0.00	0.00	0.00	1.00	0.59	12.50
248.5	0.00	0.00	0.00	1.00	0.59	10.00	0.00	0.00	0.00	4.00	2.36	40.00	0.00	0.00	0.00	0.00	0.00	0.00	3.00	1.77	30.00	2.00	1.18	20.00
249.5	0.00	0.00	0.00	0.00	0.00	0.00	0.00	0.00	0.00	7.00	4.13	53.85	1.00	0.59	7.69	2.00	1.18	15.38	0.00	0.00	0.00	3.00	1.77	23.08
250.5	2.00	1.18	25.00	0.00	0.00	0.00	0.00	0.00	0.00	3.00	1.77	37.50	0.00	0.00	0.00	0.00	0.00	0.00	3.00	1.77	37.50	0.00	0.00	0.00
251.5	1.00	0.59	14.29	0.00	0.00	0.00	0.00	0.00	0.00	4.00	2.36	57.14	0.00	0.00	0.00	0.00	0.00	0.00	1.00	0.59	14.29	1.00	0.59	14.29
252.5	0.00	0.00	0.00	0.00	0.00	0.00	0.00	0.00	0.00	1.00	0.59	100.00	0.00	0.00	0.00	0.00	0.00	0.00	0.00	0.00	0.00	0.00	0.00	0.00
253.5	1.00	0.59	12.50	0.00	0.00	0.00	0.00	0.00	0.00	3.00	1.77	37.50	0.00	0.00	0.00	0.00	0.00	0.00	3.00	1.77	37.50	1.00	0.59	12.50
254.5	0.00	0.00	0.00	0.00	0.00	0.00	0.00	0.00	0.00	0.00	0.00	0.00	0.00	0.00	0.00	0.00	0.00	0.00	2.00	1.18	50.00	2.00	1.18	50.00
255.5	0.00	0.00	0.00	0.00	0.00	0.00	0.00	0.00	0.00	1.00	0.59	50.00	0.00	0.00	0.00	0.00	0.00	0.00	0.00	0.00	0.00	1.00	0.59	50.00
256.5	1.00	0.59	12.50	0.00	0.00	0.00	0.00	0.00	0.00	1.00	0.59	12.50	0.00	0.00	0.00	0.00	0.00	0.00	6.00	3.54	75.00	0.00	0.00	0.00
257.5	0.00	0.00	0.00	0.00	0.00	0.00	0.00	0.00	0.00	0.00	0.00	0.00	0.00	0.00	0.00	0.00	0.00	0.00	3.00	1.77	75.00	1.00	0.59	25.00
258.5	2.00	1.18	28.57	0.00	0.00	0.00	0.00	0.00	0.00	2.00	1.18	28.57	0.00	0.00	0.00	0.00	0.00	0.00	3.00	1.77	42.86	0.00	0.00	0.00
259.5	0.00	0.00	0.00	0.00	0.00	0.00	0.00	0.00	0.00	0.00	0.00	0.00	0.00	0.00	0.00	0.00	0.00	0.00	0.00	0.00	0.00	0.00	0.00	100.00
260.5	0.00	0.00	0.00	0.00	0.00	0.00	0.00	0.00	0.00	1.00	0.59	16.67	0.00	0.00	0.00	0.00	0.00	0.00	4.00	2.36	66.67	1.00	0.59	16.67
261.5	2.00	1.18	22.22	0.00	0.00	0.00	0.00	0.00	0.00	1.00	0.59	11.11	0.00	0.00	0.00	0.00	0.00	0.00	5.00	2.95	55.56	1.00	0.59	11.11
262.5	0.00	0.00	0.00	0.00	0.00	0.00	0.00	0.00	0.00	3.00	1.77	37.50	0.00	0.00	0.00	0.00	0.00	0.00	4.00	2.36	50.00	1.00	0.59	12.50
263.5	0.00	0.00	0.00	0.00	0.00	0.00	0.00	0.00	0.00	0.00	0.00	0.00	0.00	0.00	0.00	0.00	0.00	0.00	1.00	0.59	100.00	0.00	0.00	0.00
264.5	2.00	1.18	22.22	0.00	0.00	0.00	0.00	0.00	0.00	3.00	1.77	33.33	0.00	0.00	0.00	0.00	0.00	0.00	3.00	1.77	33.33	1.00	0.59	11.11
265.5	1.00	0.59	20.00	0.00	0.00	0.00	0.00	0.00	0.00	0.00	0.00	0.00	0.00	0.00	0.00	0.00	0.00	0.00	3.00	1.77	60.00	1.00	0.59	20.00
266.5	0.00	0.00	0.00	0.00	0.00	0.00	0.00	0.00	0.00	0.00	0.00	0.00	0.00	0.00	0.00	0.00	0.00	0.00	2.00	1.18	100.00	0.00	0.00	0.00
267.5	0.00	0.00	0.00	0.00	0.00	0.00	0.00	0.00	0.00	0.00	0.00	0.00	0.00	0.00	0.00	0.00	0.00	0.00	2.00	1.18	66.67	1.00	0.59	33.33
268.5	0.00	0.00	0.00	0.00	0.00	0.00	0.00	0.00	0.00	0.00	0.00	0.00	0.00	0.00	0.00	0.00	0.00	0.00	5.00	2.95	71.43	2.00	1.18	28.57
269.5	0.00	0.00	0.00	0.00	0.00	0.00	0.00	0.00	0.00	1.00	0.59	20.00	1.00	0.59	20.00	0.00	0.00	0.00	3.00	1.77	60.00	0.00	0.00	0.00
270.5	1.00	0.59	16.67	0.00	0.00	0.00	0.00	0.00	0.00	1.00	0.59	16.67	0.00	0.00	0.00	0.00	0.00	0.00	4.00	2.36	66.67	0.00	0.00	0.00
271.5	0.00	0.00	0.00	0.00	0.00	0.00	0.00	0.00	0.00	0.00	0.00	0.00	0.00	0.00	0.00	0.00	0.00	0.00	2.00	1.18	100.00	0.00	0.00	0.00
272.5	0.00	0.00	0.00	0.00	0.00	0.00	0.00	0.00	0.00	0.00	0.00	0.00	0.00	0.00	0.00	0.00	0.00	0.00	2.00	1.18	100.00	0.00	0.00	0.00

4.4.3 Plates

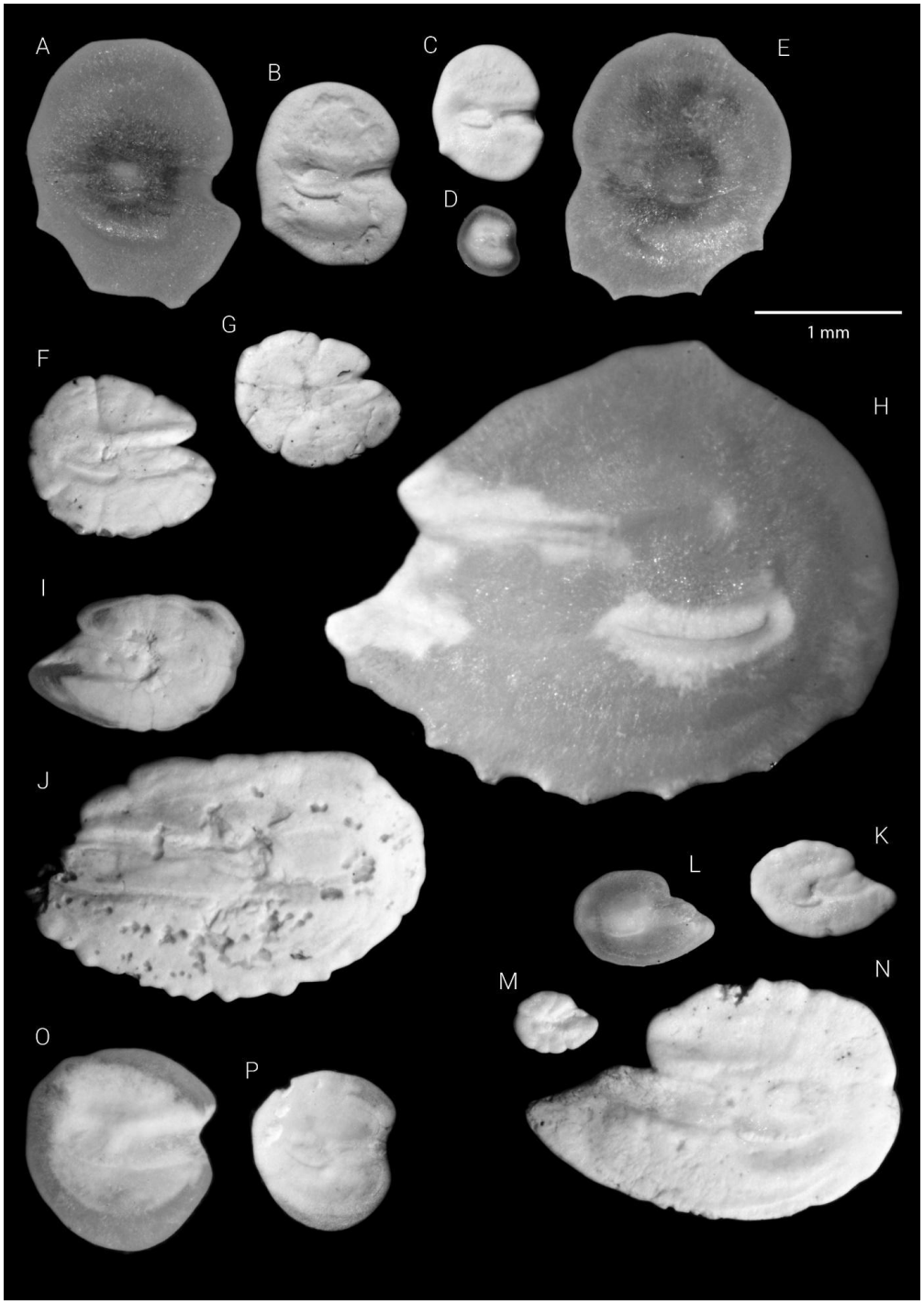

Plate S4.1: *Inner view of fossil fish otoliths from Kasten core M144 KC5-6 (central western Mediterranean Sea) belonging to family Myctophidae. A-E: Benthosema glaciale; F-H: Diaphus holti; I-J: Notoscopelus elongatus; K-N: Ceratoscopelus maderensis; O-P: Electrona risso. Scale bar 1mm.*

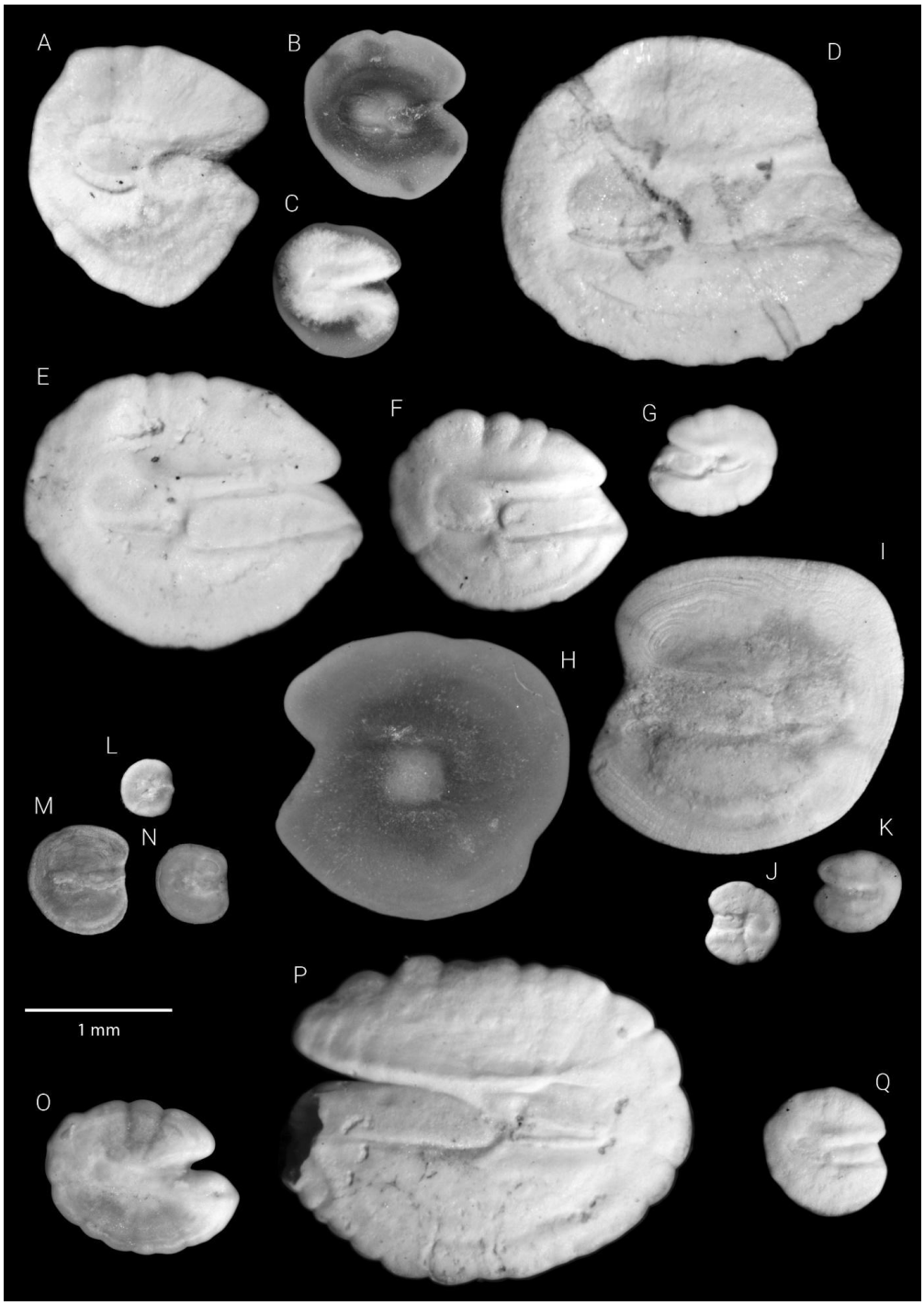

Plate S4.2: *Inner view of fossil fish otoliths from Kasten core M144 KC5-6 (central western Mediterranean Sea) belonging to family Myctophidae. A-C: Hygophum benoiti; D: Lobianchia dofleini; E-G: Myctophum punctatum; H-K: Lampanyctus crocodilus; L-N: Lampanyctus pusillus; O-P: Symbolophorus veranyi; Q: Hygophum hygomii. Scale bar 1mm.*

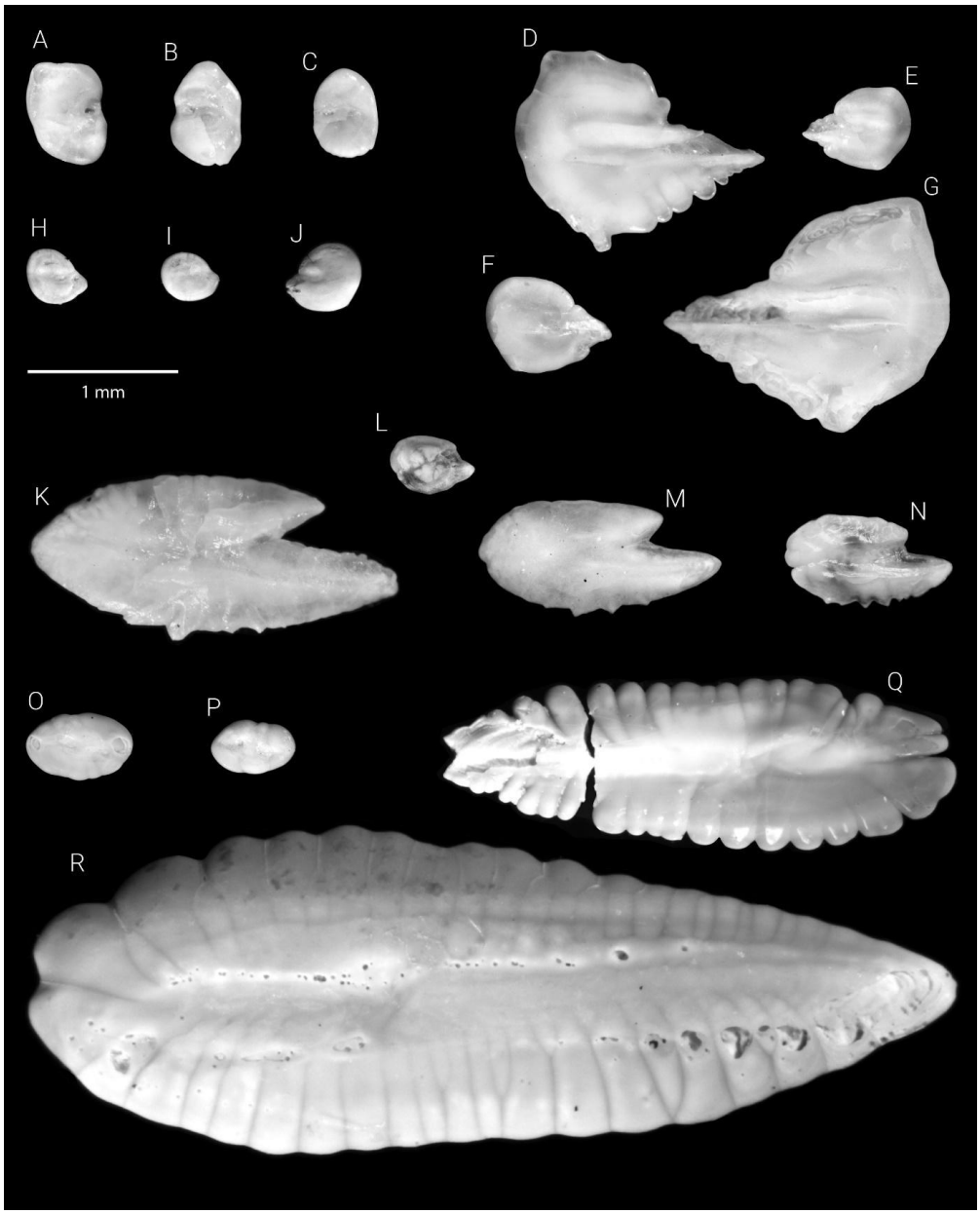

Plate S4.3: *Inner view of fossil fish otoliths from Kasten core M144 KC5-6 (central western Mediterranean Sea). A-C: Argyropelecus hemigymnus (Sternoptychidae); D-G: Maurolicus mülleri (Sternoptychidae); H-J: Gonostomatidae; K-N: Engraulis encrasicolus (Engraulidae); O-P: Gadiculus argenteus (Gadidae); Q-R: Micromesistius poutassou. Scale bar 1mm.*

CHAPTER 5

5 Synthesis and research perspectives

5.1 Synthesis

Warming, acidification, and deoxygenation processes– also referred to as the "deadly trio" – are all concerningly accelerating in today's ocean. They are assumed to have severe consequences for its biogeochemical cycling and ecosystems in ways we cannot predict as yet (Bijma et al., 2013; Gruber, 2011). The lack of temporal and spatial long-term monitoring and instrumental time series relating to biological and physicochemical parameters prevent a comprehensive evaluation of how those CO_2 induced climate change stressors impact marine biota. In laboratory experimental settings, physical and chemical parameters can be manipulated in seawater to simulate past and/or future conditions to overcome the constraints of short time series. However, they fail to capture the complex interplay and synergistic effects of ocean warming, acidification, and deoxygenation and the associated long-term responses. By overcoming those limitations mentioned above, this thesis contributes to the understanding of how those CO_2 induced climate change stressors affect marine ecosystems. This is done by providing long-term records of calcifying plankton and pelagic fish dynamics from Mediterranean Sea sediments, to test their response to the "deadly trio", or as they are referred to here: The trident of climate change impacts. The features of the Mediterranean Sea (chapter 1.4) make the basin an ocean laboratory, in which paleoceanographic changes can be studied to differentiate between natural variability of ecosystems and anthropogenic impacts. Accordingly, the thesis can advance the understanding of global change processes.

In this thesis, common and novel paleoceanographic tools are applied on geohistorical long-term records from the Mediterranean Sea to assess the response of pelagic organisms (zooplankton and fishes) to CO_2 induced climate change stressors. Undisturbed marine sedimentary archives, from multicorer, provide the necessary high temporal resolution to identify the pre-industrial baselines for calcifying plankton assemblages and their shell chemistry/morphometrics. In this way, the impacts of anthropogenic warming and acidification are tested against preindustrial variability on calcifying plankton (Chapters 2 and 3). To better understand the response of pelagic fish to future ocean deoxygenation (Chapter 4), a marine sedimentary Holocene record is extracted from the Eastern Mediterranean Sea. The

geohistorical natural variability preserved in the marine sediments allows to contrast a well-ventilated “normal” oxygen Mediterranean Sea with anoxic conditions. Here, the use of a Kasten corer guarantees the sampling of large amounts of sediment, to yield for high concentrations of fossil otoliths, being scarce in ocean deposits.

In chapter 2, the transition between preindustrial and modern times is investigated through SST reconstructions derived from alkenones and planktic foraminiferal abundance dynamics. This approach allows to test for changes in western Mediterranean climatic and oceanographic conditions induced through anthropogenic CO_2 perturbations. Particularly, relative abundance changes of the key indicator species *G. bulloides, G. inflata* and *G. truncatulinoides* shed light on hydrographic conditions and surface productivity patterns. Those findings suggest that anthropogenic warming during the 20^{th} century enhanced vertical stratification, impeding nutrient supply to surface waters, which lead to a decline in marine surface productivity, overriding the preindustrial signal of natural variability.

Chapter 3 assesses the impacts of ongoing ocean acidification on calcifying marine zooplankton. Cutting-edge stable isotope mass spectrometry analysis in fossil shells of *G. ruber* and *G. bulloides*, two surface dwelling planktic foraminifera species, show accelerated anthropogenic carbon uptake, depicted by $\delta^{13}C$ variability, and ongoing acidification, depicted by $\delta^{11}B$ variability, in the ocean. Such changes were detected for the first time in Mediterranean planktic foraminiferal shells. Size normalized weight (SNW) measurements performed in the same two species suggest that those carbon perturbations at the sea surface impaired foraminiferal calcification during the 20^{th} century.

In chapter 4, an Eastern Mediterranean otolith record is used to contrast the response of the pelagic fish community to changing ocean oxygen levels throughout the Holocene. Those microfossils have been applied in ichthyology, fishery biology and micropaleontology since over a century, but continuous marine records are very rare, as high concentrations of fossils and large amounts of sediments are needed to gain statistically significant results. Unlike planktic foraminiferal shells, which record lower trophic food web dynamics, fossil otoliths can give insights about past

ecological changes of higher trophic levels, which are so far insufficiently studied in paleoceanography. Here, it is shown that mesopelagic fish thrived during times of a well oxygenated water column but became nearly absent when mid- to bottom waters were severely anoxic. The findings suggest that accelerated ocean deoxygenation might reduce mesopelagic fish abundance in two ways. Shoaling of OMZs is expected to compress their vertical night-time habitat, thus enhances predator pressure on mesopelagic fish, while survival in the core regions of the OMZs become nearly impossible, once absolute oxygen levels fall below a certain threshold (Vaquer-Sunyer & Duarte, 2008).

The findings of that thesis, which are based on Mediterranean long-term fossil records, can provide a glimpse of how the ocean in a future high CO_2 world could look like (Fig. 5.1). SST increase, and enhanced stratification might result in ultraoligotrophic surface waters and declining biological productivity. At the same time, ongoing acidification impedes the biogenic calcification of marine calcifying plankton, while reduced ocean oxygen levels and particularly severe midwater anoxia diminishes mesopelagic fish stocks. With ocean warming, acidification, and deoxygenation expected to become more severe during the 21st century (Bopp et al., 2013), global marine ecosystem services are under threat since marine calcifying plankton and mesopelagic fish are major components of both the marine food web architecture and biogeochemical cycling in the ocean. Mesopelagic fish are key players in the marine food web, by connecting shallow with deep sea ecosystems (Eduardo et al., 2021), and controlling both, bottom-up and top-down processes (Catul et al., 2011), mediating energy transfer from primary production to top predator biomass (Hunt et al., 2015). Owing to their large biomass which equals 100x annual global fish and aquaculture production (FAO, 2022; Irigoien et al., 2014), mesopelagic fish are not only a vital food for big predatory fish and marine mammals, but also an important resource to supply aquaculture and nutraceutical markets (St. John et al., 2016). As a reliable source of essential amino acids and nutritive proteins (Koizumi et al., 2014; Seo et al., 1998), mesopelagic fish might be a potentially new nutritional resource to sustainably feed the world. Although, planktic foraminifera constitute only a small component of the global plankton biomass (Buitenhuis et al.,

2013; Knecht et al., 2023; Ziveri et al., 2023), making them less important for the marine food web, they are good indicators for overall plankton biomass changes as they are closely related to primary production. Mesopelagic fish actively transport carbon from the surface to the deep ocean through vertical migration, sustaining its biological carbon pump efficiency (Davison et al., 2013; Saba et al., 2021). Planktic foraminifera are responsible for approximately 50% of the global pelagic calcite export flux through sinking shells, highlighting their importance for long-term carbon storage in ocean sediments (Schiebel et al., 2018). Accordingly, the decline of both mesopelagic fish and planktic foraminifera due to enhanced warming, acidification, and deoxygenation in a future ocean, as indicated through this thesis, suggests a major loss of marine biomass and profound perturbations of the marine carbon pump, which would have negative knock-on effects on climate regulation, ocean's ecosystem functioning and food security.

The scientific findings presented in this work call out for a better protection of our oceans through improved sustainable management of marine resources and a reduction of CO_2 emissions. Mesopelagic fishery is a promising, new solution to provide a growing aquaculture production and a globally increasing population with nutritional food, and to counterbalance the declining worlds fish supply which is already exhausted through industrial fisheries. As indicated in this work, mesopelagic fish dynamics are highly sensitive to climate change stressors like ocean deoxygenation. Right now, the role of mesopelagic fish for carbon cycling and pelagic food webs seems to be too important to enhance pressure on the mesopelagic communities through inconsiderate exploitation of mesopelagic resources. More studies are needed to quantify the biomass of mesopelagic fish and better assess their response to ongoing climate change. Additionally, it is important to implement a precautionary approach for harvesting midwater resources, including moratoriums on deep sea fishing, the promotion of marine protected areas and the reduction of fishery subsidies. Additionally, great and effective efforts need to be done to cut carbon emissions, to slow down ocean warming, acidification, and deoxygenation, hence mitigate the effects of CO_2 induced climate change stressors on marine ecosystems, which is extremely urgent as we cannot forecast their extensive consequences. Due to

the high uncertainties regarding fundamental processes and interplay between combined CO_2 induced climate change stressors, the magnitude of marine ecosystem damage over the coming century is likely to be underestimated yet. Only a drastic reduction in carbon emissions might prevent us from unpredictable marine ecosystem collapse. Both sustainable midwater fishery and climate mitigation are two crucial components to protect and restore marine ecosystem functions, to provide for the same goods and services that satisfied our needs, also for the next generation.

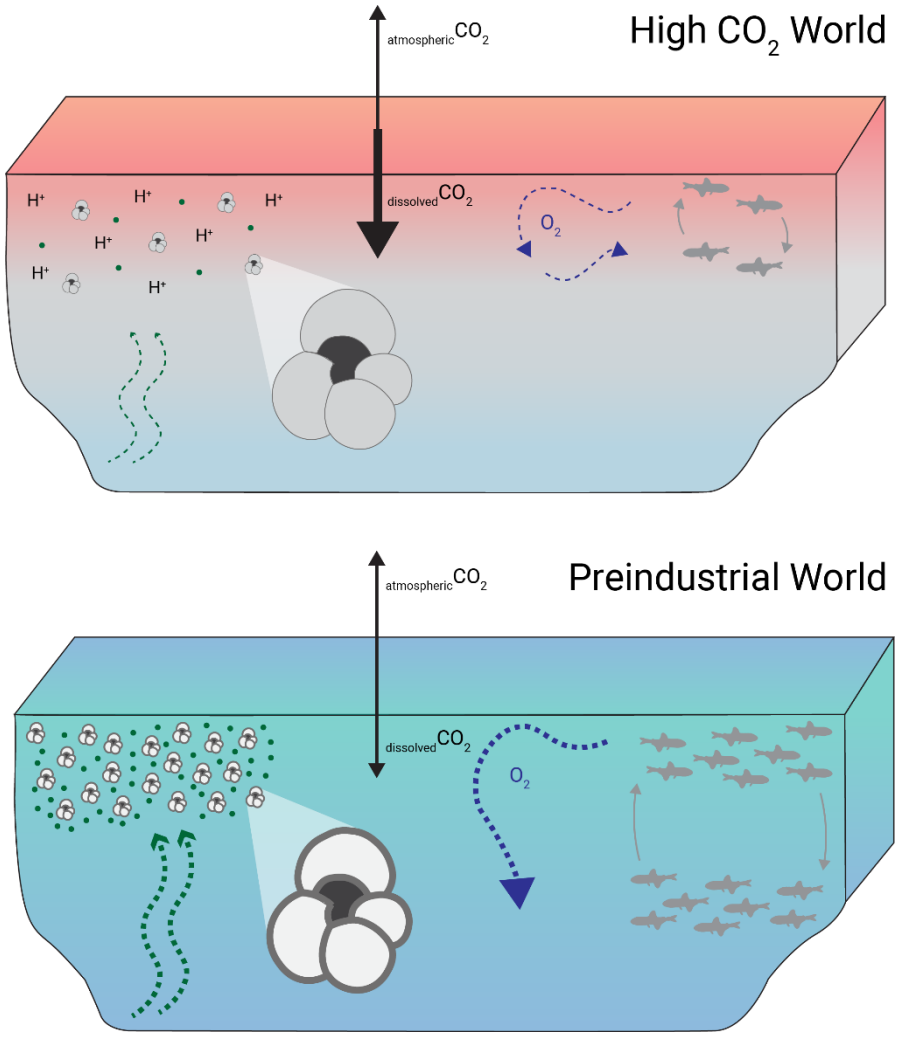

Figure 5 1: *Sketch of an ocean in a preindustrial compared to a high CO_2 world based on main findings of the thesis.*

5.2 Research perspectives

Fossil planktic foraminifera as a window to long-term biodiversity changes

Knowledge about marine biodiversity change is key to sustain ocean ecosystem functioning, however, smaller organisms are less well studied than larger taxa and plankton monitoring programs rarely span more than a century. As diversity of marine microfossils is closely related to overall diversity of marine microplankton, studying entire fossil foraminiferal species compositions will allow to quantify biodiversity dynamics over decades to millennia and assess their relation to environmental long-term changes. There is further need to use fossil planktic foraminiferal records with highest temporal resolution to extend observational zooplankton time-series back to preindustrial times, which will help assess human impact on biological plankton diversity, refine ecological model projections and evaluate nonlinear dynamics and the detection of tipping points in marine ecosystems. To better constrain zooplankton dynamics on seasonal to centennial times scales, we must overcome the lack of collaborations between zooplankton ecologists and micropaleontologists, calling for more interdisciplinarity in our research.

The need for more paleo fish records

This thesis reconstructs pelagic fish dynamics throughout the geological past by using fossil otoliths, in the same fashion as some previous studies produced long time series by means of other fish proxy types like teeth, scales, or bones. There are many other environments and time periods which need to be investigated yet, to establish a comprehensive set of historical baselines which are crucial for marine fishery conservation and management, as they can help to effectively restore degraded marine fish populations and communities. More efforts must be made to study fish response throughout climatic extreme events in the past like the Paleocene-Eocene Thermal Maximum (PETM) or glacial to interglacial cycles to better understand their responses to climate change stressors like ocean warming and acidification. Comparing long-term reconstructions of fish abundance and species composition changes with paleo

productivity might fill knowledge gaps in the complex research field embracing food web architecture and trophic web dynamics.

Proxy potentials of fossil otoliths

There are many applications for otoliths in modern fishery science, studying their morphometrics, growth rings or chemical composition which provide information about habitats or life history of fishes. As the use of otoliths in paleoceanography is quite recent, there is a great potential to apply those cutting-edge techniques of modern fishery science to fossil otoliths. Analyzing otolith size changes in sedimentary records would provide us with a proxy for fish body size and biomass. The stable isotopic composition of fossil otoliths could help to better understand past changes in species trophic level and diet ($\delta^{15}N$) or metabolic rates ($\delta^{13}C$). Measuring redox sensitive elements like Mn/Ca ratios in the calcareous structure of fossil otoliths could give insights of fish exposure to hypoxic conditions in the past. Those are just a few, selected examples of how fossil otoliths could serve as proxy archives and the short list might give a glimpse of their great potential for research in paleoceanography, paleoclimatology, and paleoecology.

Table of Figures

Chapter 1:

Chapter 2:

Chapter 3:

Chapter 4:

Chapter 5:

Table of Tables

Chapter 2:

Chapter 3:

Chapter 4:

Table of Plates

Chapter 3:

Chapter 4:

References

Abram, N. J., McGregor, H. V., Tierney, J. E., Evans, M. N., McKay, N. P., Kaufman, D. S., . . . Gunten, L. v. (2016). Early onset of industrial-era warming across the oceans and continents. *Nature, 536*, 411. doi:10.1038/nature19082

Ahmed, M., Anchukaitis, K. J., Asrat, A., Borgaonkar, H. P., Braida, M., Buckley, B. M., . . . Consortium, P. k. (2013). Continental-scale temperature variability during the past two millennia. *Nature geoscience, 6*(5), 339-346. doi:10.1038/ngeo1797

Aldridge, D., Beer, C. J., & Purdie, D. A. (2012). Calcification in the planktonic foraminifera Globigerina bulloides linked to phosphate concentrations in surface waters of the North Atlantic Ocean. *Biogeosciences, 9*(5), 1725-1739. doi:10.5194/bg-9-1725-2012

Álvarez, M., Sanleón-Bartolomé, H., Tanhua, T., Mintrop, L., Luchetta, A., Cantoni, C., . . . Civitarese, G. (2014). The CO_2 system in the Mediterranean Sea: a basin wide perspective. *Ocean Sci., 10*(1), 69-92. doi:10.5194/os-10-69-2014

Alves, E. Q., Macario, K., Ascough, P., & Bronk Ramsey, C. (2018). The worldwide marine radiocarbon reservoir effect: definitions, mechanisms, and prospects. *Reviews of Geophysics, 56*(1), 278-305. doi:10.1002/2017RG000588

Amitai, Y., Yam, R., Montagna, P., Devoti, S., Correa, M. L., & Shemesh, A. (2020). Spatial and temporal variability in Mediterranean climate over the last millennium from vermetid isotope records and CMIP5/PMIP3 models. *Global and Planetary Change, 189*, 103159. doi:https://doi.org/10.1016/j.gloplacha.2020.103159

Andersen, M. B., Matthews, A., Bar-Matthews, M., & Vance, D. (2020). Rapid onset of ocean anoxia shown by high U and low Mo isotope compositions of sapropel S1. *Geochemical Perspectives Letters, 15*, 10-14. doi:https://doi.org/10.7185/geochemlet.2027

Anderson, O. R., Spindler, M., Bé, A. W. H., & Hemleben, C. (1979). Trophic Activity of Planktonic Foraminifera. *Journal of the Marine Biological Association of the United Kingdom, 59*(3), 791-799. doi:10.1017/S002531540004577X

Appleby, P. G., & Oldfield, F. (1992). Applications of lead-210 to sedimentation studies. In M. Ivanovich & R. S. Harmon (Eds.), *Uranium series disequilibrium: applications to environmental problems* (2 ed.). United Kingdom: Clarendon Press.

Ascough, P., Cook, G., & Dugmore, A. (2005). Methodological approaches to determining the marine radiocarbon reservoir effect. *Progress in Physical Geography, 29*(4), 532-547. doi:10.1191/0309133305pp461ra

Ausín, B., Flores, J. A., Sierro, F. J., Cacho, I., Hernández-Almeida, I., Martrat, B., & Grimalt, J. O. (2015). Atmospheric patterns driving Holocene productivity in the Alboran Sea (Western Mediterranean): a multiproxy approach. *The Holocene, 25*(4), 583-595. doi:doi.org/10.1177/0959683614565952

Azharuddin, S., Govil, P., Chalk, T. B., Shekhar, M., Foster, G. L., & Mishra, R. (2022). Abrupt upwelling and CO2 outgassing episodes in the north-eastern Arabian Sea since mid-Holocene. *Scientific Reports, 12*(1). doi:10.1038/s41598-022-07774-4

Azrieli-Tal, I., Matthews, A., Bar-Matthews, M., Almogi-Labin, A., Vance, D., Archer, C., & Teutsch, N. (2014). Evidence from molybdenum and iron isotopes and molybdenum–uranium covariation for sulphidic bottom waters during Eastern Mediterranean sapropel S1 formation. *Earth and Planetary Science Letters, 393*, 231-242. doi:https://doi.org/10.1016/j.epsl.2014.02.054

Bagarinao, T., & Vetter, R. D. (1989). Sulfide tolerance and detoxification in shallow-water marine fishes. *Marine Biology, 103*(3), 291-302. doi:10.1007/BF00397262

Bárcena, M. A., & Abrantes, F. (1998). Evidence of a high-productivity area off the coast of Málaga from studies of diatoms in surface sediments. *Marine Micropaleontology, 35*(1), 91-103. doi:10.1016/S0377-8398(98)00012-7

Bárcena, M. A., Flores, J. A., Sierro, F. J., Pérez-Folgado, M., Fabres, J., Calafat, A., & Canals, M. (2004). Planktonic response to main oceanographic changes in the Alboran Sea (Western Mediterranean) as documented in sediment traps and surface sediments. *Marine Micropaleontology, 53*(3-4), 423-445. doi:10.1016/j.marmicro.2004.09.009

Barham, E. G. (1966). Deep Scattering Layer Migration and Composition: Observations from a Diving Saucer. *Science, 151*(3716), 1399-1403. doi:doi:10.1126/science.151.3716.1399

Barker, S., Broecker, W., Clark, E., & Hajdas, I. (2007). Radiocarbon age offsets of foraminifera resulting from differential dissolution and fragmentation within the sedimentary bioturbated zone. *Paleoceanography and Paleoclimatology, 22*(2). doi:10.1029/2006PA001354

Barker, S., & Elderfield, H. (2002). Foraminiferal calcification response to glacial-interglacial changes in atmospheric Co2. *Science, 297*(5582), 833-836. doi:10.1126/science.1072815

Barker, S., Greaves, M., & Elderfield, H. (2003). A study of cleaning procedures used for foraminiferal Mg/Ca paleothermometry. *Geochemistry, Geophysics, Geosystems, 4*(9). doi:10.1029/2003GC000559

Bates, N. R., Astor, Y. M., Church, M. J., Currie, K. I. M., Dore, J. E., GonzÁLez-DÁVila, M., . . . Santana-Casiano, J. M. (2014). A Time-Series View of Changing Surface Ocean Chemistry Due to Ocean Uptake of Anthropogenic CO_2 and Ocean Acidification. *Oceanography, 27*(1), 126-141.

Baumann, K. H., Andruleit, H., Böckel, B., Geisen, M., & Kinkel, H. (2005). The significance of extant coccolithophores as indicators of ocean water masses, surface water temperature, and paleoproductivity: a review. *Paläontologische Zeitschrift, 79*(1), 93 - 112. doi:10.1007/978-3-642-58646-0_4

Baumann, K. H., Čepek, M., & Kinkel, H. (1999). Coccolithophores as Indicators of Ocean Water Masses, Surface-Water Temperature, and Paleoproductivity — Examples from the South Atlantic. In G. Fischer & G. Wefer (Eds.), *Use of Proxies in Paleoceanography: Examples from the South Atlantic* (pp. 117-144). Berlin, Heidelberg: Springer Berlin Heidelberg.

Bauska, T. K., Joos, F., Mix, A. C., Roth, R., Ahn, J., & Brook, E. J. (2015). Links between atmospheric carbon dioxide, the land carbon reservoir and climate over the past millennium. *Nature geoscience, 8*(5), 383-387. doi:10.1038/ngeo2422

Bazzicalupo, P., Maiorano, P., Girone, A., Marino, M., Combourieu-Nebout, N., Pelosi, N., . . . Incarbona, A. (2020). Holocene climate variability of the Western Mediterranean: Surface water dynamics inferred from calcareous plankton assemblages. *The Holocene, 30*(5), 691-708. doi:10.1177/0959683619895580

Bé, A. W. H. (1977). An ecological, zoogeographic and taxonomic review of recent planktonic foraminifera. *Oceanic Micropaleontology*, 1-100.

Bé, A. W. H., & Tolderlund, D. S. (1971). Distribution and Ecology of Living Planktonic Foraminifera in Surface Waters of the Atlantic and Indian Ocean. In B.M. Funnel & W. R. Riedel (Eds.), *The Micropaleontology of Oceans* (pp. 104 - 149). New York: University Press.

Beaufort, L., Lancelot, Y., Camberlin, P., Cayre, O., Vincent, E., Bassinot, F., & Labeyrie, L. (1997). Insolation cycles as a major control of equatorial Indian Ocean primary production. *Science, 278*(5342), 1451-1454. doi:10.1126/science.278.5342.1451

Beaufort, L., Probert, I., de Garidel-Thoron, T., Bendif, E. M., Ruiz-Pino, D., Metzl, N., . . . de Vargas, C. (2011). Sensitivity of coccolithophores to carbonate chemistry and ocean acidification. *Nature, 476*(7358), 80-83. doi:10.1038/nature10295

Beaugrand, G., McQuatters-Gollop, A., Edwards, M., & Goberville, E. (2013). Long-term responses of North Atlantic calcifying plankton to climate change. *Nature Climate Change, 3*(3), 263. doi:10.1038/nclimate1753

Beer, C. J., Schiebel, R., & Wilson, P. (2010a). On methodologies for determining the size-normalised weight of planktic foraminifera. *Biogeosciences, 7*(7), 2193.

Beer, C. J., Schiebel, R., & Wilson, P. A. (2010b). Testing planktic foraminiferal shell weight as a surface water [CO32−] proxy using plankton net samples. *Geology, 38*(2), 103-106.

Behrenfeld, M. J., O'Malley, R. T., Siegel, D. A., McClain, C. R., Sarmiento, J. L., Feldman, G. C., . . . Boss, E. S. (2006). Climate-driven trends in contemporary ocean productivity. *Nature, 444*(7120), 752-755. doi:10.1038/nature05317

Béjard, T. M., Rigual-Hernández, A. S., Flores, J. A., Tarruella, J. P., Durrieu de Madron, X., Cacho, I., . . . Sierro, F. J. (2023). Calcification response of planktic foraminifera to environmental change in the western Mediterranean Sea during the industrial era. *Biogeosciences, 20*(7), 1505-1528. doi:10.5194/bg-20-1505-2023

Bemis, B. E., Spero, H. J., Lea, D. W., & Bijma, J. (2000). Temperature influence on the carbon isotopic composition of Globigerina bulloides and Orbulina universa (planktonic foraminifera). *Marine Micropaleontology, 38*(3-4), 213-228. doi:10.1016/S0377-8398(00)00006-2

Benkovitz, A., Matthews, A., Teutsch, N., Poulton, S. W., Bar-Matthews, M., & Almogi-Labin, A. (2020). Tracing water column euxinia in Eastern Mediterranean Sapropels S5 and S7. *Chemical Geology, 545*, 119627. doi:https://doi.org/10.1016/j.chemgeo.2020.119627

Bertrand, A., Chaigneau, A., Peraltilla, S., Ledesma, J., Graco, M., Monetti, F., & Chavez, F. P. (2011). Oxygen: A Fundamental Property Regulating Pelagic Ecosystem Structure in the Coastal Southeastern Tropical Pacific. *PLoS ONE, 6*(12), e29558. doi:10.1371/journal.pone.0029558

Bianchi, C. N. (2007). Biodiversity issues for the forthcoming tropical Mediterranean Sea. *Hydrobiologia, 580*(1), 7. doi:10.1007/s10750-006-0469-5

Bianchi, D., Galbraith, E. D., Carozza, D. A., Mislan, K. A. S., & Stock, C. A. (2013). Intensification of open-ocean oxygen depletion by vertically migrating animals. *Nature geoscience, 6*(7), 545-548. doi:10.1038/ngeo1837

Bijma, J., Faber Jr, W. W., & Hemleben, C. (1990). Temperature and salinity limits for growth and survival of some planktonic foraminifers in laboratory cultures. *Journal of Foraminiferal Research, 20*(2), 95-116. doi:10.2113/gsjfr.20.2.95

Bijma, J., Pörtner, H.-O., Yesson, C., & Rogers, A. D. (2013). Climate change and the oceans – What does the future hold? *Marine Pollution Bulletin, 74*(2), 495-505. doi:https://doi.org/10.1016/j.marpolbul.2013.07.022

Bijma, J., Spero, H. J., & Lea, D. W. (1999). Reassessing Foraminiferal Stable Isotope Geochemistry: Impact of the Oceanic Carbonate System (Experimental Results). In G. Fischer & G. Wefer (Eds.), *Use of Proxies in Paleoceanography: Examples from the South Atlantic* (pp. 489-512). Berlin, Heidelberg: Springer Berlin Heidelberg.

Bindoff, N. L., Cheung, W. W. L., Kairo, J. G., Arístegui, J., Guinder, V. A., Hallberg, R., . . . Williamson, P. (2019). Changing Ocean, Marine Ecosystems, and Dependent Communities. In H.-O. Pörtner, D. C. Roberts, V. Masson-Delmotte, P. Zhai, M. Tignor, E. Poloczanska, K. Mintenbeck, A. Alegría, M. Nicolai, A. Okem, J. Petzold, B. Rama, & N. M. Weyer (Eds.), *IPCC special report on the ocean and cryosphere in a changing climate* (pp. 447-587). Cambridge, UK and New York, NY, USA.

Bird, C., Darling, K. F., Russell, A. D., Davis, C. V., Fehrenbacher, J., Free, A., . . . Ngwenya, B. T. (2017). Cyanobacterial endobionts within a major marine planktonic calcifier (Globigerina bulloides, Foraminifera) revealed by 16S rRNA metabarcoding. *Biogeosciences, 14*(4), 901-920. doi:10.5194/bg-14-901-2017

Blaauw, M., & Christen, J. A. (2011). Flexible paleoclimate age-depth models using an autoregressive gamma process. *Bayesian analysis, 6*(3), 457-474. doi:10.1214/11-BA618

Bograd, S. J., Castro, C. G., Di Lorenzo, E., Palacios, D. M., Bailey, H., Gilly, W., & Chavez, F. P. (2008). Oxygen declines and the shoaling of the hypoxic boundary in the California Current. *Geophysical Research Letters, 35*(12). doi:https://doi.org/10.1029/2008GL034185

Bollmann, J. (1997). Morphology and biogeography of Gephyrocapsa coccoliths in Holocene sediments. *Marine Micropaleontology, 29*(3-4), 319-350. doi:10.1016/S0377-8398(96)00028-X

Bopp, L., Resplandy, L., Orr, J. C., Doney, S. C., Dunne, J. P., Gehlen, M., . . . Seferian, R. (2013). Multiple stressors of ocean ecosystems in the 21st century: projections with CMIP5 models. *Biogeosciences, 10*, 6225-6245.

Bormans, M., & Garrett, C. (1989). A simple criterion for gyre formation by the surface outflow from a strait, with application to the Alboran Sea. *Journal of Geophysical Research: Oceans, 94*(C9), 12637-12644. doi:10.1029/JC094iC09p12637

Bosc, E., Bricaud, A., & Antoine, D. (2004). Seasonal and interannual variability in algal biomass and primary production in the Mediterranean Sea, as derived from 4 years of SeaWiFS observations. *Global Biogeochemical Cycles, 18*(1). doi:10.1029/2003GB002034

Bown, P. R., & Young, J. R. (1998). Techniques. In P. R. Bown (Ed.), *Calcareous nannofossil biostratigraphy* (pp. 16-28). London: Chapman and Hall.

Boyce, D. G., Dowd, M., Lewis, M. R., & Worm, B. (2014). Estimating global chlorophyll changes over the past century. *Progress in Oceanography, 122*, 163-173. doi:10.1016/j.pocean.2014.01.004

Boyce, D. G., Lotze, H. K., Tittensor, D. P., Carozza, D. A., & Worm, B. (2020). Future ocean biomass losses may widen socioeconomic equity gaps. *Nature Communications, 11*(1), 2235. doi:10.1038/s41467-020-15708-9

Bradley, R. S. (2015a). Chapter 3 - Dating Methods I. In R. S. Bradley (Ed.), *Paleoclimatology (Third Edition)* (pp. 55-101). San Diego: Academic Press.

Bradley, R. S. (2015b). Chapter 6 - Marine Sediments. In R. S. Bradley (Ed.), *Paleoclimatology (Third Edition)* (pp. 195-277). San Diego: Academic Press.

Brassell, S., Eglinton, G., Marlowe, I., Pflaumann, U., & Sarnthein, M. (1986). Molecular stratigraphy: a new tool for climatic assessment. *Nature, 320*(6058), 129.

Breitburg, D., Levin, L. A., Oschlies, A., Grégoire, M., Chavez, F. P., Conley, D. J., . . . Zhang, J. (2018). Declining oxygen in the global ocean and coastal waters. *Science, 359*(6371), eaam7240. doi:doi:10.1126/science.aam7240

Brewer, P. G., & Peltzer, E. T. (2017). Depth perception: the need to report ocean biogeochemical rates as functions of temperature, not depth. *Philosophical Transactions of the Royal Society A: Mathematical, Physical and Engineering Sciences, 375*(2102), 20160319. doi:doi:10.1098/rsta.2016.0319

Buitenhuis, E. T., Vogt, M., Moriarty, R., Bednaršek, N., Doney, S. C., Leblanc, K., . . . Swan, C. (2013). MAREDAT: towards a world atlas of MARine Ecosystem DATa. *Earth Syst. Sci. Data, 5*(2), 227-239. doi:10.5194/essd-5-227-2013

Cacho, I., Grimalt, J. O., Canals, M., Sbaffi, L., Shackleton, N. J., Schönfeld, J., & Zahn, R. (2001). Variability of the western Mediterranean Sea surface temperature during the last 25,000 years and its connection with the Northern Hemisphere climatic changes. *Paleoceanography, 16*(1), 40-52.

Cacho, I., Grimalt, J. O., Pelejero, C., Canals, M., Sierro, F. J., Flores, J. A., & Shackleton, N. (1999). Dansgaard-Oeschger and Heinrich event imprints in Alboran Sea paleotemperatures. *Paleoceanography and Paleoclimatology, 14*(6), 698-705. doi:10.1029/1999PA900044

Cacho, I., Grimalt, J. O., Sierro, F. J., Shackleton, N., & Canals, M. (2000). Evidence for enhanced Mediterranean thermohaline circulation during rapid climatic coolings. *Earth and Planetary Science Letters, 183*(3), 417-429. doi:10.1016/S0012-821X(00)00296-X

Caldeira, K., & Wickett, M. E. (2003). Anthropogenic carbon and ocean pH. *Nature, 425*(6956), 365-365. doi:10.1038/425365a

Canals, M., Puig, P., de Madron, X. D., Heussner, S., Palanques, A., & Fabres, J. (2006). Flushing submarine canyons. *Nature, 444*(7117), 354-357. doi:10.1038/nature05271

Capet, A., Vandenbulcke, L., Veselka, M., & Grégoire, M. (2018). 3.6 Decline of the Black Sea oxygen inventory. In: Copernicus Marine Service Ocean State Report, Issue 2. *Journal of Operational Oceanography, 11*(sup1). doi:10.1080/1755876X.2018.1489208

Capotondi, L., Soroldoni, L., Principato, M. S., & Corselli, C. (2004). Late Quaternary planktonic foraminiferal distributions: problems related to size fraction. In R. Coccioni, S. Galeotti, & F. Lirer (Eds.), *Proceedings of the First Italian Meeting on Environmental Micropaleontology. Grzybowski Foundation Special Publication* (Vol. 9, pp. 1-6).

Cartes, J. E., Schirone, A., Barsanti, M., Delbono, I., Martínez-Aliaga, A., & Lombarte, A. (2017). Recent reconstruction of deep-water macrofaunal communities recorded in Continental Margin sediments in the Balearic Basin. *Deep Sea Research Part I: Oceanographic Research Papers, 125*, 52-64. doi:https://doi.org/10.1016/j.dsr.2017.04.016

Casford, J. S. L., Abu-Zied, R., Rohling, E. J., Cooke, S., Fontanier, C., Leng, M., . . . Thomson, J. (2007). A stratigraphically controlled multiproxy chronostratigraphy for the eastern Mediterranean. *Paleoceanography, 22*(4). doi:https://doi.org/10.1029/2007PA001422

Castradori, D. (1993). Calcareous nannofossils and the origin of eastern Mediterranean sapropels. *Paleoceanography, 8*(4), 459-471. doi:10.1029/93PA00756

Catul, V., Gauns, M., & Karuppasamy, P. K. (2011). A review on mesopelagic fishes belonging to family Myctophidae. *Reviews in Fish Biology and Fisheries, 21*(3), 339-354. doi:10.1007/s11160-010-9176-4

Chan, F., Barth, J. A., Blanchette, C. A., Byrne, R. H., Chavez, F., Cheriton, O., . . . Washburn, L. (2017). Persistent spatial structuring of coastal ocean acidification in the California Current System. *Scientific Reports, 7*(1), 2526. doi:10.1038/s41598-017-02777-y

Chapman, M. R. (2010). Seasonal production patterns of planktonic foraminifera in the NE Atlantic Ocean: Implications for paleotemperature and hydrographic reconstructions. *Paleoceanography, 25*(1). doi:10.1029/2008PA001708

Chavez, F. P., Messié, M., & Pennington, J. T. (2011). Marine Primary Production in Relation to Climate Variability and Change. *Annual Review of Marine Science, 3*(1), 227-260. doi:10.1146/annurev.marine.010908.163917

Cheng, L., Abraham, J., Hausfather, Z., & Trenberth, K. E. (2019). How fast are the oceans warming? *Science, 363*(6423), 128-129. doi:doi:10.1126/science.aav7619

Cheng, L., Abraham, J., Trenberth, K. E., Fasullo, J., Boyer, T., Mann, M. E., . . . Li, G. (2023). Another Year of Record Heat for the Oceans. *Advances in Atmospheric Sciences*. doi:10.1007/s00376-023-2385-2

Chiu, C. F., Sweere, T. C., Clarkson, M. O., de Souza, G. F., Hennekam, R., & Vance, D. (2022). Co-variation systematics of uranium and molybdenum isotopes reveal pathways for descent into euxinia in Mediterranean sapropels. *Earth and Planetary Science Letters, 585*, 117527. doi:https://doi.org/10.1016/j.epsl.2022.117527

Cisneros, M., Cacho, I., Frigola, J., Canals, M., Masqué, P., Martrat, B., . . . Lirer, F. (2016). Sea surface temperature variability in the central-western Mediterranean Sea during the last 2700 years: a multi-proxy and multi-record approach. *Climate of the Past, 12*(4), 849-869. doi:10.5194/cp-12-849-2016

Cisneros, M., Cacho, I., Frigola, J., Sanchez-Vidal, A., Calafat, A., Pedrosa-Pàmies, R., . . . Canals, M. (2019). Deep-water formation variability in the north-western Mediterranean Sea during the last 2500 yr: A proxy validation with present-day data. *Global and Planetary Change, 177*, 56-68. doi:10.1016/j.gloplacha.2019.03.012

Claireaux, G., & Chabot, D. (2019). The significance of ocean deoxygenation for

the physiology of marine organisms. In D. Laffoley & J. M. Baxter (Eds.), *Ocean Deoxygenation: Everyone's Problem* (pp. 461-484): IUCN.

CLIMAP Project Members, Ruddiman, W. F., Cline, R. M. L., Hays, J. D., Prell, W. L., Ruddiman, W. F., . . . Thompson, P. R. (1984). The last interglacial ocean. *Quaternary Research, 21*(2), 123-224. doi:10.1016/0033-5894(84)90098-X

Colella, S., D'Ortenzio, F., Marullo, S., Santoleri, R., Ragni, M., & d'Alcala, M. R. (2003). *Primary production variability in the Mediterranean Sea from SeaWiFS data.* Paper presented at the Proceedings of SPIE.

Coma, R., Ribes, M., Serrano, E., Jiménez, E., Salat, J., & Pascual, J. (2009). Global warming-enhanced stratification and mass mortality events in the Mediterranean. *Proceedings of the National Academy of Sciences, 106*(15), 6176-6181. doi:10.1073/pnas.0805801106

Conan, S. M. H., Ivanova, E. M., & Brummer, G. J. A. (2002). Quantifying carbonate dissolution and calibration of foraminiferal dissolution indices in the Somali Basin. *Marine Geology, 182*(3-4), 325-349. doi:10.1016/S0025-3227(01)00238-9

Conte, M. H., Sicre, M. A., Rühlemann, C., Weber, J. C., Schulte, S., Schulz-Bull, D., & Blanz, T. (2006). Global temperature calibration of the

alkenone unsaturation index (UK′ 37) in surface waters and comparison with surface sediments. *Geochemistry, Geophysics, Geosystems, 7*(2). doi:10.1029/2005GC001054

Cossarini, G., Lazzari, P., & Solidoro, C. (2015). Spatiotemporal variability of alkalinity in the Mediterranean Sea. *Biogeosciences, 12*(6).

Cramer, W., Guiot, J., Fader, M., Garrabou, J., Gattuso, J.-P., Iglesias, A., . . . Xoplaki, E. (2018). Climate change and interconnected risks to sustainable development in the Mediterranean. *Nature Climate Change, 8*(11), 972-980. doi:10.1038/s41558-018-0299-2

Crowley, T. J. (2000). Causes of Climate Change Over the Past 1000 Years. *Science, 289*(5477), 270-277. doi:10.1126/science.289.5477.270

Crowley, T. J., & Unterman, M. B. (2013). Technical details concerning development of a 1200 yr proxy index for global volcanism. *Earth System Science Data, 5*(1), 187. doi:10.5194/essd-5-187-2013

Crutzen, P. J. (2002). Geology of mankind. *Nature, 415*(6867), 23-23. doi:10.1038/415023a

D'Ortenzio, F., & Ribera d'Alcalà, M. (2009). On the trophic regimes of the Mediterranean Sea: a satellite analysis. *Biogeosciences, 6*(2), 139-148. doi:10.5194/bg-6-139-2009

Davis, A. N., Davis, C. V., Thunell, R. C., Osborne, E. B., Black, D. E., & Benitez-Nelson, C. R. (2019). Reconstructing 800 Years of Carbonate Ion Concentration in the Cariaco Basin Using the Area Density of Planktonic Foraminifera Shells. *Paleoceanography and Paleoclimatology, 34*(12), 2129-2140. doi:10.1029/2019PA003698

Davis, C. V., Rivest, E. B., Hill, T. M., Gaylord, B., Russell, A. D., & Sanford, E. (2017). Ocean acidification compromises a planktic calcifier with implications for global carbon cycling. *Scientific Reports, 7*(1), 2225-2225. doi:10.1038/s41598-017-01530-9

Davison, P. C., Checkley, D. M., Koslow, J. A., & Barlow, J. (2013). Carbon export mediated by mesopelagic fishes in the northeast Pacific Ocean. *Progress in Oceanography, 116*, 14-30. doi:https://doi.org/10.1016/j.pocean.2013.05.013

De Lange, G. J., Thomson, J., Reitz, A., Slomp, C. P., Principato, M. S., Erba, E., & Corselli, C. (2008). Synchronous basin-wide formation and redox-controlled preservation of a Mediterranean sapropel. *Nature geoscience, 1*(9), 606.

de Nooijer, L. J., Spero, H. J., Erez, J., Bijma, J., & Reichart, G. J. (2014). Biomineralization in perforate foraminifera. *Earth-Science Reviews, 135*, 48-58. doi:https://doi.org/10.1016/j.earscirev.2014.03.013

Di Donato, V., Daunis-i-Estadella, J., Martín-Fernández, J. A., & Esposito, P. (2015). Size Fraction Effects on Planktonic Foraminifera Assemblages: A Compositional Contribution to the Golden Sieve Rush.

Mathematical Geosciences, 47(4), 455-470. doi:10.1007/s11004-014-9529-y

Dickson, A. G. (1990). Standard potential of the reaction: AgCl(s) + 12H2(g) = Ag(s) + HCl(aq), and and the standard acidity constant of the ion HSO4⁻ in synthetic sea water from 273.15 to 318.15 K. *The Journal of Chemical Thermodynamics, 22*(2), 113-127. doi:10.1016/0021-9614(90)90074-Z

Dickson, A. G., & Millero, F. J. (1987). A comparison of the equilibrium constants for the dissociation of carbonic acid in seawater media. *Deep Sea Research Part A. Oceanographic Research Papers, 34*(10), 1733-1743. doi:10.1016/0198-0149(87)90021-5

Dickson, A. J., Cohen, A. S., & Coe, A. L. (2012). Seawater oxygenation during the Paleocene-Eocene Thermal Maximum. *Geology, 40*(7), 639-642. doi:10.1130/g32977.1

Dickson, R. R., Kelly, P. M., Colebrook, J. M., Wooster, W. S., & Cushing, D. H. (1988). North winds and production in the eastern North Atlantic. *Journal of Plankton Research, 10*(1), 151-169. doi:10.1093/plankt/10.1.151

Dittert, N., & Henrich, R. (2000). Carbonate dissolution in the South Atlantic Ocean: evidence from ultrastructure breakdown in Globigerina bulloides. *Deep Sea Research Part I: Oceanographic Research Papers, 47*(4), 603-620. doi:https://doi.org/10.1016/S0967-0637(99)00069-2

Doney, S. C., Fabry, V. J., Feely, R. A., & Kleypas, J. A. (2009). Ocean Acidification: The Other CO2 Problem. *Annual Review of Marine Science, 1*(1), 169-192. doi:10.1146/annurev.marine.010908.163834

Dong, S., Lei, Y., Bi, H., Xu, K., Li, T., & Jian, Z. (2022). Biological Response of Planktic Foraminifera to Decline in Seawater pH. *Biology, 11*(1), 98.

Drinkwater, K. F., Belgrano, A., Borja, A., Conversi, A., Edwards, M., Greene, C. H., . . . Walker, H. (2003). The Response of Marine Ecosystems to Climate Variability Associated with the North Atlantic Oscillation. In J. W. Hurrell, Y. Kushnir, G. Ottersen, & M. Visbeck (Eds.), *The North Atlantic Oscillation: Climatic Significance and Environmental Impact* (pp. 211-234).

Dunstan, P. K., Foster, S. D., King, E., Risbey, J., O'Kane, T. J., Monselesan, D., . . . Thompson, P. A. (2018). Global patterns of change and variation in sea surface temperature and chlorophyll a. *Scientific Reports, 8*(1), 14624. doi:10.1038/s41598-018-33057-y

Dypvik, E., & Kaartvedt, S. (2013). Vertical migration and diel feeding periodicity of the skinnycheek lanternfish (Benthosema pterotum) in the Red Sea. *Deep Sea Research Part I: Oceanographic Research Papers, 72*, 9-16. doi:https://doi.org/10.1016/j.dsr.2012.10.012

Eduardo, L. N., Bertrand, A., Mincarone, M. M., Martins, J. R., Frédou, T., Assunção, R. V., . . . Lucena-Frédou, F. (2021). Distribution, vertical

migration, and trophic ecology of lanternfishes (Myctophidae) in the Southwestern Tropical Atlantic. *Progress in Oceanography, 199*, 102695. doi:https://doi.org/10.1016/j.pocean.2021.102695

Eglinton, T. I., Conte, M. H., Eglinton, G., & Hayes, J. M. (2001). Proceedings of a workshop on alkenone-based paleoceanographic indicators. *Geochemistry, Geophysics, Geosystems, 2*(1). doi:10.1029/2000gc000122

Eide, M., Olsen, A., Ninnemann, U. S., & Eldevik, T. (2017). A global estimate of the full oceanic 13C Suess effect since the preindustrial. *Global Biogeochemical Cycles, 31*(3), 492-514. doi:10.1002/2016GB005472

Elder, K. L., Jones, G. A., & Bolz, G. (1996). Distribution of otoliths in surficial sediments of the US Atlantic continental shelf and slope and potential for reconstructing Holocene fish stocks. *Paleoceanography, 11*(3), 359-367.

Enfield, D. B., Mestas-Nuñez, A. M., & Trimble, P. J. (2001). The Atlantic multidecadal oscillation and its relation to rainfall and river flows in the continental US. *Geophysical Research Letters, 28*(10), 2077-2080. doi:doi.org/10.1029/2000GL012745

Fabry, V. J., Seibel, B. A., Feely, R. A., & Orr, J. C. (2008). Impacts of ocean acidification on marine fauna and ecosystem processes. *ICES Journal of Marine Science, 65*(3), 414-432. doi:10.1093/icesjms/fsn048

FAO. (2018). FAOSTAT statistical database: [Rome] : FAO, c2018-. Retrieved from http://www.fao.org/fishery/topic/16140/en

FAO. (2022). *The State of World Fisheries and Aquaculture 2022. Towards Blue Transformation*. FAO (Series Ed.) Retrieved from Rome, Italy:

Faust, J. C., Fabian, K., Milzer, G., Giraudeau, J., & Knies, J. (2016). Norwegian fjord sediments reveal NAO related winter temperature and precipitation changes of the past 2800 years. *Earth and Planetary Science Letters, 435*, 84-93. doi:10.1016/j.epsl.2015.12.003

Feely, R. A., Sabine, C. L., Hernandez-Ayon, J. M., Ianson, D., & Hales, B. (2008). Evidence for Upwelling of Corrosive "Acidified" Water onto the Continental Shelf. *Science, 320*(5882), 1490-1492. doi:doi:10.1126/science.1155676

Fenoglio-Marc, L., Mariotti, A., Sannino, G., Meyssignac, B., Carillo, A., Struglia, M. V., & Rixen, M. (2013). Decadal variability of net water flux at the Mediterranean Sea Gibraltar Strait. *Global and Planetary Change, 100*, 1-10. doi:10.1016/j.gloplacha.2012.08.007

Fiebig, J., Schöne, B. R., & Oschmann, W. (2005). High-precision oxygen and carbon isotope analysis of very small (10–30 µg) amounts of carbonates using continuous flow isotope ratio mass spectrometry. *Rapid Communications in Mass Spectrometry, 19*(16), 2355-2358. doi:10.1002/rcm.2060

Field, D. B., Baumgartner, T. R., Charles, C. D., Ferreira-Bartrina, V., & Ohman, M. D. (2006). Planktonic foraminifera of the California Current reflect 20th-century warming. *Science, 311*(5757), 63-66. doi:10.1126/science.1116220

Filippidi, A., & De Lange, G. J. (2019). Eastern Mediterranean Deep Water Formation During Sapropel S1: A Reconstruction Using Geochemical Records Along a Bathymetric Transect in the Adriatic Outflow Region. *Paleoceanography and Paleoclimatology, 34*(3), 409-429. doi:https://doi.org/10.1029/2018PA003459

Flecha, S., Pérez, F. F., Murata, A., Makaoui, A., & Huertas, I. E. (2019). Decadal acidification in Atlantic and Mediterranean water masses exchanging at the Strait of Gibraltar. *Scientific Reports, 9*(1), 15533. doi:10.1038/s41598-019-52084-x

Flexas, M. M., Gomis, D., Ruiz, S., Pascual, A., & León, P. (2006). In situ and satellite observations of the eastward migration of the Western Alboran Sea Gyre. *Progress in Oceanography, 70*(2), 486-509. doi:10.1016/j.pocean.2006.03.017

Foster, G. L. (2008). Seawater pH, pCO2 and [CO2-3] variations in the Caribbean Sea over the last 130 kyr: A boron isotope and B/Ca study of planktic foraminifera. *Earth and Planetary Science Letters, 271*(1-4), 254-266. doi:10.1016/j.epsl.2008.04.015

Foster, G. L., & Rae, J. W. B. (2016). Reconstructing Ocean pH with Boron Isotopes in Foraminifera. *Annual Review of Earth and Planetary Sciences, 44*(1), 207-237. doi:10.1146/annurev-earth-060115-012226

Freitas, C., Olsen, E. M., Knutsen, H., Albretsen, J., & Moland, E. (2016). Temperature-associated habitat selection in a cold-water marine fish. *Journal of Animal Ecology, 85*(3), 628-637. doi:https://doi.org/10.1111/1365-2656.12458

Freitas, C., Villegas-Ríos, D., Moland, E., & Olsen, E. M. (2021). Sea temperature effects on depth use and habitat selection in a marine fish community. *Journal of Animal Ecology, 90*(7), 1787-1800. doi:https://doi.org/10.1111/1365-2656.13497

Friedli, H., Lötscher, H., Oeschger, H., Siegenthaler, U., & Stauffer, B. (1986). Ice core record of the 13C/12C ratio of atmospheric CO2 in the past two centuries. *Nature, 324*(6094), 237-238. doi:10.1038/324237a0

Friedlingstein, P., O'Sullivan, M., Jones, M. W., Andrew, R. M., Gregor, L., Hauck, J., . . . Zheng, B. (2022). Global Carbon Budget 2022. *Earth System Science Data, 14*(11), 4811-4900. doi:10.5194/essd-14-4811-2022

Frigola, J., Moreno, A., Cacho, I., Canals, M., Sierro, F. J., Flores, J. A., . . . Curtis, J. H. (2007). Holocene climate variability in the western Mediterranean region from a deepwater sediment record. *Paleoceanography, 22*(2). doi:10.1029/2006PA001307

Fromentin, J. M., & Planque, B. (1996). Calanus and environment in the eastern North Atlantic. II. Influence of the North Atlantic Oscillation on C. finmarchicus and C. helgolandicus. *Marine Ecology Progress Series, 134*, 111-118. doi:10.3354/meps134111

Fu, W., Randerson, J. T., & Moore, J. K. (2016). Climate change impacts on net primary production (NPP) and export production (EP) regulated by increasing stratification and phytoplankton community structure in the CMIP5 models. *Biogeosciences, 13*(18), 5151-5170. doi:10.5194/bg-13-5151-2016

Garcia-Orellana, J., Pates, J. M., Masqué, P., Bruach, J. M., & Sanchez-Cabeza, J. A. (2009). Distribution of artificial radionuclides in deep sediments of the Mediterranean Sea. *Science of The Total Environment, 407*(2), 887-898. doi:10.1016/j.scitotenv.2008.09.018

Garcia-Gorriz, E., & Carr, M. E. (2001). Physical control of phytoplankton distributions in the Alboran Sea: a numerical and satellite approach. *Journal of Geophysical Research: Oceans, 106*(C8), 16795-16805. doi:10.1029/1999JC000029

Garcia, H., Boyer, T., Baranova, O., Locarnini, R., Mishonov, A., Grodsky, A. e., . . . Reagan, J. (2019). *World ocean atlas 2018*. https://www.ncei.noaa.gov/archive/accession/NCEI-WOA18.

Gascard, J. C., & Richez, C. (1985). Water masses and circulation in the Western Alboran sea and in the Straits of Gibraltar. *Progress in Oceanography, 15*(3), 157-216. doi:10.1016/0079-6611(85)90031-X

Gattuso, J. P., Magnan, A., Billé, R., Cheung, W. W. L., Howes, E. L., Joos, F., . . . Turley, C. (2015). Contrasting futures for ocean and society from different anthropogenic CO₂ emissions scenarios. *Science, 349*(6243), aac4722. doi:doi:10.1126/science.aac4722

Gehlen, M., Trang Chau, T. T., Conchon, A., Denvil-Sommer, A., Chevallier, F., Vrac, M., & Mejia, C. (2020). Section 2.10: Ocean acidification. In K. von Schuckmann & P.-Y. Le Traon (Eds.), *Copernicus Marine Service Ocean State Report, Issue 4, Journal of Operational Oceanography* (Vol. 13:sup1, pp. 64-76).

Gemayel, E., Hassoun, A., Benallal, M., Goyet, C., Rivaro, P., Saab, M. A.-A., . . . Ziveri, P. (2015). Climatological variations of total alkalinity and total inorganic carbon in the Mediterranean Sea surface waters. *Earth System Dynamics*(6), 789-800.

Gersonde, R. (2012). The expedition of the research vessel" Sonne" to the subpolar North Pacific and the Bering Sea in 2009 (SO202-INOPEX). *Berichte zur Polar-und Meeresforschung= Reports on polar and marine research, 643*.

Giamali, C., Kontakiotis, G., Koskeridou, E., Ioakim, C., & Antonarakou, A. (2020). Key Environmental Factors Controlling Planktonic Foraminiferal and Pteropod Community's Response to Late

Quaternary Hydroclimate Changes in the South Aegean Sea (Eastern Mediterranean). *Journal of Marine Science and Engineering, 8*(9), 709.

Giannoulaki, M., Iglesias, M., Tugores, M. P., Bonanno, A., Patti, B., De Felice, A., . . . Valavanis, V. (2013). Characterizing the potential habitat of European anchovy Engraulis encrasicolus in the Mediterranean Sea, at different life stages. *Fisheries Oceanography, 22*(2), 69-89. doi:https://doi.org/10.1111/fog.12005

Gilly, W. F., Beman, J. M., Litvin, S. Y., & Robison, B. H. (2013). Oceanographic and Biological Effects of Shoaling of the Oxygen Minimum Zone. *Annual Review of Marine Science, 5*(1), 393-420. doi:10.1146/annurev-marine-120710-100849

Giorgi, F. (2006). Climate change hot-spots. *Geophysical Research Letters, 33*(8). doi:10.1029/2006gl025734

Glas, M. S., Langer, G., & Keul, N. (2012). Calcification acidifies the microenvironment of a benthic foraminifer (Ammonia sp.). *Journal of Experimental Marine Biology and Ecology, 424-425*, 53-58. doi:10.1016/j.jembe.2012.05.006

Gleckler, P. J., Santer, B. D., Domingues, C. M., Pierce, D. W., Barnett, T. P., Church, J. A., . . . Caldwell, P. M. (2012). Human-induced global ocean warming on multidecadal timescales. *Nature Climate Change, 2*(7), 524-529. doi:10.1038/nclimate1553

Gogou, A., Triantaphyllou, M., Xoplaki, E., Izdebski, A., Parinos, C., Dimiza, M., . . . Martrat, B. (2016). Climate variability and socio-environmental changes in the northern Aegean (NE Mediterranean) during the last 1500 years. *Quaternary Science Reviews, 136*, 209-228. doi:0.1016/j.quascirev.2016.01.009

González-Lanchas, A., Flores, J.-A., Sierro, F. J., Bárcena, M. Á., Rigual-Hernández, A. S., Oliveira, D., . . . Grimalt, J. O. (2020). A new perspective of the Alboran Upwelling System reconstruction during the Marine Isotope Stage 11: A high-resolution coccolithophore record. *Quaternary Science Reviews, 245*, 106520. doi:10.1016/j.quascirev.2020.106520

Gonzalez-Mora, B., Sierro, F., & Flores, J. (2008). Controls of shell calcification in planktonic foraminifers. *Quaternary Science Reviews, 27*(9-10), 956-961.

Good, S. A., Martin, M. J., & Rayner, N. A. (2013). EN4: Quality controlled ocean temperature and salinity profiles and monthly objective analyses with uncertainty estimates. *Journal of Geophysical Research: Oceans, 118*(12), 6704-6716. doi:10.1002/2013JC009067

Gray, S. T., Graumlich, L. J., Betancourt, J. L., & Pederson, G. T. (2004). A tree-ring based reconstruction of the Atlantic Multidecadal Oscillation since 1567 AD. *Geophysical Research Letters, 31*(12). doi:10.1029/2004GL019932

Gray, W. R., Weldeab, S., Lea, D. W., Rosenthal, Y., Gruber, N., Donner, B., & Fischer, G. (2018). The effects of temperature, salinity, and the carbonate system on Mg/Ca in Globigerinoides ruber (white): A global sediment trap calibration. *Earth and Planetary Science Letters, 482*, 607-620. doi:10.1016/j.epsl.2017.11.026

Gregor, L., & Gruber, N. (2021). OceanSODA-ETHZ: a global gridded data set of the surface ocean carbonate system for seasonal to decadal studies of ocean acidification. *Earth Syst. Sci. Data, 13*(2), 777-808. doi:10.5194/essd-13-777-2021

Grelaud, M., Marino, G., Ziveri, P., & Rohling, E. J. (2012). Abrupt shoaling of the nutricline in response to massive freshwater flooding at the onset of the last interglacial sapropel event. *Paleoceanography, 27*(3). doi:https://doi.org/10.1029/2012PA002288

Gruber, N. (2011). Warming up, turning sour, losing breath: ocean biogeochemistry under global change. *Philosophical Transactions of the Royal Society A: Mathematical, Physical and Engineering Sciences, 369*(1943), 1980-1996. doi:doi:10.1098/rsta.2011.0003

Gruber, N., Bakker, D. C. E., DeVries, T., Gregor, L., Hauck, J., Landschützer, P., . . . Müller, J. D. (2023). Trends and variability in the ocean carbon sink. *Nature Reviews Earth & Environment, 4*(2), 119-134. doi:10.1038/s43017-022-00381-x

Gruber, N., Clement, D., Carter, B. R., Feely, R. A., van Heuven, S., Hoppema, M., . . . Wanninkhof, R. (2019). The oceanic sink for anthropogenic CO₂ from 1994 to 2007. *Science, 363*(6432), 1193-1199. doi:doi:10.1126/science.aau5153

Gruber, N., Keeling, C. D., Bacastow, R. B., Guenther, P. R., Lueker, T. J., Wahlen, M., . . . Stocker, T. F. (1999). Spatiotemporal patterns of carbon-13 in the global surface oceans and the oceanic suess effect. *Global Biogeochemical Cycles, 13*(2), 307-335. doi:10.1029/1999GB900019

Guillermic, M., Misra, S., Eagle, R., & Tripati, A. (2022). Atmospheric CO2 estimates for the Miocene to Pleistocene based on foraminiferal δ11B at Ocean Drilling Program Sites 806 and 807 in the Western Equatorial Pacific. *Clim. Past, 18*(2), 183-207. doi:10.5194/cp-18-183-2022

Harper, D. T., Hönisch, B., Zeebe, R. E., Shaffer, G., Haynes, L. L., Thomas, E., & Zachos, J. C. (2020). The Magnitude of Surface Ocean Acidification and Carbon Release During Eocene Thermal Maximum 2 (ETM-2) and the Paleocene-Eocene Thermal Maximum (PETM). *Paleoceanography and Paleoclimatology, 35*(2). doi:10.1029/2019PA003699

Hassen, N. E. H., Reguigui, N., Helali, M. A., Mejjad, N., Laissaoui, A., Benkdad, A., & Benmasour, M. (2019). Evaluating the historical sedimentation patterns in two different Mediterranean deep

environments (Sardinia and Sicily Channels). *Mediterranean Marine Science, 20*(3), 542-548. doi:10.12681/mms.19558

Hassoun, A. E. R., Bantelman, A., Canu, D., Comeau, S., Galdies, C., Gattuso, J.-P., . . . Ziveri, P. (2022). Ocean acidification research in the Mediterranean Sea: Status, trends and next steps. *Frontiers in Marine Science, 9*. doi:10.3389/fmars.2022.892670

Hassoun, A. E. R., Gemayel, E., Krasakopoulou, E., Goyet, C., Abboud-Abi Saab, M., Guglielmi, V., . . . Falco, C. (2015). Acidification of the Mediterranean Sea from anthropogenic carbon penetration. *Deep Sea Research Part I: Oceanographic Research Papers, 102*, 1-15. doi:10.1016/j.dsr.2015.04.005

Heaton, T. J., Köhler, P., Butzin, M., Bard, E., Reimer, R. W., Austin, W. E. N., . . . Skinner, L. C. (2020). Marine20—The Marine Radiocarbon Age Calibration Curve (0–55,000 cal BP). *Radiocarbon, 62*(4), 779-820. doi:10.1017/RDC.2020.68

Heburn, G. W., & La Violette, P. E. (1990). Variations in the structure of the anticyclonic gyres found in the Alboran Sea. *Journal of Geophysical Research: Oceans, 95*(C2), 1599-1613. doi:10.1029/JC095iC02p01599

Hegerl, G. C., Brönnimann, S., Schurer, A., & Cowan, T. (2018). The early 20th century warming: Anomalies, causes, and consequences. *WIREs Climate Change, 9*(4), e522. doi:10.1002/wcc.522

Helm, K. P., Bindoff, N. L., & Church, J. A. (2011). Observed decreases in oxygen content of the global ocean. *Geophysical Research Letters, 38*(23). doi:https://doi.org/10.1029/2011GL049513

Hemleben, C., Spindler, M., & Anderson, O. R. (1989). *Modern planktonic foraminifera*. New York, NY: Springer.

Henehan, M. J., Rae, J. W. B., Foster, G. L., Erez, J., Prentice, K. C., Kucera, M., . . . Elliott, T. (2013). Calibration of the boron isotope proxy in the planktonic foraminifera Globigerinoides ruber for use in palaeo-CO2 reconstruction. *Earth and Planetary Science Letters, 364*, 111-122. doi:10.1016/j.epsl.2012.12.029

Henson, S. A., Sarmiento, J. L., Dunne, J. P., Bopp, L., Lima, I., Doney, S. C., . . . Beaulieu, C. (2010). Detection of anthropogenic climate change in satellite records of ocean chlorophyll and productivity. *Biogeosciences, 7*(2), 621-640. doi:10.5194/bg-7-621-2010

Herguera, J. C., & Berger, W. H. (1991). Paleoproductivity from benthic foraminifera abundance: Glacial to postglacial change in the west-equatorial Pacific. *Geology, 19*(12), 1173-1176. doi:10.1130/0091-7613(1991)019<1173:Pfbfag>2.3.Co;2

Hernández-Almeida, I., Ausín, B., Saavedra-Pellitero, M., Baumann, K. H., & Stoll, H. M. (2019). Quantitative reconstruction of primary productivity in low latitudes during the last glacial maximum and the

mid-to-late Holocene from a global Florisphaera profunda calibration dataset. *Quaternary Science Reviews, 205*, 166-181. doi:10.1016/j.quascirev.2018.12.016

Hernández-Almeida, I., Bárcena, M. A., Flores, J. A., Sierro, F. J., Sanchez-Vidal, A., & Calafat, A. (2011). Microplankton response to environmental conditions in the Alboran Sea (Western Mediterranean): One year sediment trap record. *Marine Micropaleontology, 78*(1-2), 14-24. doi:10.1016/j.marmicro.2010.09.005

Hernández, A., Martin-Puertas, C., Moffa-Sánchez, P., Moreno-Chamarro, E., Ortega, P., Blockley, S., . . . Xu, G. (2020). Modes of climate variability: Synthesis and review of proxy-based reconstructions through the Holocene. *Earth-Science Reviews*, 103286. doi:10.1016/j.earscirev.2020.103286

Higgins, M. B., Robinson, R. S., Carter, S. J., & Pearson, A. (2010). Evidence from chlorin nitrogen isotopes for alternating nutrient regimes in the Eastern Mediterranean Sea. *Earth and Planetary Science Letters, 290*(1), 102-107. doi:https://doi.org/10.1016/j.epsl.2009.12.009

Hoegh-Guldberg, O., Cai, R., Poloczanska, E. S., Brewer, P. G., Sundby, S., Hilmi, K., . . . Jung, S. (2014). The Ocean. In V. R. Barros, C. B. Field, D. J. Dokken, M. D. Mastrandrea, K. J. Mach, T. E. Bilir, M. Chatterjee, K. L. Ebi, Y. O. Estrada, R. C. Genova, B. Girma, E. S. Kissel, A. N. Levy, S. MacCracken, P. R. Mastrandrea, & L. L. White (Eds.), *Climate Change 2014: Impacts, Adaptation, and Vulnerability. Part B: Regional Aspects. Contribution*

of Working Group II to the Fifth Assessment Report of the Intergovernmental Panel on Climate Change (pp. 1655-1731). Cambridge, United Kingdom and New York, NY, USA: Cambridge University Press.

Hönisch, B., & Hemming, N. G. (2005). Surface ocean pH response to variations in pCO2 through two full glacial cycles. *Earth and Planetary Science Letters, 236*(1), 305-314. doi:https://doi.org/10.1016/j.epsl.2005.04.027

Hunt, B. P. V., Allain, V., Menkes, C., Lorrain, A., Graham, B., Rodier, M., . . . Carlotti, F. (2015). A coupled stable isotope-size spectrum approach to understanding pelagic food-web dynamics: A case study from the southwest sub-tropical Pacific. *Deep Sea Research Part II: Topical Studies in Oceanography, 113*, 208-224. doi:https://doi.org/10.1016/j.dsr2.2014.10.023

Hurrell, J. W. (1995). Decadal trends in the North Atlantic Oscillation: regional temperatures and precipitation. *Science, 269*(5224), 676-679. doi:10.1126/science.269.5224.676

Hurrell, J. W. (2020). The Climate Data Guide: Hurrell North Atlantic Oscillation (NAO) Index (station-based), last modified 24 Apr 2020.

Retrieved from https://climatedataguide.ucar.edu/climate-data/hurrell-north-atlantic-oscillation-nao-index-station-based.

Imbrie, J., & Kipp, N. (1971). A new micropaleontological method for quantitative paleoclimatology: application to a late Pleistocene Caribbean core. *The late Cenozoic glacial ages*, 71-181.

Incarbona, A., Abu-Zied, R. H., Rohling, E. J., & Ziveri, P. (2019). Reventilation Episodes During the Sapropel S1 Deposition in the Eastern Mediterranean Based on Holococcolith Preservation. *Paleoceanography and Paleoclimatology, 34*(10), 1597-1609. doi:https://doi.org/10.1029/2019PA003626

Incarbona, A., Bonomo, S., Di Stefano, E., Zgozi, S., Essarbout, N., Talha, M., . . . Placenti, F. (2008a). Calcareous nannofossil surface sediment assemblages from the Sicily Channel (central Mediterranean Sea): palaeoceanographic implications. *Marine Micropaleontology, 67*(3-4), 297-309. doi:10.1016/j.marmicro.2008.03.001

Incarbona, A., Di Stefano, E., Patti, B., Pelosi, N., Bonomo, S., Mazzola, S., . . . Bonanno, A. (2008b). Holocene millennial-scale productivity variations in the Sicily Channel (Mediterranean Sea). *Paleoceanography, 23*(3). doi:10.1029/2007PA001581

Incarbona, A., Jonkers, L., Ferraro, S., Sprovieri, R., & Tranchida, G. (2019). Sea Surface Temperatures and Paleoenvironmental Variability in the Central Mediterranean During Historical Times Reconstructed Using Planktonic Foraminifera. *Paleoceanography and Paleoclimatology, 34*(3), 394-408. doi:10.1029/2018PA003529

Incarbona, A., Martrat, B., Mortyn, P. G., Sprovieri, M., Ziveri, P., Gogou, A., . . . Langone, L. (2016). Mediterranean circulation perturbations over the last five centuries: Relevance to past Eastern Mediterranean Transient-type events. *Scientific Reports, 6*(1), 1-10.

IPCC. (2014). Information from Paleoclimate Archives. In *Climate Change 2013 – The Physical Science Basis: Working Group I Contribution to the Fifth Assessment Report of the Intergovernmental Panel on Climate Change* (pp. 383-464). Cambridge: Cambridge University Press.

IPCC. (2019) IPCC special report on the Ocean and Cryosphere in a Changing Climate. In [H.-O. Pörtner, D. C. Roberts, V. Masson-Delmotte, P. Zhai, M. Tignor, E. Poloczanska, & N. M. Weyer (Eds.)], (pp. 255). Cambridge, UK and New York, NY, USA.

Irigoien, X., Klevjer, T. A., Røstad, A., Martinez, U., Boyra, G., Acuña, J. L., . . . Kaartvedt, S. (2014). Large mesopelagic fishes biomass and trophic efficiency in the open ocean. *Nature Communications, 5*(1), 3271. doi:10.1038/ncomms4271

Ito, T., Minobe, S., Long, M. C., & Deutsch, C. (2017). Upper ocean O2 trends: 1958–2015. *Geophysical Research Letters, 44*(9), 4214-4223. doi:https://doi.org/10.1002/2017GL073613

Jacobson, M. Z. (2005). Studying ocean acidification with conservative, stable numerical schemes for nonequilibrium air-ocean exchange and ocean equilibrium chemistry. *Journal of Geophysical Research: Atmospheres, 110*(D7). doi:10.1029/2004JD005220

Jenkyns, H. C. (2010). Geochemistry of oceanic anoxic events. *Geochemistry, Geophysics, Geosystems, 11*(3). doi:https://doi.org/10.1029/2009GC002788

Jennings, S., Mélin, F., Blanchard, J. L., Forster, R. M., Dulvy, N. K., & Wilson, R. W. (2008). Global-scale predictions of community and ecosystem properties from simple ecological theory. *Proceedings of the Royal Society B: Biological Sciences, 275*(1641), 1375-1383. doi:10.1098/rspb.2008.0192

Jentzen, A., Schönfeld, J., & Schiebel, R. (2018). Assessment of the Effect of Increasing Temperature On the Ecology and Assemblage Structure of Modern Planktic Foraminifers in the Caribbean and Surrounding Seas. *Journal of Foraminiferal Research, 48*(3), 251-272. doi:10.2113/gsjfr.48.3.251

Jimenez-Espejo, F. J., Martinez-Ruiz, F., Rogerson, M., González-Donoso, J. M., Romero, O. E., Linares, D., . . . Perez Claros, J. A. (2008). Detrital input, productivity fluctuations, and water mass circulation in the westernmost Mediterranean Sea since the Last Glacial Maximum. *Geochemistry, Geophysics, Geosystems, 9*(11). doi:https://doi.org/10.1029/2008GC002096

Jiménez-López, D., Ortega, T., Sierra, A., Ponce, R., Gómez-Parra, A., & Forja, J. (2021). Aragonite saturation state in a continental shelf (Gulf of Cádiz, SW Iberian Peninsula): Evidences of acidification in the coastal area. *Science of The Total Environment, 787*. doi:10.1016/j.scitotenv.2021.147858

Jones, P. D., Jonsson, T., & Wheeler, D. (1997). Extension to the North Atlantic oscillation using early instrumental pressure observations from Gibraltar and south-west Iceland. *International Journal of Climatology, 17*(13), 1433-1450. doi:10.1002/(SICI)1097-0088(19971115)17:13<1433::AID-JOC203>3.0.CO;2-P

Jones, W. A., & Checkley, D. M. (2019). Mesopelagic fishes dominate otolith record of past two millennia in the Santa Barbara Basin. *Nature Communications*, *10*(1), 4564. doi:10.1038/s41467-019-12600-z

Jonkers, L., Hillebrand, H., & Kucera, M. (2019). Global change drives modern plankton communities away from the pre-industrial state. *Nature, 570*(7761), 372-375. doi:10.1038/s41586-019-1230-3

Josey, S. A., Somot, S., & Tsimplis, M. (2011). Impacts of atmospheric modes of variability on Mediterranean Sea surface heat exchange. *Journal of Geophysical Research: Oceans, 116*(C2). doi:10.1029/2010jc006685

Kallel, N., Paterne, M., Duplessy, J. C., Vergnaud-Grazzini, C., Pujol, C., Labeyrie, L., . . . Pierre, C. (1997). Enhanced rainfall in the Mediterranean region during the last Sapropel Event. *Oceanologica Acta, 20*(5), 697-712.

Kapelonis, Z., Siapatis, A., Machias, A., Somarakis, S., & Markakis, K. (2019). *Distribution and vertical migration of mesopelagic fish in Corinthiakos gulf.* Paper presented at the Proceedings of 17th Panhellenic conference of Ichthyologists, Heraklion, Crete.

Kapelonis, Z., Siapatis, A., Machias, A., Somarakis, S., Markakis, K., Giannoulaki, M., . . . Tsagarakis, K. (2021). *Mesopelagic fish community and deep scattering layers in an Eastern Mediterranean Sea enclosed deep basin*. Paper presented at the ICES Annual Science Conference 2021, Remote Conference.

Kaplan, A., Cane, M. A., Kushnir, Y., Clement, A. C., Blumenthal, M. B., & Rajagopalan, B. (1998). Analyses of global sea surface temperature 1856–1991. *Journal of Geophysical Research: Oceans, 103*(C9), 18567-18589. doi:10.1029/97JC01736

Kapsenberg, L., Alliouane, S., Gazeau, F., Mousseau, L., & Gattuso, J.-P. (2017). Coastal ocean acidification and increasing total alkalinity in the northwestern Mediterranean Sea. *Ocean Science, 13*(3), 411-426. doi:10.5194/os-13-411-2017

Keeling, R. F., Körtzinger, A., & Gruber, N. (2010). Ocean Deoxygenation in a Warming World. *Annual Review of Marine Science, 2*(1), 199-229. doi:10.1146/annurev.marine.010908.163855

Keerthi, M. G., Lévy, M., & Aumont, O. (2021). Intermittency in phytoplankton bloom triggered by modulations in vertical stability. *Scientific Reports, 11*(1), 1285. doi:10.1038/s41598-020-80331-z

Kent, E. C., Kennedy, J. J., Smith, T. M., Hirahara, S., Huang, B., Kaplan, A., . . . Zhang, H.-M. (2017). A Call for New Approaches to Quantifying Biases in Observations of Sea Surface Temperature. *Bulletin of the American Meteorological Society, 98*(8), 1601-1616. doi:https://doi.org/10.1175/BAMS-D-15-00251.1

Keul, N., Langer, G., De Nooijer, L. J., & Bijma, J. (2013). Effect of ocean acidification on the benthic foraminifera Ammonia sp. is caused by a decrease in carbonate ion concentration. *Biogeosciences, 10*(10), 6185-6198. doi:10.5194/bg-10-6185-2013

Kinzer, J., Böttger-Schnack, R., & Schulz, K. (1993). Aspects of horizontal distribution and diet of myctophid fish in the Arabian Sea with reference to the deep water oxygen deficiency. *Deep Sea Research Part II: Topical Studies in Oceanography, 40*(3), 783-800. doi:https://doi.org/10.1016/0967-0645(93)90058-U

Kiss, E. (1988). Ion-exchange separation and spectrophotometric determination of boron in geological materials. *Analytica Chimica Acta, 211*(C), 243-256. doi:10.1016/S0003-2670(00)83684-3

Klevjer, T. A., Irigoien, X., Røstad, A., Fraile-Nuez, E., Benítez-Barrios, V. M., & Kaartvedt, S. (2016). Large scale patterns in vertical distribution and behaviour of mesopelagic scattering layers. *Scientific Reports, 6*(1), 19873. doi:10.1038/srep19873

Knappertsbusch, M. (1993). Geographic distribution of living and Holocene coccolithophores in the Mediterranean Sea. *Marine Micropaleontology, 21*(1-3), 219-247. doi:10.1016/0377-8398(93)90016-Q

Knecht, N. S., Benedetti, F., Hofmann Elizondo, U., Bednaršek, N., Chaabane, S., de Weerd, C., . . . Vogt, M. (2023). The Impact of Zooplankton Calcifiers on the Marine Carbon Cycle. *Global Biogeochemical Cycles, 37*(6), e2022GB007685. doi:https://doi.org/10.1029/2022GB007685

Köhler-Rink, S., & Kühl, M. (2005). The chemical microenvironment of the symbiotic planktonic foraminifer Orbulina universa. *Marine Biology Research, 1*(1), 68-78. doi:10.1080/17451000510019015

Koizumi, K., Hiratsuka, S., & Saito, H. (2014). Lipid and Fatty Acids of Three Edible Myctophids, Diaphus watasei, Diaphus suborbitalis, and Benthosema pterotum: High Levels of Icosapentaenoic and Docosahexaenoic Acids. *Journal of Oleo Science, 63*(5), 461-470. doi:10.5650/jos.ess13224

Koken, E. (1884). Ueber Fisch-Otolithen, insbesondere über diejenigen der norddeutschen Oligocän-Ablagerungen. *Zeitschrift der deutschen geologischen Gesellschaft*, 500-565.

Kontakiotis, G. (2016). Late Quaternary paleoenvironmental reconstruction and paleoclimatic implications of the Aegean Sea (eastern Mediterranean) based on paleoceanographic indexes and stable isotopes. *Quaternary International, 401*, 28-42. doi:https://doi.org/10.1016/j.quaint.2015.07.039

Kontakiotis, G., Antonarakou, A., Mortyn, P. G., Drinia, H., Anastasakis, G., Zarkogiannis, S., & Möbius, J. (2017). Morphological recognition of Globigerinoides ruber morphotypes and their susceptibility to diagenetic alteration in the eastern Mediterranean Sea. *Journal of Marine Systems, 174*, 12-24. doi:https://doi.org/10.1016/j.jmarsys.2017.05.005

Kontakiotis, G., Karakitsios, V., Mortyn, P. G., Antonarakou, A., Drinia, H., Anastasakis, G., . . . De Rafelis, M. (2016). New insights into the early Pliocene hydrographic dynamics and their relationship to the climatic evolution of the Mediterranean Sea. *Palaeogeography, Palaeoclimatology, Palaeoecology, 459*, 348-364. doi:10.1016/j.palaeo.2016.07.025

Koslow, J. A., Davison, P., Ferrer, E., Jiménez Rosenberg, S. P. A., Aceves-Medina, G., & Watson, W. (2019). The evolving response of mesopelagic fishes to declining midwater oxygen concentrations in the southern and central California Current. *ICES Journal of Marine Science, 76*(3), 626-638. doi:10.1093/icesjms/fsy154

Koslow, J. A., Goericke, R., Lara-Lopez, A., & Watson, W. (2011). Impact of declining intermediate-water oxygen on deepwater fishes in the California Current. *Marine Ecology Progress Series, 436*, 207-218.

Krishnaswamy, S., Lal, D., Martin, J. M., & Meybeck, M. (1971). Geochronology of lake sediments. *Earth and Planetary Science Letters, 11*(1-5), 407-414. doi:10.1016/0012-821X(71)90202-0

Kroeker, K. J., Kordas, R. L., Crim, R., Hendriks, I. E., Ramajo, L., Singh, G. S., . . . Gattuso, J.-P. (2013). Impacts of ocean acidification on marine organisms: quantifying sensitivities and interaction with warming. *Global Change Biology, 19*(6), 1884-1896. doi:10.1111/gcb.12179

Kroeker, K. J., Kordas, R. L., Crim, R. N., & Singh, G. G. (2010). Meta-analysis reveals negative yet variable effects of ocean acidification on marine organisms. *Ecology letters, 13*(11), 1419-1434. doi:10.1111/j.1461-0248.2010.01518.x

Kucera, M. (2007). Chapter Six Planktonic Foraminifera as Tracers of Past Oceanic Environments. In C. Hillaire–Marcel & A. De Vernal (Eds.), *Developments in Marine Geology* (Vol. 1, pp. 213-262): Elsevier.

Kuhnt, T., Schmiedl, G., Ehrmann, W., Hamann, Y., & Andersen, N. (2008). Stable isotopic composition of Holocene benthic foraminifers from the Eastern Mediterranean Sea: Past changes in productivity and deep water oxygenation. *Palaeogeography, Palaeoclimatology, Palaeoecology, 268*(1), 106-115. doi:https://doi.org/10.1016/j.palaeo.2008.07.010

La Violette, P. E. (1990). The western Mediterranean circulation experiment (WMCE): Introduction. *Journal of Geophysical Research: Oceans, 95*(C2), 1511-1514. doi:10.1029/JC095iC02p01511

Lan, X., Tans, P., & Thoning, K. W. (2023). Trends in globally-averaged CO2 determined from NOAA Global Monitoring Laboratory measurements. Retrieved from https://gml.noaa.gov/ccgg/trends/gl_data.html

Lejeusne, C., Chevaldonné, P., Pergent-Martini, C., Boudouresque, C. F., & Pérez, T. (2010). Climate change effects on a miniature ocean: the highly diverse, highly impacted Mediterranean Sea. *Trends in Ecology & Evolution, 25*(4), 250-260. doi:10.1016/j.tree.2009.10.009

Lemarchand, D., Gaillardet, J., Lewin, A., & Allègre, C. J. (2002). Boron isotope systematics in large rivers: Implications for the marine boron budget and paleo-pH reconstruction over the Cenozoic. *Chemical Geology, 190*(1-4), 123-140. doi:10.1016/S0009-2541(02)00114-6

Leung, J. Y. S., Zhang, S., & Connell, S. D. (2022). Is Ocean Acidification Really a Threat to Marine Calcifiers? A Systematic Review and Meta-Analysis of 980+ Studies Spanning Two Decades. *Small, 18*(35), 2107407. doi:https://doi.org/10.1002/smll.202107407

Levitus, S., Antonov, J. I., Boyer, T. P., Baranova, O. K., Garcia, H. E., Locarnini, R. A., . . . Zweng, M. M. (2012). World ocean heat content and thermosteric sea level change (0–2000 m), 1955–2010. *Geophysical Research Letters, 39*(10). doi:https://doi.org/10.1029/2012GL051106

Levitus, S., Antonov, J. I., Boyer, T. P., & Stephens, C. (2000). Warming of the World Ocean. *Science, 287*(5461), 2225-2229. doi:doi:10.1126/science.287.5461.2225

Lewis, E., & Wallace, D. W. R. (1998). Program Developed for CO 2 System Calculations. ORNL/CDIAC-105. Carbon Dioxide Information Analysis Center, Oak Ridge National Laboratory, US Department of Energy, Oak Ridge, Tennessee.

Li, G., Cheng, L., Zhu, J., Trenberth, K. E., Mann, M. E., & Abraham, J. P. (2020). Increasing ocean stratification over the past half-century. *Nature Climate Change, 10*(12), 1116-1123. doi:10.1038/s41558-020-00918-2

Libby, W. F., Anderson, E. C., & Arnold, J. R. (1949). Age Determination by Radiocarbon Content: World-Wide Assay of Natural Radiocarbon. *Science, 109*(2827), 227-228. doi:doi:10.1126/science.109.2827.227

Lin, C.-H., Chiang, Y.-P., Tuset, V. M., Lombarte, A., & Girone, A. (2018). Late Quaternary to Recent diversity of fish otoliths from the Red Sea, central Mediterranean, and NE Atlantic sea bottoms. *Geobios, 51*(4), 335-358. doi:https://doi.org/10.1016/j.geobios.2018.06.002

Lin, C.-H., Girone, A., & Nolf, D. (2016). Fish otolith assemblages from Recent NE Atlantic sea bottoms: A comparative study of palaeoecology. *Palaeogeography, Palaeoclimatology, Palaeoecology, 446*, 98-107. doi:https://doi.org/10.1016/j.palaeo.2016.01.022

Lin, C.-H., Taviani, M., Angeletti, L., Girone, A., & Nolf, D. (2017). Fish otoliths in superficial sediments of the Mediterranean Sea. *Palaeogeography, Palaeoclimatology, Palaeoecology, 471*, 134-143.

Lionello, P., Malanotte-Rizzoli, P., Boscolo, R., Alpert, P., Artale, V., Li, L., . . . Xoplaki, E. (2006). The Mediterranean climate: An overview of the main characteristics and issues. In P. Lionello, P. Malanotte-Rizzoli, & R. Boscolo (Eds.), *Developments in Earth and Environmental Sciences* (Vol. 4, pp. 1-26): Elsevier.

Lionello, P., & Scarascia, L. (2018). The relation between climate change in the Mediterranean region and global warming. *Regional Environmental Change, 18*(5), 1481-1493. doi:10.1007/s10113-018-1290-1

Lirer, F., Sprovieri, M., Vallefuoco, M., Ferraro, L., Pelosi, N., Giordano, L., & Capotondi, L. (2014). Planktonic foraminifera as bio-indicators for monitoring the climatic changes that have occurred over the past 2000 years in the southeastern Tyrrhenian Sea. *Integrative Zoology, 9*(4), 542-554. doi:10.1111/1749-4877.12083

Lombard, F., da Rocha, R. E., Bijma, J., & Gattuso, J. P. (2010). Effect of carbonate ion concentration and irradiance on calcification in planktonic foraminifera. *Biogeosciences, 7*(1), 247-255. doi:10.5194/bg-7-247-2010

Lombarte, A., Chic, Ò., Parisi-Baradad, V., Olivella, R., Piera, J., & García-Ladona, E. (2006). A web-based environment for shape analysis of fish otoliths. The AFORO database. *Scientia Marina, 70*(1), 147-152.

Lončarić, N., van Iperen, J., Kroon, D., & Brummer, G.-J. A. (2007). Seasonal export and sediment preservation of diatomaceous, foraminiferal and organic matter mass fluxes in a trophic gradient across the SE Atlantic. *Progress in Oceanography, 73*(1), 27-59. doi:10.1016/j.pocean.2006.10.008

Longhurst, A. (1995). Seasonal cycles of pelagic production and consumption. *Progress in Oceanography, 36*(2), 77-167. doi:10.1016/0079-6611(95)00015-1

Lopes, A. R., Trübenbach, K., Teixeira, T., Lopes, V. M., Pires, V., Baptista, M., . . . Rosa, R. (2013). Oxidative stress in deep scattering layers: Heat shock response and antioxidant enzymes activities of myctophid fishes thriving in oxygen minimum zones. *Deep Sea Research Part I: Oceanographic Research Papers, 82*, 10-16. doi:https://doi.org/10.1016/j.dsr.2013.07.014

Lüning, S., Schulte, L., Garcés-Pastor, S., Danladi, I. B., & Gałka, M. (2019). The Medieval Climate Anomaly in the Mediterranean Region. *Paleoceanography and Paleoclimatology, 34*(10), 1625-1649. doi:10.1029/2019pa003734

Maas, A. E., Frazar, S. L., Outram, D. M., Seibel, B. A., & Wishner, K. F. (2014). Fine-scale vertical distribution of macroplankton and micronekton in the Eastern Tropical North Pacific in association with an oxygen minimum zone. *Journal of Plankton Research, 36*(6), 1557-1575. doi:10.1093/plankt/fbu077

Macías, D. M., Bruno, M., Echevarría, F., Vázquez, A., & García, C. M. (2008). Meteorologically-induced mesoscale variability of the North-western Alboran Sea (southern Spain) and related biological patterns. *Estuarine, Coastal and Shelf Science, 78*(2), 250-266. doi:10.1016/j.ecss.2007.12.008

Macías, D. M., Garcia-Gorriz, E., & Stips, A. (2013). Understanding the Causes of Recent Warming of Mediterranean Waters. How Much

Could Be Attributed to Climate Change? *PLoS ONE, 8*(11), e81591. doi:10.1371/journal.pone.0081591

Macías, D. M., Garcia-Gorriz, E., & Stips, A. (2015). Productivity changes in the Mediterranean Sea for the twenty-first century in response to changes in the regional atmospheric forcing. *Frontiers in Marine Science, 2*(79). doi:10.3389/fmars.2015.00079

Macías, D. M., Garcia-Gorriz, E., & Stips, A. (2016). The seasonal cycle of the Atlantic Jet dynamics in the Alboran Sea: direct atmospheric forcing versus Mediterranean thermohaline circulation. *Ocean Dynamics, 66*(2), 137-151. doi:10.1007/s10236-015-0914-y

Macías, D. M., Garcia-Gorriz, E., Piroddi, C., & Stips, A. (2014). Biogeochemical control of marine productivity in the Mediterranean Sea during the last 50 years. *Global Biogeochemical Cycles, 28*(8), 897-907. doi:10.1002/2014GB004846

Macías, D. M., Navarro, G., Echevarría, F., García, C., & Cueto, J. (2007). Phytoplankton pigment distribution in the northwestern Alboran Sea and meteorological forcing: A remote sensing study. *Journal of Marine Research, 65*(4), 523-543. doi:10.1357/002224007782689085

Madrid, C. R. (1978). *The Nimbus 7 User's Guide*. Greenbelt, Maryland: NASA Goddard Space Flight Center.

Malevich, S. B., Vetter, L., & Tierney, J. E. (2019). Global Core Top Calibration of δ18O in Planktic Foraminifera to Sea Surface Temperature. *Paleoceanography and Paleoclimatology, 34*(8), 1292-1315. doi:10.1029/2019PA003576

Mallo, M., Ziveri, P., Mortyn, P. G., Schiebel, R., & Grelaud, M. (2017). Low planktic foraminiferal diversity and abundance observed in a spring 2013 west-east Mediterranean Sea plankton tow transect. *Biogeosciences, 14*(9). doi:10.5194/bg-14-2245-2017

Mann, M. E., Zhang, Z., Rutherford, S., Bradley, R. S., Hughes, M. K., Shindell, D., . . . Ni, F. (2009). Global signatures and dynamical origins of the Little Ice Age and Medieval Climate Anomaly. *Science, 326*(5957), 1256-1260. doi:10.1126/science.1177303

Marcellin Yao, K., Marcou, O., Goyet, C., Guglielmi, V., Touratier, F., & Savy, J.-P. (2016). Time variability of the north-western Mediterranean Sea pH over 1995–2011. *Marine Environmental Research, 116*, 51-60. doi:10.1016/j.marenvres.2016.02.016

Marcott, S. A., Bauska, T. K., Buizert, C., Steig, E. J., Rosen, J. L., Cuffey, K. M., . . . Brook, E. J. (2014). Centennial-scale changes in the global carbon cycle during the last deglaciation. *Nature, 514*(7524), 616-619. doi:10.1038/nature13799

Margaritelli, G., Cacho, I., Català, A., Barra, M., Bellucci, L. G., Lubritto, C., . . . Lirer, F. (2020a). Persistent warm Mediterranean surface waters

during the Roman period. *Scientific Reports, 10*(1), 10431. doi:10.1038/s41598-020-67281-2

Margaritelli, G., Cisneros, M., Cacho, I., Capotondi, L., Vallefuoco, M., Rettori, R., & Lirer, F. (2018). Climatic variability over the last 3000 years in the central - western Mediterranean Sea (Menorca Basin) detected by planktonic foraminifera and stable isotope records. *Global and Planetary Change, 169*, 179-187. doi:10.1016/j.gloplacha.2018.07.012

Margaritelli, G., Lirer, F., Schroeder, K., Alberico, I., Dentici, M. P., & Caruso, A. (2020b). Globorotalia truncatulinoides in Central - Western Mediterranean Sea during the Little Ice Age. *Marine Micropaleontology, 161*, 101921. doi:10.1016/j.marmicro.2020.101921

Margaritelli, G., Vallefuoco, M., Di Rita, F., Capotondi, L., Bellucci, L. G., Insinga, D. D., . . . Lirer, F. (2016). Marine response to climate changes during the last five millennia in the central Mediterranean Sea. *Global and Planetary Change, 142*, 53-72. doi:10.1016/j.gloplacha.2016.04.007

Marlowe, I., Green, J., Neal, A., Brassell, S., Eglinton, G., & Course, P. (1984). Long chain (n-C37–C39) alkenones in the Prymnesiophyceae. Distribution of alkenones and other lipids and their taxonomic significance. *British Phycological Journal, 19*(3), 203-216.

Marriner, N., Kaniewski, D., Pourkerman, M., & Devillers, B. (2022). Anthropocene tipping point reverses long-term Holocene cooling of the Mediterranean Sea: A meta-analysis of the basin's Sea Surface Temperature records. *Earth-Science Reviews*, 103986. doi:10.1016/j.earscirev.2022.103986

Marshall, B. J., Thunell, R. C., Henehan, M. J., Astor, Y., & Wejnert, K. E. (2013). Planktonic foraminiferal area density as a proxy for carbonate ion concentration: A calibration study using the Cariaco Basin ocean time series. *Paleoceanography, 28*(2), 363-376. doi:10.1002/palo.20034

Martinez, E., Antoine, D., D'Ortenzio, F., & Gentili, B. (2009). Climate-Driven Basin-Scale Decadal Oscillations of Oceanic Phytoplankton. *Science, 326*(5957), 1253-1256. doi:doi:10.1126/science.1177012

Martrat, B., Grimalt, J. O., Lopez-Martinez, C., Cacho, I., Sierro, F. J., Flores, J. A., . . . Hodell, D. A. (2004). Abrupt temperature changes in the Western Mediterranean over the past 250,000 years. *Science, 306*(5702), 1762-1765. doi:10.1126/science.1101706

Martrat, B., Jimenez-Amat, P., Zahn, R., & Grimalt, J. O. (2014). Similarities and dissimilarities between the last two deglaciations and interglaciations in the North Atlantic region. *Quaternary Science Reviews, 99*, 122-134. doi:10.1016/j.quascirev.2014.06.016

Marullo, S., Artale, V., & Santoleri, R. (2011). The SST multidecadal variability in the Atlantic–Mediterranean region and its relation to AMO. *Journal of Climate, 24*(16), 4385-4401. doi:10.1175/2011JCLI3884.1

Masqué, P., Fabres, J., Canals, M., Sanchez-Cabeza, J., Sanchez-Vidal, A., Cacho, I., . . . Bruach, J. (2003). Accumulation rates of major constituents of hemipelagic sediments in the deep Alboran Sea: a centennial perspective of sedimentary dynamics. *Marine Geology, 193*(3-4), 207-233. doi:10.1016/S0025-3227(02)00593-5

McGregor, H. V., Evans, M. N., Goosse, H., Leduc, G., Martrat, B., Addison, J. A., . . . Ersek, V. (2015). Robust global ocean cooling trend for the pre-industrial Common Era. *Nature geoscience, 8*(9), 671-677. doi:10.1038/ngeo2510

McNeil, B. I., & Matear, R. J. (2008). Southern Ocean acidification: A tipping point at 450-ppm atmospheric CO₂. *Proceedings of the National Academy of Sciences, 105*(48), 18860-18864. doi:doi:10.1073/pnas.0806318105

MedECC. (2020). *Climate and Environmental Change in the Mediterranean Basin – Current Situation and Risks for the Future*. W. Cramer, J. Guiot, & K. Marini (Series Ed.) Retrieved from Marseille, France:

Medoc, G. (1970). Observation of Formation of Deep Water in the Mediterranean Sea, 1969. *Nature, 227*(5262), 1037-1040. doi:10.1038/2271037a0

Mehrbach, C., Culberson, C. H., Hawley, J. E., & Pytkowicx, R. M. (1973). Measurement of the apparent dissociation constants of carbonic acid in seawater at atmospheric pressure. *Limnology and oceanography, 18*(6), 897-907. doi:10.4319/lo.1973.18.6.0897

Mekik, F. (2014). Radiocarbon dating of planktonic foraminifer shells: A cautionary tale. *Paleoceanography and Paleoclimatology, 29*(1), 13-29. doi:10.1002/2013PA002532

Mellon, S., Kienast, M., Algar, C., de Menocal, P., Kienast, S. S., Marchitto, T. M., . . . Thomas, H. (2019). Foraminifera Trace Anthropogenic CO2 in the NW Atlantic by 1950. *Geophysical Research Letters, 46*(24), 14683-14691. doi:10.1029/2019GL084965

Merchant, C. J., Embury, O., Bulgin, C. E., Block, T., Corlett, G. K., Fiedler, E., . . . Donlon, C. (2019). Satellite-based time-series of sea-surface temperature since 1981 for climate applications. *Scientific data, 6*(1), 223. doi:10.1038/s41597-019-0236-x

Mertens, C., & Schott, F. (1998). Interannual Variability of Deep-Water Formation in the Northwestern Mediterranean. *Journal of Physical Oceanography, 28*(7), 1410-1424. doi:10.1175/1520-0485(1998)028<1410:Ivodwf>2.0.Co;2

Meyer, J., & Riebesell, U. (2015). Reviews and Syntheses: Responses of coccolithophores to ocean acidification: a meta-analysis. *Biogeosciences, 12*(6), 1671-1682. doi:10.5194/bg-12-1671-2015

Millero, F. J., Morse, J., & Chen, C.-T. (1979). The carbonate system in the western Mediterranean Sea. *Deep Sea Research Part A. Oceanographic Research Papers, 26*(12), 1395-1404. doi:10.1016/0198-0149(79)90007-4

Millot, C. (1999). Circulation in the Western Mediterranean Sea. *Journal of Marine Systems, 20*(1), 423-442. doi:10.1016/S0924-7963(98)00078-5

Moel, H., Ganssen, G., Peeters, F., Jung, J.-S., Kroon, D., Brummer, G.-J., & Zeebe, R. E. (2009). Planktic foraminiferal shell thinning in the Arabian Sea due to anthropogenic ocean acidification? *Biogeosciences, 6*. doi:10.5194/bgd-6-1811-2009

Mojtahid, M., Manceau, R., Schiebel, R., Hennekam, R., & de Lange, G. J. (2015). Thirteen thousand years of southeastern Mediterranean climate variability inferred from an integrative planktic foraminiferal-based approach. *Paleoceanography, 30*(4), 402-422. doi:10.1002/2014pa002705

Molfino, B., & McIntyre, A. (1990). Precessional forcing of nutricline dynamics in the equatorial Atlantic. *Science, 249*(4970), 766-769. doi:10.1126/science.249.4970.766

Morard, R., Füllberg, A., Brummer, G.-J. A., Greco, M., Jonkers, L., Wizemann, A., . . . Kucera, M. (2019). Genetic and morphological divergence in the warm-water planktonic foraminifera genus Globigerinoides. *PLoS ONE, 14*(12), e0225246. doi:10.1371/journal.pone.0225246

Moreno, A., Pérez, A., Frigola, J., Nieto-Moreno, V., Rodrigo-Gámiz, M., Martrat, B., . . . Valero-Garcés, B. L. (2012). The Medieval Climate Anomaly in the Iberian Peninsula reconstructed from marine and lake records. *Quaternary Science Reviews, 43*, 16-32. doi:10.1016/j.quascirev.2012.04.007

Morey, A. E., Mix, A. C., & Pisias, N. G. (2005). Planktonic foraminiferal assemblages preserved in surface sediments correspond to multiple environment variables. *Quaternary Science Reviews, 24*(7), 925-950. doi:10.1016/j.quascirev.2003.09.011

Moy, A. D., Howard, W. R., Bray, S. G., & Trull, T. W. (2009). Reduced calcification in modern Southern Ocean planktonic foraminifera. *Nature geoscience, 2*(4), 276. doi:10.1038/ngeo460

Müller, P. J., & Fischer, G. (2001). A 4-year sediment trap record of alkenones from the filamentous upwelling region off Cape Blanc, NW Africa and a comparison with distributions in underlying sediments. *Deep Sea Research Part I: Oceanographic Research Papers, 48*(8), 1877-1903. doi:10.1016/S0967-0637(00)00109-6

Naik, S. S., Godad, S. P., & Naidu, P. D. (2011). Does carbonate ion control planktonic foraminifera shell calcification in upwelling regions? *Current Science, 101*(10), 1370-1375.

NASA Goddard Space Flight Center, O. E. L., Ocean Biology Processing Group. (2020). *Moderate-resolution Imaging Spectroradiometer (MODIS) Aqua Chlorophyll Data; 2018 Reprocessing. NASA OB.DAAC, Greenbelt, MD, USA.*

Netburn, A. N., & Koslow, J. A. (2015). Dissolved oxygen as a constraint on daytime deep scattering layer depth in the southern California current ecosystem. *Deep Sea Research Part I: Oceanographic Research Papers, 104*, 149-158. doi:https://doi.org/10.1016/j.dsr.2015.06.006

Nieto-Moreno, V., Martínez-Ruiz, F., Gallego-Torres, D., Giralt, S., García-Orellana, J., Masque, P., . . . Ortega-Huertas, M. (2015). Palaeoclimate and palaeoceanographic conditions in the westernmost Mediterranean over the last millennium: an integrated organic and inorganic approach. *Journal of the Geological Society, 172*(2), 264-271. doi:10.1144/jgs2013-105

Nieto-Moreno, V., Martínez-Ruiz, F., Giralt, S., Jiménez-Espejo, F., Gallego-Torres, D., Rodrigo-Gámiz, M., . . . De Lange, G. (2011). Tracking climate variability in the western Mediterranean during the Late Holocene: a multiproxy approach. *Climate of the Past, 7*(4), 1395-1414. doi:10.5194/cpd-7-635-2011

Nieto-Moreno, V., Martínez-Ruiz, F., Willmott, V., García-Orellana, J., Masqué, P., & Damsté, J. S. (2013). Climate conditions in the westernmost Mediterranean over the last two millennia: An integrated biomarker approach. *Organic Geochemistry, 55*, 1-10. doi:10.1016/j.orggeochem.2012.11.001

Nittrouer, C. A., DeMaster, D. J., McKee, B. A., Cutshall, N. H., & Larsen, I. L. (1984). The effect of sediment mixing on Pb-210 accumulation rates for the Washington continental shelf. *Marine Geology, 54*(3), 201-221. doi:10.1016/0025-3227(84)90038-0

NOAA National Centers for Environmental Information. (2021). State of the Climate: Global Climate Report for Annual 2020. Retrieved from https://www.ncdc.noaa.gov/sotc/global/202013

Nriagu, J. O. (1990). Human influence on the global cycling of trace metals. *Palaeogeography, Palaeoclimatology, Palaeoecology, 82*(1), 113-120. doi:https://doi.org/10.1016/S0031-0182(12)80025-3

Nriagu, J. O. (1996). A History of Global Metal Pollution. *Science, 272*(5259), 223-223. doi:doi:10.1126/science.272.5259.223

Numberger, L., Hemleben, C., Hoffmann, R., Mackensen, A., Schulz, H., Wunderlich, J.-M., & Kucera, M. (2009). Habitats, abundance patterns and isotopic signals of morphotypes of the planktonic foraminifer Globigerinoides ruber (d'Orbigny) in the eastern Mediterranean Sea

since the Marine Isotopic Stage 12. *Marine Micropaleontology, 73*(1-2), 90-104. doi:10.1016/j.marmicro.2009.07.004

O'Reilly, C. H., Woollings, T., & Zanna, L. (2017). The dynamical influence of the Atlantic Multidecadal Oscillation on continental climate. *Journal of Climate, 30*(18), 7213-7230. doi:10.1175/JCLI-D-16-0345.1

Ohman, M. D., & Venrick, E. L. (2003). CalCOFI in a changing ocean. *Oceanography, 16 (3),* 76-85. doi:https://doi.org/10.5670/oceanog.2003.34

Olivar, M. P., Castellón, A., Sabatés, A., Sarmiento-Lezcano, A., Emelianov, M., Bernal, A., . . . Brierley, A. S. (2022). Variation in mesopelagic fish community composition and structure between Mediterranean and Atlantic waters around the Iberian Peninsula. *Frontiers in Marine Science, 9*. doi:10.3389/fmars.2022.1028717

Olsen, J., Anderson, N. J., & Knudsen, M. F. (2012). Variability of the North Atlantic Oscillation over the past 5,200 years. *Nature geoscience, 5*(11), 808-812. doi:10.1038/ngeo1589

Orr, J. C., Fabry, V. J., Aumont, O., Bopp, L., Doney, S. C., Feely, R. A., . . . Joos, F. (2005). Anthropogenic ocean acidification over the twenty-first century and its impact on calcifying organisms. *Nature, 437*(7059), 681-686. doi:10.1038/nature04095

Osborn, T. J. (2004). Simulating the winter North Atlantic Oscillation: the roles of internal variability and greenhouse gas forcing. *Climate Dynamics, 22*(6-7), 605-623. doi:10.1007/s00382-004-0405-1

Osborne, E. B., Thunell, R. C., Gruber, N., Feely, R. A., & Benitez-Nelson, C. R. (2020). Decadal variability in twentieth-century ocean acidification in the California Current Ecosystem. *Nature geoscience, 13*(1), 43-49. doi:10.1038/s41561-019-0499-z

Osborne, E. B., Thunell, R. C., Marshall, B. J., Holm, J. A., Tappa, E. J., Benitez-Nelson, C., . . . Chen, B. (2016). Calcification of the planktonic foraminifera Globigerina bulloides and carbonate ion concentration: Results from the Santa Barbara Basin. *Paleoceanography, 31*(8), 1083-1102. doi:10.1002/2016PA002933

Oschlies, A., Brandt, P., Stramma, L., & Schmidtko, S. (2018). Drivers and mechanisms of ocean deoxygenation. *Nature geoscience, 11*(7), 467-473. doi:10.1038/s41561-018-0152-2

Oviedo, A., Ziveri, P., Álvarez, M., & Tanhua, T. (2015). Is coccolithophore distribution in the Mediterranean Sea related to seawater carbonate chemistry? *Ocean Sci., 11*(1), 13-32. doi:10.5194/os-11-13-2015

Pagani, M., Liu, Z., LaRiviere, J., & Ravelo, A. C. (2010). High Earth-system climate sensitivity determined from Pliocene carbon dioxide concentrations. *Nature geoscience, 3*(1), 27-30. doi:10.1038/ngeo724

Pallacks, S., Ziveri, P., Martrat, B., Mortyn, P. G., Grelaud, M., Schiebel, R., . . . Anglada-Ortiz, G. (2021). Planktic foraminiferal changes in the western Mediterranean Anthropocene. *Global and Planetary Change, 204*, 103549. doi:doi.org/10.1016/j.gloplacha.2021.103549

Parisi-Baradad, V., Manjabacas, A., Lombarte, A., Olivella, R., Chic, Ò., Piera, J., & García-Ladona, E. (2010). Automated Taxon Identification of Teleost fishes using an otolith online database—AFORO. *Fisheries Research, 105*(1), 13-20. doi:https://doi.org/10.1016/j.fishres.2010.02.005

Pauly, D., Piroddi, C., Hood, L., Bailly, N., Chu, E., Lam, V., . . . Palomares, M. L. D. (2021). The Biology of Mesopelagic Fishes and Their Catches (1950–2018) by Commercial and Experimental Fisheries. *Journal of Marine Science and Engineering, 9*(10), 1057.

Peeters, F. J. C., Brummer, G.-J. A., & Ganssen, G. (2002). The effect of upwelling on the distribution and stable isotope composition of Globigerina bulloides and Globigerinoides ruber (planktic foraminifera) in modern surface waters of the NW Arabian Sea. *Global and Planetary Change, 34*(3), 269-291. doi:10.1016/S0921-8181(02)00120-0

Peliz, A., Boutov, D., & Teles-Machado, A. (2013). The Alboran Sea mesoscale in a long term high resolution simulation: Statistical analysis. *Ocean Modelling, 72*, 32-52. doi:10.1016/j.ocemod.2013.07.002

Penman, D. E., Hönisch, B., Zeebe, R. E., Thomas, E., & Zachos, J. C. (2014). Rapid and sustained surface ocean acidification during the Paleocene-Eocene Thermal Maximum. *Paleoceanography, 29*(5), 357-369. doi:https://doi.org/10.1002/2014PA002621

Pérez-Folgado, M., Sierro, F. J., Flores, J. A., Cacho, I., Grimalt, J. O., Zahn, R., & Shackleton, N. (2003). Western Mediterranean planktonic foraminifera events and millennial climatic variability during the last 70 kyr. *Marine Micropaleontology, 48*(1), 49-70. doi:10.1016/S0377-8398(02)00160-3

Perissoratis, C., & Piper, D. J. W. (1992). Age, regional variation, and shallowest occurrence of S1 sapropel in the northern Aegean Sea. *Geo-Marine Letters, 12*(1), 49-53. doi:10.1007/BF02092108

Philippart, C. J. M., Anadón, R., Danovaro, R., Dippner, J. W., Drinkwater, K. F., Hawkins, S. J., . . . Reid, P. C. (2011). Impacts of climate change on European marine ecosystems: Observations, expectations and indicators. *Journal of Experimental Marine Biology and Ecology, 400*(1), 52-69. doi:10.1016/j.jembe.2011.02.023

Philippsen, B. (2013). The freshwater reservoir effect in radiocarbon dating. *Heritage Science, 1*(1), 24. doi:10.1186/2050-7445-1-24

Pierrot, D., Lewis, E., & Wallace, D. (2006). MS Excel program developed for CO2 system calculations. *ORNL/CDIAC-105a. Carbon Dioxide Information Analysis Center, Oak Ridge National Laboratory, US Department of Energy, Oak Ridge, Tennessee, 10*.

Pisano, A., Marullo, S., Artale, V., Falcini, F., Yang, C., Leonelli, F. E., . . . Buongiorno Nardelli, B. (2020). New Evidence of Mediterranean Climate Change and Variability from Sea Surface Temperature Observations. *Remote Sensing, 12*(1), 132. doi:doi:10.3390/rs12010132

Polovina, J. J., Howell, E. A., & Abecassis, M. (2008). Ocean's least productive waters are expanding. *Geophysical Research Letters, 35*(3). doi:https://doi.org/10.1029/2007GL031745

Praetorius, S. K., Mix, A. C., Walczak, M. H., Wolhowe, M. D., Addison, J. A., & Prahl, F. G. (2015). North Pacific deglacial hypoxic events linked to abrupt ocean warming. *Nature, 527*(7578), 362-366. doi:10.1038/nature15753

Priede, I. G. (2017). List of Deep-Sea Fish Families and Their Taxonomic Classification. In I. G. Priede (Ed.), *Deep-Sea Fishes: Biology, Diversity, Ecology and Fisheries* (pp. 406-414). Cambridge: Cambridge University Press.

Prince, E. D., & Goodyear, C. P. (2006). Hypoxia-based habitat compression of tropical pelagic fishes. *Fisheries Oceanography, 15*(6), 451-464. doi:https://doi.org/10.1111/j.1365-2419.2005.00393.x

Prince, E. D., Luo, J., Goodyear, C. P., Hoolihan, J. P., Snodgrass, D., Orbesen, E. S., . . . Schirrip, M. J. (2010). Ocean scale hypoxia-based habitat compression of Atlantic istiophorid billfishes. *Fisheries Oceanography, 19*(6), 448-462. doi:https://doi.org/10.1111/j.1365-2419.2010.00556.x

Pross, J., Bahr, A., Berke, M., Blum, M., Brzelinski, S., Campos, H., . . . Raeke, A. (2021). *Eastern Mediterranean Paleoclimate and Ecosystems during the Rise of Early Civilizations, Cruise No. M144, December 27, 2017 - January 18, 2018, Heraklion (Greece) - Catania (Italy)* (2195-8475). Retrieved from Bonn: https://www.tib.eu/de/suchen/id/awi%3A132ff752be9c30ba658681b1b47cd916c1e60f6a

Proud, R., Cox, M. J., & Brierley, A. S. (2017). Biogeography of the Global Ocean's Mesopelagic Zone. *Current Biology, 27*(1), 113-119. doi:https://doi.org/10.1016/j.cub.2016.11.003

Puig, P., Masqué, P., Martín, J., Paradis, S., Juan-Dfaz, X., Toro, M., & Palanques, A. (2015). Changes in sediment accumulation rates within NW Mediterranean submarine canyons caused by bottom trawling activities. In F. Briand (Ed.), *Submarine canyon dynamics in the Mediterranean and tributary seas- An integrated geological,*

oceanographic and biological perspective. (Vol. CIESM Monograph 47 pp. 232). Monaco: CIESM Publisher.

Pujol, C., & Grazzini, C. V. (1995). Distribution patterns of live planktic foraminifers as related to regional hydrography and productive systems of the Mediterranean Sea. *Marine Micropaleontology, 25*(2), 187-217. doi:10.1016/0377-8398(95)00002-I

Quay, P. D., Tilbrook, B., & Wong, C. S. (1992). Oceanic Uptake of Fossil Fuel CO₂: Carbon-13 Evidence. *Science, 256*(5053), 74-79. doi:doi:10.1126/science.256.5053.74

R Core Team. (2023). R: A Language and Environment for Statistical Computing. Vienna, Austria: R Foundation for Statistical Computing. Retrieved from https://www.R-project.org/

Rae, J. W. B. (2018). Boron Isotopes in Foraminifera: Systematics, Biomineralisation, and CO2 Reconstruction. In H. Marschall & G. Foster (Eds.), *Boron Isotopes: The Fifth Element* (pp. 107-143). Cham: Springer International Publishing.

Rae, J. W. B., Foster, G. L., Schmidt, D. N., & Elliott, T. (2011). Boron isotopes and B/Ca in benthic foraminifera: Proxies for the deep ocean carbonate system. *Earth and Planetary Science Letters, 302*(3-4), 403-413. doi:10.1016/j.epsl.2010.12.034

Raja, M., & Rosell-Melé, A. (2021). Appraisal of sedimentary alkenones for the quantitative reconstruction of phytoplankton biomass. *Proceedings of the National Academy of Sciences, 118*(2), e2014787118. doi:10.1073/pnas.2014787118

Rasool, S. I., & Schneider, S. H. (1971). Atmospheric Carbon Dioxide and Aerosols: Effects of Large Increases on Global Climate. *Science, 173*(3992), 138-141. doi:doi:10.1126/science.173.3992.138

Rayner, N., Parker, D. E., Horton, E., Folland, C. K., Alexander, L. V., Rowell, D., . . . Kaplan, A. (2003). Global analyses of sea surface temperature, sea ice, and night marine air temperature since the late nineteenth century. *Journal of Geophysical Research: Atmospheres, 108*(D14). doi:10.1029/2002JD002670

Rebotim, A., Voelker, A. H., Jonkers, L., Waniek, J. J., Meggers, H., Schiebel, R., . . . Kucera, M. (2017). Factors controlling the depth habitat of planktonic foraminifera in the subtropical eastern North Atlantic. *Biogeosciences, 14*(4), 827-859. doi:10.5194/bg-14-827-2017

Regenberg, M., Schröder, J. F., Jonas, A.-S., Woop, C., & Gorski, L. (2013). WEIGHT LOSS AND ELIMINATION OF PLANKTONIC FORAMINIFERAL TESTS IN A DISSOLUTION EXPERIMENT. *Journal of Foraminiferal Research, 43*(4), 406-414. doi:10.2113/gsjfr.43.4.406

Reid, P. C., & Hill, C. (2016). Ocean warming: setting the scene. In D. Laffoley & J. M. Baxter (Eds.), *Explaining ocean warming: Causes, scale,*

effects and consequences (1 ed., Vol. 17, pp. 17-45). Gland, Switzerland: IUCN.

Reimer, P. J., Bard, E., Bayliss, A., Beck, J. W., Blackwell, P. G., Ramsey, C. B., . . . Friedrich, M. (2013). IntCal13 and Marine13 radiocarbon age calibration curves 0–50,000 years cal BP. *Radiocarbon, 55*(4), 1869-1887. doi:10.2458/azu_js_rc.55.16947

Reiss, P. T., & Todd Ogden, R. (2009). Smoothing parameter selection for a class of semiparametric linear models. *Journal of the Royal Statistical Society: Series B (Statistical Methodology), 71*(2), 505-523. doi:https://doi.org/10.1111/j.1467-9868.2008.00695.x

Renault, L., Oguz, T., Pascual, A., Vizoso, G., & Tintoré, J. (2012). Surface circulation in the Alborán Sea (western Mediterranean) inferred from remotely sensed data. *Journal of Geophysical Research: Oceans, 117*(C8). doi:10.1029/2011JC007659

Retailleau, S., Schiebel, R., & Howa, H. (2011). Population dynamics of living planktic foraminifers in the hemipelagic southeastern Bay of Biscay. *Marine Micropaleontology, 80*(3), 89-100. doi:10.1016/j.marmicro.2011.06.003

Reynolds, R. W., & Smith, T. M. (1994). Improved global sea surface temperature analyses using optimum interpolation. *Journal of Climate, 7*(6), 929-948. doi:10.1175/1520-0442(1994)007<0929:IGSSTA>2.0.CO;2

Rhein, M., Rintoul, S. R., S. Aoki, S., Campos, E., Chambers, D., Feely, R. A., . . . Wang, F. (2013). Observations: Ocean. In T. F. Stocker, D. Qin, G.-K. Plattner, M. Tignor, S. K. Allen, J. Boschung, A. Nauels, Y. Xia, V. Bex, & P. M. Midgley (Eds.), *Climate Change 2013: The Physical Science Basis. Contribution of Working Group I to the Fifth Assessment Report of the Intergovernmental Panel on Climate Change* (pp. 255-316). Cambridge, United Kingdom and New York, NY, USA: Cambridge University Press.

Richardson, A. J., Walne, A. W., John, A. W. G., Jonas, T. D., Lindley, J. A., Sims, D. W., . . . Witt, M. (2006). Using continuous plankton recorder data. *Progress in Oceanography, 68*(1), 27-74. doi:10.1016/j.pocean.2005.09.011

Riesch, R., Tobler, M., & Plath, M. (2015). Hydrogen Sulfide-Toxic Habitats. In R. Riesch, M. Tobler, & M. Plath (Eds.), *Extremophile Fishes: Ecology, Evolution, and Physiology of Teleosts in Extreme Environments* (pp. 137-159). Cham: Springer International Publishing.

Rigual-Hernández, A. S., Sierro, F. J., Bárcena, M. A., Flores, J. A., & Heussner, S. (2012). Seasonal and interannual changes of planktic foraminiferal fluxes in the Gulf of Lions (NW Mediterranean) and their implications for paleoceanographic studies: two 12-year sediment trap

records. *Deep Sea Research Part I: Oceanographic Research Papers, 66*, 26-40. doi:10.1016/j.dsr.2012.03.011

Robbins, J. A. (1978). Geochemical and geophysical applications of radioactive lead. In J. O. Nriagu (Ed.), *Biogeochemistry of Lead in the Environment* (pp. 285-393). Amsterdam: Elsevier Scientific.

Rohling, E. J. (1994). Review and new aspects concerning the formation of eastern Mediterranean sapropels. *Marine Geology, 122*(1), 1-28. doi:https://doi.org/10.1016/0025-3227(94)90202-X

Rohling, E. J., Abu-Zied, R., Casford, J., Hayes, A., & Hoogakker, B. (2009). The marine environment: present and past. In J. C. Woodward (Ed.), *The physical geography of the Mediterranean* (Vol. 8, pp. 33-67). Oxford: Oxford University Press.

Rohling, E. J., & Hilgen, F. (1991). The eastern Mediterranean climate at times of sapropel formation: a review. *Netherlands Journal of Geosciences/Geologie en Mijnbouw*(Classic Papers).

Rohling, E. J., Hopmans, E. C., & Sinninghe Damsté, J. S. (2006). Water column dynamics during the last interglacial anoxic event in the Mediterranean (sapropel S5). *Paleoceanography, 21*(2). doi:https://doi.org/10.1029/2005PA001237

Rohling, E. J., Marino, G., & Grant, K. (2015). Mediterranean climate and oceanography, and the periodic development of anoxic events (sapropels). *Earth-Science Reviews, 143*, 62-97.

Rohling, E. J., Rijk, S. D., Myers, P. G., & Haines, K. (2000). Palaeoceanography and numerical modelling: the Mediterranean Sea at times of sapropel formation. *Geological Society, London, Special Publications, 181*(1), 135-149. doi:doi:10.1144/GSL.SP.2000.181.01.13

Rohling, E. J., Sprovieri, M., Cane, T., Casford, J. S. L., Cooke, S., Bouloubassi, I., . . . Kroon, D. (2004). Reconstructing past planktic foraminiferal habitats using stable isotope data: a case history for Mediterranean sapropel S5. *Marine Micropaleontology, 50*(1), 89-123. doi:10.1016/S0377-8398(03)00068-9

Rothwell, R. G. (2004). Deep ocean pelagic oozes. In R. C. Selley, R. M. Cocks, & I. R. Plimer (Eds.), *Encyclopedia of Geology*. Oxford: Elsevier.

Ruddiman, W. F. (2008). *Earth's climate : past and future* (2nd ed.). New York: W.H. Freeman.

Russell, A. D., Hönisch, B., Spero, H. J., & Lea, D. W. (2004). Effects of seawater carbonate ion concentration and temperature on shell U, Mg, and Sr in cultured planktonic foraminifera. *Geochimica et Cosmochimica Acta, 68*(21), 4347-4361. doi:https://doi.org/10.1016/j.gca.2004.03.013

Rutherford, S., D'Hondt, S., & Prell, W. (1999). Environmental controls on the geographic distribution of zooplankton diversity. *Nature, 400*(6746), 749-753. doi:10.1038/23449

Saba, G. K., Burd, A. B., Dunne, J. P., Hernández-León, S., Martin, A. H., Rose, K. A., . . . Wilson, S. E. (2021). Toward a better understanding of fish-based contribution to ocean carbon flux. *Limnology and oceanography, 66*(5), 1639-1664. doi:https://doi.org/10.1002/lno.11709

Sabatier, P., Dezileau, L., Colin, C., Briqueu, L., Bouchette, F., Martinez, P., . . . Von Grafenstein, U. (2012). 7000 years of paleostorm activity in the NW Mediterranean Sea in response to Holocene climate events. *Quaternary Research, 77*(1), 1-11. doi:10.1016/j.yqres.2011.09.002

Sabbatini, A., Bassinot, F., Boussetta, S., Negri, A., Rebaubier, H., Dewilde, F., . . . Morigi, C. (2011). Further constraints on the diagenetic influences and salinity effect on Globigerinoides ruber (white) Mg/Ca thermometry: Implications in the Mediterranean Sea. *Geochemistry, Geophysics, Geosystems, 12*(10). doi:https://doi.org/10.1029/2011GC003675

Sachs, J. P., & Repeta, D. J. (1999). Oligotrophy and Nitrogen Fixation During Eastern Mediterranean Sapropel Events. *Science, 286*(5449), 2485-2488. doi:doi:10.1126/science.286.5449.2485

Salvatteci, R., Gutierrez, D., Field, D., Sifeddine, A., Ortlieb, L., Caquineau, S., . . . Bertrand, A. (2019). Fish debris in sediments from the last 25 kyr in the Humboldt Current reveal the role of productivity and oxygen on small pelagic fishes. *Progress in Oceanography, 176*, 102114. doi:https://doi.org/10.1016/j.pocean.2019.05.006

Salvatteci, R., Schneider, R. R., Galbraith, E., Field, D., Blanz, T., Bauersachs, T., . . . Bertrand, A. (2022). Smaller fish species in a warm and oxygen-poor Humboldt Current system. *Science, 375*(6576), 101-104. doi:doi:10.1126/science.abj0270

Sampaio, E., Santos, C., Rosa, I. C., Ferreira, V., Pörtner, H.-O., Duarte, C. M., . . . Rosa, R. (2021). Impacts of hypoxic events surpass those of future ocean warming and acidification. *Nature Ecology & Evolution, 5*(3), 311-321. doi:10.1038/s41559-020-01370-3

Sánchez-Cabeza, J., Masqué, P., & Ani-Ragolta, I. (1998). 210Pb and210Po analysis in sediments and soils by microwave acid digestion. *Journal of Radioanalytical and Nuclear Chemistry, 227*(1-2), 19-22. doi:10.1007/bf02386425

Sarhan, T., Garcı, x, a Lafuente, J., Vargas, M., Vargas, J. M., & Plaza, F. (2000). Upwelling mechanisms in the northwestern Alboran Sea. *Journal of Marine Systems, 23*(4), 317-331. doi:10.1016/S0924-7963(99)00068-8

Sassa, C., Kawaguchi, K., Hirota, Y., & Ishida, M. (2004). Distribution patterns of larval myctophid fish assemblages in the subtropical–tropical waters of the western North Pacific. *Fisheries Oceanography, 13*(4), 267-282. doi:https://doi.org/10.1111/j.1365-2419.2004.00289.x

Schiebel, R. (2002). Planktic foraminiferal sedimentation and the marine calcite budget. *Global Biogeochemical Cycles, 16*(4), 3-1-3-21. doi:10.1029/2001GB001459

Schiebel, R., Barker, S., Lendt, R., Thomas, H., & Bollmann, J. (2007). Planktic foraminiferal dissolution in the twilight zone. *Deep Sea Research Part II: Topical Studies in Oceanography, 54*(5-7), 676-686.

Schiebel, R., & Hemleben, C. (2000). Interannual variability of planktic foraminiferal populations and test flux in the eastern North Atlantic Ocean (JGOFS). *Deep Sea Research Part II: Topical Studies in Oceanography, 47*(9), 1809-1852. doi:https://doi.org/10.1016/S0967-0645(00)00008-4

Schiebel, R., & Hemleben, C. (2005). Modern planktic foraminifera. *Paläontologische Zeitschrift, 79*(1), 135-148. doi:10.1007/BF03021758

Schiebel, R., & Hemleben, C. (2017). *Planktic foraminifers in the modern ocean*. Berlin, Heidelberg: Springer.

Schiebel, R., Smart, S. M., Jentzen, A., Jonkers, L., Morard, R., Meilland, J., . . . Haug, G. H. (2018). Advances in planktonic foraminifer research: New perspectives for paleoceanography. *Revue de Micropaléontologie, 61*(3), 113-138. doi:10.1016/j.revmic.2018.10.001

Schiebel, R., Waniek, J., Bork, M., & Hemleben, C. (2001). Planktic foraminiferal production stimulated by chlorophyll redistribution and entrainment of nutrients. *Deep Sea Research Part I: Oceanographic Research Papers, 48*(3), 721-740. doi:10.1016/S0967-0637(00)00065-0

Schiebel, R., Waniek, J., Zeltner, A., & Alves, M. (2002). Impact of the Azores Front on the distribution of planktic foraminifers, shelled gastropods, and coccolithophorids. *Deep Sea Research Part II: Topical Studies in Oceanography, 49*(19), 4035-4050. doi:10.1016/S0967-0645(02)00141-8

Schiebel, R., Zeltner, A., Treppke, U. F., Waniek, J. J., Bollmann, J., Rixen, T., & Hemleben, C. (2004). Distribution of diatoms, coccolithophores and planktic foraminifers along a trophic gradient during SW monsoon in the Arabian Sea. *Marine Micropaleontology, 51*(3-4), 345-371. doi:10.1016/j.marmicro.2004.02.001

Schirrmacher, J., Weinelt, M., Blanz, T., Andersen, N., Salgueiro, E., & Schneider, R. R. (2019). Multi-decadal atmospheric and marine climate

variability in southern Iberia during the mid-to late-Holocene. *Climate of the Past, 15*(2), 617-634. doi:10.5194/cp-15-617-2019

Schlesinger, M. E., & Ramankutty, N. (1994). An oscillation in the global climate system of period 65–70 years. *Nature, 367*(6465), 723-726. doi:10.1038/367723a0

Schlitzer, R. (2019). Ocean Data View. Retrieved from https://odv.awi.de

Schmidt, D. N., Renaud, S., Bollmann, J., Schiebel, R., & Thierstein, H. R. (2004). Size distribution of Holocene planktic foraminifer assemblages: Biogeography, ecology and adaptation. *Marine Micropaleontology, 50*(3-4), 319-338. doi:10.1016/S0377-8398(03)00098-7

Schmidtko, S., Stramma, L., & Visbeck, M. (2017). Decline in global oceanic oxygen content during the past five decades. *Nature, 542*(7641), 335-339. doi:10.1038/nature21399

Schmiedl, G., Kuhnt, T., Ehrmann, W., Emeis, K.-C., Hamann, Y., Kotthoff, U., . . . Pross, J. (2010). Climatic forcing of eastern Mediterranean deep-water formation and benthic ecosystems during the past 22 000 years. *Quaternary Science Reviews, 29*(23), 3006-3020. doi:https://doi.org/10.1016/j.quascirev.2010.07.002

Schneider, A., Tanhua, T., Körtzinger, A., & Wallace, D. W. R. (2010). High anthropogenic carbon content in the eastern Mediterranean. *Journal of Geophysical Research: Oceans, 115*(C12). doi:10.1029/2010JC006171

Schneider, A., Wallace, D. W., & Körtzinger, A. (2007). Alkalinity of the Mediterranean sea. *Geophysical Research Letters, 34*(15). doi:10.1029/2006GL028842

Schneider, C. A., Rasband, W. S., & Eliceiri, K. W. (2012). NIH Image to ImageJ: 25 years of image analysis. *Nature Methods, 9*(7), 671-675. doi:10.1038/nmeth.2089

Schroeder, K., Garcìa-Lafuente, J., Josey, S. A., Artale, V., Nardelli, B. B., Carrillo, A., . . . Zodiatis, G. (2012). 3 - Circulation of the Mediterranean Sea and its Variability. In P. Lionello (Ed.), *The Climate of the Mediterranean Region* (pp. 187-256). Oxford: Elsevier.

Schroeder, K., Taillandier, V., Vetrano, A., & Gasparini, G. P. (2008). The circulation of the western Mediterranean Sea in spring 2005 as inferred from observations and from model outputs. *Deep Sea Research Part I: Oceanographic Research Papers, 55*(8), 947-965. doi:10.1016/j.dsr.2008.04.003

Schulz, K. G., Hartley, S., & Eyre, B. (2019). Upwelling Amplifies Ocean Acidification on the East Australian Shelf: Implications for Marine Ecosystems. *Frontiers in Marine Science, 6*(636). doi:10.3389/fmars.2019.00636

Seibel, B. A. (2011). Critical oxygen levels and metabolic suppression in oceanic oxygen minimum zones. *Journal of Experimental Biology, 214*(2), 326-336. doi:10.1242/jeb.049171

Seibel, B. A., & Wishner, K. F. (2019). The Significance of Ocean Deoxygenation for Mesopelagic Communities. In D. Laffoley & J. M. Baxter (Eds.), *Ocean Deoxygenation: Everyone's Problem* (pp. 265-276): IUCN.

Seo, H.-S., Endo, Y., Moku, M., Muramoto, K., Fujimoto, K., & Kawaguchi, K. (1998). Amino Acid Composition of Proteins in Myctophid Fishes in the Subarctic and Tropical Pacific Ocean. *Fisheries science, 64*(4), 652-653. doi:10.2331/fishsci.64.652

Shaffer, G., Olsen, S. M., & Pedersen, J. O. P. (2009). Long-term ocean oxygen depletion in response to carbon dioxide emissions from fossil fuels. *Nature geoscience, 2*(2), 105-109. doi:10.1038/ngeo420

Shaltout, M., & Omstedt, A. (2014). Recent sea surface temperature trends and future scenarios for the Mediterranean Sea. *Oceanologia, 56*(3), 411-443. doi:10.5697/oc.56-3.411

Siani, G., Paterne, M., Arnold, M., Bard, E., Métivier, B., Tisnerat, N., & Bassinot, F. (2000). Radiocarbon reservoir ages in the Mediterranean Sea and Black Sea. *Radiocarbon, 42*(2), 271-280. doi:10.1017/S0033822200059075

Sicre, M.-A., Jalali, B., Martrat, B., Schmidt, S., Bassetti, M.-A., & Kallel, N. (2016). Sea surface temperature variability in the North Western Mediterranean Sea (Gulf of Lion) during the Common Era. *Earth and Planetary Science Letters, 456*, 124-133. doi:10.1016/j.epsl.2016.09.032

Simpson, G. L. (2018). Modelling Palaeoecological Time Series Using Generalised Additive Models. *Frontiers in Ecology and Evolution, 6*(149). doi:10.3389/fevo.2018.00149

Skliris, N., Sofianos, S., Gkanasos, A., Mantziafou, A., Vervatis, V., Axaopoulos, P., & Lascaratos, A. (2012). Decadal scale variability of sea surface temperature in the Mediterranean Sea in relation to atmospheric variability. *Ocean Dynamics, 62*(1), 13-30. doi:10.1007/s10236-011-0493-5

Slomp, C. P., Thomson, J., & de Lange, G. J. (2004). Controls on phosphorus regeneration and burial during formation of eastern Mediterranean sapropels. *Marine Geology, 203*(1), 141-159. doi:https://doi.org/10.1016/S0025-3227(03)00335-9

Smith, A. C., Wynn, P. M., Barker, P. A., Leng, M. J., Noble, S. R., & Tych, W. (2016). North Atlantic forcing of moisture delivery to Europe throughout the Holocene. *Scientific Reports, 6*(1), 24745. doi:10.1038/srep24745

Smith, R. O., Bryden, H. L., & Stansfield, K. (2008). Observations of new western Mediterranean deep water formation using Argo floats 2004-2006. *Ocean Sci., 4*(2), 133-149. doi:10.5194/os-4-133-2008

Somarakis, S., Isari, S., & Machias, A. (2011). Larval fish assemblages in coastal waters of central Greece: reflections of topographic and oceanographic heterogeneity. *Scientia Marina, 75*(3), 605-618.

Spero, H. J. (1992). Do planktic foraminifera accurately record shifts in the carbon isotopic composition of seawater ΣCO2? *Marine Micropaleontology, 19*(4), 275-285. doi:https://doi.org/10.1016/0377-8398(92)90033-G

Spero, H. J., Bijma, J., Lea, D. W., & Bemis, B. E. (1997). Effect of seawater carbonate concentration on foraminiferal carbon and oxygen isotopes. *Nature, 390*(6659), 497. doi:10.1038/37333

Spero, H. J., & Lea, D. W. (1996). Experimental determination of stable isotope variability in Globigerina bulloides: implications for paleoceanographic reconstructions. *Marine Micropaleontology, 28*(3), 231-246. doi:10.1016/0377-8398(96)00003-5

Spero, H. J., Lerche, I., & Williams, D. F. (1991). Opening the carbon isotope 'vital effect' black box, 2, Quantitative model for interpreting foraminiferal carbon isotope data. *Paleoceanography, 6*(6), 639-655. doi:10.1029/91PA02022

Sprovieri, R., Di Stefano, E., Incarbona, A., & Gargano, M. E. (2003). A high-resolution record of the last deglaciation in the Sicily Channel based on foraminifera and calcareous nannofossil quantitative distribution. *Palaeogeography, Palaeoclimatology, Palaeoecology, 202*(1), 119-142. doi:https://doi.org/10.1016/S0031-0182(03)00632-1

St. John, M. A., Borja, A., Chust, G., Heath, M., Grigorov, I., Mariani, P., . . . Santos, R. S. (2016). A Dark Hole in Our Understanding of Marine Ecosystems and Their Services: Perspectives from the Mesopelagic Community. *Frontiers in Marine Science, 3*. doi:10.3389/fmars.2016.00031

Stainbank, S., Kroon, D., Rüggeberg, A., Raddatz, J., de Leau, E. S., Zhang, M., & Spezzaferri, S. (2019). Controls on planktonic foraminifera apparent calcification depths for the northern equatorial Indian Ocean. *PLoS ONE, 14*(9), e0222299. doi:10.1371/journal.pone.0222299

Stambler, N. (2014). The Mediterranean Sea – Primary Productivity. In S. Goffredo & Z. Dubinsky (Eds.), *The Mediterranean Sea. Its history and present challenges* (pp. 113-121). Dordrecht Heidelberg New York London: Springer.

Stein, K., Tor, K., & Jens Christian, H. (1998). Schooling of the vertically migrating mesopelagic fish Maurolicus muelleri in light summer nights. *Marine Ecology Progress Series, 170*, 287-290.

Steinhilber, F., Abreu, J. A., Beer, J., Brunner, I., Christl, M., Fischer, H., . . . McCracken, K. G. (2012). 9,400 years of cosmic radiation and solar activity from ice cores and tree rings. *Proceedings of the National Academy of Sciences, 109*(16), 5967-5971. doi:10.1073/pnas.1118965109

Steinhilber, F., Beer, J., & Fröhlich, C. (2009). Total solar irradiance during the Holocene. *Geophysical Research Letters, 36*(19). doi:10.1029/2009GL040142

Stewart, J. S., Hazen, E. L., Bograd, S. J., Byrnes, J. E. K., Foley, D. G., Gilly, W. F., . . . Field, J. C. (2014). Combined climate- and prey-mediated range expansion of Humboldt squid (Dosidicus gigas), a large marine predator in the California Current System. *Global Change Biology, 20*(6), 1832-1843. doi:10.1111/gcb.12502

Stoll, H. M., Arevalos, A., Burke, A., Ziveri, P., Mortyn, G., Shimizu, N., & Unger, D. (2007). Seasonal cycles in biogenic production and export in Northern Bay of Bengal sediment traps. *Deep Sea Research Part II: Topical Studies in Oceanography, 54*(5), 558-580. doi:https://doi.org/10.1016/j.dsr2.2007.01.002

Storz, D., Schulz, H., Waniek, J. J., Schulz-Bull, D. E., & Kučera, M. (2009). Seasonal and interannual variability of the planktic foraminiferal flux in the vicinity of the Azores Current. *Deep Sea Research Part I: Oceanographic Research Papers, 56*(1), 107-124. doi:10.1016/j.dsr.2008.08.009

Stramma, L., Johnson, G. C., Sprintall, J., & Mohrholz, V. (2008). Expanding Oxygen-Minimum Zones in the Tropical Oceans. *Science, 320*(5876), 655-658. doi:doi:10.1126/science.1153847

Stramma, L., Prince, E. D., Schmidtko, S., Luo, J., Hoolihan, J. P., Visbeck, M., . . . Körtzinger, A. (2012). Expansion of oxygen minimum zones may reduce available habitat for tropical pelagic fishes. *Nature Climate Change, 2*(1), 33-37. doi:10.1038/nclimate1304

Stramma, L., Schmidtko, S., Levin, L. A., & Johnson, G. C. (2010). Ocean oxygen minima expansions and their biological impacts. *Deep Sea Research Part I: Oceanographic Research Papers, 57*(4), 587-595. doi:https://doi.org/10.1016/j.dsr.2010.01.005

Stratford, K., Williams, R. G., & Myers, P. G. (2000). Impact of the circulation on Sapropel Formation in the eastern Mediterranean. *Global Biogeochemical Cycles, 14*(2), 683-695. doi:https://doi.org/10.1029/1999GB001157

Struglia, M. V., Mariotti, A., & Filograsso, A. (2004). River discharge into the Mediterranean Sea: climatology and aspects of the observed variability. *Journal of Climate, 17*(24), 4740-4751. doi:10.1175/JCLI-3225.1

Stuiver, M., & Reimer, P. J. (1993). Extended 14C Data Base and Revised CALIB 3.0 14C Age Calibration Program. *Radiocarbon, 35*(1), 215-230. doi:10.1017/S0033822200013904

Tachikawa, K., Sépulcre, S., Toyofuku, T., & Bard, E. (2008). Assessing influence of diagenetic carbonate dissolution on planktonic foraminiferal Mg/Ca in the southeastern Arabian Sea over the past 450 ka: Comparison between Globigerinoides ruber and Globigerinoides sacculifer. *Geochemistry, Geophysics, Geosystems, 9*(4). doi:https://doi.org/10.1029/2007GC001904

Tanhua, T., Hainbucher, D., Schroeder, K., Cardin, V., Álvarez, M., & Civitarese, G. (2013). The Mediterranean Sea system: a review and an introduction to the special issue. *Ocean Science, 9*, 789-803. doi:10.5194/os-9-789-2013

Tans, P., & Keeling, R. F. (2020). Trends in Atmospheric Carbon Dioxide. Retrieved from https://www.esrl.noaa.gov/gmd/ccgg/trends/data.html

Thiede, J. (1975). Distribution of foraminifera in surface waters of a coastal upwelling area. *Nature, 253*(5494), 712-714. doi:10.1038/253712a0

Thomson, J., Crudeli, D., de Lange, G. J., Slomp, C. P., Erba, E., Corselli, C., & Calvert, S. E. (2004). Florisphaera profunda and the origin and diagenesis of carbonate phases in eastern Mediterranean sapropel units. *Paleoceanography, 19*(3). doi:https://doi.org/10.1029/2003PA000976

Thunell, R. C. (1978). Distribution of recent planktonic foraminifera in surface sediments of the Mediterranean Sea. *Marine Micropaleontology, 3*(2), 147-173. doi:10.1016/0377-8398(78)90003-8

Titschack, J., Fink, H. G., Baum, D., Wienberg, C., Hebbeln, D., & Freiwald, A. (2016). Mediterranean cold-water corals – an important regional carbonate factory? *The Depositional Record, 2*(1), 74-96. doi:10.1002/dep2.14

Todd, C. L., Schmidt, D. N., Robinson, M. M., & De Schepper, S. (2020). Planktic Foraminiferal Test Size and Weight Response to the Late Pliocene Environment. *Paleoceanography and Paleoclimatology, 35*(1), e2019PA003738. doi:10.1029/2019pa003738

Touratier, F., & Goyet, C. (2009). Decadal evolution of anthropogenic CO2 in the northwestern Mediterranean Sea from the mid-1990s to the mid-2000s. *Deep Sea Research Part I: Oceanographic Research Papers, 56*(10), 1708-1716. doi:10.1016/j.dsr.2009.05.015

Toyofuku, T., Matsuo, M. Y., de Nooijer, L. J., Nagai, Y., Kawada, S., Fujita, K., . . . Kitazato, H. (2017). Proton pumping accompanies calcification in foraminifera. *Nature Communications, 8*(1), 14145. doi:10.1038/ncomms14145

Trouet, V., Esper, J., Graham, N. E., Baker, A., Scourse, J. D., & Frank, D. C. (2009). Persistent positive North Atlantic Oscillation mode dominated

the medieval climate anomaly. *Science, 324*(5923), 78-80. doi:10.1126/science.1166349

Tsimplis, M. N., Calafat, F. M., Marcos, M., Jordá, G., Gomis, D., Fenoglio-Marc, L., . . . Chambers, D. P. (2013). The effect of the NAO on sea level and on mass changes in the Mediterranean Sea. *Journal of Geophysical Research: Oceans, 118*(2), 944-952. doi:10.1002/jgrc.20078

Tuset, V. M., Lombarte, A., & Assis, C. A. (2008). Otolith atlas for the western Mediterranean, north and central eastern Atlantic. *Scientia Marina, 72*(S1), 7-198.

Ulbrich, U., Lionello, P., Belusic, D., Jacobeit, J., Knippertz, P., Kuglitsch, F. G., . . . Ziv, B. (2012). 5 - Climate of the Mediterranean: Synoptic patterns, temperature, precipitation, winds and their extremes. In P. Lionello (Ed.), *The Climate of the Mediterranean Region* (pp. 301-346). Oxford: Elsevier.

Uppstrom, L. R. (1974). The boron/chlorinity ratio of deep-sea water from the Pacific Ocean. *Deep Sea Res., 21*, 161-162. doi:10.1016/0011-7471(74)90074-6

Usoskin, I., Gallet, Y., Lopes, F., Kovaltsov, G., & Hulot, G. (2016). Solar activity during the Holocene: the Hallstatt cycle and its consequence for grand minima and maxima. *Astronomy & Astrophysics, 587*, A150. doi:10.1051/0004-6361/201527295

Vallefuoco, M., Lirer, F., Ferraro, L., Pelosi, N., Capotondi, L., Sprovieri, M., & Incarbona, A. (2012). Climatic variability and anthropogenic signatures in the Gulf of Salerno (southern-eastern Tyrrhenian Sea) during the last half millennium. *Rendiconti Lincei, 23*(1), 13-23. doi:10.1007/s12210-011-0154-0

Van Raden, U. J., Groeneveld, J., Raitzsch, M., & Kucera, M. (2011). Mg/Ca in the planktonic foraminifera Globorotalia inflata and Globigerinoides bulloides from Western Mediterranean plankton tow and core top samples. *Marine Micropaleontology, 78*(3-4), 101-112.

Vaquer-Sunyer, R., & Duarte, C. M. (2008). Thresholds of hypoxia for marine biodiversity. *Proceedings of the National Academy of Sciences, 105*(40), 15452-15457. doi:doi:10.1073/pnas.0803833105

Vargas-Yáñez, M., García, M. J., Salat, J., García-Martínez, M., Pascual, J., & Moya, F. (2008). Warming trends and decadal variability in the Western Mediterranean shelf. *Global and Planetary Change, 63*(2-3), 177-184. doi:10.1016/j.gloplacha.2007.09.001

Vargas-Yáñez, M., Moya, F., García-Martínez, M. C., Tel, E., Zunino, P., Plaza, F., . . . Serra, M. (2010). Climate change in the Western Mediterranean Sea 1900–2008. *Journal of Marine Systems, 82*(3), 171-176. doi:10.1016/j.jmarsys.2010.04.013

Vargas-Yáñez, M., Plaza, F., García-Lafuente, J., Sarhan, T., Vargas, J. M., & Vélez-Belchi, P. (2002). About the seasonal variability of the Alboran Sea circulation. *Journal of Marine Systems, 35*(3), 229-248. doi:10.1016/S0924-7963(02)00128-8

Vignudelli, S., Gasparini, G., Astraldi, M., & Schiano, M. (1999). A possible influence of the North Atlantic Oscillation on the circulation of the Western Mediterranean Sea. *Geophysical Research Letters, 26*(5), 623-626. doi:10.1029/1999GL900038

Volkman, J. K., Barrerr, S. M., Blackburn, S. I., & Sikes, E. L. (1995). Alkenones in Gephyrocapsa oceanica: Implications for studies of paleoclimate. *Geochimica et Cosmochimica Acta, 59*(3), 513-520. doi:10.1016/0016-7037(95)00325-T

Volkman, J. K., Eglinton, G., Corner, E. D. S., & Forsberg, T. E. V. (1980). Long-chain alkenes and alkenones in the marine coccolithophorid Emiliania huxleyi. *Phytochemistry, 19*(12), 2619-2622.

von Schuckmann, K., Le Traon, P.-Y., Smith, N., Pascual, A., Djavidnia, S., Gattuso, J.-P., . . . Fanjul, E. Á. (2020). Copernicus Marine Service Ocean State Report, Issue 4. *Journal of Operational Oceanography, 13*(sup1), S1-S172. doi:10.1080/1755876X.2020.1785097

Vonhof, H. B., de Graaf, S., Spero, H. J., Schiebel, R., Verdegaal, S. J. A., Metcalfe, B., & Haug, G. H. (2020). High-precision stable isotope analysis of <5 μg CaCO3 samples by continuous-flow mass spectrometry. *Rapid Communications in Mass Spectrometry, 34*(19), e8878. doi:10.1002/rcm.8878

Waelbroeck, C., Duplessy, J.-C., Michel, E., Labeyrie, L., Paillard, D., & Duprat, J. (2001). The timing of the last deglaciation in North Atlantic climate records. *Nature, 412*(6848), 724-727. doi:10.1038/35089060

Wang, J., Yang, B., Ljungqvist, F. C., Luterbacher, J., Osborn, Timothy J., Briffa, K. R., & Zorita, E. (2017). Internal and external forcing of multidecadal Atlantic climate variability over the past 1,200 years. *Nature geoscience, 10*(7), 512-517. doi:10.1038/ngeo2962

Wang, L. (2000). Isotopic signals in two morphotypes of Globigerinoides ruber (white) from the South China Sea: implications for monsoon climate change during the last glacial cycle. *Palaeogeography, Palaeoclimatology, Palaeoecology, 161*(3-4), 381-394. doi:10.1016/S0031-0182(00)00094-8

Waters, C. N., Zalasiewicz, J., Summerhayes, C., Barnosky, A. D., Poirier, C., Gałuszka, A., . . . Wolfe, A. P. (2016). The Anthropocene is functionally and stratigraphically distinct from the Holocene. *Science, 351*(6269), aad2622. doi:10.1126/science.aad2622

Watson, A. J. (2016). Oceans on the edge of anoxia. *Science, 354*(6319), 1529-1530. doi:doi:10.1126/science.aaj2321

Wefer, G., Berger, W. H., Bijma, J., & Fischer, G. (1999). Clues to Ocean History: a Brief Overview of Proxies. In G. Fischer & G. Wefer (Eds.), *Use of Proxies in Paleoceanography: Examples from the South Atlantic* (pp. 1-68). Berlin, Heidelberg: Springer Berlin Heidelberg.

Weinkauf, M. F. G., Kunze, J. G., Waniek, J. J., & Kučera, M. (2016). Seasonal variation in shell calcification of planktonic foraminifera in the ne atlantic reveals species-specific response to temperature, productivity, and optimum growth conditions. *PLoS ONE, 11*(2). doi:10.1371/journal.pone.0148363

Weiss, R. F. (1974). Carbon dioxide in water and seawater: the solubility of a non-ideal gas. *Marine Chemistry, 2*(3), 203-215. doi:10.1016/0304-4203(74)90015-2

Whitney, F. A., Freeland, H. J., & Robert, M. (2007). Persistently declining oxygen levels in the interior waters of the eastern subarctic Pacific. *Progress in Oceanography, 75*(2), 179-199. doi:https://doi.org/10.1016/j.pocean.2007.08.007

Wishner, K. F., Outram, D. M., Seibel, B. A., Daly, K. L., & Williams, R. L. (2013). Zooplankton in the eastern tropical north Pacific: Boundary effects of oxygen minimum zone expansion. *Deep Sea Research Part I: Oceanographic Research Papers, 79*, 122-140. doi:https://doi.org/10.1016/j.dsr.2013.05.012

Wood, S. N. (2011). Fast stable restricted maximum likelihood and marginal likelihood estimation of semiparametric generalized linear models. *Journal of the Royal Statistical Society: Series B (Statistical Methodology), 73*(1), 3-36. doi:10.1111/j.1467-9868.2010.00749.x

Wood, S. N., Pya, N., & Säfken, B. (2016). Smoothing Parameter and Model Selection for General Smooth Models. *Journal of the American Statistical Association, 111*(516), 1548-1563. doi:10.1080/01621459.2016.1180986

Yamamoto, M., Shimamoto, A., Fukuhara, T., Naraoka, H., Tanaka, Y., & Nishimura, A. (2007). Seasonal and depth variations in molecular and isotopic alkenone composition of sinking particles from the western North Pacific. *Deep Sea Research Part I: Oceanographic Research Papers, 54*(9), 1571-1592. doi:10.1016/j.dsr.2007.05.012

Yasuhara, M., Rabalais, N. N., Conley, D. J., & Gutiérrez, D. (2019). Palaeo-records of histories of deoxygenation and its ecosystem impact. In D. Laffoley & J. M. Baxter (Eds.), *Ocean Deoxygenation: Everyone's Problem* (pp. 213-224): IUCN.

Young, J. R. (1994). Functions of coccoliths. In A. Winter & W. G. Siesser (Eds.), *Coccolithophores* (pp. 63-82): Cambridge Univ. Press.

Young, J. R., Geisen, M., Cros, L., Kleijne, A., Sprengel, C., Probert, I., & Østergaard, J. (2003). A guide to extant coccolithophore taxonomy. *Journal of Nannoplankton Research, Special Issue, 1*, 1-132.

Zachos, J. C., Röhl, U., Schellenberg, S. A., Sluijs, A., Hodell, D. A., Kelly, D. C., . . . Kroon, D. (2005). Rapid Acidification of the Ocean During the Paleocene-Eocene Thermal Maximum. *Science, 308*(5728), 1611-1615. doi:doi:10.1126/science.1109004

Zarkogiannis, S., Kontakiotis, G., & Antonarakou, A. (2020). Recent planktonic foraminifera population and size response to Eastern Mediterranean hydrography. *Revue de Micropaléontologie, 69*, 100450. doi:https://doi.org/10.1016/j.revmic.2020.100450

Zeebe, R. E. (2012). History of seawater carbonate chemistry, atmospheric CO 2, and ocean acidification. *Annual Review of Earth and Planetary Sciences, 40*(141), 2012.

Zeebe, R. E., & Rae, J. W. B. (2020). Equilibria, kinetics, and boron isotope partitioning in the aqueous boric acid–hydrofluoric acid system. *Chemical Geology, 550*, 119693. doi:10.1016/j.chemgeo.2020.119693

Zeebe, R. E., Ridgwell, A., & Zachos, J. C. (2016). Anthropogenic carbon release rate unprecedented during the past 66 million years. *Nature geoscience, 9*(4), 325-329. doi:10.1038/ngeo2681

Zeebe, R. E., & Zachos, J. C. (2013). Long-term legacy of massive carbon input to the Earth system: Anthropocene versus Eocene. *Philosophical Transactions of the Royal Society A: Mathematical, Physical and Engineering Sciences, 371*(2001), 20120006. doi:doi:10.1098/rsta.2012.0006

Zielhofer, C., von Suchodoletz, H., Fletcher, W. J., Schneider, B., Dietze, E., Schlegel, M., . . . Mikdad, A. (2017). Millennial-scale fluctuations in Saharan dust supply across the decline of the African Humid Period. *Quaternary Science Reviews, 171*, 119-135. doi:https://doi.org/10.1016/j.quascirev.2017.07.010

Ziveri, P., Baumann, K.-H., Böckel, B., Bollmann, J., & Young, J. R. (2004). Biogeography of selected Holocene coccoliths in the Atlantic Ocean. In H. R. Thierstein & J. R. Young (Eds.), *Coccolithophores: From Molecular Processes to Global Impact* (pp. 403-428). Berlin, Heidelberg: Springer Berlin Heidelberg.

Ziveri, P., Gray, W. R., Anglada-Ortiz, G., Manno, C., Grelaud, M., Incarbona, A., . . . Berelson, W. (2023). Pelagic calcium carbonate production and shallow dissolution in the North Pacific Ocean. *Nature Communications, 14*(1), 805. doi:10.1038/s41467-023-36177-w

Zuo, Z., Eisma, D., Gieles, R., & Beks, J. (1997). Accumulation rates and sediment deposition in the northwestern Mediterranean. *Deep Sea Research Part II: Topical Studies in Oceanography, 44*(3), 597-609. doi:10.1016/S0967-0645(96)00083-5